SHEAR STRENGTH AND DRIFT CAPACITY OF REINFORCED CONCRETE AND HIGH-PERFORMANCE FIBER REINFORCED CONCRETE LOW-RISE WALLS SUBJECTED TO DISPLACEMENT REVERSALS

by

Adamantia Athanasopoulou

A dissertation submitted in partial fulfillment
of the requirements for the degree of
Doctor of Philosophy
(Civil Engineering)
in The University of Michigan
2010

Doctoral Committee:

Associate Professor Gustavo J. Parra-Montesinos, Chair
Professor Sherif El-Tawil
Professor James K. Wight
Professor Alan S. Wineman

ACKNOWLEDGEMENTS

This research was possible through the financial support provided by the National Science Foundation under Grant No. CMS 0324519. The opinions expressed in this report are those of the writer and do not necessarily reflect the views of the sponsors.

The writer greatly appreciates to have been advised both academically and personally by Associate Professor Gustavo J. Parra-Montesinos. His invaluable and continuous support fulfilled the writer's Ph.D. learning process and was instrumental in the completion of this dissertation. The writer is also grateful for having the opportunity to be taught by Professors James K. Wight, Sherif El-Tawil and Alan S. Wineman. The writer wishes to thank them for their participation in her doctoral committee and for their valuable comments throughout this research project. Their research enthusiasm and broad knowledge will definitely inspire and benefit the writer in her professional career.

The author wishes to thank her friends and fellow students at the University of Michigan, in particular, Hai Dinh, Matt Fadden, Katie Farnum, Peter Heeringa, Terry McGovern, Heather Munoz, Monthian Setkit, and Elisabeth Windsor for their kind help. Many special thanks to Remy Lequesne and Min Yuan Cheng for their tremendous help in the lab and friendship along the way. Sincere thanks are also due to the University of Michigan Structures Laboratory manager, Jan Pantolin and technicians, Robert Spence and Robert Fischer, for their invaluable help during the experimental phase of this research.

Finally, the writer wishes to thank her beloved family, her parents Anastasios and Maria and her sisters Katerina and Alexia, whose endless love and encouragement were always with her. The author also wishes to express her gratitude to Kostas for his unconditional love, support and understanding throughout the course of this research.

TABLE OF CONTENTS

LIST OF TABLES

LIST OF FIGURES

CHAPTER 1

INTRODUCTION

1.1 BACKGROUND AND RESEARCH MOTIVATION

Since the 1960s, considerable research, as well as lessons learned from previous earthquakes, have led to improved understanding of the seismic behavior of structural walls. Among the first reported observations concerning the seismic behavior of structural walls were those after the Chilean earthquake of 1960, as reported in the Advance Engineering Bulletin No. 6 issued by the Portland Cement Association, where the efficiency of structural walls in controlling structural damage during severe earthquakes was noted. In the early 1970s, Fintel (1974) indicated that properly designed structural walls could be used effectively as the primary lateral-load resisting system for both wind and earthquake loading in multistory buildings. Structural wall systems have also been recognized as a favorable alternative to ductile moment-resistant frames (Sittipunt et al., 2001). Today, reinforced concrete structural walls are frequently used as the primary component of the lateral load-resisting system in buildings located in earthquake-prone regions because of their substantial contribution to building lateral strength and stiffness.

The seismic design of reinforced concrete structural walls in the U.S. follows the provisions of Chapter 21 of the ACI Building Code (ACI Committee 318, 2008). These are perhaps the most widely used provisions for the design of structural walls located in earthquake-prone regions. Typical reinforcement requirements for structural walls, besides flexural reinforcement, include distributed vertical and horizontal reinforcement in the web of the wall. Special confinement reinforcement at the wall edges, in the form

of closely spaced hoops, is often required to avoid early concrete crushing when the expected compression strain and/or stress demand is large. Fig. 1-1 shows the typical reinforcement detailing in the boundary regions of RC structural walls.

Low-rise walls are typically defined as those having a height-to-length ratio smaller than two and thus, they exhibit a behavior highly influenced by shear. Low-rise walls can be found in low-rise buildings such as parking structures, and in high-rise structures, when the walls extend only a few stories above the foundation level (Pauley et al., 1981). The required seismic detailing of low-rise structural walls, even though it is believed to lead to an acceptable level of performance, can translate into severe reinforcement congestion and construction difficulties. In addition, experimental studies focusing on the behavior of reinforced concrete low-rise walls have generally revealed limited drift capacity, in some cases as low as 0.3% (Barda et al., 1977; Pauley et al., 1981; Hidalgo et al., 2002). Thus, there is room for improvements in performance and possibly, for simplifications in reinforcement detailing.

A design alternative that could lead to enhanced seismic behavior while allowing for simplifications in reinforcement detailing in low-rise walls is the use of discontinuous, randomly oriented steel fibers added to the concrete. Fiber reinforcement can be very effective for bridging cracks in any direction because of the random orientation of the fibers. Also, the use of fiber reinforcement often leads to a reduced crack spacing with the associated narrower crack widths and increase in shear strength and damage tolerance. Of particular interest for use in low-rise wall construction is High-Performance Fiber Reinforced Concrete (HPFRC), which is a new type of fiber reinforced concrete that exhibits a strain-hardening behavior under direct tension. This material has been used in shear-critical elements with very promising results in terms of shear resistance, deformation capacity and damage tolerance (Parra, 2005).

Kim and Parra (2003) proposed the use of HPFRC in lieu of regular concrete in low-rise walls. A pilot experimental study that consisted of the testing of two HPFRC low-rise walls under displacement reversals showed that the use of an HPFRC material offers the potential for a significant relaxation in the required web and confinement reinforcement while enhancing wall displacement capacity and damage tolerance.

To the writer's knowledge, no work other than the pilot study by Kim and Parra (2003) has been conducted on the behavior of HPFRC low-rise structural walls under displacement reversals. Thus, prior to this study, very limited information was available on the shear strength and deformation capacity of HPFRC walls subjected to reversed cyclic loading. Based on the encouraging results from the pilot study by Kim and Parra (2003), a comprehensive experimental and analytical research project was therefore undertaken to evaluate in depth the seismic behavior of HPFRC low-rise walls and to develop analytical tools for their modeling and design.

1.2 RESEARCH OBJECTIVE AND SCOPE

The main objective of this research was to evaluate the potential of using HPFRC materials in low-rise walls in order to simplify transverse reinforcement detailing while enhancing shear resistance, deformation capacity and damage tolerance when subjected to earthquake-induced lateral displacements.

The scope of this thesis was limited to rectangular cantilever low-rise walls constructed with either regular concrete or an HPFRC material. Two shear span-to-length ratios were evaluated, 1.2 and 1.5, and no axial load was applied to the walls. The HPFRCs used contained either steel or ultra-high molecular weight polyethylene (Spectra) fibers in volume fractions between 1.5% and 2.0%.

In order to achieve the research objective, the following tasks were performed:

Task 1: Literature Review

The review of the relevant literature covered two basic topics. The first topic focused on the behavior and design of reinforced concrete walls under lateral loading. In particular, previous experimental studies on reinforced concrete low-rise walls were reviewed so that the parameters that influence wall shear strength and deformation capacity could be identified. This review was followed by a presentation of the design philosophy for reinforced concrete structural walls with emphasis on the seismic provisions of the 2005 ACI Code (ACI Committee 318, 2005). The second review topic focused on the behavior of HPFRC materials and their application in shear-critical elements, with emphasis on existing methods for estimating the shear strength of fiber-reinforced concrete members under monotonic and reversed cyclic loading.

Task 2: Experimental Studies

The experimental program included the design and testing of seven low-rise walls under reversed cyclic displacements. Four specimens were constructed with regular concrete, which were designed according to the seismic provisions (Chapter 21) of the 2005 ACI Code (ACI Committee 318, 2005). The use of an HPFRC material in combination with a simplified reinforcing detailing was evaluated through the testing of HPFRC low-rise wall specimens under approximately the same shear stress level as their companion RC walls. The main experimental parameters were: 1) average shear stress level; 2) wall height-to-length ratio; 3) web and tension reinforcement ratio; 4) use of fiber reinforced concrete versus fiber reinforced mortar, and 5) effect of addition of dowel bars at the wall-foundation interface for HPFRC walls.

Task 3: Experimental Results and Analytical Studies

The evaluation of the experimental behavior of the RC and HPFRC test walls was mainly based on the load versus displacement hysteresis response, sliding shear response, rotations along the wall height, shear distortions, and energy dissipation capacity. Emphasis was also given to the identification of the different deformation mechanisms

and their contribution to overall drift, so that conclusions could be drawn about the modeling of low-rise walls. In this part of the study, the test results reported by Kim and Parra (2003) from the pilot study on HPFRC low-rise walls were further analyzed and included in the analytical program.

Task 4: Summary and Conclusions

The final task consisted of a summary of the main aspects of the research program and conclusions drawn from the experimental and analytical studies.

1.3 ORGANIZATION OF THE THESIS

This report is organized in six chapters. In the first chapter a brief introduction to the research project is given, followed by a statement of the research objective and scope. A review of relevant research work on the behavior of RC low-rise walls and structural applications of HPFRC materials is presented in Chapter 2. Chapter 3 focuses on the experimental program, where the reinforcing details of the specimens, the materials used, the test protocol, and other testing issues are discussed. Chapter 4 presents the basic experimental results, whereas Chapter 5 focuses on the analytical studies and in-depth discussion of the behavior of the test specimens. Conclusions and recommendations drawn from this study are provided in Chapter 6.

CHAPTER 2

LITERATURE REVIEW

2.1 INTRODUCTION

In this chapter, a literature review on topics related to this research study is presented. A short review on the behavior and design of low-rise reinforced concrete structural walls is presented in Section 2.2. Emphasis is given on experimental investigations on isolated low-rise walls with similar characteristics to those of the specimens tested in this study. A review of the 2005 ACI Code seismic provisions (ACI Committee 318, 2005) for low-rise shear walls is then followed by a discussion of predictive equations for the shear strength of structural walls. Section 2.3 provides an overview of the behavior and characteristics of High-Performance Fiber Reinforced Concrete (HPFRC) materials and a discussion of their structural applications on shear-critical members subjected to displacement reversals.

2.2 BEHAVIOR OF REINFORCED CONCRETE STRUCTURAL WALLS

2.2.1 General

Reinforced concrete structural walls are deep and relatively thin, vertical cantilever members, also referred to as “shear walls”. Structural walls are widely used in reinforced concrete buildings located in earthquake-prone regions as the primary lateral-load resisting mechanism, because of their efficiency to provide lateral strength and stiffness, and control the lateral drift. Structural walls can also be an effective solution to rehabilitate deficient existing structures. As documented by several researchers (for example Fintel, 1991; Wood, 1991), buildings with reinforced concrete walls have shown good performance during recent earthquakes, which has made structural concrete walls a

quite popular alternative to reinforced concrete frames in regions of high seismicity, such as the west coast of the U.S., New Zealand, Chile, among others.

Structural walls can be found in various shapes and sizes, with different configurations in the building plan. Symmetrical sections, for example rectangular and barbell shaped, are quite frequent, although "flanged", asymmetrical wall sections such as T- and L-shaped sections are also often used. The effect of the wall cross-section shape on the seismic behavior of a shear wall has been investigated by several researchers and it has been shown that the wall strength, stiffness, and ductility depend greatly on the shape of the wall (Paulay, 1986[(a)]; Wallace and Moehle, 1989).

One of the most common classifications of structural walls is with respect to their overall height-to-length ratio (wall aspect ratio, h_w/l_w). Walls with aspect ratio greater than two are usually referred to as "slender walls" and have a behavior mainly dominated by flexure. Slender walls are quite common in tall buildings because of their efficiency in resisting lateral loads and limiting lateral drift. Structural walls with an aspect ratio smaller than two are usually called "low-rise" walls, where shear tends to govern the overall wall response. "Squat walls" are typically defined as walls with an aspect ratio smaller than one. Low-rise walls find application in residential buildings, parking structures, industrial buildings, nuclear power plants, and also in highway overpasses and bridge abutments. Furthermore, low shear span-to-length ratios (shear aspect ratio, a/l_w) can be found in slender walls at the basement of high-rise structures if the magnitude of the bending moment at the foundation level is significantly reduced from its maximum value, at the top of the basement (Salonikios, 2007).

Since the 1960s, several research projects have focused on the behavior of slender and low-rise walls under monotonic and reversed lateral cyclic loading. Based on experimental investigations, factors that affect the behavior of structural walls, especially their deformation capacity, include the wall aspect ratio and configuration, axial load,

shear stress demand, and wall reinforcement ratios (Wallace and Moehle, 1992; Wallace, 1994; 1995[(a)]; 1995[(b)]). The philosophy often used in the design of concrete walls focuses on providing the required strength and stiffness to avoid or limit damage under frequent earthquakes (limited or no inelastic behavior) while ensuring sufficient wall deformation capacity so that the lateral load capacity can be maintained during the inelastic response expected during stronger, less frequent earthquakes (Massone and Wallace, 2004). Structural walls must also be able to dissipate energy after yielding to survive strong ground motions, as noted by Pauley et al. (1982), and should not be susceptible to sudden failures due to shear or local instabilities.

The ultimate shear strength of shear walls and the design criteria to adequately resist shear has been the focus of many experimental and analytical studies (Hidalgo et al., 2002). Two different approaches have been used by researchers for predicting the ultimate shear strength of shear walls: the derivation of empirical expressions based on test results (for example Barda et al., 1977; Aktan and Bertero, 1985; Wood, 1989; Wood, 1990), and the application of shear models based on structural mechanics through the use of equilibrium, compatibility and material constitutive relationships (for example Collins and Mitchell, 1986; Aoyama, 1991). Most of the seismic design provisions found in modern building codes, such as the ACI Code provisions (ACI Committee 318, 2008), use empirical or semi-empirical equations to estimate the ultimate shear strength of shear walls.

2.2.2 Experimental Research on the Behavior of Low-Rise Reinforced Concrete Structural Walls

2.2.2.1. General Background

Before the 1970s, experimental research on reinforced concrete structures was primarily directed towards the understanding of the behavior of moment resisting frames. Limited work was reported on the behavior of structural walls under earthquake-type loading (Lopes, 2001[(b)]). Benjamin and Williams (1957; 1958; 1960) conducted one of the

earliest experimental investigations on the behavior and strength of one-story plain and reinforced concrete structural walls. Later, in 1968, the U.S. Portland Cement Association (PCA) undertook an extensive test program in order to generate information on the behavior and strength characteristics of structural walls for high and low-rise buildings (Cardenas et al., 1973; 1980; Oesterle et al., 1976; 1979).

After the 1970s, the interest on the seismic behavior of isolated and coupled structural walls grew. Fintel (1991) documented the superiority of structural walls to resist lateral forces induced by seismic excitations and several experimental investigations focusing on structural walls were carried out in the U.S., Europe, New Zealand, and Japan. In particular, the remarkably good performance of structural wall dominant buildings during the 1985 Chilean earthquake inspired an increase in the amount of research on the seismic behavior and detailing requirements of reinforced concrete walls in the U.S. (Thomsen and Wallace, 1995).

2.2.2.2 Behavior of Low-Rise Walls under Lateral Loading

The behavior of low-rise walls may be quite different from that of slender walls because of the effect of the wall aspect ratio (deep member behavior versus beam-type behavior for low-rise and slender walls, respectively). Typical failure modes observed in low-rise walls subjected to lateral loading (monotonic or cyclic) are well documented and include: diagonal tension failure, diagonal compression failure (or web crushing and/or splitting failure), and sliding shear failure at the base of the wall (Pauley et al., 1982). Fig. 2-1 schematically presents the diagonal tension and diagonal compression failure modes. A typical corner-to-corner diagonal tension failure is shown in Fig. 2-1(a) whereas Fig. 2-1(b) illustrates a case where a steeper diagonal crack leads to failure. Figs. 2-1(c) and (d), on the other hand, present a diagonal compression and a web crushing failure under monotonic and cyclic loading, respectively.

The development of a ductile flexural response is generally favorable since failures due to shear can lead to limited ductility and premature degradation in stiffness and strength. Shear failure should thus be avoided in seismic design. Diagonal tension failure can be avoided by providing sufficient horizontal and vertical shear reinforcement, whereas limitations in the wall flexural strength (and thus in shear stress demand) can insure that a diagonal compression failure mechanism will not govern. Oesterle et al. (1984) suggested that low-rise walls are more susceptible to web crushing prior to flexural yielding compared with slender walls. It is also possible that in cases of high axial compression and flexure in rectangular walls, the boundary zone under compression may fail through out-of-plane instability (Aktan and Bertero, 1985). Furthermore, walls that are lightly reinforced are also prone to failure by fracture of the reinforcement, particularly in cases where axial tension can be developed by the foundation system, as reported by Wood (1989).

Even though diagonal tension and compression failure mechanisms can be avoided, a significant reduction in stiffness and a consequent reduction in the energy dissipation capacity of the wall could occur because of sliding shear deformations. The start of the mechanism of sliding shear is illustrated in Figure 2-2(a), as reported by Paulay et al. (1982). At this stage, the shear force is primarily transmitted at the wall base across the uncracked flexural compression zone. Typically, sliding shear deformations are observed after significant flexural yielding has occurred during load reversals and flexural cracks connect to form a continuous horizontal crack along a deteriorated cracked region at or near the base (Pauley et al., 1982), as shown in Fig. 2-2(b). At this point, the wall may rotate as a rigid body and because of the progressive yielding, when the load is reversed, sliding displacement occurs along the horizontal crack. Fig. 2-3(c) illustrates the transmission of flexural compression stresses after yielding of the compression steel, which allows closing of the horizontal crack at the compression end of the wall. Prior to sliding shear failure, shear is transferred primarily by “dowel action because of the significant deterioration of the shear friction mechanism along the plane of the sliding shear deformations.

Sliding shear deformations can be significant for walls with increased shear demand or with low axial compression force, as noted by Pauley et al. (1982). Corley et al. (1981) reported that damage by sliding shear is anticipated in the range of nominal shear stresses from approximately $3\sqrt{f_c'}$ to $7\sqrt{f_c'}$ (psi), where f_c' is the concrete cylinder compression strength in psi. In the same study by Corley et al., it was reported that when the shear stress demand exceeds $7\sqrt{f_c'}$ (psi), the formation of a concrete diagonal strut may preclude the development of a sliding shear failure mechanism.

Barda et al. (1977) investigated the behavior of six cantilever structural wall specimens with shear span-to-length ratios, a/l_w, ranging from 0.25 to 1.0. All the specimens had a flanged cross-section and boundary elements with transverse reinforcement. Two of the specimens were subjected to load reversals, whereas the rest of the tests were conducted under monotonic loading. The specimens were tested under a high level of shear stress, ranging from $8\sqrt{f_c'}$ to $14\sqrt{f_c'}$ (psi). Very limited drift capacities were reported at failure (less than 1.0%), in addition to a significant loss of stiffness and strength after the peak load. Based on the test results it was concluded that horizontal reinforcement was ineffective for shear resistance in walls with shear span-to-length ratios less than 0.5. Vertical reinforcement was found to be mostly effective for walls with shear span-to-length ratios between 0.25 and 0.5 and less effective for walls with a ratio of 1.0. However, the research results clearly indicated that minimum horizontal and vertical web reinforcement should be provided in all walls regardless of their aspect ratio because it results in more evenly distributed cracks with reduced widths. It was also pointed out that a significant portion of shear introduced at the top of the wall is transmitted directly to the foundation by diagonal compression. The authors also reported in the same study that the shear strength of the specimen with a shear aspect ratio of 1.0 was about 20% lower than that of the specimens with smaller aspect ratios (i.e. ratios of 0.25 and 0.5), verifying the advantageous effect of a low wall shear span-to-length ratio on the shear strength of structural walls.

Cardenas et al. (1980) reported on the results of seven rectangular reinforced concrete walls with a shear span-to-length ratio of 1.1 and no special boundary elements. The reinforcing detailing of the specimens is shown in Fig. 2-3. Only one specimen was subjected to cyclic loading, whereas the other walls were tested under monotonic lateral loading. Major parameters in the study were the amount and distribution of the vertical and horizontal reinforcement. It was concluded that both the vertical and horizontal reinforcement contribute to the shear strength of low-rise walls, but their relative effectiveness was not studied further. The authors reported drifts at failure in the range of 0.6% to 1.9% for the wall tested under monotonic loading, whereas the specimen subjected to cyclic loading failed at a drift of approximately 0.5%. An upper limit in the order of $10\sqrt{f_c'}$ (psi) was proposed for the shear strength of low-rise walls. It should be noted that the authors defined the average shear stress based on the effective depth of the section, d, rather than the length of the wall, ℓ, which is used in the 2005 ACI Code.

Synge (1980) and Pauley et al. (1982) addressed the issue of ductility and sliding shear deformations in low-rise walls. The study was based on the response of four walls with a shear span-to-length ratio of 0.6, tested under reversed cyclic loading. The walls had either a rectangular or a flanged cross section and were reinforced with an orthogonal grid of web reinforcement. Bi-diagonal web reinforcement, as shown in Fig. 2-4, was added in two specimens to evaluate its effectiveness in resisting sliding shear. Transverse reinforcement in the wall boundary regions was provided to prevent premature buckling of the longitudinal reinforcement. Maximum shear stresses for the specimens were in the range of $6.2\sqrt{f_c'}$ to $6.8\sqrt{f_c'}$ (psi). It was reported that the rectangular wall specimen reinforced with an orthogonal grid of web reinforcement exhibited a substantial loss of strength in the second cycle to a drift of 0.6%, when sliding deformations became significant (approximately 65% of the applied lateral displacement). In the wall specimen with a flanged section and orthogonal grid of web reinforcement, excessive sliding and loss of stiffness was observed when 0.35% drift was reached, leading to an overall inferior performance in terms of energy dissipation capacity compared with the wall with rectangular cross section. An enhanced response in terms of energy dissipation and

improved control of sliding shear deformations was observed in the specimens where diagonal reinforcement was used. Strength loss was reported in the diagonally reinforced rectangular specimen during the second cycle to a drift of 0.8% while buckling of the diagonal bars was observed at 1.3% drift. The flanged wall specimen with diagonal reinforcement maintained its strength up to a drift of 0.4% and exhibited a more gradual loss of strength compared with the flanged specimen without diagonal reinforcement. Buckling of the diagonal bars in this specimen was reported at a drift of 1.5%.

Wiradinata and Saatcioglu (1986) tested two reinforced concrete walls with rectangular cross-section and a shear span-to-length ratio of 0.3 and 0.6. Fig. 2-5 shows the dimensions of the two specimens. The taller wall reached a peak shear stress of about $7.0\sqrt{f_c'}$ (psi) and failed by diagonal tension at a drift of 1.7%. The specimen with a shear aspect-to-length ratio of 0.3 exhibited a highly pinched hysteretic behavior that was attributed to excessive sliding deformations at the base of the wall, which contributed more than 70% to the lateral displacement at the end of the test. In the specimen with a shear span-to-length ratio of 0.6, even though flexural and shear deformations were both significant throughout the test, shear deformations clearly governed once the wall strength started to degrade. Based on the limited test results, the authors concluded that walls with a shear span-to-length ratio of approximately 0.3 are more susceptible to sliding shear failures compared to more slender walls. It should be noted, however, that even though the shorter wall could not develop its flexural strength prior to a sliding shear failure, the reported drift at failure was surprisingly high (2.6%). No discussion was provided by the authors though. The test results also confirmed the observation made by other researchers that vertical reinforcement is highly effective in resisting shear in squat walls.

Lefas et al. (1990) studied the strength, deformation characteristics and failure mechanism of wall specimens with a shear span-to-length ratio of 1.1 and 2.1. All the specimens had a rectangular cross-section with transverse reinforcement in the boundary elements. In terms of wall strength, the advantageous arching effect with a decreasing

shear aspect ratio was verified by the test results. The walls with a shear span-to-length ratio of 1.1 sustained shear stresses in the range of $8.0\sqrt{f_c'}$ to $12.0\sqrt{f_c'}$ (psi), while maximum shear stresses of $5.0\sqrt{f_c'}$ to $7.7\sqrt{f_c'}$ (psi) were measured in the group of specimens with a shear span-to-length ratio of 2.1. Drifts at failure ranged from about 1.0% to 1.5%, the specimens with a shear span-to-length ratio of 2.1 reaching the larger drifts. All the specimens were reported to fail due a nearly vertical splitting of the compressive zone close to the wall base, with a more extensive failure region for the lower aspect ratio walls and the specimens that were subjected to axial load. The authors discussed the effectiveness of the compression zone as a shear transfer mechanism at the wall base, and concluded that it is associated with the development of triaxial compressive stress conditions near the base of the wall, suggesting that the horizontal web reinforcement and the aggregate interlock did not significantly affect the load-capacity of the walls tested.

Tests on structural walls with a shear span-to-length ratio of 1.2 were reported by Maier (1992). Main parameters in the tests were the wall cross section (rectangular or barbell shape), the effect of boundary elements, and the type of loading (monotonic or cyclic). Based on the test results, it was concluded that an increase in the horizontal reinforcement ratio had a small effect on the wall shear strength, but it was quite beneficial with regards to the specimen deformation capacity.

Salonikios et al. (1999; 2000) reported on tests of low-rise shear walls detailed according to the Eurocode 8 (EC8) provisions. Eleven specimens with a shear span-to-length ratio of either 1.0 or 1.5 were tested under cyclic loading. The walls were reinforced for shear with an orthogonal grid of web reinforcement, while some specimens had cross-inclined bars also. Moderate levels of shear stress were recorded during the tests ($2.5\sqrt{f_c'}$ to $5.5\sqrt{f_c'}$ (psi)) with the more slender walls sustaining an average drift of 1.5% compared with 1.0% in the specimens with a shear span-to-length ratio of 1.0. Even though web shear cracking was the first to be observed, all the specimens failed in a

predominantly flexural mode, characterized by concrete crushing and reinforcement buckling at the confined wall edges. Diagonal cracking of the web and sliding at the wall base were also observed, and the authors suggested that the degree of pinching was controlled by bond-slip and horizontal sliding, rather than by the opening of inclined shear cracks. The test results indicated that sliding shear resistance provided by the diagonal bars led to an increase in the energy dissipation capacity of the walls with a shear span-to-length ratio equal to 1.0. However, the effect of the diagonal reinforcement was less significant for the walls with higher shear span-to-length ratios, particularly when axial compression was present. Furthermore, no improvement in wall drift capacity was observed with the addition of diagonal reinforcement. The authors also suggested that walls with an aspect ratio of 1.5 and with low longitudinal reinforcement ratio in the boundary region (boundary region reinforcing ratio as defined in the ACI Code less than 2.0%) could exhibit a flexural dominated behavior and as a result, the confinement of the boundary region, rather than the shear reinforcement, is the critical design parameter.

Sittipunt et al. (2001) also evaluated the influence of diagonal reinforcement on the hysteretic response of low-rise walls. In total, four barbell shape wall specimens with a shear span-to-length ratio of 1.4 were tested to failure. Two walls contained conventional web vertical and horizontal reinforcement, while the other two specimens were only reinforced with a grid of inclined web reinforcement, as shown in Fig. 2-6. Web crushing was reported in the walls reinforced with the conventional layout of web reinforcement, whereas the diagonal reinforcement changed the failure mode in the other two specimens to crushing of the concrete in the boundary elements. It should be noted that the wall reinforcing details were appropriate for low to moderate seismicity regions and as a result, the transverse reinforcement in the boundary elements was not intended to provide confinement to the concrete core. The behavior of the walls with diagonal reinforcement was quite similar to that reported by Salonikios et al. (1999; 2000), and was characterized by a decrease in the shear distortions at the plastic hinge region compared with the specimens with conventional web reinforcement. However, after yielding of the diagonal reinforcement, the magnitude of shear distortions was comparable in all the specimens with no appreciable effect on deformation capacity. Low-rise walls (shear span-to-length

ratio of 0.75) with diagonal reinforcement were also tested by Choi (2006) under a peak shear stress ranging from $6.1\sqrt{f_c'}$ to $11.3\sqrt{f_c'}$ (psi). Similar conclusions to the study by Sittipunt et al. (2001) were drawn from this study. The beneficial effect of the diagonal reinforcement was also verified by an analytical study reported by Sittipunt and Wood (1995) that showed that diagonal reinforcement provides a mechanism that is more effective in transferring the lateral forces into the foundation, leads to lower shear strains close to the base of the wall, and improves energy dissipation capacity. However, before choosing the use of diagonal reinforcement in the web of walls, the difficulties associated with the placement of the diagonal bars during construction should be considered.

Hidalgo et al. (2002) tested 26 low-rise walls with varying shear span-to-length ratios (ranging from 0.35 to 1.0) under displacement reversals. The walls were designed to exhibit a shear mode of failure in order to investigate the behavior of buildings with walls exhibiting a non-ductile failure mode. The test set-up used in this investigation is shown in Fig. 2-7. The research study indicated that deformation capacity of walls decreases as the shear span-to-length ratio decreases, as reported by other investigators. Diagonal cracking was observed at 0.1% drift, while drifts at failure varied from as low as 0.3% to 1.3%. No significant influence of the amount of distributed reinforcement on drift at first cracking was observed, as expected. On the other hand, the amount of distributed web reinforcement was found to somewhat affect the drift at ultimate. In contrast with observations in other experimental projects, it was reported that the distributed web reinforcement had little or no effect on the maximum shear strength. As noted by the authors, however, the test setup had a significant influence on these observations since these walls were tested under double curvature. It was also suggested that the energy absorption capacity of the specimens was not influenced by the variation of wall aspect ratio.

Lopes (2001[(a)]; 2001[(b)]) reported on the tests of four walls with a shear span-to-length ratio of 1.1. The test set-up is shown in Fig. 2-8 and the main parameters studied were the amount and detailing of the horizontal and confinement reinforcement. The specimens

were tested under high shear stresses ($7.2\sqrt{f_c'}$ to $9.3\sqrt{f_c'}$ (psi)) and exhibited the same drift capacity (approximately 1.0%). No sliding shear failure was reported. Three specimens failed in diagonal tension whereas one specimen (the wall that sustained the higher shear stress) failed by concrete crushing. It was observed that the specimens that failed in shear by diagonal tension achieved their ultimate loads at much lower levels of displacement and had spalling of concrete at earlier stages compared with the specimen that failed by concrete crushing. However, the specimens that failed in diagonal tension exhibited a considerable ability to deform in the post-ultimate range with a moderate drop in strength.

The issue of strength degradation with repeated loading cycles for low-rise walls has not been widely investigated (Gulec et al., 2008). However, test results indicate that walls subjected to load reversals often experience a significant loss of shear strength with repeated cycling for displacements equal to or greater than the displacement corresponding to the peak strength, as expected for all shear-critical elements. Also, a low shear span aspect ratio is expected to have a significantly negative effect on the loss of wall strength and stiffness (Salonikios et al., 1999; Hidalgo et al., 2002; Gulec et al., 2008; 2009).

A summary of tests results from the experimental studies discussed above is presented in Tables 2-1 and 2-2 for specimens with rectangular and barbell (or flanged) section, respectively. It should be mentioned that in the reported tests various types of failure modes were observed. Two important experimental results are presented: 1) the peak shear stress; and 2) the lateral drift at ultimate. The peak shear stress, v_{max}, was calculated by dividing the maximum reported lateral load, F_{max}, by the area bounded by the wall thickness, t_w, and the wall length, l_w, i.e.:

$$v_{max} = \frac{F_{max}}{t_w l_w} \tag{2-1}$$

The peak shear stress is expressed in multiples of $\sqrt{f_c'}$ (psi) to facilitate comparison between the different tests and with available strength equations. The reported concrete cylinder compressive strength was used as the value for f_c'. In cases where the authors reported the cube compressive strength, the cylinder strength was estimated as 80% of the cube strength (Mindess et al., 2003). Drift is defined as the ratio between the lateral displacement at the point of the application of the load and the distance from this point to the base of the wall. A sudden loss of strength or the point at which the load carrying capacity dropped below 80% of the peak strength is taken as the ultimate condition in these tables.

Besides the studies discussed above, several other results from monotonic and cyclic tests on low-rise reinforced concrete structural walls are reported in the literature, but the test set-up, scope of the investigation, test parameters, etc. were not relevant to the low-rise walls tested for this study. For example, Palermo and Vecchio (2000) evaluated the behavior of 3-dimensional flanged low-rise walls and concluded on the beneficial effect of a minimal axial load, 5.4% of f_c', on wall drift capacity. Gupta and Rangan (1998) investigated the experimental behavior of barbell shape walls with a shear aspect ratio of 1.1 constructed with high-strength concrete (f_c' in the range of 9 ksi to 14 ksi). Shake-table tests of low-rise walls have also been reported by Mo and Kuo (1998). Wood (1990), and more recently Gulec et al. (2008; 2009), compiled all the available test results on isolated cantilever low-rise shear walls subjected to lateral load (monotonic or cyclic) in order to study their shear strength. For an extensive list of experimental studies on low-rise shear walls, the reader is referred to these two publications.

2.2.3 Design Philosophy and Review of Seismic Design Provisions for Reinforced Concrete Walls in the 2005 ACI Code

Design criteria for reinforced concrete shear walls were first incorporated in the ACI Committee 318 Building Code in 1971 (ACI Committee 381, 1971). As noted by Cardenas et al. (1973), prior to publication of the 1971 ACI Code the only provisions for

the design of structural walls in the United States were those contained in the 1967 and 1970 Uniform Building Code (UBC 1967; 1970). Limited studies were available at that time and most of the provisions in the early versions of the ACI Code were based on experimental investigations undertaken by the Portland Cement Association (PCA) in the late 1960s, and the subsequent recommendations by Cardenas et al. (1973). These early provisions were basically intended to ensure that the walls possessed adequate shear strength and the emphasis was on the evaluation of flexural and shear strength under monotonic loading.

The 2005 ACI Code design requirements for structural walls located in regions of high seismicity are given in Section 21.9, "Special structural walls and coupling beams" (ACI Committee 318, 2005). The reinforcement in structural walls typically included distributed vertical and horizontal reinforcement spread uniformly over the length and the height of the wall, respectively. Well distributed reinforcement is generally preferred in the walls because it provides cracking control to the diagonal compression strut and improves the conditions for dowel action, which in turn enhances the sliding shear resistance at the base of the wall (Pauley et al., 1982). Concentrated vertical reinforcement is usually placed at the edges of the wall (referred to as the "boundary elements") and is tied with transverse reinforcement. Minimum reinforcing ratios and maximum allowable spacing for the web distributed reinforcement follows the ACI Code provisions for ordinary shear walls (Section 11.9.9 of 2005 ACI Code). The required minimum ratio of horizontal reinforcement area to gross area of the wall is specified as 0.0025. In addition, for low-rise walls (wall height-to-length ratio, h_w/l_w, less than 2.0), it is required that the vertical reinforcing ratio be no less than the horizontal reinforcing ratio, recognizing the observation reported by several researchers that the vertical reinforcement in low-rise walls is more efficient than the horizontal reinforcement in controlling the width and growth of diagonal cracks (Cardenas, 1973; Barda et al., 1977; Wood, 1990; Lefas et al., 1990).

During strong seismic excitations, structural walls will likely undergo inelastic deformations, since it is not practical to design a structural wall to remain elastic during such events (Wallace and Moehle, 1992). But when inelastic deformations are allowed, usually occurring at the wall base, the wall must be specially detailed at those critical regions. Special transverse reinforcement should be provided at the wall edges, when high compression demands (stress and/or strain) are expected, to avoid early concrete crushing and to prevent or delay buckling of the longitudinal reinforcement so that adequate ductility can be achieved. The evaluation for need of "special boundary elements" can be carried out either through a stress-based check or a displacement-based approach.

Prior to 1994, strength requirements were primarily governing the design of reinforced concrete structural walls in the U.S. code provisions, for example, the 1989 ACI Code (ACI Committee 318, 1989) and the 1991 UBC Code (UBC, 1991). As a result, the stress-based approach for evaluating the need for special boundary elements was used in the 1989 ACI Code and the 1991 UBC Code (Thomsen and Wallace, 2004). The required deformability was achieved through the use of heavily confined boundary elements when the extreme fiber stress due to combined axial and lateral loads exceeded $0.2f_c'$ psi. This evaluation was performed using a linear elastic analysis with element stiffness values based on gross concrete cross-sectional dimensions. It was also required to continue the special transverse reinforcement at the wall boundaries up to the wall height at which the computed stress was less than $0.15f_c'$ (Wallace and Orakcal, 2002; Thomsen and Wallace, 2004).

A displacement-based design methodology for shear walls was proposed in the early 1990s (Moehle and Wallace, 1989; 1994, Wallace and Moehle, 1992) and presented an alternative and less conservative design for the boundary regions of shear walls compared with the "stress-based" approach. Based on these studies, new provisions for evaluating the need for special detailing requirements using a "displacement-based" approach were first incorporated in the 1994 UBC Code and later in the 1999 ACI Code (ACI

Committee 318, 1999). Using the displacement-based approach, the need for boundary elements is evaluated based on the maximum strain demand calculated from an estimated plastic hinge rotation (or drift) demand. Section 21.9.6.2 of the 2005 ACI Code (ACI Committee 318, 2005) requires that structural walls be detailed with special boundary elements when:

$$c \geq \frac{l_w}{600(\delta_u/h_w)} \tag{2-2}$$

where c is the neutral axis depth, δ_u is the design lateral displacement and δ_u/h_w should not be less than 0.007. The 2005 ACI Code also states that the "boundary elements should extend horizontally from the extreme compression fiber a distance not less than the larger of $(c - 0.1l_w)$ and $c/2$". For flanged wall sections, it is also required that the boundary element be extended at least 12 in. into the web.

Eq. (2-2) was developed assuming that special detailing should be provided when the compression strain at the extreme fiber exceeds a limiting value of 0.004 (Wallace and Orakcal, 2002). The wall height over which confinement should extend, specified as the larger of l_w and $M_u/4V_u$, (where M_u and V_u refer to the factored moment and shear force at the critical wall section, respectively) is based on a conservative estimate of the plastic hinge length for structural walls (Paulay, 1986; Wallace, 1994). The stress-based approach is still maintained in the 2005 ACI Code (ACI Committee 318, 2005), mainly to address configurations where the displacement approach is not appropriate (for example perforated walls or walls with setbacks) (Wallace and Orakcal, 2002). It can also be argued that the check for boundary elements in walls highly dominated by shear, such as walls with very low shear span-to-length ratios, should be based on the stress check, because in such cases the assumption of plane sections remaining plane after loading is not valid (Wallace, 1995[(b)]). In slender walls, particular attention to the confinement reinforcement is required for asymmetrical walls or walls with high levels of axial stress, but generally the "displacement-based" approach is less stringent for evaluating the need

for special transverse reinforcement when compared to the "stress-based" approach (Wallace and Moehle, 1989; Wallace, 1995[(a)]).

When special boundary elements are required in structural walls, the confining reinforcement should not be less than (Section 21.9.6.4 of the 2005 ACI Code):

$$A_{sh} = 0.09 s b_c \, f_c' / f_{yt} \tag{2-3}$$

where A_{sh} is the total cross-sectional area of the confinement reinforcement perpendicular to b_c , s is the transverse spacing of the confinement reinforcement, b_c is the concrete core dimension perpendicular to the tie legs that constitute A_{sh}, and f_{yt} is the specified yield strength of the confinement reinforcement. In addition, the spacing, s, should not exceed: (a) one-quarter of the minimum member dimension, (b) six times the diameter of the smallest longitudinal bar, and (c) the quantity s_o, defined as follows:

$$s_o = 4 + \left(\frac{14 - h_x}{3}\right) \geq 4 \text{ (in.)} \tag{2-4}$$

where, h_x is taken as the largest centerline to centerline distance between tie legs used in the boundary elements.

The requirements for the flexural and axial load strength of walls are contained in Section 21.6.5.1 of the 2005 ACI Code (ACI Committee 318, 2005). A strain-compatibility analysis assuming plane sections (linear strain distribution) is allowed to be used to assess flexural strength. Before the 1999 edition of the ACI Code, the web vertical reinforcement contribution to the wall flexural strength was neglected and the boundary elements were required to resist the full overturning moment and axial load. The application of this requirement resulted in flexural overstrength of the wall, with important implications on wall shear demand and the forces in the foundations. However, based on the 2005 edition of the ACI Code, reinforcement in the boundary elements and the web of the wall should be included in the strength calculations.

It should be noted that the provisions of the 2005 ACI Code for “Special structural walls” are basically the same as in the latest edition of the code published in 2008 ((ACI Committee 318, 2008). The only change in the 2008 edition of the code was with respect to the 2005 provision that the spacing of the confinement reinforcement in the boundary elements should not exceed one-quarter of the minimum member dimension. In the 2008 ACI Code, one-third of the minimum member dimension is allowed as maximum spacing.

2.2.4 Estimation of Shear Strength of Low-Rise Reinforced Concrete Structural Walls

Equations for the estimation of maximum shear strength of reinforced concrete shear walls can be found in building codes and the literature in general. A number of parameters have been found to affect the wall strength, such as wall aspect ratio, vertical and horizontal web reinforcement ratio, concrete strength, and applied axial force (Gulec et al., 2008; 2009). Some of these expressions are discussed next. The reader should be aware, however, of the significant scatter observed when comparing predicted resuls for the shear strength (Wood, 1990, Gulec et al 2008; 2009).

2.2.4.1 2005 ACI Code and Eurocode EC8

The 2005 ACI Code (ACI Committee 318, 2005), which is widely used in earthquake-prone regions, provides two sets of equations to determine the nominal shear strength of walls. The same equations are given in the 2008 edition of the ACI Code. One equation is given in Section 21.7 (Special reinforced concrete structural walls and coupling beams) and is indented to be used for seismic design. The second equation is used for general design and is given in Section 11.10 (Special provisions for walls). Both equations are semi-empirical and are based on the widely used modified truss analogy (Cardenas, 1973; Wood, 1990). Based on the modified truss analogy, the nominal shear strength of structural walls (V_n) is attributed to the contribution of the steel reinforcement (V_s) and the contribution of the “concrete” (V_c). The concrete contribution consists of the shear

carried in the compression zone, dowel action and aggregate interlock, whereas steel contribution refers to shear carried by horizontal web reinforcement through a truss action.

The nominal shear strength expression for concrete walls in Section 21.7 of the 2005 ACI Code (also the same in 2008 ACI Code) has the following form, in U.S. customary units:

$$V_n = \left(a_c\sqrt{f_c'} + \rho_h f_y\right)A_w \leq 10\sqrt{f_c'}A_w \tag{2-5}$$

where a_c is an aspect ratio coefficient that varies linearly from 3.0 (psi units) for walls with wall height-to-length ratio, h_w/l_w, less than 1.5, to 2.0 for walls with a ratio greater than 2.0, f_c' is the compressive strength of the concrete (psi units), ρ_h is the horizontal web reinforcement ratio, f_y is the yield strength of the horizontal reinforcement (psi units), and A_w is the area of the wall bounded by the wall thickness and the wall length (in^2 units). Eq. (2-5) clearly recognizes the higher shear strength in walls with low height-to-length ratio by specifying a concrete contribution of $3\sqrt{f_c'}$ (psi) for height-to-length ratios less that 1.5, reducing it to $2\sqrt{f_c'}$ (psi) for ratios greater than 2.0. This provision accounts indirectly for the beneficial effect of resisting part of the shear through a direct diagonal compression strut for short walls (Salonikios et al., 1999). Also, recognizing that web crushing is a potential limit on the capacity of structural walls, an upper limit of $10\sqrt{f_c'}$ (psi) is imposed on the wall shear stress. This limit is based mainly recommendations by Cardenas et al. (1973), but tests by Oesterle et al. (1984) indicated that this limit may not eliminate web crushing as a possible failure mode for walls subjected to extremely large inelastic deformations, especially for walls with concrete compressive strength lower than 5000 psi and subjected to low axial stresses.

The nominal shear strength equations for walls constructed with normal weight concrete, as given in Section 11.10 of the 2008 ACI Code (non-seismic design), is described below in U.S. customary units:

$$V_n = V_c + V_s \leq 10\sqrt{f_c'}t_w d_1 \tag{2-6}$$

$$V_c = 3.3\sqrt{f_c'}t_w d_1 + \frac{N_u d_1}{4l_w} \tag{2-7}$$

$$V_c = \left[0.6\sqrt{f_c'} + \frac{l_w\left(1.25\sqrt{f_c'} + \frac{0.2N_u}{l_w t_w}\right)}{\frac{M_u}{V_u} - \frac{l_w}{2}}\right] t_w d_1 \tag{2-8}$$

$$V_s = \frac{A_v f_y d_1}{s} \tag{2-9}$$

where t_w is the wall thickness (in.), d_1 is the effective depth which can be assumed equal to $0.8l_w$ (in.), N_u is the axial load which is negative in tension (lbs), M_u is the factored moment at the section under consideration (lbs-in.), A_v is the area of the horizontal reinforcement within a distance s (in.^{2}) and s is the spacing of the wall horizontal reinforcement (in.). The contribution of the concrete is taken as the lesser of the values provided by Eqs. (2-7) and (2-8). The first equation for the concrete contribution (Eq. 2-7) was derived for web-shear cracking and mostly applies to low-rise shear walls (Cardenas et al., 1973), whereas the second equation (Eq. 2-8) corresponds to flexural-shear cracking. It should be also mentioned that Eq. (2-8) does not apply when:

$$\frac{M_u}{V_u} - \frac{l_w}{2} \leq 0 \tag{2-10}$$

The provisions in the current Eurocode EC8 (CEN Technical Committee 250/SC8) for the estimation of the shear strength of shear walls are more complicated compared with those in Section 21.7 of ACI Code. Eurocode 8 provides separate equations for the shear resistance of structural walls subjected to seismic loading, based on the different possible failure modes, namely diagonal tension, diagonal compression (including web crushing), and sliding shear. Similarly to the ACI Code provisions, the equation for diagonal tension resistance is based on the modified truss analogy. But in contrast to the ACI provisions, Eurocode 8 provisions do not account for any increase in concrete contribution in walls

with low aspect ratio. In addition, the contribution to shear strength from web reinforcement in Eurocode 8 is estimated on the basis of the moment-to-shear ratio a_s $\left(a_s = {M_u}/{V_u l_w}\right)$. The design equation recommended in Eurocode 8 implies that for $a_s \geq 1.3$, only horizontal reinforcement contributes to shear strength, whereas for $a_s \leq 0.3$, only the vertical reinforcement resists shear; both types of reinforcement are considered effective for intermediate values.

Another important difference between American and European practice concerns the possibility of sliding shear failure of low-rise walls, which is recognized in the Eurocode 8 and a corresponding design procedure is suggested. The resistance of walls against sliding shear, according to Eurocode 8, is assumed to be made up of contributions from dowel action of vertical bars, shear resistance of cross-inclined bars, and frictional resistance. The possibility of sliding shear failure is not explicitly accounted for in the ACI Code. However, it is believed to be indirectly addressed by the upper limit to the nominal shear stress of $10\sqrt{f_c'}$ (psi) (Salonikios et al., 1999). It is worth pointing out that the equations concerning wall shear resistance against sliding shear currently specified in the Eurocode 8 provisions are quite complex and mostly semi-empirical, and were developed using the recommendations by Pauley et al. (1982).

2.2.4.2 Wood (1990)

Wood (1990) made an extensive investigation in order to collect, compile and evaluate test data of low-rise concrete walls subjected to lateral loads. The investigation focused on laboratory tests of one- and two-story isolated reinforced concrete walls (rectangular, barbell or flanged) with shear span-to-length ratios less than 2.0. The selected specimens were tested under either lateral monotonic loading or lateral load reversals. The compiled data showed a significant scatter with regards to the reported maximum average shear stress for low-rise walls, but a trend of increasing maximum average shear stress with an increase in the product $\varrho_h f_y$ (where ϱ_h is the horizontal web reinforcement ratio) was

verified. Specimen size did not seem to affect shear strength for the sizes considered while the loading scheme was found to have a negligible influence. Wood (1990) pointed out that the modified truss analogy appeared to overestimate the rate of increase of shear strength attributable to the web reinforcement in low-rise walls and as a result, the 1983 ACI Code (ACI Committee 318, 1983) equations for shear tended to underestimate the nominal shear strength of lightly reinforced walls and to overestimate the strength walls with more than 1.5 times the minimum web reinforcement ratio of 0.25%. A lower bound of $6\sqrt{f_c'}$ (psi) was recommended for the shear strength of low-rise walls with minimum distributed web reinforcement ratios, which seemed independent of web reinforcement ratio. In the same study, it was proposed that an increase in the shear strength beyond this lower bound could be attributed to the contribution of the vertical reinforcement (longitudinal reinforcement in the boundary elements and web vertical reinforcement), which can be approximated using a friction model. The shear stress upper limit of $10\sqrt{f_c'}$ (psi) in the ACI Code, and also suggested by several researchers (for example Cardenas et al., 1973), was considered to be reasonable. In summary, the work by Wood (1990) resulted in the following equation for predicting the shear strength of low-rise walls in U.S. customary units:

$$6\sqrt{f_c'}A_w \leq V_n \leq \frac{A_{vf}f_y}{4} \leq 10\sqrt{f_c'}A_w \tag{2-11}$$

where A_{vf} is the area of total vertical reinforcement (sum of web and boundary element reinforcement) crossing the shear plane (in.^{2}) and f_y is the reinforcement yield stress for the combination of vertical web and boundary element reinforcement (psi units).

2.2.4.3 Barda et al. (1977)

Barda et al. (1977) proposed an equation for the prediction of the shear strength of low-rise walls, based on test results and the use of the truss analogy. An alternate formulation for the “concrete” contribution to shear strength was recommended because the ACI Code provisions that were in effect at the time (ACI Committee 318, 1971) were found to be quite conservative. The proposed equation is as follows, in U.S. customary units:

$$V_n = \left(8\sqrt{f_c'} - 2.5\sqrt{f_c'}\frac{h_w}{l_w} + \frac{N_u}{4l_w t_w} + \rho_v f_{yv}\right) t_w d_2 \quad (2\text{-}12)$$

where ρ_v is the vertical web reinforcement ratio, f_{yv} is the yield stress of the vertical web reinforcement (psi units), and d_2 is the distance from the extreme compression fiber to centroid of wall vertical reinforcement in tension (in.). No upper limit for the shear strength was proposed in the study.

2.2.4.4 Comments on the Design Equations for Shear Strength of RC Low-Rise Walls

Recently, Gulec et al. (2008; 2009) compiled most of the existing tests results for low-rise walls with rectangular cross section as well as with boundary barbells or flanges and reported on the adequacy of several equations for predicting wall shear strength. The investigation led to the conclusion that the equation proposed by Wood (1990) gave the best prediction of the peak shear strength of rectangular low-rise walls and in most cases, the proposed lower limit of $6\sqrt{f_c'}$ (psi) governed the shear strength. The procedure of Barda et al. (1977) discussed above was found to overestimate the peak shear strength of rectangular walls and the authors recommended that it should not be used in walls with rectangular cross section. On the other hand, in walls with boundary elements (barbells or flanges), even though Wood's equation gave generally quite conservative results, the equation of Barda et al. led to reasonable estimates of the peak shear strength, especially for heavily reinforced walls. Gulec et al. (2009) also commented on the significant scatter of the peak shear strength predicted using different equations and on the lack of procedures that consider the influence of the barbell or flange area on the shear resistance, as well as the effect of out-of-plane loading.

With regards to the Eurocode 8 provisions, based on the experimental investigation conducted by Salonikios et al. (1999; 2000), it was demonstrated that the calculated sliding shear capacity of low-rise walls, based on the equations in Eurocode 8, significantly underestimated the measured maximum shear. Salonikios et al. (2000) also concluded that the Eurocode 8 estimation for shear resistance corresponding to diagonal

tension failure tends to be more conservative than the equation in the 1999 ACI Code (ACI Committee 318, 1999), which is the same equation as in the 2005 and 2008 ACI Code.

2.3 BEHAVIOR AND STRUCTURAL APPLICATIONS OF HIGH PERFORMANCE FIBER REINFORCED CONCRETE (HPFRC)

2.3.1 Overview and General Characteristics of HPFRC

Fiber reinforced cementitious composites (FRCCs) consist of concrete or mortar reinforced with discontinuous fibers, which provide post-cracking tensile resistance. The beneficial effects of the addition of discontinuous fibers to the concrete or mortar have been realized by engineers since the turn of the last century, but this technology was not extensively developed until the early 1960s (Naaman, 1985). Several fiber materials and cross sectional shapes have been used with different results, including steel (flat, crimped, hooked, twisted), polypropylene (PP), polyvinyl alcohol (PVA), glass, and carbon fibers. Since the 1990s, production of higher strength fiber reinforced concrete, use of polymers that enhance the fiber-mortar interaction, and development of polymer-based and high strength steel fibers, are just some of the technological improvements in the field of fiber reinforced concrete.

High-Performance Fiber Reinforced Cementitious Composites (HPFRCCs) and High-Performance Fiber Reinforced Concrete (HPFRC) are a special category of Fiber Reinforced Cementitious Composites (FRCCs) and are defined as those that develop a pseudo strain-hardening behavior in tension (Naaman and Reinhardt, 1996). In this report, the term HPFRC will be used to describe both materials for simplicity. However, a distinction will be made in cases where no coarse aggregate (i.e. mortar mixture) was used in the HPFRC mixture.

Nowadays, a pseudo strain-hardening behavior in tension can be achieved with the use of relatively low volume fraction of fibers, typically lower than 2.0% (Parra, 2005).

Multiple cracking and high energy absorption capacity are typically observed with this pseudo strain-hardening behavior. A qualitative stress-strain behavior of an HPFRC material is illustrated in Fig. 2-9 (Naaman, 1998). It should be mentioned that not all fiber types can lead to this high-performance behavior, and the fiber content required to achieve strain-hardening behavior highly depends on the fibers, matrix properties and fiber-matrix interaction. Steel fibers (hooked and twisted) and ultra-high molecular-weight polyethylene (Spectra) fibers have been used to develop HPFRC materials with successful applications in earthquake-resistant structures (Parra, 2005). Factors that have been reported to affect the tensile and compression response of FRCC and HPFRC materials include fiber volume fraction, fiber material and geometry, cementitious matrix composition, average bond strength versus slip response along the fiber-matrix interface, and distribution of fibers in the mix (Naaman, 1998).

The compressive stress-strain properties of FRCC and HPFRC materials with various types of fibers have been extensively studied (for example Shah and Rangan, 1971; Shah and Naaman, 1976; Shah et al., 1978). In those investigations, it was found that the compressive strength of the mortar or concrete is not appreciably improved by the addition of fibers, unless a high volume of fibers is used. However, a significant enhancement in compression ductility is possible, especially in the case of HPFRC, which can sustain large compression strains with no material spalling because the fibers can resist the lateral expansion and preserve the concrete integrity. In tension, the response of HPFRC is characterized by a nearly linear behavior up to first cracking, followed by a pseudo-strain hardening region up to the strain at which crack saturation damage localization) occurs, typically observed at strains in the range of 2.0% to 5.0% (Naaman and Reinhardt, 1996). Overall, the superior ductile tensile performance of HPFRC materials leads to a multiple cracking pattern, with smaller crack widths and generally superior damage tolerance in structural elements.

2.3.2 Shear Strength of Fiber Reinforced Cementitious Composite (FRCC) Members

It can be argued that the parameters that influence the shear resistance of FRCC members include those that affect the shear strength of conventional reinforced concrete members, with the additional significant contribution from the post-cracking tensile strength of the FRCC material (Khuntia et al., 1999). However, little is known about the interaction between the shear resistance provided by the fibers and that provided by the concrete and the steel reinforcement (Chompreda and Parra, 2005). As a result, the development of expressions that predict the ultimate shear strength of FRCC members, either through analytical work or experimental investigations, is quite challenging. Most of the studies available refer to the shear behavior of FRCC beams and provide semi-empirical strength equations that are mainly applicable to slender beams under monotonic loading (for example Ashour et al., 1992; Li et al., 1992; Mansur et al., 1986; Narayanan and Darwish, 1987; Sharma, 1986). Little is therefore known about the shear strength FRCC and HPFRC members subjected to displacement reversals.

A common approach in many predictive equations for the shear strength of FRCC beams is based on the idea of the modified "truss model" that is used in conventional reinforced concrete members for shear strength predictions, but including an additional independent term for the contribution of the fibers, v_f. As a result, an equation of this general form is as follows:

$$v_n = v_c + v_S + v_f \tag{2-13}$$

The contribution on the fibers in many equations is dependant, among others, on the fiber volume fraction and aspect ratio, the beam aspect ratio, and the anchorage conditions for the fibers (Kwak et al., 2002). Narayanan and Darwish (1988) reported that the beneficial effect of arch action that is present in deep members, and usually reflected in the "V_c" term, improves noticeably with the inclusion of steel fibers, which control the growth of splitting cracks.

Narayanan and Darwish (1987), based on tests of FRCC beams with no stirrups, proposed the following equation for the contribution of the fibers and the concrete, in MPa:

$$v_{frc} = v_c + v_f = 2.8\frac{d}{a}\left(0.24f'_{sp} + 80\rho_{st}\frac{d}{a}\right) + 0.41\tau F_1 \text{ for } a/d < 2.8 \quad (2\text{-}14)$$

where a is the shear span length (mm), d is the beam effective depth (mm), f'_{sp} is the split cylinder strength of the FRCC (MPa), ρ_{st} is tensile reinforcement ratio, τ is the fiber-matrix interfacial bond stress, and F_1 is a fiber factor defined as:

$$F_1 = \beta V_f \frac{l_f}{d_f} \quad (2\text{-}15)$$

where β is a bond factor that accounts for the shape and surface characteristic of the fiber, V_f is the fiber volume fraction (%), l_f is the fiber length (mm), and d_f is the diameter of the fiber (mm). In this equation, the contribution of the "concrete", v_c, is assumed dependant on the split-cylinder strength of the FRCC, while one of the most significant parameters in evaluating the fiber contribution is the fiber-matrix interface bond. It should be noted, however, that this quantity is very difficult to estimate (Khuntia et al., 1999), which poses severe limitations on the applicability of this type of design equation.

Khuntia et al. (1999) proposed a simple equation for the shear strength of FRCC members without transverse reinforcement subjected to monotonic loading, which can be applied to both slender and deep beams, in MPa:

$$v_{frc} = v_c + v_f = (0.167\alpha + 0.25F_1)\sqrt{f'_c} \quad (2\text{-}16)$$

where f'_c is the cylinder compressive strength of FRCC (MPa) and α is defined as:

$$\alpha = \begin{Bmatrix} 2.5\frac{a}{d} \leq 3 \text{ for } \frac{a}{d} < 2.5 \\ 1 \text{ for } \frac{a}{d} \geq 2.5 \end{Bmatrix} \qquad (2\text{-}17)$$

It should be mentioned that Eq. (2-16) was developed by collecting data from several research projects that focused on the use of straight, crimped, and hooked steel fibers. The equation is quite conservative and assumes correlation between the post-cracking strength, σ_{pc}, and compressive strength ($\sigma_{pc} = 0.41F_1\tau$), which may not be adequate for some types of fibers. In addition, it assumes $\tau = 0.68\sqrt{f_c'}$ (MPa).

The above mentioned equations assume a somewhat independent contribution of the concrete and the fibers. A different approach could be based on the Modified Compression Field Theory (Vecchio and Collins, 1986), which relates the "V_c" term in reinforced concrete beams to the tensile stress carried by the concrete in between the cracks. It could be argued, therefore, that the contributions from the concrete and the fibers are related and may be lumped into a single term. However, this possibility requires further investigation.

2.3.3 Application of HPFRC in Shear-Critical Elements Subjected to Displacement Reversals

The ductile behavior of HPRFC, characterized by multiple cracking, high energy absorption, and superior deformation capacity, has led researchers to explore the application of HPFRC in earthquake-resistant structures. In such structures, the behavior is mainly controlled by the regions where the inelastic activity occurs and therefore, the use of HPFRC in those critical regions is very attractive because the superior deformation capacity and damage tolerance of HPFRC can significantly enhance structural behavior, while allowing for simplifications in reinforcement detailing. Experimental studies have verified that the addition of fibers to the cementitious matrix has favorable effects in terms of shear strength, shear deformation capacity, and stiffness retention, especially for

shear-critical reinforced concrete elements subjected to cyclic loading when compared with the response of traditionally reinforced concrete members (Parra, 2003). Applications of HPFRC in shear-critical elements include column-beam connections, plastic hinges in flexural members under high shear, structural walls, coupling beams, precast concrete frame conections, and precast infill panels for seismic retrofit of buildings. Most of the investigations on the application of HPFRC in earthquake-resistant structures have been conducted at the University of Michigan and a brief discussion of some of these experimental investigations is reviewed in the following paragraphs.

The use of FRCCs with hooked-end steel fibers in reinforced concrete coupling beams was investigated by Wight and Erki (1995). The experimental results indicated that the use of an FRCC material with 1.5% volume fraction of hooked steel fibers in diagonally reinforced coupling beams, where the confinement around the diagonal bars was eliminated, exhibited a superior performance to diagonally reinforced coupling beams with standard detailing. Canbolat et al. (2005) further investigated the behavior of HPFRC (mortar mixture) diagonally reinforced beams and verified that a simplification in the reinforcement detailing is possible in coupling beams. Fig. 2-10 shows the reinforcing detailing of the four coupling beam specimens of the study by Canbolat et al. (2005). Specimen 1 was designed according to the seismic provisions of the ACI Code and constructed with regular concrete, whereas the other three specimens were constructed with an HPFRC material. In this study, it was found that the use of HPFRC may result in the elimination of transverse reinforcement around diagonal bars since the HPFRC material can provide adequate confinement to prevent the buckling of those bars. Specimens with either 2% volume fraction of ultra-high molecular weight polyethylene (Spectra) fibers or 1.5% volume fraction of steel Torex (twisted) fibers exhibited enhanced performance compared to that of well detailed coupling beams. Both HPFRC coupling beams exhibited substantially higher shear strength and energy dissipation capacity with a superior damage tolerance, characterized by less concrete spalling and a dense network of microcracks up to damage localization. Even after a fiber pullout had occurred due to diagonal tension, the HPFRC material was able to provide confinement to the diagonal bars.

An attractive application for FRCCs and HPFRC is in connections between beams and columns in reinforced concrete frame structures, where the required reinforcement detailing leads to significant reinforcement congestion in the joint region. Henager (1977) investigated the behavior of a beam-column connection, constructed with an FRC with a 1.7% volume fraction of steel fibers, where all the column stirrups in the joint region were eliminated. An increase in strength, stiffness and damage tolerance was reported for the FRCC joint, compared with the behavior of a control specimen detailed according to the 1971 ACI Code (ACI Committee 318, 1971). The results were further verified by later experimental studies conducted by Craig et al. (1984) and Filiatrault et al. (1994; 1995). Parra and Wight (2000) also demonstrated the possibility for reduction and even elimination of the transverse reinforcement in RC Column-to-Steel Beam (RCS) connections while increasing bearing strength with the use of an HPFRC material (Engineered Cementitious Composite – ECC [Li, 1993]) with a 1.5% volume fraction of ultrahigh molecular weight polyethylene (Spectra) fibers. A peak shear distortion of about 2.0% was reported for the HPFRC connection, with only minor damage, as well as an enhancement in strength in comparison with a standard RCS connection tested for comparison purposes.

Besides the use of HPFRC material in shear-dominated members, Parra and Chompreda (2007) investigated the use of HPFRC (mortar mixture) in the plastic hinge region of beams subjected to shear reversals. The goal was to study the shear strength decay and a potential reduction in transverse reinforcement requirements in HPFRC flexural members under inelastic displacement reversals. The beam specimens were constructed with an HPFRC (mortar) that contained either Spectra or hooked steel fibers in volume fractions of 1.5% and 2.0%, respectively. The results showed a very promising application for HPFRC, since all the specimens exhibited a stable hysteretic response at drifts exceeding 4.0%. At this drift level, only hairline crack formation was visible in the beam plastic hinge region, except for the beam-column interface, and no buckling of the longitudinal bars was observed, indication that the HPFRC can provide significant confinement to the bars, even when no transverse reinforcement was used. An important general conclusion

from the study was that a shear strength of $3.5\sqrt{f_c'}$ (psi) represented a lower limit for the shear resistance of HPFRC members, regardless of the rotation demand.

2.3.4 Application of FRCC Materials in Structural Walls

Kim and Parra (2003) investigated the hysteretic response of low-rise walls constructed with an HPFRC material (mortar mixture) containing either steel or Spectra fibers in a 2.0% and 1.5% volume fraction, respectively. Two low-rise walls with a shear span to-wall length ratio of 1.5 were tested under reversed cyclic displacements. Web vertical and horizontal distributed reinforcing ratios were less than the minimum reinforcing ratio of 0.25% specified in the ACI Code and equal to 0.21% and 0.13%, respectively. In addition, no special transverse reinforcement was used in the wall boundary regions. The wall specimens exhibited only moderate damage at 1.5% drift and a drift capacity of approximately 2.0%. Hysteresis loops were stable up to a maximum shear deformation of approximately 2.0%. Multiple cracking was observed with crack widths less than 2 mm up to 1.5% drift. Further, no instability was observed in the wall edges, despite the lack of special confining reinforcement and the high compressive stresses developed. It was also estimated that about 80% of the wall diagonal tension capacity was attributed to the fibers. The results of the tests performed by Kim and Parra (2003) showed the potential for a new simplified design for low-rise structural walls that can lead to enhanced displacement capacity and damage tolerance while allowing for a relaxation of wall web and confinement reinforcement requirements. These tests served as a pilot study for the investigation presented in this report. Further details with analysis of test results are provided in Chapters 4 and 5.

A study of the behavior of slender structural walls constructed with FRCC material was conducted by Parra et al. (2006). The main goal of the study was to eliminate the confinement reinforcement in the special boundary regions of the walls through the use of FRCC in the wall plastic hinge region. One wall was designed according to the seismic provisions of the 2002 ACI Code (ACI Committee 318, 2002), whereas three specimens were constructed with FRCC in the plastic hinge region. The FRCCs evaluated contained

steel fibers in either a 1.5% or 2.0% volume fraction. Even though special confinement was not used in the boundary regions of the FRC walls, the drift capacity of the specimens ranged from 2.5% to 3.0%. A wall specimen with 2.0% volume fraction of hooked steel fibers (HPFRC mortar material) exhibited superior damage tolerance, no instability of the boundary regions, and failed due to fracture of the main longitudinal reinforcement at 3.5% drift. The test results indicated that all the FRC walls had a flexure-dominated response, as opposed to the RC specimen, which exhibited significant shear-related damage at the end of the test. This RC wall, designed according to Chapter 21 of the 2002 ACI Code, behaved well when subjected to cycles up to 3.5% drift, despite the substantial shear related damage during the later loading cycles.

Buzzini et al. (2006) reported on three tests of structural walls constructed with Hybrid Fiber Concrete (HFC). HFC refers to a high-strength HPFRC with self-compacting properties that contains a mix of fibers of different shapes (straight, crimped and hooked) and of various lengths that are added to a mortar in volume fractions ranging from 1% to 4% (Markovic et al., 2003; 2004). Buzzini et al. (2006) investigated the behavior of two slender walls with a rectangular cross-section and a shear span-to-wall length ratio of 2.8. An additional wall with a barbell shape and a shear span-to-wall length ratio of 1.9 was also tested. All the walls had the same amount of flexural reinforcement and web vertical reinforcement, but neither horizontal web reinforcement nor transverse reinforcement in the boundary regions was provided, such as to evaluate the efficiency of the fibers to provide shear resistance and confinement. A cold joint existed in all the specimens between the wall and the foundation and sliding shear deformations significantly influenced the hysteretic behavior of the specimens. The authors suggested placing sleeves in the longitudinal bars close to the footing so as to prevent bond between the longitudinal bars and the concrete and spread the yielding of the longitudinal bars over a larger region. All the specimens showed a stable hysteretic behavior, with a drift capacity ranging from 3.2% to 4.0%. Minimum concrete spalling was reported at failure, which occurred due to fracture of the longitudinal reinforcement. Overall, a superior serviceability and adequate inelastic deformation capacity was reported for all the specimens when compared to conventional reinforced concrete structural walls. It should

be noted, however, that in these tests, the applied shear stress level was low and ranged from $1.8\sqrt{f_c'}$ to $3.0\sqrt{f_c'}$ (psi).

2.4 SUMMARY

The design of reinforced concrete structural walls to sustain the deformation demands imposed by strong ground motions requires the use of special reinforcement details to ensure adequate inelastic displacement capacity. These reinforcement requirements consist of a grid of vertical and horizontal web reinforcement and special confining reinforcement in the wall boundary elements. Construction difficulties and reinforcement congestion are usually associated with this detailing. Even though the desired level of shear strength can be achieved with the current design philosophy, there is evidence that low-rise walls posses limited displacement and energy dissipation capacity. Furthermore, no comprehensive information is available on the relation between wall drift capacity and shear stress demand. Researchers have proposed the use of diagonal reinforcement in the web of the wall to enhance overall behavior, as well as resistance against sliding shear. However, before choosing the use of inclined reinforcement on the web of walls, the difficulties associated with the placement of the diagonal bars during construction should be considered.

A potential simplified reinforcement detailing, consisting of relaxed requirements for the wall distributed reinforcement and partial or even total elimination of the confinement reinforcement in the boundary regions can potentially be achieved through the use of randomly oriented fiber reinforcement. Results from prior research have shown that the use of strain-hardening fiber reinforced cement composites in shear-critical elements (coupling beams, beam-column connections, and shear walls) can enhance their performance in terms of deformation capacity and damage tolerance. Experimental research has also shown that fiber reinforcement can be used to partially replace confinement and shear reinforcement, without any compromise in terms of strength and ductility.

Prior to this research, very limited information was available on the behavior of low-rise walls constructed with High-Performance Fiber Reinforced Concrete (HPFRC). Thus, a comprehensive experimental research program was undertaken with the goal of generating required information in order to understand the hysteretic behavior of HPFRC low-rise walls and propose an alternative simplified design for these walls when used in regions of high seismicity. The results of this study will also help to better understand the seismic behavior of RC and HPFRC low-rise walls and the influence of several parameters, most importantly wall aspect ratio and shear stress demand, on wall behavior.

CHAPTER 3

EXPERIMENTAL PROGRAM

3.1 INTRODUCTION

The purpose of this research program was to investigate the inelastic behavior of High-Performance Fiber Reinforced Concrete (HPFRC) low-rise structural walls, with emphasis on their displacement capacity, shear behavior and damage tolerance. As described in Section 2.2.4, two HPFRC low-rise walls were tested under large displacement reversals in a previous study conducted by Kim and Parra (2003). The reported results showed great potential, through the use of HPRC materials, for a significant reduction in the confining reinforcement in the wall boundary regions, as well as a relaxation in distributed web reinforcement. In this investigation, seven low-rise walls constructed with either HPFRC or conventional reinforced concrete were tested to further evaluate the application of HPFRC materials in low-rise structural walls, which could result in an simplified reinforcement detailing without compromising seismic performance.

Based on past experimental investigations, discussed in Section 2.1.2, several parameters have been found to affect the behavior of reinforced concrete low-rise walls, including wall configuration, aspect ratio, amount and layout of web reinforcement, shear stress level, and axial load. The series of tests conducted in this research project were designed to study the influence of the following factors on the seismic response of reinforced concrete and HPFRC low-rise walls:

- average shear stress level;
- wall aspect ratio;
- web reinforcement ratio;
- tension reinforcement ratio;
- use of fiber reinforced concrete versus fiber reinforced mortar; and
- use of dowel reinforcement at the base of the wall.

In the following sections, a detailed description of the tests conducted, including the materials used, specimen geometry and design, and test set up and instrumentation, is presented. Details of the specimens tested by Kim and Parra (2003) are also given because the results from these tests are compared with those of a companion RC specimen tested as part of this study.

3.2 TEST SPECIMENS

3.2.1 General Description of Test Specimens

Nine large-scale cantilever low-rise wall specimens were constructed and tested under displacement reversals in the Structural Engineering Laboratory at the University of Michigan. Seven of the specimens were tested by the writer, whereas two specimens were part of a preliminary study on HPFRC low-rise walls conducted by Kim and Parra (2003). The dimensions of the test specimens are shown in Fig. 3-1. Each specimen consisted of a wall fixed connected to a 72 in. long, 24 in. deep and 24 in. wide heavily reinforced concrete base block anchored to the laboratory strong floor. A 16 in. deep by 16 in. wide reinforced concrete top block was used for loading purposes. The load was applied through a hydraulic actuator connected to the mid-depth of the top beam at one end and to the laboratory reaction wall at the other end. The bottom and top blocks in all the specimens were constructed with regular concrete, whereas the wall was constructed with either regular concrete or an HPFRC mixture, depending on the design parameters of the specimen.

In all the specimens, the wall had a rectangular cross section, 40 in. long and 4.0 in thick. In order to investigate the influence of the wall height-to-length ratio $\left({}^{h_w}/_{\ell_w}\right)$ on the behavior of reinforced concrete and HPFRC low-rise walls, two different ratios were considered for the wall specimens. In one group of specimens, the wall had a height of 40 in., which translated into a wall height-to-length ratio of 1.0. For the rest of the specimens, the height-to-length ratio was 1.3, leading to a wall height of 52 in. The ratio between the shear span, a, i.e. the distance from the loading point (mid-height of top block) to the base of the wall, and the wall length $\left({}^{a}/_{\ell_w}\right)$ was 1.2 and 1.5, respectively, for the two groups of specimens. The main features of the test specimens are summarized in Table 3-1.

3.2.2 Design of Test Specimens

The main design parameters of the test units were the shear stress demand and type of cement-based material. Moderate intensity shear stress reversals [$5\sim7\sqrt{f_c'}$ (psi)] were the target for Specimens S1, S2, S6, S7, and S8, whereas Specimens S4, S5, S9 and S10 were designed for a higher shear stress demand [$8\sim10\sqrt{f_c'}$ (psi)]. Thus, the longitudinal and transverse reinforcement in each wall was chosen such that the target shear stress level could be attained without a premature shear failure. It should be noted that a Specimen S3, originally planned as part of the experimental program, was not tested, which is the reason for skipping Specimen S3 in the list of test specimens.

The walls constructed with regular reinforced concrete (Specimens S1, S4, S6 and S9) were designed following the seismic provisions in Chapter 21 of the 2005 ACI Code (318 ACI Committee, 2005). However, the design of the RC specimens also complied with the provisions of the 2008 ACI Code since the only difference in the two editions of the code is related to a relaxation in the maximum allowable spacing of the confinement reinforcement in the wall edges, as discussed in Section 2.2.3. For each wall, the main longitudinal wall reinforcement was concentrated in the wall edges and web horizontal and vertical distributed reinforcement was also provided. All longitudinal bars were

continued along the wall height and were fully anchored in the base block by means of a standard hook. Because large inelastic deflections were expected to be imposed on the test walls, special boundary elements were provided in all the reinforced concrete walls, as will be discussed later.

The configuration of the reinforcement for the HPFRC specimens (Specimens S2, S5, S7, S8 and S10) followed the same basic layout as their companion reinforced concrete walls. The longitudinal wall reinforcement was chosen such that the shear stress demand would be approximately the same as that in the companion RC specimen. The ACI Code provisions for the web distributed reinforcement and the confining reinforcement in the boundary elements were not explicitly followed in the design of the HPFRC specimens, as a major goal in this study was the evaluation of a possible relaxation in the reinforcement configuration.

Because of the construction sequence, which was meant to simulate that in real construction, a cold joint existed between the specimen base block and the bottom section of the wall. In the case of conventional reinforced concrete construction, the effect of this cold joint can be minimized by proper roughening of the surface of the footing. For the HPFRC walls, on the other hand, the cold joint is more critical because the joint section could be significantly weaker than the adjacent sections above the foundation due to the lack of fibers bridging the base-wall interface. Furthermore, because of the excellent bond between reinforcement and HPFRC materials (Parra et al., 2005; Chao et al., 2007), the longitudinal reinforcement would likely yield only in the region close to the cold joint. This concentration of yielding at the base of the wall could ultimately result in a sliding shear failure or even fracture of the reinforcement with a detrimental effect on wall displacement capacity. Thus, dowel bars were added in most HPFRC walls, as it will discussed in Section 3.2.3, to strengthen the wall-foundation interface and prevent concentration of inelastic rotations at this cold joint.

The maximum flexural strength at the base of each wall, M_{max}, was predicted using a sectional analysis and assuming plane sections remain plane after loading. Both the reinforcement concentrated in the boundary elements and the distributed web reinforcement were included in the strength computations. The concrete compressive strength, f_c', was assumed to be equal to 5000 psi for the regular concrete and the HPFRC mixtures. A 1.25 multiplier was applied to the nominal yield strength of the steel, f_y, to account for material overstrength and strain hardening, as specified in Chapter 21 of the ACI Code. It was also assumed that the dowel bars, when used in the HPFRC specimens, could develop 50% of their yield strength. The maximum base shear, V_{max}, was computed by dividing the predicted maximum flexural strength by the shear span length, a, as shown in Eq. (3-1).

$$V_{max} = \frac{M_{max}}{a} \tag{3-1}$$

The wall transverse reinforcement (i.e. the web horizontal distributed reinforcement) was chosen such that the shear demand, based on the predicted maximum flexural strength, would not exceed the nominal shear strength according to the ACI Code. The only exception was the design of Specimens S7 and S8, tested by Kim and Parra (2003), in which the wall transverse reinforcement was selected such that the nominal flexural strength of the wall would be approximately 1.2 times its assumed shear strength. The vertical web reinforcement ratio was chosen to be equal to the horizontal reinforcement ratio, as required by the ACI Code for structural walls with a height-to-length ratio less than 2.0.

For the reinforced concrete walls, the nominal shear strength, V_n, was calculated from Section 21.7.4.1 of the 2005 ACI Code, as follows:

$$V_n = \left(3\sqrt{f_c'} + \rho_h f_y\right) A_w \tag{3-2}$$

where the contribution of "concrete" to wall shear strength is equal to $3\sqrt{f_c'}$ (psi) for structural walls with a height-to-length ratio less than 2.0. The shear strength of the HPFRC specimens, on the other hand, was estimated assuming an increased contribution from the cementitious matrix because of the strain-hardening properties of the HPFRC material. Chompreda and Parra (2005), based on tests of HPFRC beams under displacement reversals, concluded that a shear strength of $3.5\sqrt{f_c'}$ (psi) represented a lower limit for the shear resistance of HPFRC flexural members with no transverse reinforcement, regardless of the rotation demand. However, for the HPFRC low-rise walls tested in this study, the "fiber-concrete" contribution to shear strength was assumed to be $5\sqrt{f_c'}$ (psi) because of the beneficial effect of arch action on the shear resistance of low-rise walls. The maximum base shear and the nominal shear strength values used for the design of the specimens are given in Table 3-2.

Shear transfer at the base of the RC and HPFRC walls was checked based on Section 11.6 of the 2005 ACI Code, as required for "interfaces between two concretes cast at different times". The nominal shear strength for shear transfer, V_n, based on a shear-friction model, is given by the following equation:

$$V_n = A_{vf} f_y \mu \tag{3-3}$$

where A_{vf} is the area of the shear-friction reinforcement perpendicular to the shear-friction plane, i.e. the total vertical reinforcement crossing the wall base, $f_y$is the yield strength of the shear-friction reinforcement (with a maximum value of 60,000 psi) and μ is a coefficient of friction in accordance with 2005 ACI Code Section 11.6.4.3. In the case of the RC walls in this study, the value of μ was taken equal to 0.6 ("concrete placed against hardened concrete not intentionally roughened"). In addition, the nominal strength for shear-transfer cannot exceed the smallest of $0.2f_c'A_c$ (equal to 160 kips for $f_c' = 5000$ psi) or $800A_c$ (equal to 128 kips), as required in ACI Code Section 11.6.5. Table 3-3 lists the values of V_n for shear transfer at the wall base for all the specimens. It can be observed that for all the RC walls, the nominal strength for shear-transfer

exceeded the maximum base shear, V_{max}, and thus, no additional dowel reinforcement had to be provided based on the ACI Code provisions. In the case of the HPFRC walls, dowel reinforcement was added because, as mentioned before, the cold joint was considered to be more critical than in the RC companion specimens.

The check for special boundary elements for the RC walls was performed based on the "stress check" of Chapter 21 of the 2005 ACI Code (Section 21.9.6.3). The stress-based check is considered more appropriate than the displacement-based check for use in low-rise walls such as those tested in this study. Table 3-4 lists the value of the extreme fiber compressive stress corresponding to the maximum flexural strength at the wall base for all test specimens. A linear elastic model and gross section properties were considered, as required by the ACI Code. The stress values for the HPFRC walls are also included in the table for comparison purposes, even though confinement reinforcement was eliminated or significantly relaxed. It can be observed that in the RC walls, the maximum compressive stress greatly exceeded the limit of $0.2f_c'$ (equal to 1000 psi for $f_c' = 5000$ psi) in all cases. As a result, special boundary elements had to be provided in the RC walls. It should also be noted that performing the check based on the displacement-based approach would have also resulted in the same conclusion.

The bottom and top beam in each specimen were designed to remain elastic thought the test. The bottom block was designed using a standard 2-D strut-and-tie model. The bottom block had the same dimensions in all the specimens, and slightly increased longitudinal reinforcement ratio for the specimens tested under higher shear stress. The dimensions and the reinforcement of the top block were chosen so that the load could be safely transferred to the specimen and to accommodate the connection with the hydraulic actuator. The dimensions and reinforcing details for the bottom and top blocks are provided in Figs. 3-2 and 3-3.

3.2.3 Reinforcing Details of Test Specimens

The reinforcing details for all the specimens are listed in Table 3-5 and the reinforcement configuration for each specimen is shown in Figs. 3-4 through 3-13. In the following, a summary of the design details for all the specimens is given.

3.2.3.1 Specimens with Shear Span-to-Length Ratio of 1.2

Specimen S1 was constructed with regular concrete and designed according to the seismic provisions of the 2005 ACI Building Code (ACI Committee 318, 2005). The wall longitudinal reinforcement was selected such that an average shear stress demand in the range of $5\sqrt{f_c'}$ (psi) to $6\sqrt{f_c'}$ (psi) would be imposed on the wall. The purpose of this test was to obtain a representative behavior of modern reinforced concrete walls with a shear span-to-length ratio close to 1.2 when subjected to shear stress reversals of moderate intensity.

The wall main longitudinal reinforcement in Specimen S1 consisted of 4 No. 4 (0.5 in. diameter) Grade 60 bars in each boundary region, placed in two layers, continuous through the wall and fully anchored in the base beam. This amount of wall main longitudinal reinforcement translated into a wall boundary reinforcement ratio, ρ_{bound}, of 5.0% according to Chapter 21 of the ACI Code, and a tension reinforcement ratio, ρ, of 0.53% ($\rho = \frac{A_s}{l_w t_w}$, where $A_s$is the area of main longitudinal reinforcement and t_w is the wall thickness). Two layers of smooth No. 2 (0.25 in. diameter) bars spaced at 3.5 in. on center were used as web horizontal reinforcement, resulting in a web reinforcement ratio of 0.71%. The web vertical reinforcement ratio was also chosen equal to 0.71%. The confining reinforcement in the wall boundary regions was provided through closed hoops made of 0.162 in. diameter smooth wire spaced at 1.0 in. The required confinement reinforcement ratio, rather than the maximum allowed spacing, governed the design. For a concrete compressive strength of 5000 psi and wire reinforcement yield strength of 29 ksi, the hoop spacing, as calculated from Equation (2-3), was equal to 0.9 in. However, for ease of construction, it was decided to use a spacing of 1.0 in. since this would not

compromise the behavior of the specimen. The reinforcing details for the wall of Specimen S1 are given in Fig. 3-4.

In the wall of Specimen S2, an HPFRC material containing a 2.0% volume fraction of hooked steel fibers was used. This specimen was the first wall in this investigation constructed with a fiber cementitious material and the HPFRC material chosen was the same as that used in Specimen S7 tested earlier by Kim and Parra (2003). Information on HPFRC mixture used in Specimen S2 is given in Section 3.3.1 and Tables 3-6 and 3-7. The main longitudinal reinforcement at the wall edges was the same as that in the control RC Specimen S1 such that the peak shear stress demand would be approximately the same in the two specimens. However, a possible relaxation of the web horizontal and vertical reinforcement was investigated in Specimen S2. Two layers of smooth No. 2 bars, spaced at 8.0 in. on center, were chosen for the web reinforcement, which corresponded to a horizontal and vertical reinforcement ratio of 0.31%. This ratio is less than one half of that used in Specimen S1 and is close to the minimum reinforcing ratio of 0.25% specified in the ACI Code. Thus, the shear strength provided by the horizontal web reinforcement, assuming a vertical projection of the critical diagonal crack equal to ℓ_w, represented less than 50% of the expected shear stress demand and was estimated to be in the order of $2.4\sqrt{f_c'}$ (psi).

The confining reinforcement in the boundary region of Specimen S2 was completely eliminated and as a result, the transverse reinforcement at the wall edges consisted only of the extension of the web horizontal reinforcement, terminated with a 135 degree hook at one end and a 90 degree hook at the other end. The elimination of the special confining reinforcement was decided based on the promising results obtained from the earlier study by Kim and Parra (2003) and allowed the evaluation of the ability of the HPFRC material to sustain large compressive strain demands and provide confinement to the wall longitudinal reinforcement. Further, this allowed an evaluation of whether HPFRC materials can provide sufficient lateral support to prevent buckling of the longitudinal bars in the wall boundary region.

As discussed earlier, sliding shear failure was considered as a possible failure mechanism in the HPFRC walls because of the presence of the cold joint at the wall base (see Section 3.2.2). However, given the low wall aspect ratio, it was assumed that concentrated flexural deformations at the wall base would likely not be large enough to result into a sliding shear failure and thus, no dowel reinforcement was placed at the wall base of Specimen S2. The lack of dowel reinforcement in Specimen S2 would also allow the evaluation of the influence of the cold joint on the behavior of HPFRC low-rise walls. Reinforcing details for Specimen S2 are provided in Fig. 3-5.

Specimens S4 (RC) and S5 (HPFRC) had the same geometry as that of Specimens S1 and S2, but were designed with an increased longitudinal reinforcement ratio in the boundary regions such that a higher shear stress demand in the range of $8.5\sqrt{f_c'}$ (psi) to $9.5\sqrt{f_c'}$ (psi) would be imposed on the walls. The testing of these two specimens would thus allow the evaluation of the influence of shear stress demand on the behavior of RC and HPFRC walls when subjected to displacements reversals.

Specimen S4 was constructed with regular concrete. Two No. 6 and 2 No. 5 Grade 60 bars were used in each boundary region of the wall, which translated into a wall boundary reinforcement ratio of 9.4% and a wall tension reinforcement ratio of 1.0%. No dowel bars were used to strengthen the wall-foundation interface. A deformed wire was chosen for the web distributed reinforcement to better simulate the behavior of walls with standard deformed bars (more information about the properties of these bars is given in Section 3.3.3). It should be mentioned that these small diameter deformed bars were difficult to find and thus, they were not available for use in all the wall specimens. Two layers of D5 wire (area = 0.05 in.^{2}) at 3.0 in. on center were used as horizontal and vertical wall reinforcement in Specimen S4, which translated into a web reinforcing ratio of 0.83%. The confining reinforcement in the boundary regions was the same as that in RC Specimen S1. The reinforcement layout for Specimen S4 is given in Fig. 3-6.

The wall in Specimen S5 was constructed with a relatively new type of HPFRC material. A self-consolidating, high performance fiber reinforced concrete with a 1.5% volume fraction of high-strength (330 ksi) hooked steel fibers was chosen in order to facilitate concrete casting (Liao et al., 2007). This HPFRC mixture contains coarse aggregate ($^{3}/_{8}$ in. maximum size), which makes the material more attractive for large-scale applications. Information on this mixture will be given in Section 3.3.1

As it will be discussed in Chapter 4, sliding shear deformations played a significant role in the behavior of HPFRC Specimen S2, which was constructed without the addition of dowel reinforcement at the wall-foundation interface. Thus, dowel bars were provided at the wall base of Specimen S5 in order to strengthen the wall-base block interface and force flexural yielding to primarily occur above the cold joint. In order to prevent the occurrence of a predominant flexural crack caused at the termination of the dowel bars, these dowel bars were extended, debonded, beyond the wall plastic hinge region, as shown in Fig. 3-7. A close-up photo of the dowel bars and the debonded regions is shown in Fig. 3-8. The use of diagonal bars in the web of the concrete walls, even though it has been generally proven effective to prevent a sliding shear failures was considered to be difficult to implement in practice and thus, it was ruled out as an alternative to the use of dowel reinforcement.

The main vertical wall reinforcement in HPFRC Specimen S5 consisted of 4 No. 5, Grade 60 bars in each boundary region and two layers of 4 No. 4 dowel bars, distributed as shown in Fig. 3-9. The spacing of the wall distributed horizontal and vertical reinforcement was relaxed compared to that in Specimen S4. D5 wire reinforcement was spaced at 4.0 in. on center, corresponding to a horizontal and vertical reinforcing ratio of 0.63%. Based on the preliminary results of the tests of Specimens S7 and S8 (Kim and Parra, 2003) and Specimen S2, the complete elimination of special confining reinforcement in the wall boundary regions through the use of HPFRC seemed a feasible design solution. However, given the high intensity of the stress demand that would be imposed on Specimen S5, some confining reinforcement was used. Single hoops made of

0.162 in. diameter wire at 4.0 in. spacing was provided in the wall boundary regions, which corresponded only to one-fourth of the confinement reinforcement in the companion RC Specimen S4.

3.2.3.2 Specimens with Shear Span-to-Length Ratio of 1.5

Specimen S6 was designed as a conventional reinforced concrete structural wall for an average shear stress demand between $6.5\sqrt{f_c'}$ (psi) and $7.5\sqrt{f_c'}$ (psi). This specimen represented a control specimen for the HPFRC low-rise walls with a shear span-to-length ratio of 1.5 and the shear stress level was chosen to be approximately equal to the shear stress level of Specimens S7 and S8, which were previously tested by Kim and Parra (2003). The wall was designed based on the provisions of the 2005 ACI Code, as for RC Specimen S1. Main vertical tension reinforcement ratio was approximately 1.0%, consisting of two No. 5 and two No. 6 bars. For the vertical and horizontal web reinforcement, smooth No. 2 bars, spaced at 3.5 in. on center, were used, which translated into a reinforcement ratio of 0.71%. The confinement reinforcement in the boundary regions consisted of singe hoops made out of a 0.162 in. diameter wire, spaced at 1.0 in. Reinforcement detailing for Specimen S6 is shown in Fig. 3-10.

Specimens S7 and S8 were designed and tested by Kim and Parra (2003) and, to the writer's knowledge, were the first HPFRC low-rise walls tested under displacement reversals. Specimens S7 and S8 were constructed with an HPFRC material containing hooked steel fibers and ultra-high molecular weight polyethylene (Spectra) fibers, respectively. The reinforcing bars in these two specimens were placed in a single layer, given the lack of experience at the time in casting HPFRC in these elements. It was argued that the use of one layer of reinforcement would not compromise the behavior of the walls because of the beneficial effect of using a ductile concrete material in tension. However, casting of the walls in Specimens S7 and S8 did not present any significant challenge and thus, it was decided to use two layers of reinforcement in all the HPFRC specimens designed for this study.

The longitudinal reinforcement in Specimen S7 and S8 consisted of 3 No. 7 bars at each edge, which corresponded to a tension reinforcement ratio of 1.1%, while 4 No. 5 bars were added as dowel reinforcement. Smooth No. 2 bars at 10 in. and 6.0 in. on center were provided as distributed horizontal and vertical wall reinforcement, respectively. No special boundary confinement reinforcement was used, as in HPFRC Specimen S2. The reinforcing details for HPFRC Specimens S7 and S8 are shown in Fig. 3-11.

The last two specimens (S9 and S10) were designed for a high shear stress demand (between $8.5\sqrt{f_c'}$ (psi) and $9.5\sqrt{f_c'}$ (psi)). For Specimen S9, which was constructed with regular concrete, 2 No. 7 and 2 No. 6 bars were used as the main flexural reinforcement based on the target shear stress level. The chosen bars corresponded to a boundary reinforcement ratio of 13% and a tension reinforcement ratio of 1.4%. The wall horizontal and vertical distributed reinforcement was provided in the form of crimped wire (more information in Section 3.3.2). Two layers of D4 crimped wire (area=0.04 $in.^2$) at 3.0 in. on center were provided, which translated into a horizontal and vertical distributed reinforcement ratio of 0.67%. The boundary confining reinforcement was the same as that in all the reinforced concrete specimens (0.162 in. diameter wire at 1.0 in. spacing). The elevation and cross-section of Specimen S9 can be seen in Fig. 3-12.

For Specimen S10, 4 No. 6 bars were used as the wall main longitudinal reinforcement, which along with the two layers of 4 No. 4 dowel bars, resulted in a moment capacity at the wall base approximately equal to that of the companion RC Specimen S9. The upper end of the dowel bars was also debonded, as in Specimen S5. The web distributed reinforcement (D4 wire) was spaced at 4.0 in., resulting in a horizontal and vertical distributed reinforcement ratio of 0.5%. For Specimen S5, single hoops (0.162 in. diameter) at 4.0 in. spacing were provided in each boundary element. Fig. 3-13 provides the details of the reinforcement for this specimen.

3.3 MATERIALS USED IN THE STUDY

3.3.1 Concrete Mixtures

3.3.1.1 Mixing Proportions

The concrete used for the wall in the specimens constructed with conventional reinforced concrete (Specimens S1, S4, S6 and S9) was mixed in the Structural Engineering Laboratory at the University of Michigan. The proportions by weight of this mixture were 1:1.55:1.45:0.48 (cement: sand: coarse aggregate: water). Type III cement (high early strength) was used and the coarse aggregate consisted of crushed limestone with 1/2 in. maximum aggregate size. The sand used was 2NS sand, which according to Section 902 of the 2003 Standard Specifications for Construction of the Michigan Department of Transportation (Aggregate Div., Levy Corporate, Dec. 2008, http://www.edwclevy.com) refers to natural sand with particles sized from 3/8 in. to mesh #200 (diameter of 0.00295 in.). A rheobuild 1000 high-range water reducing admixture was used in some cases to achieve adequate workability.

The fiber reinforced mortar mixture used for HPFRC Specimen S2 was the same as that used in previous investigations on the seismic behavior of HPFRC structural members (for example Canbolat et al., 2005), and it was also used in Specimen S7 tested by Kim and Parra (2003). The mortar was mixed in the Structural Engineering Laboratory with proportions by weight of 1:2:0.48:0.20 for Type III cement, #16 silica sand, water, and class C fly ash. The silica sand is a product referred to as “Flint Silica #16”, manufactured by U.S. Silica Company, with particles sized from mesh #20 (diameter of 0.03346 in.) to mesh #140 (diameter of 0.00417 in.). Regular strength (160 ksi) hooked steel fibers, 1.2 in. long and 0.022 in. diameter (Bekaert ZP 305) in a volume fraction of 2.0%, were used in this mixture, denoted as HPFRC-SH mixture. For the wall of Specimen S8 (Kim and Parra, 2003), the mixture proportions by weight of the fiber cementitious material were 1:1:0.5:0.15 (type III cement: silica sand: water: class C fly ash). Ultra high molecular weight polyethylene (Spectra) fibers in a volume fraction of 1.5% were used in this mixture, which was denoted as HPFRC-PE mixture.

The mixture used for HPFRC Specimens S5 and S10 is one of a series of self-consolidating HPFRC mixtures developed at the University of Michigan for seismic applications (Liao et al., 2007). This mixture was chosen such as to investigate its use in structural applications and to ease the casting of the wall specimens, given the small thickness of the walls (4 in.). The mixing ratio of this HPFRC material by weight was 1:2.2:1.2:0.8:0:885:0.005:0.038 for Type III cement, #16 Silica sand, coarse aggregate, water, class C fly ash, superplasticizer, and a viscosity modifying admixture (VMA). The coarse aggregate consisted of solid crushed limestone with a maximum size of $^{3}/_{8}$ in. The superplasticizer used was a polycarboxylate-based plasticizer and the VMA agent was basically used to enhance the viscosity and reduce fiber segregation in the presence of higher water-to-cementitious ratios. A 1.5% volume fraction of 1.2 in. long, 0.015 in. diameter, high-strength (330 ksi) hooked steel fibers was used in this mix denoted as SCHPFRC mixture.

The bottom and top block of the specimens were constructed with regular concrete. The concrete mixture for the bottom block for all the specimens was provided by a local ready-mix concrete supplier, whereas the mixture for the top block was either delivered by a ready-mix concrete supplier or prepared in the Structural Engineering Laboratory. The ready-mix concrete was specified as a 4000 psi compressive strength mixture, with 3/8 in. maximum aggregate size and 6 in. slump. The regular concrete mixed in the laboratory, on the other hand, had the same proportions as those for the regular concrete used in the walls of Specimens S1, S4, S6 and S9. Table 3-6 lists the details for the different mixtures used in this study. It should be mentioned that the compressive strength of the ready-mix concrete used in the bottom block of Specimen S10 was less than the specified strength of 4000 psi because the mixture had a substantially higher water-to-cement ratio than the ratio originally specified in the mixture due to an error of the concrete supplier.

3.3.1.2 Mixing Process

The regular concrete mixture mix was prepared in the laboratory in either a 5 or a 1.5 cubic feet capacity mixer (Fig. 3-14). The mixing process followed standard practice for mixing regular concrete. Due to the capacity of the mixers and the required volume of concrete, several batches had to be prepared to complete the casting for each of the walls. The 1.5 cubic feet capacity mixer was also used for the HPFRC material used in the wall of Specimen S2. The fibers were added last to the mixer. Although concrete slump was not measured before the fibers were added, it was obvious that the workability of the mixture was affected. However, the casting of the wall was performed without significant problems.

The mixing procedure and mixing time for the self-consolidating HPFRC mix used in Specimens S5 and S10 followed the recommendations by Liao et al. (2007). The mixing procedure, including the sequence by which different materials are placed in the mixer, and the mixing time are critical to successfully achieve a self-consolidating concrete mixture. For the mixture used in this study, the cement, fly ash and sand had first to be dry-mixed for 30 seconds and then the pre-mixed liquid (water, superplasticizer and VMA) was added slowly such as to limit the formation of lumps in the paste. The coarse aggregate was then added and after 2 minutes, the steel fibers were added slowly to the mixture. The mixing process was continued for approximately 3 minutes after the addition of fibers was completed.

3.3.2 Fibers

Three types of fibers, two made of steel and one made out of ultra high molecular weight polyethylene, were evaluated in this study and their properties are listed in Table 3-7. The steel fibers had a circular cross-section with their ends bent such as to create a hook and enhance the mechanical bond with the concrete matrix (Fig. 3-15(a)). These fibers are commercially available through Bekaert S.A., Belgium, by the name Dramix. The first Dramix fiber used is referred to as ZP305 fiber. This fiber has been used in many

applications, such as slabs, retaining walls, precast members, sprayed concrete, and pavements. Dramix ZP305 fibers are 1.2 in. long with a diameter of 0.022 in. The tensile strength of the fiber, as reported by the manufacturer, is in the range of 160 ksi to 200 ksi, with an elastic modulus of 29,000 ksi. These fibers were used in Specimens S2 and S7.

The other Dramix fiber used in this study is referred to as RC-80/30-BP fiber. It is a high-strength hooked steel fiber, 1.2 in. long, and with a diameter of 0.015 in. The specified tensile strength of this fiber was 335 ksi (2300 MPa). This high-strength hooked steel fiber was used in Specimens S5 and S10.

Ultrahigh molecular weight polyethylene (Spectra) fibers were used in Specimen S8 (Fig. 3-15(b)). Spectra fibers are widely used in fiber reinforced polymers for the aerospace industry. The fibers had a length of 1.5 in. and a diameter of 0.0015 in. The fiber tensile strength and elastic modulus reported by the manufacturer were 375 ksi and 17,000 ksi, respectively.

The fibers used in this experimental program were selected on the basis of previous large-scale tests conducted at the University of Michigan. Test results from direct tensile tests on FRC (mortar) with Dramix ZP305 fibers were reported by Chompreda and Parra (2005). They reported a tensile strain-hardening behavior in composites with a 2% fiber volume fraction, while a strain-softening behavior with gradual strength decay was reported for composites with a 1.5% fiber volume fraction. Further, the preliminary results from the low-rise wall test (Specimen S7) by Kim and Parra (2003) showed great potential for the application of these fibers in structural walls. The HPFRC mixture with the Spectra fibers was reported to have maximum tension strength of approximately 0.51 ksi and an average peak strain of 2.0% (Kim and Parra, 2003). The Dramix RC-80/30-BP fiber was used in combination with the self-consolidating HPFRC mixture described above. As reported in the study by Liao et al. (2007), this self-consolidating mixture

exhibits a strain-hardening behavior in tension, up to a strain in the range of 0.25% to 0.5% with a peak stress of approximately 0.5 ksi.

3.3.3 Reinforcing Steel

In all the specimens, the deformed reinforcing bars (No. 4, 5, 6 and 7 bars) were made out of Grade 60 steel. The No. 2 bars used in Specimens S1, S2, S6, S7 and S8 were smooth bars because deformed No. 2 bars could not be obtained. These bars did not conform with ASTM standards. Separate steel orders were made for the reinforcement used in Specimens S1 and S2, S4 and S5, S6, S7 and S8, and S9 and S10.

For Specimens S9 and S10, a crimped wire (D4, area=0.04 $in.^2$) was used for the wall web reinforcement in order to enhance the bond between the reinforcement and the matrix. The crimped wire was obtained from Milliken Steel Sales Ltd. in Canada and it was basically a smooth wire that was driven through a crimping machine to create indentations (Fig. 3-16(a)). The manufacturer reported that this material does not have a yield plateau and rather exhibits a cold-formed steel behavior with a yield stress based on the 0.2% offset method of about 90 ksi and an ultimate stress of about 96 ksi. A deformed wire (D5, area=0.05 $in.^2$) that conforms to ASTM Standard A 496-02 “Standard Specification for Steel Wire, Deformed, for Concrete Reinforcement” was used in Specimens S4 and S5 because it was considered a better alternative to the previously used crimped wire (Fig. 3-16(b)). This wire was obtained from Wire Products Inc. in Florida and is described as a “positive deformation pattern” wire with a nominal yield stress of 75 ksi.

The boundary confining reinforcement for all the specimens was constructed from a 0.162 in. diameter smooth wire. The wire was a general purpose low carbon steel wire that met the ASTM A853 requirements for coating only. This wire had a yield and ultimate strength of 29 ksi and 47 ksi, respectively, based on test results from previous

studies (Chompreda and Parra, 2005). The wire was delivered in the form of a coil and the hoops were prepared in the laboratory.

3.3.4 Material Testing

3.3.4.1 Concrete and HPFRC Materials

The average compressive strength of the concrete and HPFRC mixtures was determined through compressive tests of 4×8 in. cylinders. For each batch of material prepared in the laboratory and for all ready-mix concrete delivered, six cylinders were prepared. Three cylinders were tested at 28 days and the other three were used to record the concrete strength one day after the test. Tests were conducted using an Instron testing machine operated under displacement control. The average compressive strength obtained from the cylinder tests performed one day after the test day are listed in Table 3-8.

In addition to cylinder tests for evaluation of compressive strength, beam specimens with dimension of $6 \times 6 \times 20$ in. were prepared for the HPFRC material used in Specimens S5 and S10. Five beams were cast for Specimen S5, three from the first batch and two from the second batch. For Specimen S10, three beam specimens were made from each of the two batches. All beams were tested under third-point loading with an 18 in. span length, according to ASTM 1609-05 (Fig. 3-17). Net midspan deflections were measured through two linear potentiometers with a ∓ 0.1 in. stroke length connected to an instrumentation frame, as shown in Fig. 3-17. Key results from the tests are given in Table 3-9. First peak load (cracking load) is defined, according to ASTM 1609-05 (Section 10.2), as the load value at the first point on the load versus deflection curve where the tangent slope is zero. Figs. 3-18 and 3-19 show the load versus deflection response for the beam specimens tested for Specimens S5 and S10, respectively. Strengths at deflection levels equal to 0.03 in. (span length/300) and 0.12 in. (span length/150) are provided in Table 3-9. The tests were terminated after a midspan deflection of 0.12 in. was reached, as required by ASTM 1609-05 (Section 9.5).

Kim and Parra (2003) reported on results from tension tests of the HPFRC materials used in Specimens S7 and S8. Based on the tensile stress-strain response of the HPFRC material with hooked steel fibers and Spectra fibers, the first cracking strength was approximately 0.43 ksi both materials. The HPFRC material with hooked steel fibers (ZP305) showed a pea tensile stress of 0.60 ksi at a strain of approximately 0.5%. On the other hand, the peak tensile stress and corresponding strain for the HPFRC material with Spectra fibers were 0.51 ksi and 2%, respectively.

3.3.4.2 Reinforcing Steel

Samples of the reinforcing steel used to construct the wall of the specimens were tested under direct tension to determine their yield and ultimate strength. For each bar size in each shipment, two or three 24-in. long coupons were randomly selected and tested. The results are summarized in Table 3-10. The stress-strain curve for the D4 wire, as obtained from direct tension tests, is shown in Fig. 3-20.

3.4 CONSTRUCTION OF SPECIMENS

All the specimens were constructed in the Structural Engineering Laboratory at the University of Michigan. To ensure realistic construction-site conditions, all test units were built in the fully upright position. This construction process was deemed to be necessary to ensure a realistic distribution and orientation of the fibers in the HPFRC walls. However, the casting of the specimens was somewhat challenging in some cases because of the small wall thickness (4 in.). The construction sequence is briefly presented below.

First, the reinforcement of the base block was tied and the cage was placed in a wooden formwork (Fig. 3-21). PVC pipes were embedded in the formwork for the placement of the high strength threaded rods that were used to connect the specimen to the strong floor. Then, the wall longitudinal bars, which were continuous over the wall height, were assembled and concrete was poured in the base block using ready-mix concrete provided by a local supplier. Fig. 3-22 shows a specimen ready for casting of the base block.

Subsequently, the wall transverse reinforcement above the base block was placed (Fig. 3-23), the formwork of the wall was put in place (Fig. 3-24), and the wall concrete was cast in one lift. In Fig. 3-25, Specimen S4 is shown after the completion of the wall casting and the removal of the formwork. Finally, the formwork for the top beam was put in place, the top block reinforcement was assembled (Fig. 3-26), and regular concrete was poured. Concrete cylinders were prepared for every batch of concrete prepared in the laboratory and for every ready-mix concrete delivery.

After each concrete casting, the exposed concrete was covered with plastic sheets for 2-3 days. The forms were removed about one week after casting. Once the specimen construction was completed (Fig. 3-27), the specimen was lifted with the crane and placed into the test set up. Concrete material samples were also covered with plastic sheets for approximately two days, at which point they were demolded and placed in a water tank until testing.

As discussed previously, the specimen casting sequence resulted in a cold joint between the specimen base block and the bottom section of the wall. For the regular concrete specimens and HPFRC Specimen S2 the cold joint was left unreinforced. In the other HPFRC specimens, dowel bars were used to strengthen the wall-base interface and force inelastic deformations to occur within the HPFRC wall.

Difficulties were encountered during the casting of the wall of Specimen S10, which was the first wall in the study to be constructed with the self-consolidating HPFRC mixture. A self-consolidating mixture could not be achieved for this specimen. Further, the mixture showed poor workability during casting and significant vibration was necessary to make sure that the material would flow throughout the wall. However, the removal of the formwork revealed air voids in the wall, there were generally away from the expected plastic hinge region. A grout mixture was used to patch those regions and the behavior of the specimen was not compromised, as was evident during the test.

3.5 SPECIMENS INSTRUMENTION

Strains in the reinforcement were measured using electrical resistance strain gauges attached to the reinforcing bars at several locations. The location and label for the strain gauges placed on the wall reinforcing bars are shown in Figs. A-1 to A-8 in Appendix A.

One face of each specimen was instrumented with linear potentiometers positioned vertically, horizontally and diagonally to monitor average shear strain distortions and rotations. Vertical potentiometers were also placed adjacent to both side edges of the walls to measure rotations at the wall base. Rigid body horizontal displacement (sliding) of the bottom block and sliding of the wall with respect to the base block were recorded through potentiometers attached to a fixed location. The rotation of the bottom and top blocks was monitored using clinometers. A typical arrangement of the potentiometers and inclinometers is shown in Figs. 3-28 and 3-29. A load cell and a Linear Variable Differential Tranformer (LVDT) were used to monitor the applied load and lateral displacement of the actuator, respectively. The readings from all the instruments were collected simultaneously through a data acquisition system at a sampling rate of 2 Hz.

An Optotrak Certus motion capture system, manufactured by NDI, Canada, was also used during the testing of Specimens S4, S5, S9 and S10. Optotrak is a non-contact motion measurement system that tracks the position in space of small sensors. Only one position sensor is required to determine the 3D location of the point to which the sensor is applied. In this investigation, the sensors were attached to one face of the specimen, forming 5 in. $\times$ 5 in. grid, as can be seen in Fig. 3-30. Using the recorded coordinates of the sensors during the test, average strains and rotations were determined at various locations. For the specimens where both potentiometers and Optotrak markers were used, it was possible to compare the results from the two instrumentation procedures and conclude on their overall accuracy. Photos of the instrumentation schemes are shown in Figs. 3-31 and 3-32.

3.6 TEST SET UP AND TEST PROCEDURE

All the specimens were constructed in an area adjacent to the testing space in the Structural Engineering Laboratory at the University of Michigan and were then moved into the test location using an overhead crane. The specimens were anchored to the laboratory strong floor through eight 1-1/2 in. diameter threaded rods. Liquid grout forming an approximately 1/2 in. thick layer was cast between the top surface of the bottom block and the 1-1/4 in. thick steel bearing plates connected to the threaded rods. The specimens were also braced laterally at the top block to restrain out-of-plane movements, as shown in Fig. 3-33. Subsequently, the external instrumentation was placed and shortly before the test the horizontal hydraulic actuator was connected to the strong wall at the mid-depth of the top block. A specimen ready for testing is shown in Fig. 3-34.

A 100-kip hydraulic actuator with a ±15 in. stroke was used for the application of lateral displacements for the specimens designed for moderate shear stress demands, (i.e. Specimens S1, S2 and S6). However, for the specimens where high shear stresses were expected, (i.e. Specimens S4, S4, S9 and S10), a 300-kip hydraulic actuator with an ±8 in. stroke was used. The typical test set-up is shown in Fig. 3-35.

The specimens were subjected to quasi-static reversed cyclic displacements, with the peak displacement at a given cycle ranging from 0.125% drift to 3.0% drift. Drift was calculated as the lateral displacement at mid-depth of the top block in relation to the top of the base block divided by the initial distance between those two sections. Every displacement cycle up to 2.0% drift was performed twice to evaluate any decrease in strength and stiffness with repeated displacement cycles. The loading scheme used in this study was the same used for Specimens S7 and S8 by Kim and Parra (2003), allowing the test results to be compared with existing data. However, it should be mentioned that there is no widely accepted reversed cyclic loading scheme for RC members and it has been reported that the loading scheme can have a significant effect on the behavior and ductility of RC members (Lehman et al., 2004; Matamoros and Sozen, 2003).

The target lateral displacement history is shown in Fig. 3-36. Ideally, the specimen would be subjected to this drift history. During the test, the applied drift was corrected to account for the sliding of the base block through the use of a horizontal potentiometer attached to the base block (Figs. 3-28 and 3-29). The measured drift was further corrected, after the test, to account for the rotation of the bottom block, as will be described in Section 4.1. Drifts reported throughout this report are the corrected ("actual") drifts.

CHAPTER 4

EXPERIMENTAL RESULTS

4.1 DEFINITIONS

Before the test results are presented, some basic terms are first defined. This section describes the calculation of average shear stress, wall drift, shear strains, rotations along the wall height, and strains, including principal strains and directions.

4.1.1 Average Shear Stress

Average shear stress, v, was obtained by dividing the applied lateral load, P, by the product of the wall length, ℓ_w, and thickness, t_w, i.e. the wall cross sectional area, as follows:

$$v = \frac{P}{\ell_w t_w} \tag{4-1}$$

The applied lateral load represents the load cell reading from the hydraulic actuator.

In this report, shear stress is often expressed in multiples of $\sqrt{f_c'}$ in psi to facilite the comparison with the shear strength equations given in the ACI Building Code. For example, as discussed in Section 2.2.4, the shear strength attributed to concrete for seismic design of low-rise walls $(h_w/\ell_w \leq 2)$ is $3.0\sqrt{f_c'}$ (psi), whereas the upper

strength limit is $10\sqrt{f_c'}$ (psi). The normalization of the magnitude of the shear stress also allows for an easy comparison of the shear stresses imposed on all the test specimens.

4.1.2 Drift

Drift is defined as the ratio between the lateral displacement of the wall and shear span:

$$\delta = \frac{\Delta}{a} \tag{4-2}$$

where Δ is the lateral displacement at the mid-depth of the top block and a is the shear span length, defined as the distance from the base of the wall to the mid-depth of the top block.

The lateral displacement of the wall was obtained after correcting the displacement applied through the actuator to account for rigid body displacements (rotation and slip) of the bottom beam. The bottom beam rigid body displacements were measured with the use of inclinometer CL1 and potentiometer P11, shown in Figs. 3-28 and 3-29. Thus, the lateral displacement of the wall was calculated as follows (Fig. 4-1):

$$\Delta = \Delta_a - s_b - \beta(h_a - h_{P11}) \tag{4-3}$$

where, Δ_a (in.) is the lateral displacement of the actuator, monitored through a Linear Variable Differential Tranducer (LVDT), s_b (in.) is the horizontral movement obtained from potentiometer P11 attached to the base beam, h_{P11} (in.) is the elevation of potentiometer P11 with repect to the laboratory strong floor, β (rad) is the base block rotation obtained from inclimometer CL1 attached to the base beam, and h_a (in.) is the elevation of the actuator with respect to the strong floor. The rigid body displacements of the base block was also calculated using the data obtained from the Optotrak system markers' coordinates, when applicable, but no significant difference was found compared to the measurements of the pontetiometer and inclinometer.

A correction to account for the flexibility in the loading fixtures also had to be considered, as can be observed by comparing the displacement at the mid-depth of the top block recorded from the actuator LVDT and the top block displacement as calculated based on the lateral displacement and rotation of the top row of Optotrak markers (wall portion above top row of markers was assumed to rotate as a rigid body)(). Fig. 4-2 shows a comparison plot of the top-block displacement in Specimen S5 obtained from the two instrumentation methods (Optotrak markers system and actuator LVDT). Only the load versus displacement response envelope for the first cycle at each drift level is plotted in the figure. It can be seen that there is some difference in the top-block displacements, especially in the negative (pulling) loading direction. The Optotrak system data gave smaller displacements at each drift level and this can be attributed to the flexibility associated to the loading apparatus, particularly to the deformation of the rods used to tie the actuator to the top block (see Fig. 3-35). The difference in the displacements was rather constant after the peak load was achieved for both loading directions. Very similar plots were obtained for Specimens S4, S9 and S10 and as a result, the displacement obtained from the Optotrak system, when availiable, was used to calculate the applied lateral displacement of the wall Δ_a in Eq. (4-3). For Specimens S1, S2, S6, S7 and S8, a correction to account for the relaxation of the test set up could not be performed because data from the Optotrak system was not availiable. Thus, the wall drift was calculated from Eq. (4-3) based on the actuator displacement.

4.1.3 Shear Strain

The average shear strain (shear distortion) in the lower part of the wall was determined using the data obtained through the diagonal potentiometers P1 and P2 or the Optotrak system marker coordinates, when available (see Figs. 3-28 to 3-20). The average shear strain can be calculated using the expression by Oesterle et al. (1976), based on the change in length in the two diagonals:

$$\gamma = \frac{(d_1' - d_1)d_1 - (d_2' - d_2)d_2}{2HL} \tag{4-4}$$

where γ (rad) is the average shear strain and the rest of the variables are defined in Fig. 4-3.

Eq. (4-4) is theoretically correct when the element experiences a constant curvature along the height H. For the low-rise walls in this study, it can therefore be argued that the values obtained for the diagonal lengths d_1' and d_2' were affected by the distribution of the curvature along the height of the wall. However, the measured shear strain can be corrected so that the shear distortion is not overestimated because of the flexural deformations in the wall. A method to perform the correction was presented by Massone and Wallace (2004), which required the readings from vertically, horizontally and diagonally placed potentiometers. Even though the instrumentation scheme used in this study included diagonal, vertical and horizontal potentiometers (see Fig. 3028 and Fig. 3029), the horizontal potentiometers did not work properly in some tests and thus, the correction could not be performed in all the cases. Therefore, the shear strain was first calculated for all the specimens using Eq. (4-4) and additionally, a more accurate calculation was performed for the specimens where the Optotrak system was used. As will be described in Section 4.1.6, it was possible to calculate the average shear strain for each quadrilateral element in the marker grid using the Optotrak markers' coordinates. As shown in Fig. 4-4, the wall could then be divided in several horizontal strips along its height. Each strip had a height of 5 in. and comprised seven quadrilateral elements. Given the relatively small height of each strip, curvature was assumed to be constant in each strip, allowing the shear strain to be estimated as the average shear strain of the seven quadrilateral elements. This procedure allowed then the calculation of the shear strain distribution, as well as the average shear strain in the walls over a region 35 in.$\times$ 35 in. A comparison plot for the two procedures will be shown and discussed in Section 4.5.

4.1.4 Flexural Rotations

Concentrated rotations at the bottom of the wall were calculated using the deformations measured through the potentiometers attached to the sides of the wall, i.e. potentiometers P7 through P10 (see Figs. 3-28 and 3-29). Using the same potentiometers, the rotation at

a height of 0.3*h*, where *h* refers to the wall height, could be also calculated. Rotations at other sections along the wall height were also obtained using the inclinometers and the data from the Optotrak markers.

4.1.5 Horizontal Slip at the Wall Base

The horizontal slip at the wall-base block interface was monitored with the use of potentiometer P12 (see Figs. 3-28 and 3-29). The readings of the potentiometer were corrected to account for the rigid body motion of the base block, as follows:

$$s = s_{P12} - s_{p11} - \beta \times \left(h_{p12} - h_{P11}\right) \tag{4-5}$$

where s (in.) is the slip at the cold joint, s_{P12} (in.) is the reading from potentiometer P12, β (rad) is the rotation of the bottom block, and h_{P12} (in.) is the elevation of potentiometer P12 with respect to the laboratory strong floor. The slip was also calculated using the data from the the Optotrak markers located at 4 in. above the wall base, resulting in similar values. It should be mentioned that potentiometer P12 monitored the horizontal displacement of the wall at approximately 3 in. from the base block. Thus, the measurements were slighly affected by the deformation and rigid body rotation of the wall in this region.

4.1.6 Calculation of Strain Field from Optotrak Data

Using the coordinates of the Optotrak markers, the average strains in the wall plane for each quadrilateral element were calculated. The coordinates of the markers were first transformed to a coordinate system in the plane of the wall (such that the x- and y-axis defined the plane of the wall) in order to obtain the in-plane displacement of the markers. With the displacements of the markers known, the average strains were calculated.

Consider a quadrilateral element deformed as shown in Fig. 4-5. If the coordinates and displacements of all four nodes 1, 2, 3, and 4 are known, the average strains $\varepsilon_x, \varepsilon_y$ and γ_{xy} can be calculated as follows:

$$\varepsilon_x = \frac{1}{2}\left(\frac{u_3 - u_2}{\Delta x_{23}} + \frac{u_4 - u_1}{\Delta x_{14}}\right) \tag{4-6}$$

$$\varepsilon_y = \frac{1}{2}\left(\frac{v_1 - v_2}{\Delta y_{12}} + \frac{v_4 - v_3}{\Delta y_{43}}\right) \tag{4-7}$$

$$\gamma_{xy} = \frac{1}{2}(\beta_1 + \beta_2) + \frac{1}{2}(\beta_3 + \beta_4) = \\ = \frac{1}{2}\left(\frac{u_1 - u_2}{\Delta y_{12}} + \frac{u_4 - u_3}{\Delta y_{43}}\right) + \frac{1}{2}\left(\frac{v_3 - v_2}{\Delta x_{23}} + \frac{v_4 - v_1}{\Delta x_{14}}\right) \tag{4-8}$$

where:

$$\Delta y_{12} = |y_1 - y_2| \tag{4-9}$$

$$\Delta y_{43} = |y_4 - y_3| \tag{4-10}$$

$$\Delta x_{14} = |x_4 - x_1| \tag{4-11}$$

$$\Delta x_{23} = |x_3 - x_2| \tag{4-12}$$

Once the strain field is available, the principal strains and directions are computed as follows:

$$\varepsilon_1 = \tfrac{1}{2}(\varepsilon_x + \varepsilon_y) + \tfrac{1}{2}\sqrt{(\varepsilon_x - \varepsilon_y)^2 + \gamma_{xy}^2} \tag{4-13}$$

$$\varepsilon_2 = \frac{1}{2}(\varepsilon_x + \varepsilon_y) - \frac{1}{2}\sqrt{(\varepsilon_x - \varepsilon_y)^2 + \gamma_{xy}^2} \tag{4-14}$$

$$\theta = \frac{1}{2}tan^{-1}\left(\frac{\gamma_{xy}}{\varepsilon_x - \varepsilon_y}\right) \tag{4-15}$$

The calculated shear strain in each quadrilateral element, γ_{xy}, was also used to obtain the average shear distortion in the wall, as discussed in Section 4.1.3.

4.2 DAMAGE PROGRESSION IN THE WALL SPECIMENS

Minor flexural cracks were visible in all the specimens at the end of the first cycle at a drift of 0.25%. Damage at drifts of 0.5% consisted of hairline flexural-shear and diagonal cracks with widths of less than 0.01 in. However, as the applied drift increased, differences were observed in the behavior of the specimens that led to different failure modes. The overall behavior of each specimen will be described in the following sections and photos of the cracking patterns will also be provided. The test results for all the specimens are also summarized in Table 4-1. As noted in the table, the drift capacity of the wall is defined as the maximum drift up to which the specimen could sustain at least 80% of the peak load in each loading direction.

4.2.1 Reinforced Concrete Wall Specimens

Specimen S1, with a wall shear span-to-length ratio of 1.2, was constructed with regular concrete and detailed according to the seismic provisions of Chapter 21 of the ACI Code (ACI Committee 318, 2005). This specimen sustained a drift of 2.3% with an average peak shear stress of $5.9\sqrt{f_c'}$ (psi) ($6.2\sqrt{f_c'}$ and $5.5\sqrt{f_c'}$ (psi)) for the positive and negative loading direction, respectively). The main crack formation in Specimen S1 had already occurred by the end of the 0.7% drift cycle and it consisted of three major diagonal cracks in each direction and some hairline-size flexural cracks. As the test progressed, the existing diagonal cracks extended and widened and at 1.0% drift, the maximum diagonal crack width was approximately 0.03 in. Fig. 4-6(a) shows the damage of Specimen S1 at 1.0% drift. At drifts larger than 1.0%, the damage in the wall concentrated at a few major diagonal cracks and in the cold joint at the wall-foundation interface. Vertical cracking in the wall compression zone and some concrete spalling at the wall edges was noticeable at the base of the wall at a drift of 1.7%. In the last loading cycles, damage was concentrated in the lower part of the wall with diagonal crack widths of up to 0.12 in. On

the wall tension side, there was a gap of approximately 0.2 in. at the interface between the bottom of the wall and the base block due to yielding and slip of the main vertical reinforcement. At this stage, sliding shear deformations at the wall base clearly governed the behavior of the specimen and a decision was made to terminate the test, even though the wall could still sustain 90% of the peak load. Fig. 4-6(b) shows the state of damage for Specimen S1 at the final drift of 2.3%, while Fig. 4-6(c) presents a close-up of the damage in the wall boundary region.

Specimen S4 had the same aspect ratio as Specimen S1, but was designed for a higher shear stress demand. For this specimen the average maximum shear stress demand was $8\sqrt{f_c'}$ (psi) ($7.7\sqrt{f_c'}$ and $8.2\sqrt{f_c'}$ (psi) for the positive and negative loading direction, respectively) and the drift capacity was approximately 1.5%. At a drift of 1.0% a more dense array of cracks had formed compared to Specimen S1, as can been in Fig. 4-7(a). Appreciable shear-related damage on the lower part of the wall was evident at the end of the 1.3% drift cycle, with measured diagonal crack widths equal to 0.07 in. At a drift of 1.5%, the wall exhibited significant concrete cover spalling and concrete crushing in the web region at the lower part of the wall. At this drift the specimen started to loose strength and the maximum crack width increased to 0.1 in. As the applied displacement increased, a rapid deterioration of the concrete core in the web of the wall was obvious, along with a residual opening of the gap at the cold joint, leading to a significant drop in the lateral load capacity during the drift cycles to 1.5% and 1.9%. The state of damage at a drift of 1.9% is shown in Fig. 4-7(b). The test was terminated after the wall was pushed to 2.4% drift and it could sustain only 30% of the peak load. After the removal of the load, the condition of the concrete core in the wall lower level was examined. Extensive cover spalling was observed at the wall boundary regions, but no indication of buckling of the main longitudinal reinforcement was observed. On the other hand, the concrete core in the wall web was crushed and several vertical bars were fractured. Figure 4-7(c) shows the extensive damage in the lower part of the wall at the end of the test. Compared to RC Specimen S1, the damage was more extensive because of the increased shear stress reversals applied to Specimen S4.

Specimen S6, with a shear span-to-wall length ratio of 1.5, sustained a maximum shear stress equal to $6.7\sqrt{f_c'}$ (psi). The damage progress in the early cycles was similar to that in the other reinforced concrete specimens. An array of intersecting diagonal cracks had already formed in the web of the wall at a drift of 0.5%, along with several hairline-size flexural-shear cracks that propagated towards the compression zone. The damage at the drift level of 0.9% can be seen in Fig. 4-8(a) and is similar to that in Specimen S1. A maximum crack width of 0.02 in. was measured at this drift level. Gradual opening of the existing cracks rather than the development of new cracks, as well as damage concentration at the wall compression corner as a result of the initiation of a sliding shear mechanism, characterized the damage progression up to a drift of 1.4%. In the cycles leading to a drift of 1.9%, there was deterioration of the concrete in the compression zone and eventually concrete crushing in the wall compression edges, but no significant loss of the lateral load capacity was observed. The test was not continued after the drift level of 2.1% because of the substantial damage in the wall boundary elements. Vertical splitting along the longitudinal reinforcement in the boundary elements was also noticeable. Fig. 4-8(b) shows the state of the damage for Specimen S6 at the end of the test, while a close-up of the boundary region is shown in Fig. 4-8(c).

Specimen S9 had the same geometry as Specimen S6, but the maximum applied shear stress was equal to $9.5\sqrt{f_c'}$ (psi). In the cycles leading to a drift of 0.7%, several flexural cracks formed and intersecting flexural-shear and diagonal cracks extended towards the wall compression zone, as can been in Fig. 4-9(a). At this stage, the damage state was characterized by narrower crack spacing and slightly wider crack widths compared to Specimen S6. During the cycle at 1.0% drift, the opening of a 0.1 in. wide gap was noticed on the tension face at the wall base. Specimen S9 maintained its strength up to a drift of 1.2%. At this drift, the maximum diagonal crack width was equal to 0.08 in. and 0.15 in. for the web and boundary region, respectively. Vertical splitting cracks were also observed at the wall edges. The wall of Specimen S9 experienced a drop in the lateral load-carrying capacity during the cycle leading to a drift of 1.5%. Significant concrete cover spalling and concrete crushing at the lower portion of the wall was evident at a drift

of 1.8%. At this drift level, the specimen had lost approximately 25% of its peak load. Fig. 4-9(b) shows a close look at the wall boundary region after the 1.8% drift cycle was completed. At the final drift of 2.2%, severe damage concentration at the compression edge in the lower part of the wall was observed, as can be seen in Fig. 4-9(c). Examination of the wall after the end of the test revealed several fractured vertical web bars and a severely damaged wall web.

4.2.2 High-Performance Fiber Reinforced Concrete Wall Specimens

Specimen S2 had the same aspect ratio as Specimen S1, but was constructed with a hooked steel fiber reinforced cementitious material. The provided horizontal and vertical web distributed reinforcement was only one-third compared to companion RC Specimen S1 and the confining reinforcement in the boundary regions was completely eliminated. Despite the relaxed reinforcement detailing, Specimen S2 sustained a drift of 3.0% with a maximum shear stress of $4.1\sqrt{f_c'}$ (psi) and $4.7\sqrt{f_c'}$ (psi) in the positive and negative loading direction, respectively. Up to a drift level of 1.2%, minor shear-related damage was observed in the wall, as can been seen in Fig. 4-10(a). At this stage the maximum diagonal crack width was approximately 0.02 in., but a gap along the base cold joint could already be seen. At a drift of 1.5%, no appreciable damage was observed on the extreme compression fibers at the wall base for both loading directions even though no confinement reinforcement was used in the wall boundary regions. Several cracks, however, had formed in the wall boundary regions. As the wall was displaced to a drift of 1.5%, some new vertical splitting cracks formed in the compression zone at the wall base (Fig. 4-10(b)). At this stage, several cracks of smaller width compared to RC Specimen S1 were observed, as the fibers were effective in bridging these cracks. In addition, concrete spalling was minor, even at the boundary regions. As the applied displacement increased to 2.3% drift, the wall was able to maintain its strength in the negative loading direction, but experienced some loss of strength in the positive loading direction. At a drift of 3.0%, it was obvious that the slip at the wall base was excessive and the test was terminated. Fig. 4-10(c) shows the extent of the damage at the end of the test, while a close-up shot of the boundary region is shown in Fig. 4-10(d). It should be mentioned

that no dowel reinforcement at the wall base was added in this specimen, in an effort to evaluate whether strengthening the cold joint at the wall base was needed in very short walls in which shear deformations, rather than flexural yielding, would likely dominate the wall behavior. However, as it will be discussed in Section 4.6, the results from the test of Specimen S2 clearly indicated the need for such reinforcement in order to prevent the opening of a wide through crack at the wall base that can adversely control the wall behavior.

Specimen S5 was constructed with a self-consolidating HPFRC material with high strength hooked steel fibers and was designed to resist a higher shear stress demand (approximately $6.5\sqrt{f_c'}$ (psi)) compared to Specimen S2. Specimen S5 exhibited a drift capacity of 1.5%, as companion RC Specimen S4, despite the relaxation in the confinement reinforcement in the wall boundary regions (one-fourth of the confinement reinforcing ratio provided in Specimen S4). In terms of damage progression, up to the drift at which the wall experienced the peak load (0.85%), a significantly larger number of flexural and diagonal cracks was observed compared to Specimen S4, which can be attributed to the multiple cracking behavior of the strain-hardening HPFRC matrix (Fig. 4-11(a)). Diagonal crack widths of about 0.02 in. were measured at this stage. At the drift of 1.3%, the damage started concentrating at the horizontal crack that formed along the end of the bonded region of the dowel bars, as can be seen in Fig. 4-11(b), and the wall started to experience a gradual loss of strength. At a drift of 1.7%, the maximum width of this horizontal crack was 0.1 in. and a noticeable slip was observed along this crack. In addition, concrete spalling was considered relatively minor compared to that in Specimen S4 and no vertical splitting at the boundary elements was observed. In the cycle leading to a 1.9% drift, the pull-out of the fibers bridging the horizontal crack was followed by significant sliding shear deformations that led to a 30% loss of the specimen strength. At this stage, concrete spalling was relatively minor and there was no indication of instability in the boundary regions despite the low confinement reinforcement ratio (Fig. 4-11(c)). The test continued up to a drift of 2.4% and the extensive damage along the

horizontal crack at the end of the bonded region of the dowels at this drift can been seen in Fig. 4-11(d).

Specimen S7 had the same geometry as RC Specimen S6, but was reinforced with a 2.0% volume fraction of hooked steel fibers. This specimen exhibited a diagonal tension failure at a drift of approximately 2.4%. Diagonal cracks started to form in the wall at 0.25% drift, along with some flexural cracks. At 0.5% drift, the wall was crossed by several diagonal cracks and at 1.0% drift, the crack width was 0.02 in. (Fig. 4-12(a)). In the subsequent drift cycles, the damage in the wall started to concentrate on these cracks, leading to a crack width of 0.08 in. at 1.5% drift. At 2.0% drift, some minor crushing was observed on the extreme compression fibers at the wall base, and there was no significant gap on the tension side at the wall-base block interface. However, flexural-diagonal cracks were observed near the end line of the dowel bars. Specimen S7 was subjected to a maximum shear stress of $6.2\sqrt{f_c'}$ (psi) and sustained about the same drift as the companion RC Specimen S6 (2.1%), even though the provided reinforcement in the web and boundary regions of the wall was significantly reduced and placed in one layer. The state of damage in Specimen S7 at the end of the test is shown in Fig. 12(b).

The damage progression in Specimen S8 with the same geometry and reinforcement as Specimen S7 but with a 1.5% volume fraction of Spectra fibers, was similar to that in Specimen S7. At 0.5% drift, the wall was crossed by four main diagonal cracks corresponding to each loading direction and at 1.0% drift, new diagonal cracks had formed with approximately 4 in. spacing and a maximum width of 0.03 in. The use of Spectra fibers resulted in a more dense array of cracks compared to Specimen S7, as can be observed in Fig. 4-13(a). At 1.5% drift, tens of hairline diagonal cracks had formed near the major cracks, and the maximum width of the major diagonal cracks was 0.06 in. On the tension side of the wall, there was a 0.15 in. gap at the interface between the wall bottom and the base block due to yielding and slip of the main vertical reinforcement. At displacements larger than 1.5% drift, the damage in the wall was concentrated on a few major diagonal cracks, and some minor crushing on the extreme compression fiber of the

wall base was observed. Specimen S8 sustained a maximum shear stress of $6.5\sqrt{f_c'}$ (psi) at a drift of 2.1%. Fig. 4-13(b) shows the condition of the specimen at 2.1% drift. At the final drift of 2.3%, the wall lost more than 20% of its peak strength.

The use of a self-consolidating HPFRC material in Specimen S10, with a shear span-to-length ratio of 1.5, led to an enhanced behavior compared to that of Specimen S9, constructed with regular concrete and reduced transverse reinforcement. It should be reminded that some problems were encountered during the casting of the wall in this specimen, as discussed in Section 3.3.1.2. Specimen S10 sustained a peak drift of 2.2% with a maximum applied shear stress of $8.9\sqrt{f_c'}$ and $8.2\sqrt{f_c'}$ (psi) for the positive and negative loading direction, respectively. During the cycles to drifts ranging from 0.15% to 0.7%, several hairline-size diagonal cracks formed for each loading direction, with the cracking progressing in the wall web and the extreme compression fiber. The maximum crack with at 0.7% drift was equal to 0.015 in. No appreciable shear-related damage was noticeable at a drift of 1.0% and a dense array of narrow flexural and diagonal cracks was observed in the wall, as in all the HPFRC specimens (Fig. 4-14(a)). At a drift of 1.4%, a horizontal crack had completely formed in the web of the wall along the end line of the dowel bars, similar to Specimen S5 (Fig. 4-14(b)). This crack connected with existing cracks at the boundary elements and in the subsequent loading cycles, damage concentrated along this crack with visible slip. At a drift of 1.9%, there was minor concrete spalling with no appreciable damage in the boundary elements (Fig. 4-14(c)) despite the relaxed confinement reinforcement and the high shear stress demands. The test was terminated at a drift of 2.2% because of damage concentration along the major horizontal crack. At this drift level, the wall could sustain more than 90% of the peak load in both loading directions. The state of damage at the lower part of the wall when the test was terminated is shown in Fig. 4-14(d).

4.2.3 Summary of Test Observations

The RC low-rise walls designed according to the seismic provisions of the ACI Code (ACI Committee 318, 2005) exhibited a stable hysteretic behavior with no premature shear failure. However, a horizontal crack at the wall-foundation interface developed in the RC walls and the sliding shear deformation mechanism had a significant effect in the wall behavior at later stages of the test. Damage concentrated in the lower part of the wall and shear-related diagonal cracking was considered moderate. Specimens S1, S6 and S9 exhibited a similar failure pattern, which was characterized by crushing on the extreme compression fibers at the wall base and vertical splitting cracks in the wall boundary regions. In Specimen S4, severe concrete spalling, followed by crushing of the web concrete, characterized the wall failure at the end of the test. In general, a more dense array of cracks developed in the RC walls that were tested at a high shear stress level (i.e. Specimens S4 and S9) compared to the specimens tested under moderate shear stress reversals (i.e. Specimens S1 and S6).

HPFRC Specimen S2 had a similar failure pattern compared to the companion RC Specimen S1, but the effect of the sliding shear mechanism at the wall base was substantially more pronounced. The addition of dowel bars in Specimens S5 and S10 resulted in flexural-diagonal cracks near the end line of the dowels that ultimately led to failure when the fibers bridging those cracks pulled-out. Specimen S8, reinforced with Spectra fibers, failed by diagonal tension, whereas loss of strength in Specimen S7 was due to a combined diagonal tension failure and opening of a horizontal crack along the end line of the dowel bars. A dense array of narrow cracks developed in the HPFRC walls. Concrete spalling, if any, was not substantial, even at drifts in the order of 2.0%. All the HPFRC test units showed a stable hysteretic behavior despite the relaxed confining reinforcing detailing in the boundary regions. Moreover, the premature sliding shear failure of Specimen S2 demonstrated the need for dowel reinforcement at the wall-foundation interface in HPFRC low-rise walls.

4.3 LATERAL LOAD VERSUS DISLACEMENT RESPONSE

The lateral load versus drift responses for all the test specimens are shown in Figs. 4-15(a) to (i). The drift in the plots corresponds to the wall lateral displacement with respect to the wall base and was calculated as described in Section 4.1.2. In each plot, a line corresponding to the probable shear demand associated to a flexural failure, V_{pr}, is shown. The probable shear demand was calculated based on the peak moment obtained from a moment versus curvature nonlinear section analysis using actual material properties. More information on the nonlinear section analysis is given in Section 5.2.3. Also shown in the plots is a line that corresponds to the nominal shear strength, V_n. In the case of the RC walls, the nominal shear strength was calculated based on the 2005 ACI Code equation (see Section 3.2.2. For the HPFRC walls, the nominal shear strength was estimated assuming a contribution from the "fiber-reinforced concrete" equal to $5\sqrt{f_c'}$ (psi), as described in Section 3.2.2. In all cases, measured steel yield strength and concrete cylinder strength were used for calculation of the nominal shear strength. The values of the probable shear demand and nominal shear strength are listed in Table 4-2.

From Figs. 4-15(a) to (i), it can be seen that the strength of the test specimens was very close to the predicted strength. Except for Specimens S7 and S8, which were designed to exhibit a diagonal tension failure, the predicted strength corresponded to the shear at peak moment calculated from a moment versus curvature analysis. In these specimens, the nominal shear strength exceeded the probable shear demand by at least 24% (Specimen S9) and by as much as 107% (Specimen S1). In Specimens S7 and S8, on the other hand, the nominal shear strength was slightly lower than the probable shear demand corresponding to a flexural failure and was very similar to the measured shear strength.

In all the specimens, significant pinching can be seen in the hysteresis loops even for low drift levels, as expected for low-rise walls, due to major effect of shear at the behavior of low-rise walls. The well known characteristic in RC elements subjected to cyclic loading of the unloading and reloading stiffness reduction is also evident in the hysteresis loops.

The pinching of the loops in the wall specimens constructed with HPFRC materials is comparable to that of the RC wall specimens. This is attributed to the fact that the fibers do not provide appreciable resistance against crack closing, despite their effectiveness in restraining crack opening. It can also be noticed that the load versus drift response for most of the specimens was not completely symmetrical, mainly due to the correction of the applied drift to account for the rigid body rotation of the specimens. During the test of the specimens, the applied lateral displacement was only corrected for the horizontal displacement of the base block, while the effect of rigid body rotation above Potentiometer P11 was accounted for only when the results were analyzed. In most cases, it was found that the rotation of the base block was larger when the actuator was "pushing" the wall, resulting in somewhat smaller actual applied drifts in this loading direction (positive direction).

The load versus displacement relationship for RC Specimen S1 is shown in Fig. 4-15(a). The specimen was loaded uni-axially in the west-east direction, the east direction being the positive direction in the plot. The first loading half-cycle to a target drift of 0.125% was in the west direction, corresponding to the actuator "pulling" the specimen. The specimen exhibited a stable hysteretic response, which indicates that RC low-rise walls designed according to the seismic provisions of the ACI Code (ACI Committee 318, 2005) can perform adequately under moderate shear demands. Yielding of the main longitudinal bars was first detected at a drift of 0.75% in the negative loading direction and by 1.2% drift, yielding had spread along the main longitudinal bars over half the height of the wall on both sides. At this drift level, sliding deformations at the base of the wall became significant for the negative loading direction, resulting in a slightly lower wall shear resistance of the specimen for this loading direction. However, the wall was able to sustain the peak load up to a drift of 2.3% and 2.5% in the positive and negative loading direction, respectively. This drift cycle was the last to be applied Specimen S1. At the end of the test, slip at the wall-foundation interface accounted for approximately 50% of the applied displacement and as a result, the flexural and shear deformation demands imposed on the wall were relatively small.

The hysteretic response of HPFRC Specimen S2 is shown in Fig. 4-15(b). The sign convention in the plot is the same as that used for Specimen S1, i.e. positive displacement corresponded to “pushing” the specimen. Specimen S2 had the same amount of boundary longitudinal reinforcement as the companion RC Specimen S1, but the web vertical and horizontal reinforcement was less than one-half of that provided in Specimen S1. In addition, no confinement reinforcement was used in the wall boundary regions, relying solely in the fibers to delay crushing of the concrete and buckling of the longitudinal bars.

In the early cycles the hysteretic response of Specimen S2 was similar to that of Specimen S1, but a reduced stiffness was recorded for the positive loading direction for no apparent reason after 0.5% drift. The main longitudinal reinforcement started yielding at a drift of 0.7% and 0.9% for the negative and positive loading direction, respectively. At this drift level, strains above yield were recorded up to the mid-height of the wall. In the cycle after the onset of yielding of the main vertical reinforcement, the peak shear stress was reached, with a smaller value in the positive loading direction compared to the negative loading direction. Sliding shear deformations at the cold joint were clearly significant at this point. The slip along the horizontal crack at the wall base for the positive loading direction was approximately 8 times that for the negative loading direction, which resulted in a reduced strength and stiffness for the positive loading direction. Specimen S2 sustained the full peak stress in the negative loading direction (up to approximately 3.0% drift) and more than 80% of the peak stress in the positive loading direction at a drift of 2.3%. After the cycle to 2.3% drift was completed, the drift was unintentionally increased to approximately 3.0% in the positive loading direction. At this drift level no loss of strength was observed, but the test was terminated because excessive base sliding shear deformations had occurred and the wall was “rocking” about its lower corners, with minor flexural and shear deformation demands above the wall base.

Figs. 4-15(c) and (d) show the lateral load versus drift response for Specimens S4 and S5, respectively. Specimen S4 was constructed with regular concrete, whereas a self-consolidating HPFRC material was used in Specimen S5, allowing for some relaxation in

the required reinforcement. Dowel bars were also used to strengthen the wall-foundation interface, based on the test results of Specimen S2. The initial cracked stiffness for both specimens was greater compared to that of Specimens S1 and S2 because of the increased longitudinal reinforcement ratio. Yielding in the main longitudinal bars in the boundary region was first detected at a drift of approximately 0.4%, and strains above yield were recorded in the main vertical reinforcement over half the height of the wall. In Specimen S5, the strains in the dowel reinforcement were below the yield strain. RC Specimen S4 wall sustained a peak load 20% greater than that of the HPFRC low-rise wall because of the greater flexural capacity of Specimen S4. As can be seen in the plots, HPFRC Specimen S5 exhibited a gradual loss of strength and stiffness for drifts larger than 1.0% and maintained at least 80% of the peak strength up to approximately 1.5% drift. On the other hand, strength degradation was faster in RC Specimen S4 due to the extensive concrete crushing in the lower part of the wall. However, Specimen S4 could be considered to have approximately the same drift capacity as Specimen S4.

Fig. 4-15(e) shows the hysteretic response for RC Specimen S6, with a wall shear span-to-length ratio of 1.5. The load versus drift response was very similar to that of the shorter RC Specimen S1. The wall sustained the peak stress of $6.7\sqrt{f_c'}$ (psi) up to a drift of 2.1%, despite the damage in the extreme compression fibers at the wall base. A stable hysteretic response was also exhibited by Specimens S7 and S8, as shown in Figs. 4-15(f) and (g), respectively. The shear stress that was sustained by these specimens was approximately equal to that of the control RC Specimen S6. Specimens S7 and S8 did not experience any significant loss of strength up to 2.1% drift. The type of the fibers used (hooked steel fibers versus Spectra fibers) did not seem to affect the deformation capacity of the specimens and the ultimate drift for both specimens was 2.1% and 2.3% for Specimens S7 and S8, respectively.

The hysteretic response for Specimens S9 and S10, the two specimens with a shear span-to-wall length ratio of 1.5 that were tested under high shear stress reversals, is given in Figs. 4-15(h) and (i), respectively. Specimen S9 was constructed with regular reinforced

concrete, whereas hooked steel fibers were used in Specimen S10, which had reduced web distributed and confining reinforcement ratios compared to those in RC Specimen S4. The load versus displacement response was quite similar in the two test walls for drifts up to 1.5%. In the cycle leading to a drift of 1.75%, a substantial loss of strength was observed for Specimen S9 due to concrete crushing in the lower part of the wall. The HPFRC specimen, on the other hand, sustained most of the peak load with a rather gradual loss of stiffness up to a drift of 2.2%. Fig. 4-16 shows a comparison plot for the shear stress (normalized by $\sqrt{f_c'}$ in psi units) versus the drift response for these two specimens. The peak shear stress level sustained by the HPFRC specimen was slightly lower than that for the RC wall due to differences in longitudinal reinforcement detailing. The stable hysteretic response and enhanced deformation capacity of Specimen S10 under such high level of shear stress and despite the reduced reinforcement detailing is a clear indication of the ability of the HPFRC material to contribute to wall shear strength and deformation capacity.

4.4 LOAD VERSUS DRIFT ENVELOPE RESPONSE

The load versus drift envelope response for all specimens is plotted in Figs. 4-17(a) to (i). In the figures, every point in the envelope represents the maximum drift and corresponding load in each cycle. The first and second cycles to each drift level are plotted separately with a solid and dashed line, respectively. The values of maximum drift and load in each cycle for all the specimens are listed in Tables 4-3 to 4-11.

Specimens S4, S5, S9 and S10, designed for a higher shear stress level, seemed to have a higher stiffness compared to the rest of the specimens, especially in the earlier cycles. Even though an increased initial stiffness was expected due to the higher reinforcement ratio, this observation should be taken with some precaution because of the difference in the calculation of wall drift, as discussed earlier (see Section 4.1.2). The applied displacement in Specimens S1, S2, S6, S7 and S8 was not corrected to account for potential slip in the load application mechanism and as a result, the response of these specimens was slightly “softer”, especially in the earlier drift cycles.

Within the elastic range, the load versus drift envelope response for the second cycle at each drift was very similar to that for the first cycle. A small decrease in strength was observed in some test units after the peak load.

4.5 AVERAGE SHEAR STRAINS

As it was discussed in Section 4.1.3, the average wall shear strain was calculated using two diagonal potentiometers (see Figs. 3-28 and 3-29) over a wall area of $27\ \text{in.} \times 27\ \text{in.}$ The lateral load versus average shear distortion response for all test units except fir Specimen S1 is shown in Figs. 4-18(a) to (h). During the test of Specimen S1 the two diagonal potentiometers performed poorly and no meaningful calculation could be made for the average shear strain. As was discussed earlier, the RC walls generally experienced concrete spalling for drifts larger than 1.5%. As a result, the readings from the potentiometers were affected and the data presented had to be cut off when they were considered unreliable. This was not the case for the HPFRC specimens.

For specimens where the Optotrak markers were also used, the average shear strain calculated from Eq. (4-4) could also be obtained using the data from the corner markers over a wall area of $25\ \text{in.} \times 25\ \text{in.}$ (see Fig. 3-30). A comparison of shear strains obtained through the two instrumentation schemes is presented in Fig. 4-19 for Specimen S5. The two instrumentation schemes generally gave similar results, but the potentiometers slightly underestimated the shear distortion of the wall.

The load versus average shear strain hysteresis loops for all the RC and HPFRC walls except for Specimen S2 (and Specimen S1 for which data were not reliable) exhibited significant pinching. As it was discussed earlier, pinched hysteresis loops are expected for the HPFRC specimens since the fibers that bridge the cracks cannot offer appreciable resistance during crack closing, leading to a lower stiffness until the cracks are fully closed, as is the case for RC members.

Generally, the shear distortion capacity of the RC specimens was not significantly affected by either the wall aspect ratio or the level of the applied shear stress. The RC walls exhibited smaller shear strains compared with the HPFRC specimens, especially for drifts after peak load. Figs. 4-18(b) and (g) show the load versus shear strain hysteresis loops for Specimens S4 and S9, respectively. The data were clipped off at about 1.9% and 1.2% drift for Specimens S4 and S9, respectively, and the two walls exhibited similar behavior up to shear strains of approximately 0.005 rad (up to 1.0% drift). As it can be seen in Fig. 4-18(b), Specimen S4 sustained a shear distortion of 0.007 rad and 0.014 rad in the positive and negative loading direction, respectively, before a significant drop in strength occurred at 1.9% drift. At this stage, the shear related damage could be described as moderate. Shear strains were slightly smaller in Specimen S9, with values of about 0.005 rad at 1.2% drift. As can been seen in Fig. 4-9(c), the damage in Specimen S9 was concentrated at the bottom corners of the wall, resulting in smaller shear distortions. Fig. 4-18(d) presents the load versus average shear distortion response for Specimen S6 up to a drift of 1.6%. The maximum shear strain measured up to that stage was approximately 0.007 rad and the overall behavior was similar to that in the other RC walls. Based on the above results, and even though shear strains could not be accurately measured up to failure of the RC specimens, it can be concluded that moderate shear related damage in RC walls is associated with shear strains varying between approximately 0.005 rad and 0.007 rad .

The load versus shear distortion response for the wall of Specimen S2 is shown in Fig. 4-18(a). Specimen S2, reinforced with hooked steel fibers, exhibited minor shear-related damage with a maximum shear strain of 0.002 rad (negative loading direction). It is clear that shear deformations had a negligible role in the behavior of Specimen S2, which was governed by the sliding shear mechanism as well as rocking at the base of the wall, as explained earlier. It is worth mentioning that the shear strains were even smaller in the positive loading direction, for which the recorded slip at the cold joint was greater and less diagonal cracking was observed.

Shear distortions in all the other HPFRC specimens (Specimens S5, S7, S8 and S10) were larger when compared to their companion RC specimens. Shear strains in excess of 0.02 rad were recorded in these specimens and only minor shear related damage was evident in the walls at distortions of about 0.01 rad. Damage localization started at shear strains larger than 0.015 rad, which can be conservatively considered as the shear distortion capacity of the HPFRC specimens.

Figs. 4-20(a) and (b) show the shear distortion versus drift envelope curves for the half-cycle direction that corresponded to the larger shear strain values (positive or negative loading direction) for the RC and HPFRC specimens, respectively. From the figures, it is clear that the rate of shear strain increase was larger for the HPFRC specimens compared to the RC specimens. It can also be seen that the shear strains for Specimen S2 were insignificant and basically had no effect on the behavior of the wall specimen. For drifts lower than 1.0% (limited yielding had occurred at this drift level) the shear distortion was approximately 0.005 rad for all the HPFRC specimens, except for Specimen S2. For drifts larger than 1.0%, on the other hand, the shear strains increased at slightly different rates in the HPFRC walls and at a drift of 2.0%, the maximum shear strain ranged between 0.018 and 0.024 rad, with Specimen S5 sustaining the largest shear distortion.

A comparison of the shear distortion calculated using Eq. (4-4) and by averaging the shear strain calculated over the different longitudinal strips along the wall is presented in Fig. 4-21 for Specimen S4. For drifts up to 1.0% there is good agreement between the two methods. For the cycles leading to a drift of 2.0%, however, shear distortions calculated using Eq. (4-4) overestimated the shear distortion with an error in the range of 10% to 20%. For drifts larger than 2.0%, the difference in the results from the two methods seemed to increase, but the error estimate is not considered accurate because the recorded data could be unreliable due to concrete spalling. It is worth mentioning that Massone and Wallace (2004), based on slender RC wall tests, reported that the calculation of shear distortions using the diagonal transducers mounted within the

yielding region of the wall tends to overestimate the shear distortion by as much as 30%. This conclusion generally agrees with the results from this study.

Fig. 4-22(a) shows the shear strain versus drift envelope response for the different strips (see Fig. 4-4) in Specimen S4 (only the positive loading direction is shown) calculated from the Optotrak markers data. A similar response was obtained for the RC Specimen S9. For drifts up to 0.75%, the shear strain was similar for all the strips. However, as the applied displacement increased, the lower part of the wall (strip 1) exhibited increased shear strains. Shear strains of up to 0.01 rad were measured in wall strips 2 through 5, whereas for drifts larger than 1.0% the shear strain in the lower strip increased rapidly with drift, reaching strains in excess of 0.06 rad. This is explained by the concentration of shear-related damage on the lower part of the wall after the peak load was reached.

In contrast, increased shear strain values were recorded over a larger area of the wall for the HPFRC Specimens S5 and S10. The shear strain versus drift envelope for the positive loading direction in Specimen S10 can be seen in Fig. 4-22(b). Wall strips 1 and 2 exhibited a similar increase in the shear strain after a drift of 0.75%, with strains of about 0.06 rad at the end of the test. It is worth mentioning that Specimens S5 and S10 were reinforced with dowel bars at the wall-foundation interface and a major horizontal crack formed in the region where the bonded area of the dowel bars terminated. Horizontal slip occurred along this crack, which affected the measured values of shear strain for strips 1 and 2, especially during the last drift cycles.

4.6 SLIDING SHEAR RESPONSE

The horizontal slip at the wall-foundation interface was monitored with the use of potentiometer P12 (see Figs. 3-28 and 3-29), as discussed previously. Fig. 4-23(a) shows the load versus the base horizontal slip response for Specimen S1. The overall sliding shear response was not symmetrical for the two loading directions and after the cycle to a drift of 0.5%, residual slip started accumulating in the negative loading direction. As a

result, the shear and flexural deformation demand imposed on the wall was greater in the positive loading direction and yielding of the longitudinal bars at the boundary zone initiated at a drift of 0.7% for the positive loading direction compared to 1.2% drift in the negative loading direction. The slip kept increasing in the negative loading direction, reaching a maximum value of 0.55 in. during the last drift cycle. The load versus slip hysteresis loops exhibited the well-known pinching resulting in low energy dissipation capacity for this deformation mechanism.

Significant slip was also recorded in RC Specimen S6, as can be seen in Fig. 4-23(b). For drifts up to 0.75% the slip was not substantial, with values of less than 0.05 in. After the onset of yielding of the longitudinal bars in the boundary regions, the wall exhibited increased sliding shear deformations, especially in the positive loading direction. The contribution of slip to the overall deformation of the wall in the negative loading direction was fairly constant throughout the test, but the wall experienced a larger rate of slip increase in the positive loading direction. In the last drift cycle a slip of 0.5 in. was recorded, as in Specimen S1.

RC Specimens S4 and S9, which were designed to sustain an increase shear stress demand, experienced less slip at the cold joint compared with Specimens S1 and S6. The load versus slip response for Specimens S4 and S9 can been seen in Figs. 4-23(c) and (d), respectively. The maximum slip was approximately 0.25 in. in both specimens before a significant drop in load occurred. The observed decrease in slip compared to that in Specimens S1 and S6 can be attributed to the increased dowel action of the vertical reinforcement, which led to increased contributions from flexural and shear deformations to the total drift. In addition, a comparison of the load versus slip response of the RC specimens did not reveal any influence of wall aspect ratio on the sliding shear deformations at the base of the walls.

For Specimen S2 the potentiometer that was used to monitor the slip at the cold joint did not work properly for most of the test and reliable results could only be obtained after the second cycle to a drift of 1.75%. The measured load versus slip response from that point is shown in Fig. 4-24. As can be seen, the recorded slip at peak displacement for each cycle was almost constant and, as discussed earlier, the wall experienced larger slip in the positive loading direction. The sliding shear mechanism in Specimen S2 was initiated early in the test due to the lack of fibers crossing the wall-foundation interface (and its effect on concentration of inelastic flexural deformation at the cold joint) and the insufficient dowel action of the vertical reinforcement at the cold joint. Despite the low aspect ratio of the wall, the concentrated flexural deformations at the wall base were large enough to result into a sliding shear failure for this specimen.

All the other HPFRC walls (Specimens S5, S7, S8 and S10) were reinforced with dowel bars at the cold joint. The addition of the dowel bars forced flexural yielding to primarily occur above the base of the wall and the measured slip at the wall base did not exceed 0.2 in. for all the HPFRC specimens with dowel bars. However, sliding shear deformations occurred at the section where the bonded portion of the dowel reinforcement ended and a predominant horizontal crack developed. For Specimens S5 and S10 it was possible to obtain data on slip along the horizontal crack using the data from the Optotrak system markers (see Fig. 3-30). The hysteresis loops are presented in Figs. 4-25(a) and (b) for Specimen S5 and S10, respectively. In both specimens the measured slip was below 0.15 in. up to the peak load. In the following cycles, the slip increased at a faster rate, with a noticeable decrease in the slip stiffness and significant pinching. However, the slip behavior was relatively stable with maximum values of slip of approximately 0.5 in. at the end of the test. The effect of the slip along the horizontal crack at the end line of the dowel bars was less significant in Specimens S7 and S8, which failed predominately by diagonal tension.

4.7 HORIZONTAL WALL DILATIONS

Wall dilations were measured through potentiometers P3 and P4 (see Fig. 3-28 and 3-29). In the lower part of the wall, the potentiometers were placed at 4 in. from the wall base, whereas in the top part of the wall they were positioned at 31 in. from the base. As a result, for specimens with a shear aspect ratio of 1.2, dilations were obtained at a height of 0.1*h* and 0.8*h*, whereas for the walls with a shear span-to-length ratio of 1.5, dilations were measured at a height of 0.1*h* and 0.6*h*, where *h* refers to the wall height excluding the top block.

Figs. 4-26(a) to (c) show the measured dilations at a height of 0.1*h* and 0.6*h* for Specimens S6, S7 and S8, respectively. The dilations at a height of 0.6*h* in RC Specimen S6 were 3 to 4 times greater than those at the base of the wall, but were below 0.1 in. throughout the test (average strain of 0.37%). The same trend was recorded in HPFRC Specimen S8, but the dilations were larger, with maximum values of 0.1 in. (average strain of 0.37%) and 0.3 in. (average strain of 1.1%) at the bottom and top of the wall, respectively. In contrast, dilations in HPFRC Specimen S7 at a height of 0.1*h* and 0.6*h* were similar up to drifts of 2%, with values of up to 0.2 in. (average strain of 0.74%). Beyond 2% drift, the dilations at the wall base became unsymmetrical and greater than 0.6 in. (average strain of 2.2%).

A comparison of the dilations at the base of the wall for Specimens S9 and S10 is presented in Fig. 4-27. Greater dilation values were obtained for HPFRC Specimen S10, which correlates well with the spread of the damage in the lower part of the wall because of sliding along the horizontal crack at the end of the bonded portion of the dowel bars.

Generally, no significant trend could be obtained with regards to the dilations for the RC and HPFRC specimens. However, the measured dilations seemed to correlate well with the damage in the specimens.

4.8 ROTATIONS

4.8.1 Concentrated Rotations at the Wall Base

As described in Section 4.1.4, the concentrated flexural deformations at the wall base (over 2 in.) were calculated using the recorded data from potentiometers P7 through P10 (see Figs. 3-28 and 3-29). During the drift cycles leading to failure, there was concrete spalling and crushing and thus, data recorded from the potentiometers became unreliable for some specimens. The data were therefore cut off at the point beyond which the potentiometer measurements were believed to be unreliable. Figs. 4-28(a) to (i) show the lateral load versus concentrated rotation at the base of the wall for all the specimens. The concentrated rotation at the wall base was strongly related to the crack opening on the tension face at the bottom of the wall. As a result, the load versus rotation hysteretic response became distinctly pinched after the vertical wall reinforcement yielded at the wall base.

In Fig. 4-28(a) the lateral load versus concentrated rotation response for Specimen S1 was clipped in the second 1.0% drift half-cycle in the positive loading direction, while the entire data for Specimen S2 are presented in Fig. 4-28(b). Concentrated rotations were small (below 0.002 rad) in both specimens at the onset of yielding of the wall main vertical reinforcement. For the RC specimen the concentrated rotation remained small (approximately 0.003 rad) up to the drift of 1.0%, when the potentiometers stopped functioning properly. In Specimen S2, for drifts larger than 1.0%, the concentrated rotations increased at a faster rate for the negative loading direction compared with the positive loading direction. The maximum value for the concentrated rotation for the negative loading direction was approximately 0.01 rad, whereas the maximum rotation demand at the wall base in the positive loading direction was 5 times smaller because of the substantial contribution of slip to the total drift in this loading direction.

The response of RC Specimen S4 in terms of concentrated rotations is shown in Fig. 4-28(c), while for HPFRC Specimen S5 the data were cut off at the end of the cycle to

1.4% drift (Fig. 4-28(d)). The response of both specimens remained linear up to the onset of yielding of the longitudinal reinforcement at a drift of 0.4%. At this stage the measured concentrated rotation was, on average, approximately 0.001 rad. Up to a drift of 1.0%, both specimens exhibited similar response with rotations smaller than 0.004 rad. For larger drifts, the rotation remained relatively constant for the HPFRC specimen (Specimen S5) with a value of 0.005 rad up to the time the potentiometers started performing poorly. In contrast, after the cycle to 1.0% drift, the rotations in Specimen S4 increased faster compared to the previous cycles, with a maximum concentrated rotation at failure of approximately 0.01 rad.

The behavior of Specimen S6 is shown in Fig. 4-28(e) up to a drift of 1.4%. Small concentrated rotations (less than 0.002 rad) were measured at a drift of 0.6% when yielding of the longitudinal reinforcement started. Specimen S6 exhibited higher rotations compared to Specimen S1 up to a drift of 1.0% (between 0.0025 rad and 0.004 rad). At a drift of 1.4%, a rotation of 0.007 rad was measured in the negative loading direction, whereas the wall exhibited a substantially smaller rotation in the positive loading direction (approximately 0.002 rad). As can been seen in Figs. 4-28(f) and (g), Specimens S7 and S8 exhibited similar behavior up to a drift of 1.3%, at which the data were cut off for Specimen S8. At this stage, the peal rotation for Specimens S8 was 0.013 rad. The rotation at peak load was approximately 0.004 rad for Specimen S7, and a value of 0.007 rad was measured at the end of the test.

RC Specimen S9 exhibited slightly larger rotations compared to the shorter RC Specimen S4. The load versus concentrated rotation response for this specimen is shown in Fig. 4-28(h) only up to a drift of 1.0%. At this level the average rotation was 0.006 rad and 0.01 rad for the positive and negative loading directions, respectively. The response for HPFRC Specimen S10 is presented in Fig. 4-28(i). This specimen exhibited similar behavior compared with that of RC Specimen S9 up to a drift of 1.0% and by the end of the test (drift 2.2%), the wall had sustained a concentrated rotation of 0.006 rad.

4.8.2 Distribution of Rotations along the Wall Height

The maximum total rotations at three sections over the wall height (excluding the top block), h, measured during the first cycle at each drift level, are shown in Figs. 4-29(a) to (i). The average value of the rotation for the two loading directions is plotted in the figures. In Specimen S1, the maximum wall rotations at the height of $0.5h$ were about two times those at the height of $0.1h$ and the rotations kept increasing with the increase of drift level. In Specimen S2 most of the rotation experienced by the wall was concentrated at the height of $0.1\ h$, whereas the rotation at the height of 0.5 h was smaller compared with Specimen S1. This correlated well with the predominant sliding shear deformations observed at the bottom of the wall in Specimen S2.

A similar trend was observed in the rotations of Specimens S4 and S5, but the HPFRC specimen (Specimen S5) exhibited larger rotations at a height of $0.1h$ and $0.2h$ due to the horizontal crack that developed in the section where the bonded region of the dowel bars terminated. The rotations kept increasing with an increase in drift for both specimens up to a drift of 1.3%. At this point the shear deformations became more significant and maximum rotations started decreasing.

The rotations in RC Specimen S6 were similar to those in Specimen S1. Up to a drift of about 1.3% the rotations at a height of $0.9h$ were almost two times those at the height of $0.1h$. For larger drifts, though, the rotations at a height of $0.1h$ increased at a faster rate and a maximum value of 0.005 rad was recorded at the end of the test. HPFRC Specimen S8 exhibited a similar tendency as RC Specimen S6. For HPFRC Specimen S7, however, the maximum rotations at a height of 0.6h and 0.9h started decreasing beyond 1.8% drift. This phenomenon correlates well with the fact that the dilations at the wall base of Specimen S7 were significant after 2.0% drift, which resulted in damage concentration at the lower part of the wall. After the drift cycle at 1.8% drift, the rotations at $0.1h$ in Specimen S7 could not be accurately measured and therefore, were not included in the plot.

RC Specimen S9 had a very similar behavior compared with RC Specimen S4, but Specimen S9 exhibited slightly larger rotations. At a height of $0.1h$, the rotations were more significant when compared with the rotations at a height of $0\ 0.2h$, $0.35h$ and $0.55h$. For drifts larger than 1.3%, the rotations remained fairly constant since shear distortions started contributing more significantly to the overall drift. In HPFRC Specimen S10, the rotations at the lower part of the wall ($0.1h$) were constant for drifts ranging from 1.0% to 2.0%, whereas the rotations at a height of $0.2h$ increased at a nearly constant rate with an increase in drift and were up to 3 times larger than the rotations at a height of $0.1h$. Substantial rotations were also observed at a height of $0.35h$, but these rotation decreased for drifts beyond 1.8%. At this drift level the rotations in the lower part of the wall started to increase rapidly due to damage concentration at the horizontal crack along the end line of the dowel bars.

4.9 STEEL STRAINS

Strains in the reinforcing steel were measured through linear strain gauges. The strain gauges were attached at several locations on the main vertical reinforcement, the web vertical and horizontal reinforcement, and the dowel bars. The location and label for the strain gauges in each specimen is shown in Appendix A (Figs. A-1 to A-8). Before discussing the strains recorded in the test units it should be mentioned that strain measurements in reinforcing bars embedded in fiber reinforced concrete tend to be more sensitive to crack location than those in bars embedded in regular concrete, which is attributed to the increased bond strength provided by the fibers (Chao et al., 2009). Thus, the measured strains should not be taken as the only indicator of the degree of inelastic activity in the wall specimens. Wall rotations and the distribution of curvature along the wall height also provide a measurement of the inelastic deformations experienced by the specimens.

In Specimen S1 strains above yield were first recorded in the main vertical reinforcement at the wall edge near the base (gauges V1, V2 and V3) during the cycle at 0.95% drift. Yielding spread to mid-height of the wall (gauges V4, V5 and V6) and all strains gauges

placed on the vertical main and web reinforcement in the lower part of the wall indicated yielding of the steel. Strains in the main vertical reinforcement at the wall edges located at the top of the wall (gauges V8, V9) exhibited strains closed to the theoretical yield value. For drifts exceeding 1.3%, a residual tensile strain at the end of each cycle was measured in the vertical reinforcement because the bars experienced less compression strain demands compared to the tension strain demands due to crack opening and wall "growth". At the end of the test, tensile strains in the vertical reinforcement of approximately 1% and 2% were recorded at the base and mid-height of the wall, respectively. The strain histories for gauges V1 and V5, located at the bottom and the mid-height of the wall of Specimen S1, respectively, are presented in Fig. 4-30.

Strains in the horizontal bars remained elastic throughout the test and little difference could be seen between the strain histories recorded at different locations in the horizontal bars. The strains did not exceed 0.1% and a characteristic strain response is presented in Fig. 4-31 for a horizontal bar located at $0.1h$ from the wall base (gauge H4). It is worth mentioning that the theoretical yield strain, as obtained from tensile tests, was 0.33% for the smooth No. 2 horizontal bars used in Specimen S1.

For the companion HPFRC Specimen S2, a similar strain history response was observed in the main vertical reinforcement at the base of the wall compared with Specimen S1. As was discussed earlier, the imposed flexural deformation demands were greater in the negative loading direction because of the unsymmetrical sliding shear response for this specimen. As a result, yielding was first detected in the bars that were in tension for the negative loading direction (gauges V4, V2 and V5) during the cycle to a drift of 0.65%. On the hand, for the positive loading direction, strains above yield were first recorded during the cycle to a drift of 1.3%The spread of yielding was limited and at wall mid-height the maximum strain at the end of the test was approximately 0.3%.. Strains in the horizontal reinforcement were smaller compared to those in Specimen S1, which was consistent with the minor shear-related damage observed in the wall.

In Specimen S4, readings from the strains gauges located at the bottom of the wall (gauges F1-1 and F1-2) gave indication of yielding at a drift of 0.5%. Yielding of the main vertical reinforcement extended over at least $0.25h$ and at mid-height of the wall, a strain of 0.3% was recorded at 1.0% drift, just before the strain gauges at this location stopped giving reliable data. The vertical web reinforcement remained elastic for most of the test and the theoretical yield strain of 0.3% was exceeded at a drift of 1.7% at gauges located at $0.25h$ from the wall base (gauges V1-1 and V1-2). A representative strain response for the vertical web bars is shown in Fig. 4-32. The high shear stress demand in RC Specimen S4 resulted in larger strains in the horizontal web reinforcement compared to those in Specimen S1. At a drift of 1.0%, strains in the horizontal bars of 0.2% were recorded at all the instrumented locations. Inelastic strains were measured in the horizontal bar located at $0.25h$ from the base of the wall (gauges H3-1 and H3-3).

Similar observations were made in Specimen S5 with regards to the recorded strain histories in the main vertical reinforcement. The inelastic activity was limited to approximately $0.5h$ from the base of the wall and the strains were in the range of 0.3% to 0.5% (generally larger than those in Specimen S4). The dowel bars that were added to reinforce the wall-foundation interface remained elastic, but strains in the range of 0.08% to 0.16% were measured in these bars. The strains in the web vertical and horizontal reinforcement were generally similar to those in Specimen S4. Yielding in some horizontal bars took place for drifts larger than 1.5%. Fig. 4-33 shows the recorded strain history obtained for a horizontal bar located at $0.5h$ for Specimens S4 and S5 (gauges H4-1 and H5-1, respectively).

There was no significant difference in the strain histories for RC Specimen S6 when compared with RC Specimen S1. In the lower part of the wall strains in excess of 2.0% were recorded in the main vertical reinforcement at the boundary regions. Fig. 4-34 presents the strain history for a strain gauge located in the mid-height of the wall (gauge V19) with a maximum recorded strain of 0.6%. Strains in the web vertical and horizontal reinforcement were either below or approximately at the theoretical yield strain. A

representative strain history for horizontal bars located at $0.2h$ and $0.5h$ from the wall base can be seen in Fig. 4-35.

Readings from linear strain gauges attached to the vertical reinforcement in Specimens S7 and S8 revealed that most of the reinforcement yielded during the cycles ranging from 0.8 to 1.3% drift. First yielding of the main vertical reinforcement was observed at 0.8% drift in Specimen S7, and at 1.0% drift in Specimen S8. The dowel bars did not yield during the test, as was also observed in Specimen S5, but their maximum strain was as large as approximately 0.1%. Strains close to the theoretical yield strain in the horizontal reinforcement were observed during the cycle to 1.5% and 1.0% drift for Specimens S7 and S8, respectively. Inelastic strains were also observed in the horizontal bars of Specimen S8, which failed by diagonal tension.

Yielding at the lower part of the wall for Specimens S9 and S10 was first observed during the cycle to 0.5% drift. Inelastic activity spread up to $0.4h$ from the wall base for Specimen S10 and strains exceeding 2.0% were recorded during the last cycles. In contrast, maximum strains of about 0.3% were measured in Specimen S9 at the wall mid-height, and the strain histories suggested that no yielding took place in that location in the main vertical reinforcement. Strains in the web vertical reinforcement were in the range of 0.1% to 0.3% for both specimens. Larger differences were observed for the web horizontal reinforcement. Fig. 4-36 shows a comparison of the strain history for a strain gauge located in a horizontal bar at a height of $0.3h$ for Specimens S9 and S10 (gauges H3-1 and H3-2, respectively).

Figs. 4-37(a) and (b) show the strain versus drift envelop response obtained from strain gauges placed on the main vertical wall reinforcement and located at 1.0 in. from the wall base in the RC and HPFRC specimens, respectively. For Specimen S1, the strain increased almost linearly with an increase in drift up to approximately 1.3% drift, followed by a faster strain increased for large drifts. For Specimens S4, S6 and S9 when

the strain reached the yield strain (at a strain of about 0.23%), the strain increased at a much higher rate with an increase in drift. In addition, the strains at ultimate in these specimens were 2 to 3 times larger than the strains in Specimen S1. Similar observations were made for the strains in the HPFRC specimens, where yielding started at drifts ranging from 0.4% to 1.0%.

From Fig. 4-38 (a), which presents the strain versus drift, envelop response obtained from strain gauges placed on the main vertical reinforcement at the wall mid-height in the RC specimens, it can be seen that yielding spread up to that location, particularly in Specimens S1 and S6. Unlike the strain measured at 1 in. from the wall base, the strain increase at wall mid-height was much greater in Specimen S1 compared with the rest of the RC walls for drifts larger than 1.7%. In Specimen S9, the damage was concentrated in the lower part of the wall and as a result, the strain beyond 0.8% drift remained fairly constant with an increase in the drift.

The strains for the HPFRC specimens at the wall mid-height are shown in Fig. 4-38(b). Strains in Specimens S2 and S5 with a shear span-to-length ratio of 1.2 remained constant at about the yield strain, whereas for Specimen S10 a fast increase in strain with drift was observed after yielding, with strains at ultimate close to 2.0%. A similar trend was observed during the early loading cycle for Specimens S7 and S8, but the strain gauges stopped working at a drift of 1.4% and 1.0%, respectively.

The strains for the dowel reinforcement in the HPFRC test units (Specimens S5, S7, S8 and S10) are presented in Fig. 4-39. As was discussed earlier, the strain gauges located on the dowel bars at 1.0 in. from the wall base showed no sign of yielding and maximum strains were in the range of 0.1% to 0.16%. Studies by Chao et al. (2009) have concluded that reinforcing bars embedded in HPFRC materials exhibit a superior bond resistance compared to regular concrete matrices because of the confinement that the fiber reinforcement offers, along with the crack control.

Based on the readings of the strain gauges located on the dowel bars in Specimens S5 and S10 at 1 in. from the wall base and at the section where the bonded region of the dowels terminated, an estimation of the average bond stress could be made. For Specimen S5 the peak average bond stress was 580 psi (calculated at a drift of 1.0%), whereas a value of 650 psi was estimated for Specimen S10. Using the readings of the strain gauges at the base of the dowel bars in Specimens S7 and S8, the average bond stress was estimated to be approximately 550 psi and 700 psi, respectively. It should be mentioned that a larger bond stress developed in the dowel bars of Specimen S8, which was reinforced with Spectra fibers, compared to the specimens reinforced with steel fibers.

Figs. 4-40 to 4-42 show plots of strain versus drift for wall horizontal bars located at a height of $0.1h$, $0.25h$ and $0.5h$, respectively. The measured strains in the horizontal bars located at $0.1h$ for the RC walls were significantly affected by the level of the shear stress and consequently the shear damage experienced by the walls in the lower part. A similar trend, but less pronounced, was observed in the HPFRC specimens. The strains measured in the horizontal reinforcement located at $0.5h$ were similar in all the specimens, except for Specimen S2, where much smaller strains were recorded due to insignificant shear-related damage.

4.10 STIFFNESS RETENTION CAPACITY

The stiffness of the wall specimens was evaluated in terms of the secant stiffness values determined from peak-to-peak displacement for each hysteresis loop. As can be observed from the load versus displacement hysteresis loops, the stiffness decreased with an increase in the drift and the rate of the stiffness decay decreased as the drift increased. HPFRC specimens had a lower initial stiffness compared with the companion RC specimens due to the reduced reinforcement in the wall and the lack of aggregates in the cement-based mixture for Specimens S2, S7 and S8.

In order to better evaluate the stiffness retention capacity of the specimens, the peak-to-peak displacement secant stiffness values were normalized with respect to the secant stiffness at approximately 0.15% drift for each specimen, in order to take into account variations in specimen parameters, such as the reinforcing ratio and the lack of coarse aggregate in some of the HPFRC walls. Table 4-12 presents the value of the secant stiffness used for the normalization in each specimen and the corresponding average drift level.

Figs. 4-43 (a) to (d) show the normalized peak-to-peak displacement stiffness versus drift for the first and second cycle for the test units. Specimen S8 showed a similar trend compared with that in Specimen S7 and thus, it was omitted from the figures. All the HPFRC specimens had a higher normalized stiffness compared to the RC companion specimens at the same drift level and maintained a higher percentage of their initial stiffness at the end of the test. The stiffness values for the second cycles at each drift level were very close to the first cycle values. It was also observed that shear stress level had an adverse effect on the normalized stiffness decay because the specimens tested under moderate shear stress levels exhibited a more gradual loss of stiffness compared to the specimens subjected to higher shear stresses. This trend can be seen in Figs. 4-44 and 4-45, where the normalized stiffness versus drift is plotted separately for the RC and HPFRC walls, respectively, and the level of shear stress sustained by each specimen is noted for easy comparison.

It should be noted, however, that yielding of the wall main longitudinal reinforcement had a substantial effect on the decay of peak-to-peak displacement stiffness with an increase in drift, but this does not necessarily translated into critical damage in the wall. As a result, the decay of peak-to-peak stiffness should not be taken as the only indication for the state of damage in the specimens.

The experimental initial stiffness of the walls was also compared to the theoretical elastic stiffness accounting for the effect of shear deformation. However, the experimental initial stiffness was found to be more than 80% below the theoretical value. Other studies that have reported pre-cracking stiffness based on shear wall tests generally revealed a wide scatter in the stiffness values (Cardenas et al., 1980; Farrar, 1990). The difference in the experimental and theoretical stiffness values can be attributed to the several factors, particularly elastic opening and slip along the cold joint, as well as slip in the test set-up. In this study, the instrumentation was not originally designed to accurately measure the pre-cracking stiffness and further comparison of the experimental and theoretical stiffness was not considered appropriate.

4.10 ENERGY DISSIPATION CAPACITY

A desirable characteristic in the behavior of low-rise walls, besides adequate displacement capacity, is a good energy dissipation capacity. The energy dissipated by the specimens during each loading cycle was calculated as the area enclosed by the applied load versus displacement hysteresis loops. Figs. 4-46(a) and (b) show the dissipated energy versus drift for the wall specimens with a shear span-to-length ratio of 1.2 and 1.5, respectively. In these plots, the drift is the average drift reached for the positive and negative loading directions at each cycle. The first and second cycle at each drift are plotted separately with a solid and dashed line, respectively. For drifts smaller than 0.5%, the energy dissipated was quite small, but for larger drifts a nearly linear energy increase with respect to an increase in drift level can be observed. In all the specimens, the energy dissipated during the first cycle was slightly larger compared to that in the second cycle at the same drift level, mainly because of the small decay in the strength and stiffness that the specimens experienced during the second cycle. Specimens S7 and S8, which had the same reinforcing detailing but reinforced with steel and Spectra fibers, respectively, revealed no significant difference in the amount of energy dissipated, with only a minor change in the trend during the last cycles due to a difference in the failure mechanism.

The dissipated energy was also normalized such that specimens with different load-carrying capacities could be adequately compared. The dissipated energy was normalized by the energy dissipated by an equivalent elasto-plastic system. The value of the normalized energy, therefore, provided information about the degree of pinching in the load versus displacement hysteresis loops. For the calculation of the area enclosed by the elasto-plastic system, the peak strength of the elasto-plastic system was set equal to the strength measured in the specimens for each cycle at a given drift level. The stiffness of the system was set equal to the peak-to-peak stiffness at the first loading cycle to 0.5% drift. The value of the stiffness for smaller drifts was not considered reliable since it was greatly affected by the flexibility in the test set up. Nonetheless, the values of the normalized dissipated energy were quite sensitive to the chosen stiffness definition of the elasto-plastic system and more attention should, thus, be given to the general trends rather than the actual values.

The plots of normalized energy dissipated versus average drift for all specimens are shown in Figs. 4-47(a) and (b). The wall specimens with a shear span-to-length ratio of 1.2 exhibited an almost constant normalized energy dissipation capacity for drifts ranging from 0.5% to 1.5%. Specimen S2, which failed by sliding shear at the wall base, had slightly smaller normalized energy than the companion RC Specimen S1, whereas HPFRC Specimen S5 exhibited a larger normalized energy than RC Specimen S4. In the group of specimens with an aspect ratio of 1.5, the normalized energy generally increased with an increase in drift. HPFRC Specimen S10 had the best energy dissipation capacity among all the specimens for drifts larger than 1.0%. Overall, the HPFRC walls that were tested under higher shear stress reversals (Specimens S5 and S10) had a higher value of dissipated energy than the companion RC specimens (Specimens S4 and S9).

CHAPTER 5
ANALYTICAL STUDIES

5.1 DEFORMATION COMPONENTS

Several deformation mechanisms contribute to wall drift, the most important ones being: shear distortion, sliding at the base of the wall, and flexural rotations (elastic and inelastic). In this section, an attempt was made to determine the relative contributions from each of these components to total drift.

The deformation components were calculated using the data recorded from either the potentiometers and clinometers or the Optotrak system. For Specimens S4, S5, S9 and S10, the Optotrak marker coordinates were used to calculate the deformation components following the procedure described below. A similar procedure was used for the specimens where only data from potentiometers and clinometers were available.

The drift due to the shear distortion of the wall (δ_γ) was calculated as:

$$\delta_\gamma = \frac{\sum_{i=1}^{5}(\gamma_i \times h_i)}{\alpha} \tag{5-1}$$

where γ_i is the average shear strain in a strip *i* (where *i* ranges from 1 through 5 as shown in Fig. 5-1), h_i is the height of each strip (i.e. 5 in.), and α is the wall shear span equal to 48 in. and 60 in. for the wall specimens with a shear span-to-length ratio of 1.2 and 1.5, respectively. The shear strain in each strip was calculated as described in Section 4.1.3, based on the coordinates of the Optorak markers.

The drift due to sliding at the wall base (δ_s) was estimated based on the difference between the horizontal coordinates of the Optotrak markers at the base of the wall (i.e. first row of markers in the wall) and the foundation block as follows:

$$\delta_s = \frac{\bar{x}}{a} \tag{5-2}$$

where $\bar{x}$ is the average horizontal displacement of the markers at the base of the wall (in.) with respect to the foundation block, corrected to account for the flexural rotations within the lower 4 in. of the wall.

The drift due to the flexural rotations (δ_θ) within the region instrumented with Optotrak markers was determined based on the average curvature calculated for each strip by double integration of the curvature along the wall elevation:

$$\delta_\theta = \frac{\sum_{i=1}^{6} \phi_i \times \overline{x_i} \times \Delta x_i}{\alpha} \tag{5-3}$$

where ϕ_i is the average curvature for strip *i* calculated as described in Section 5.2.1 (rad/in.), $\overline{x_i}$ is the distance from the middle of strip *i* to the mid-depth of the top beam (in.), and Δx_i is the height of strip *i* (in.). These terms are also defined in Fig. 5-2. Elastic flexural rotations (δ_{el}) above the wall area instrumented with Optotrak markers were determined assuming elastic uncracked behavior.

The total calculated drift was then obtained as follows:

$$(\delta_{pred}) = \delta_\gamma + \delta_s + \delta_\theta + \delta_{el} \tag{5-4}$$

Figs. 5-3 (a) through 5-3 (d) show plots of the predicted drift normalized by the applied drift for Specimens S4, S5, S9 and S10. The average contributions for the two loading directions are plotted in the figures because similar behavior was obtained for the positive and negative loading direction. The plots have been separated in three areas. The lower

region corresponds to the drift due to flexural rotations over the area instrumented with the Optotrak markers (elastic and inelastic). The contribution of the elastic rotations above the instrumented region was insignificant (less than 3% in all the specimens) and thus, it was not added to the plotted contribution from flexural rotations. The middle area gives the contribution of shear distortions, followed by the upper region, which represents the contribution of the horizontal slip at the wall base. It can be observed that the summation of the drift components was in reasonable agreement with the applied drift, the analytical value ranging between 85% and 110% of the "actual" drift.

The behavior of Specimens S4 and S9 should be representative of that for an RC wall designed according to the ACI Code Seismic Provisions and subjected to shear stress reversals of high intensity. The plot of the deformation components for these specimens is shown in Figs. 5-3 (a) and (b), respectively. Figs. 5-3 (c) and (d), on the other hand, show the drift components for Specimens S5 and S10, respectively, which refer to the companion HPFRC walls. It is worth mentioning that the wall of Specimens S5 and S10 was reinforced with dowel bars at the wall-foundation interface and ultimately failed due to the formation of a wide flexural crack along the end line of the dowel bars, along with concrete crushing in the lower part of the wall.

Between 50% and 60% of the drift applied to RC Specimen S4 for drifts up to of 1.0% was contributed by flexural deformations. For larger drifts, however, the contribution of flexural rotations decreased and the specimen started exhibiting appreciable shear-related damage in the lower wall region. At the onset of concrete spalling at 1.5% drift, flexural rotations contributed approximately 35% of the applied lateral displacement. At approximately 2.0% drift, shear distortion and slip contributed over 70% of the total drift, the displacement at which the wall experienced a significant loss of strength.

In RC Specimen S9, which experienced substantial concrete crushing in the wall edges close to the wall base, flexural rotations played a more important role compared to that in

Specimens S4. The contribution from shear distortions to total drift in this specimen was relatively constant throughout the test (approximately 20%), while sliding deformations became significant (greater than 30%) when rotations started decreasing at drifts larger than 1.3%.

HPFRC Specimens S5 and S10, with a shear span-to-length ratio of 1.2 and 1.5, respectively, exhibited the same failure mode. The slip contribution at the wall base for both specimens was less than 10% because of the use of dowel reinforcement. Despite the similar failure pattern, the increased slenderness of Specimen S10 led to an increase in the rotation contribution compared to Specimen S5 when the drift exceeded 1.4%. Conversely, shear distortions contributed more significantly to total drift in Specimen S5 and at a drift of 1.8%, shear distortions contributed more than 50% of the applied drift. It should be noted, however, that some slip occurred along the horizontal crack that developed in the region where the bonded part of the dowel reinforcement terminated for both specimens. This slip translated into an “apparent” shear strain that could not be separated from the “actual” shear strain. Thus, the shear distortion contributions in Specimens S5 and S10 also included the contribution of slip along this horizontal crack.

Overall, rotations in Specimens S4, S5, S9 and S10 contributed approximately 60% of the total lateral displacement for drifts up to 1.0%. For larger deformation levels, however, the contribution of horizontal slip (either at the cold joint or in the region where the bonded length of the dowel bars terminated) and shear strains increased, reducing the wall rotation contribution to total drift.

For Specimens S1, S2, S6, S7 and S8, a similar analysis was performed based on the data recorded from the potentiometers and clinometers (see Fig. 3-29). In Specimen S1, the rotations at a height of 0.1h, where h refers to the height of the wall (excluding the top block), had an almost constant contribution to the total drift throughout the test, approximately equal to 20% and 10% for the positive and negative loading direction,

respectively. Rotations between sections located at 0.1*h* and 0.45*h* from the wall base, on the other hand, had an increased contribution to total drift. For the positive loading direction, a contribution of 25% was calculated for the early cycles, increasing to 40% for drift levels close to failure. For the negative loading direction, this contribution was somewhat constant and corresponded approximately to 20% of the total wall drift. Sliding shear deformations had a significant effect on the behavior of Specimen S1 and contributed up to 40% of the total drift for the negative loading direction, which explains the smaller contribution of inelastic rotations at the wall base to total drift.

HPFRC Specimen S2 exhibited a different behavior in terms of drift components compared to the companion RC Specimen S1. Rotations at 0.1*h* had an increasing relative contribution to total drift with an increase in drift demand. For the negative loading direction, this contribution varied from 30% in the early cycles to 70% in the last cycles. With respect to the drift contribution in the positive loading direction, flexural rotations at 0.1*h* contributed between 10% and 30% of the applied drift. Rotations between 0.1*h* and 0.45*h* had a negligible contribution to total drift (less than 10%). The small contribution of rotations in this region was due to the predominant sliding shear mechanism exhibited by the wall. The contribution from sliding deformations was approximately 60% in the cycles close to failure for the positive loading direction, but this contribution was only 20% for the negative loading direction, where rotations at 0.1*h* played a dominant role. Shear distortions had a negligible contribution, less than 5%, to total drift. It seems that the relative low shear stress demand on the specimen, combined with the significant sliding deformations that led to an increased rocking at the wall base, did not allow for the development of large shear distortions.

Concentrated rotations at the wall base in RC Specimen S6 accounted for approximately 20% of the total drift, whereas inelastic rotations over the rest of the wall height contributed about 50% of the total drift for both loading directions. Shear deformations were about six times larger than those in HPFRC Specimen S2, with a contribution of approximately 20% to total drift. For HPFRC Specimens S7 and S8, wall base rotations

accounted for less than 50% of the applied lateral displacement, while shear distortions had an increased contribution (approximately 40% at drifts larger than 1.8%) compared to the companion RC Specimen S6.

5.2 CURVATURE

5.2.1 Curvature Distribution

Curvature along the wall elevation was computed from the readings of the Optotrak markers. It was assumed that cross sections remained plane after loading and thus, Eq. (5-4) was used to compute curvature along the wall height:

$$\phi_i = \frac{\left(y_2^i - y_2^{i-1}\right) - \left(y_1^i - y_1^{i-1}\right)}{\Delta x_i \times \ell} \tag{5-5}$$

where ϕ_i is the average curvature (rad/in.) over each strip i of height Δx_i(in.), y_2^i and y_1^i, and y_2^{i-1} and $y_1^{i-1}$are the y-coordinates of the edge markers at the top and bottom corners of strip i (in.), respectively, and ℓ is the horizontal distance between the edge markers, equal to 35 inches.

The curvature profile along the wall height for Specimens S4, S5, S9 and S10 is plotted for the first cycle at each drift level in Figs. 5-4 through 5-7. Curvature distribution for the positive and negative loading directions is plotted separately. In some instances, particularly near the end of the tests, curvature could not be calculated due to concrete spalling, which made the deformation measurements unreliable. In each plot, a line denoting the theoretical yield curvature was added, as obtained from a non-linear section analysis (see Section 5.2.3). The values for the theoretical yield curvature for Specimens S4, S5, S9 and S10 are listed in Table 5-1.

For RC Specimen S4, the values of curvature above the lower strip (Fig. 5-2) were below or at the theoretical yield curvature, ϕ_y, for drifts up to approximately 0.6%. The

curvature at the bottom strip in the wall, however, was two to four times larger than ϕ_y at this drift level. For larger drifts, inelastic deformations spread up to 14 in. (0.3*h*) from the wall base, whereas the rest of the wall had curvature values below the theoretical yield curvature.

HPFRC Specimen S5 had a similar curvature distribution compared to that in the companion RC specimen (Specimen S4) for low drift levels (less than 0.6%). The use of dowel reinforcement, however, led to increased average curvatures in the strip where the bonded portion of the dowel bars ended (4 in. to 9 in. from the wall base). Curvatures at the wall base were also larger for HPFRC Specimen S5 compared to RC Specimen S4. A behavior similar to that of RC Specimen S4 and HPFRC Specimen S5, respectively, was observed in Specimens S9 and S10.

5.2.2 Plastic Hinge Length and Curvature Capacity

Several equations exist for the prediction of plastic hinge length in RC beams and columns, but limited studies have addressed the length of plastic hinges in low-rise shear walls. Pauley and Priestley (1993) proposed an equation for RC walls that relates the wall plastic hinge length with its aspect ratio, as follows:

$$\ell_p = (0.2 + 0.044A_r)\ell_w \tag{5-6}$$

where ℓ_p is the plastic hinge length (in.), i.e. a hypothetical length over which the maximum curvature is assumed to be constant, A_r is the wall aspect ratio, and ℓ_w is the wall length (in.). Table 5-2 lists the values of the plastic hinge length for Specimens S4, S5, S9 and S10 as obtained from Eq. (5-6), as well as those obtained from the test. The experimental value of the plastic hinge length, ℓ_p, was estimated based on the curvature distribution obtained from the Optotrak markers (see Section 5.2.1) and corresponded to the length over which the experimentally obtained maximum curvature could be assumed constant such that it resulted in approximately the same contribution to wall drift.

From Table 5-2, it can be observed that specimens with increased slenderness exhibited a shorter plastic hinge length, as the walls experienced increased concentrated rotations at the wall base compared with the shorter walls. In the case of the HPFRC walls, the addition of the dowel bars in the wall-foundation interface led to a wider spreading of inelastic activity compared to the companion RC specimens. Pauley and Priestley suggested that Eq. (5-6) is a rather conservative estimation of the plastic hinge length. However, as it can be observed from the comparison of the values in Table 5-2, the equation predicted a longer plastic hinge for the RC walls (also for the HPFRC Specimens) compared with the experimentally estimated plastic hinge length. Thus, for the case of the specimens in this study Eq. (5-6) would underestimate the curvature ductility demands.

5.2.3 Section Modeling for Prediction of Moment versus Curvature Response

In order to predict the moment versus curvature response of the critical section in the wall specimens, a nonlinear section analysis was performed using a computer program originally written by Parra in the late 1990s (Parra and Naaman, 2001). The program is based on the common assumption that plane sections remain plane after bending (i.e. linear strain distribution). This assumption is generally valid for beams that have relatively long spans compared with their depth, but it could be questionable for deep members, as in the case of low-rise walls. A linear strain distribution, however, was assumed for simplicity and the results compared well with the experimental moment versus curvature response of the walls.

The nonlinear section analysis was performed for Specimens S4, S5, S9 and S10 for which the analytical results could be compared with the experimental moment versus curvature response obtained from the Optotrak system. For RC Specimens S4 and S9, the critical section considered was at the wall base. For the HPFRC specimens, on the other hand, two sections were analyzed, the section at the wall base and the section where the bonded region of the dowel bars ended. For the section at the wall base (cold joint), no tension stresses were allowed in the concrete (for both RC and HPFRC walls).

For modeling the tensile stress-strain response of the HPFRC material, a piece-wise linear relationship was used, as shown in Fig. 5-8. The values for the four points were obtained by fitting the model to the average stress-strain response reported by Liao et al. (2007). The tensile behavior of regular concrete was assumed linear up to the cracking point, assumed to occur at a stress of $7.5\sqrt{f_c'}$ (psi). The values used in the analyses are summarized in Table 5-3.

The model shown in Fig. 5-9 was used for simulating the compressive behavior of the regular concrete and the HPFRC material. The ascending portion of the stress-strain response can be satisfactory modeled as linear up to peak stress (Roy and Sozen, 1964), followed by a linear stress decay until the compression strain capacity of the material is reached. This simple model was chosen since the flexural behavior of RC members is not particularly sensitive to the shape of the matrix compressive stress-strain response. As it can been seen in Fig. 5-9, the parameters needed to define the compressive stress-strain response are: the compressive strength f_c', the strain at maximum stress ε_o, the slope parameter Z for the descending branch, and the ultimate strain ε_{cu}.With these parameters defined, the equations that describe the model are as follows:

For $\varepsilon_c < \varepsilon_o$:

$$f_c = \frac{\varepsilon_c}{\varepsilon_o} f_c' \tag{5-7}$$

For $\varepsilon_o \leq \varepsilon_c \leq \varepsilon_{cu}$

$$f_c = f_c'[1 - \mathrm{Z}(\varepsilon_c - \varepsilon_o)] \tag{5-8}$$

Table 5-4 summarizes the input parameters that were used for the HPFRC matrix in Specimens S5 and S10. The values were obtained from cylinders tests conducted as part of this study, combined with the results reported by Liao et al. (2007) for the same

HPFRC mixture. For the regular concrete mixture used in Specimens S4 and S9, the value of the maximum compressive strength was obtained from cylinder tests, whereas the values of the strain at maximum stress and the slope parameter Z are shown in Table 5-4.

The behavior of the steel reinforcement was modeled as shown in Fig. 5-10. The required parameters are the steel yield strength f_y, modulus of elasticity E_s, strain at the beginning of the strain-hardening region ε_{sh}, initial modulus of the strain hardening branch E_{sh}, tensile strength f_{su}, and the strain at tensile strength ε_u. The equations that describe the model are as follows:

For $\varepsilon \leq \varepsilon_y$:

$$f_s = E_s \varepsilon_s \tag{5-9}$$

For $\varepsilon_y < \varepsilon \leq \varepsilon_{sh}$:

$$f_s = f_y \tag{5-10}$$

For $\varepsilon_{sh} < \varepsilon \leq \varepsilon_{sm}$:

$$f_s = f_y + \left(f_{su} - f_y\right)\left[2\left(\frac{\varepsilon - \varepsilon_{sh}}{\varepsilon_{sm} - \varepsilon_{sh}}\right) - \left(\frac{\varepsilon - \varepsilon_{sh}}{\varepsilon - \varepsilon_{sh}}\right)^2\right] \tag{5-11}$$

For $\varepsilon_{sm} < \varepsilon \leq \varepsilon_u$:

$$f_s = f_{su} \tag{5-12}$$

where:

$$\varepsilon_{sm} = \varepsilon_{sh} + \frac{2\left(f_{su} - f_y\right)}{E_{sh}} \tag{5-13}$$

The values for the yield strength and the tensile strength of the steel reinforcement were obtained from direct tension tests (see Table 3-6). However, the strains in the steel were not always measured reliably. Thus, the following values were used, which in general represented well the stress-strain response of the steel for the cases where it could not be obtained experimentally: $E_s = 29{,}000\ ksi$, $\varepsilon_{sh} = 0.006$, $E_{sh} = 1250\ ksi$ and $\varepsilon_u = 0.14$.

In order to estimate the curvature capacity of both RC and HPFRC wall sections, a concrete compression strain capacity needed to be assumed. For the regular concrete matrix used in RC Specimens S4 and S9, a maximum compressive strain of 0.008 was assumed because of the good confinement of the concrete core in the wall boundary regions. The analysis was also performed for a maximum strain values in the range from 0.005 to 0.008, but the results showed that these values are too low to get a reasonable prediction of curvature capacity. An increased strain capacity was used for the HPFRC material in the section analysis for Specimens S5 and S10. Parra et al. (2005) reported a crushing strain of approximately 0.01 in HPFRC (mortar mixture) beams subjected to displacement reversals. As a result, this limit was used as a first approximation, and resulted in reasonable predictions of the curvature capacity for the section at the end line of the dowel bars.

Figs. 5-11 to Fig. 5-14 show moment-curvature plots for Specimens S4, S5, S9 and S10, respectively. In each plot, the moment-curvature response obtained from the nonlinear analysis (at the critical section) was compared with the behavior obtained from the experiments. It can be observed that prior to yielding, the analytical response did not agree well with the experimental moment-curvature response that corresponded to the applied moment at the wall base and the average curvature obtained over the lower 4 in. of the wall. The experimental response was substantially softer compared with the analytical response, which is attributed to strain accumulation (and potentially slip) of the wall vertical reinforcement in the base block. However, the curvatures that were experimentally measured in the wall region from 4 in. up to 9 in. from the wall base were in very good agreement with the analysis results for curvatures within the elastic range.

Compared with the experimental data, the results from the theoretical analysis showed higher moment capacities. As mention earlier, a basic assumption in the analysis was a linear strain distribution in the wall sections. As a result, the analysis did not consider any shear-moment interaction, which could be significant in low-rise walls. For Specimen S5 in particular, it seems that the weak region in the section where the bonded part of the dowel bars terminated affected significantly the wall strength and resulted in a lower moment capacity compared with that predicted through the nonlinear analysis (Fig. 5-12).

In RC Specimens S9 that failed by concrete crushing at the wall corners near the base, the curvature capacity (average value for the positive and negative loading directions) at the wall base was equal to 1.1×10^{-3} (rad/in.). This curvature capacity is approximately 13 times larger than the theoretical yield curvature for Specimen S9, as obtained from the nonlinear section analysis. In comparison, RC Specimen S4, which exhibited a web compression failure and whose behavior was characterized by a reduced contribution from flexural rotations to total drift, exhibited a curvature capacity equal to 0.73×10^{-4} (rad/in.) or about 7.5 times the theoretical yield curvature.

Table 5-5 lists the values of the compressive strains ε_1, ε_2, and ε_3, measured at the edge of the wall in the regions from 0 in. to 4 in., 4 in. to 9 in., and 9 in. to 14 in. from the wall base, respectively, for various drift levels. The strains were first calculated using the outer Optotrak markers and then the strain at the wall edges was estimated based on the average curvature calculated for that drift level. In Specimen S4, strain ε_2, in the regions where web concrete crushing was concentrated, was estimated to be 0.0012 at 1.0% drift and increased to 0.0026 at 2.0% drift. For Specimen S9, the compressive strain ε_1 at a drift of 1.5% was approximately 0.004, and increased to 0.0085 near the end of the test (2.0% drift).

5.3 SHEAR FRICTION MODEL

Several studies have revealed a relation between the shear strength of deep beams and the amount of horizontal reinforcement (for example, dePavia et al., 1965; Smith and Vantsiotis, 1982). Based on these observations, Wood (1990) suggested that the shear strength of RC low-rise walls could be related to the total amount of vertical reinforcement (longitudinal reinforcement in the boundary elements and wall web vertical reinforcement), as also discussed in Section 2.2.4.2. Using a shear friction analogy and assuming a sliding mechanism to develop along the critical horizontal crack, the nominal shear strength of the low-rise test walls could be estimated as:

$$v_{nsf} = \frac{\mu A_{vf} f_y}{A_{cv}} \tag{5-14}$$

where μ is the shear friction coefficient, A_{vf} is the area of steel crossing the shear plane (in.^{2}), f_y is the yield stress of the vertical steel (ksi), and A_{cv} is the area of the shear plane (in.^{2}). In case that bars with different yield strengths are used in the boundary elements and the wall web, the quantity $A_{vf} f_y$ can be determined as:

$$A_{vf} f_y = 2A_{sbe} f_{ybe} + A_{swv} f_{yv} \tag{5-15}$$

where $A_{sbe}$is the steel area in one boundary region (in.^{2}), f_{ybe} is the yield stress of the steel in the boundary region (ksi), A_{swv} is the area of web vertical reinforcement (in.^{2}), and f_{yv} is the yield stress of the web vertical reinforcement (ksi).

The value of the friction coefficient is generally not known and a reasonable lower bound for low-rise walls equal to $1/4$ was proposed by Wood (1990). Fig. 5-15 shows a plot of the ratio v_{max}/v_{nsf} versus the shear friction strength corresponding to $\mu = 1.0$. The ordinate values correspond to the experimental shear friction coefficient, μ. The vertical reinforcement considered was the total reinforcement crossing the critical horizontal crack that developed in each wall. In the case of the RC walls and the HPFRC specimen with no dowel bars (Specimen S2), the section considered was at the wall base. On the

other hand, for the HPFRC walls with dowel bars (Specimens S5, S7, S8, and S10), the section considered corresponds to the horizontal crack that formed along either the end line of the dowel reinforcement or at the section where the bonded part of the dowel bars ended. As can be seen, the friction coefficient was found to be in the range of 0.35 to 0.52 and the material used (regular concrete versus HPFRC) did not seem to have an effect on the shear friction coefficient. Table 5-6 lists the value of μ for all the test walls.

Figure 5-16 presents a plot of the peak shear stress sustained by the specimens versus the shear friction capacity assuming $\mu = 1.0$. A nearly linear increase for the wall shear strength with an increase in vertical reinforcement strength is observed, as also reported by Wood (1990). Based on the test results from this study a simple relationship, using linear regression analysis, was found for the shear strength of the wall specimens as a function of the vertical reinforcement strength:

$$v_{max} = 0.25 \times \left(\frac{A_{vf} f_y}{A_{cv}}\right) + 180 \text{ (psi)} \qquad (5\text{-}16)$$

The wall peak shear stress, normalized by $\sqrt{f_c'}$ (psi), is shown in Fig. 5-17. All the specimens, except for HPFRC Specimen S2, had shear strengths greater than $6.0\sqrt{f_c'}$ (psi), which is the lower limit suggested by Wood (1990) for low-rise walls. It is worth emphasizing that Specimen S2 was the only HPFRC wall without dowel bars at the wall-foundation interface, which led to excessive sliding along this section with the associated loss of stiffness and strength. It can be concluded, therefore, that the use of dowel reinforcement in HPFRC walls to strengthen the wall-foundation interface is also critical so that the minimum shear strength of $6.0\sqrt{f_c'}$ (psi) can be achieved. Nonetheless, the lower limit of $6.0\sqrt{f_c'}$ (psi) proposed by Wood for RC low-rise walls was verified by the results of this study.

Fig. 5-18 shows the envelope (for the first loading cycle at each drift level) of the shear force normalized by the shear friction strength (for $\mu = 1.0$) versus the sliding at the horizontal crack for several of the test walls. The responses shown correspond to the

average response for the positive and loading direction. The reader should be reminded that for all the RC specimens and HPFRC Specimen S2 the horizontal crack was developed at the wall base, whereas for the HPFRC specimens with dowel bars, the crack was formed in the region where the bonded part of the dowel terminated. The data for Specimen S1 were not included in the plot because the load versus sliding response was highly unsymmetrical for the two loading directions (see Fig. 4-23(a)). Also, data were not available for Specimens S2, S7 and S8 such that the response envelope could be obtained.

The nearly linear ascending portion of the curves in Fig. 5-18 provides an estimation of an "elastic sliding stiffness", which can be normalized by the shear friction strength assuming $\mu = 1$. Table 5-7 lists the values of normalized elastic sliding stiffness obtained from the envelope responses shown in Fig. 5-18. The elastic sliding stiffness was calculated as the secant stiffness at 80% of the shear friction strength. As can be seen, the experimentally obtained values were relatively consistent (ranging from 7.5/in. to 8.9/in.), although HPFRC Specimens S5 and S10 showed a lower sliding stiffness at the section where the bonded portion of the dowel bars terminated compared to the sliding stiffness at the base of the RC walls. Also identified in Fig. 5-18 are discrete values for the concentrated rotation at the horizontal crack. For concentrated rotations of approximately 0.15% (0.0015 rad), sliding at the horizontal crack did not exceed 0.05 in. However, the magnitude of the sliding became greater than 0.1 in. for rotations larger than 0.35%.

The data plotted in Fig. 5-18 suggest that a shear coefficient of 0.25, as suggested by Wood (1990), may be adequate to control excessive sliding. In order to evaluate this possibility, Fig. 5-19 shows a plot of the shear force, normalized by the shear friction strength (for $\mu = 1.0$), versus sliding at the base of the wall (cold joint) for HPFRC Specimens S5 and S10. The shear friction capacity at the wall base of these two specimens was higher because of the addition of dowel bars. It can be seen that the peak normalized shear force at the wall base was approximately 0.25 for both specimens and

sliding did not exceed 0.06 in. These limited results thus support the use of Wood's proposed shear friction coefficient for preventing substantial stiffness degradation due to shear sliding.

5.4 WALL SLIP VERSUS CRACK WIDTH

For HPFRC Specimens S5 and S10, for which a wide flexural crack and subsequent sliding developed at the section where the bonded area of the dowel bars ended, it was possible to obtain a relationship between the magnitude of sliding and the average crack width using the data from the Optotrak system. Fig. 5-20 presents a plot of "sliding stiffness", K_s, (i.e. ratio of average shear stress to horizontal slip) versus average crack width for these two specimens. In Fig. 5-21, the sliding stiffness was normalized by the shear friction capacity, V_{nsf}, for a friction coefficient, μ, equal to 1.0. A plot of sliding stiffness (and absolute slip) versus crack width at the edge of the wall tension side is shown in Figs. 5-22 and 5-23 for Specimen S5 and S10, respectively. As expected, sliding stiffness decreased as crack width (either average or at wall tension side) increased. Damage concentration at the horizontal crack was evident for average crack widths larger than 0.05 in. At this stage, the sliding stiffness value was below 100 ksi/in., whereas the normalized sliding stiffness had a value below 0.5 1/in. For the cycles leading to failure the average crack width was, on average, 0.1 in. Based on the behavior of these two specimens, it was concluded that once the magnitude of sliding stiffness decreases below 100 ksi/in., the opening of the horizontal crack and associated sliding governed the behavior of the specimens. It can also be observed that the width of the horizontal crack at the wall tension side of Specimen S10 exceeded 0.1 in. only during the last negative loading half cycle, whereas for Specimen S5 the crack width was larger than 0.1 in. for drifts above 1.0%.

5.5 SHEAR DISTORTION AND ROTATION INTERACTION

Specimens S7 and S8 were the only walls in the study that were designed to fail by diagonal tension. Thus, the results from the test of these two specimens were used to

evaluate the interaction between flexural rotations and shear distortions. A plot of shear distortion, γ, versus the shear stress for Specimens S7 and S8 is shown in Figs. 5-24 (a) and (b), respectively. Because no Optotrak markers were used in these two specimens, shear distortions were calculated from two diagonal potentiometers (see Fig. 3-29), while rotations correspond to those at a section 0.3*h* from the wall base, where *h* refers to the wall height excluding the top block. The two specimens exhibited similar behavior and the shear strain remained below 0.5% for average shear stress less than $5.5\sqrt{f_c'}$ (psi). However, shear strains increased significantly in both specimens, particularly in the loading direction in which a diagonal tension failure ultimately developed (positive and negative direction for Specimens S7 and S8, respectively). Damage concentration along the diagonal crack that led to failure was observed for shear strains greater than approximately 1.0%, and peak shear distortions reached 2.0% when a diagonal tension failure occurred.

Figs. 5-25 (a) and (b) show a plot between the shear strain and the rotation ratio (γ/θ) in the lower part of the wall versus average shear stress for HPFRC Specimens S7 and S8, respectively. Specimens S7 and S8 had γ/θ ratios below 1.2 up to a shear stress level of $5.0\sqrt{f_c'}$ (psi). For the loading direction at which diagonal tension failure ultimately occurred, the γ/θ ratio increased rapidly for higher shear stress cycles. This substantial increase in the γ/θ ratio indicates a rapid deterioration in shear stiffness that resulted in degradation of the shear resisting mechanisms.

The shear stress at which a substantial increase of the γ/θ ratio occurred can be considered as an upper shear stress limit for use in design of HPFRC low-rise walls. However, for design purposes, it is useful to determine the contribution of the HPFRC matrix, v_c, in member shear resistance. Theoretically, the shear stress on the matrix in every cycle can be estimated as the difference between the total average shear stress

demand, v_d, and the shear stress contribution from the wall web reinforcement,v_s, as follows:

$$v_c = v_d - v_s \tag{5-17}$$

Using the readings from the strain gauges attached the web horizontal reinforcement, v_s was roughly estimated, assuming a diagonal crack with a vertical projection equal to the wall length. The shear strength contribution from the HPFRC matrix for Specimens S7 and S8 at the peak shear stress demand was found to be $4.5\sqrt{f_c'}$ (psi). As was mentioned in Section 3.2, Chompreda and Parra (2007) proposed an HPFRC shear contribution of $3.0\sqrt{f_c'}$ (psi) in flexural members, based on cyclic tests of HPFRC beams. An increased matrix contribution in the case of low-rise walls is expected due to arch action. It should be noted, however, that the above calculation of matrix contribution in the wall shear resistance can only be considered an approximation because for low-rise wall vertical reinforcement may play a more important role that the horizontal reinforcement, as suggested by many researchers (for example Barda et al., (1977); Cardenas, (1980); Wood, (1990)) and also verified by the results of this study (see Section 5.3). Nonetheless, the limit of $4.5\sqrt{f_c'}$ (psi) for the HPFRC contribution is believed to provide a reasonable estimate for the design of HPFRC low-rise walls.

5.6 SHEAR STRENGTH AND DRIFT CAPACITY OF TEST SPECIMENS AND COMPARISON WITH OTHER STUDIES

Fig. 5-26 presents the drift capacity versus peak strength for all the test specimens in this study. As expected, there is a general trend of a decreasing wall drift with increased shear stress demand. The HPFRC walls, despite the relaxed reinforcement detailing, exhibited similar or larger drift capacities compared to the companion RC specimens. It can also be observed that for the wall specimens in this study, the wall shear span-to-length ratio (1.2 or 1.5) did not seem to have a significant effect on the wall deformation capacity.

In Section 2.2.2.2, several experimental studies on the behavior of RC low-rise walls were discussed and a summary of these studies was presented in Tables 2-1 and 2-2. In order to compare the shear strength and drift capacity of the HPFRC walls with that of RC walls with similar reinforcement detailing, specimens with the following characteristics were chosen:

- Rectangular wall sections;
- Tests with no axial load;
- Cantilever wall specimens;
- Specimens with no diagonal reinforcement;
- Walls with shear span-to-length ratios ranging from 1.0 to 1.5;
- Tests with shear stress demands in the range of $2.0\sqrt{f_c'}$ to $10\sqrt{f_c'}$ (psi).
- Walls with no confinement reinforcement or with confinement reinforcement that did not comply with the 2005 ACI Code requirements for special boundary elements.

The characteristics of these test specimens, as well as their shear strength and drift capacity, are summarized in Table 5-8. The RC and HPFRC walls tested in this study were also included in the table for easy comparison. The specimens in the study by Lefas et al. (1990) had confinement in the boundary regions that did not comply with the provision of the 2005 ACI Code, whereas the reinforcing detailing of the walls tested by Salonikios and al. (1999) followed the provisions of Eurocode EC8. All the low-rise wall specimens in the studies by Cardenas et al. (1980) (except for specimen SW13), Lefas et al. (1990), and Maier (1992) were tested under monotonic loading, but they were included in Table 5-7 because of the similarity in their characteristics with the specimens of this study. As a result, the drift capacity of these specimens should be considered as an upper bound, as testing the same specimens under reversed cycle loading would have likely resulted in reduced drift capacities. This is the case of Specimens SW9 and SW13 in the study by Cardenas et al. (1980), which had the same characteristics but were tested under monotonic and reversed cyclic loading, respectively. Specimen SW9 sustained a peak shear stress of $8.6\sqrt{f_c'}$ (psi) and failed by diagonal compression at a drift of 0.6%.

On the other hand, Specimen SW13 sustained a lower peak stress ($8.0\sqrt{f_c'}$ (psi)) and failed by diagonal compression, as Specimen SW9, at a drift of approximately 0.5%.

Fig. 5-27 presents a comparison of the shear stress versus drift capacity relationship for RC specimens (all tested under monotonic loading) with no confinement reinforcement in the wall boundary regions with that of the HPFRC walls tested in this study (no or little confinement reinforcement at the wall boundaries). It can be generally observed that the HPFRC specimens exhibited higher drift capacities when compared to the RC specimens that had no confinement reinforcement, even though the RC walls were tested under monotonic loading. For shear stress levels of approximately $4.0\sqrt{f_c'}$ (psi), the RC wall with no confinement reinforcement sustained a drift of 1.2%, whereas HPFRC Specimen S2 exhibited a drift capacity of about 3.0%. For increased shear stress levels, in the range of $6.0\sqrt{f_c'}$ to $7.0\sqrt{f_c'}$ (psi), drift capacity for the RC walls ranged between 1.0% and 1.4%, while the drift capacity in the HPFRC specimens ranged between 1.5% and 2.2%. For high shear stresses (about $9.0\sqrt{f_c'}$ (psi)), the RC and HPFRC walls sustained similar drifts, but very limited test data were available for walls with such high shear stress demands.

It is interesting to discuss the behavior of Specimen SW13 in the study by Cardenas et al. (1980), tested under displacement reversals, with that of the HPFRC walls of this study. Specimen SW13 had no confinement reinforcement and web vertical and horizontal reinforcement ratio equal to 2.8% and 1.0%, respectively. The vertical reinforcement in this specimen was uniformly distributed and thus, no vertical reinforcement was concentrated at the wall edges. This specimen was subjected to a peak shear stress demand equal to $8.0\sqrt{f_c'}$ (psi) and failed by diagonal compression at a drift of approximately 0.5%. On the other hand, HPFRC Specimen S5 from this study, with a similar shear span-to-length ratio, exhibited a drift capacity of 1.5% under a peak shear stress of $6.4\sqrt{f_c'}$ (psi). Further, Specimen S10, subjected to a peak shear stress demand of $8.6\sqrt{f_c'}$ (psi), exhibited a drift capacity greater than 2.0%.

Fig. 5-28 presents a plot of shear strength versus drift capacity for all the specimens listed in Table 5-8. It should be emphasized that except for the specimens tested in this study and Specimen SW13 by Cardenas et al. (1980), all RC specimens shown in Fig. 5-28 were tested under monotonic loading. A relatively wide scatter can be observed in the drift capacity of RC walls with no confinement reinforcement (0.5% to 1.9%). Specimens SW11 and SW12 in the study by Cardenas et al. (1980) showed the largest drift capacity in this group. These two specimens failed by diagonal tension, but inadequate development length of the vertical reinforcement in the upper part of the walls was also reported. RC walls with a volumetric confinement reinforcement ratio of 0.67% and detailing in the wall boundary regions that did not comply with the 2005 ACI Code generally exhibited similar drift capacities (in the range of 1% to 1.4%) compared to those of the RC specimens with no confinement reinforcement. On the other hand, the HPFRC walls with no confinement reinforcement and shear stress demands of about $6.0\sqrt{f_c'}$ (psi) showed similar deformation capacities as the RC walls with 1.0% volumetric confinement ratio. A confinement reinforcement ratio of 1.0% resulted in an enhanced drift capacity in the RC walls, with drift capacities in the range 1.5% to 2.4%. However, specimens with a confinement ratio equal to 1.7% (walls tested by Salonikios et al., 1999) exhibited an inferior performance in terms of drift capacity. It should be noted, thought, that these specimens failed by sliding shear at the wall base.

CHAPTER 6

SUMMARY AND CONCLUSIONS

6.1 SUMMARY

Reinforced concrete low-rise walls are frequently used as the primary component of the lateral-load resisting system in low-rise buildings located in earthquake prone regions. Low-rise walls, usually defined as walls with a height-to-length ratio less than two, exhibit a behavior highly influenced by shear and find applications in residential buildings, parking structures, industrial buildings, and nuclear power plants, among others. The reinforcement detailing in RC structural walls specified in Chapter 21 of the 2008 ACI Code (318 ACI Committee, 2008) typically consists of main vertical reinforcement at the wall edges, and distributed horizontal and vertical web reinforcement to provide cracking control and diagonal tension resistance. When large inelastic deformations are expected, special transverse reinforcement is provided at the wall edges to increase concrete ductility and to restrain (or delay) buckling of the longitudinal reinforcement.

The ACI Code required seismic detailing for low-rise structural walls generally ensures an acceptable level of performance in terms of shear resistance and stiffness, but can result in severe reinforcement congestion and construction difficulties. In addition, some experimental studies have revealed inadequate wall deformation capacity and extensive damage under large shear reversals.

In this study, the use of tensile strain-hardening, High-Performance Fiber Reinforced Concrete (HPFRC) in low-rise walls was experimentally evaluated as a means to simplify reinforcement detailing and enhance their overall seismic performance and damagetolerance. The HPFRCs evaluated in this study were reinforced with either hooked steel fibers in a 1.5% or 2% volume fraction or with ultrahigh molecular weight polyethylene (Spectra) fibers in a 2% volume ratio.

Nine low-rise wall specimens with shear span-to-wall length ratio of either 1.2 or 1.5 and shear stress demands ranging from $4.4\sqrt{f_c'}$ to $9.4\sqrt{f_c'}$ (psi) were tested under displacement reversals in the University of Michigan Structures Laboratory. Four of the specimens were constructed with regular concrete and detailed according to the seismic provisions of the 2005 ACI Code (318 ACI Committee, 2005). Besides the wall main flexural reinforcement and the web distributed vertical and horizontal reinforcement, closely spaced transverse reinforcement was provided in the boundary regions of the reinforced concrete (RC) walls to avoid early concrete crushing and provide lateral bar support. On the other hand, the HPFRC low-rise walls had little or no confinement reinforcement in the boundary regions and the wall distributed reinforcement ratio was reduced compared with that in the RC walls.

6.2 CONCLUSIONS

From the experiments and analysis conducted in this research, the following conclusions can be drawn:

1) The RC low-rise walls (shear span-to-length ratio of 1.2 or 1.5) designed according to the seismic provisions of the 2005 ACI Code (ACI Committee 318, 2005) and tested under moderate $\left(5.9\sqrt{f_c'} \text{ to } 6.7\sqrt{f_c'} \text{ (psi)}\right)$ and high $\left(8\sqrt{f_c'} \text{ to } 9.4\sqrt{f_c'} \text{ (psi)}\right)$ shear stress reversals exhibited a stable hysteretic behavior with drift capacities of approximately 2.1% and 1.5%, respectively. All the RC specimens exhibited an opening of the wall-foundation cold joint that led to significant sliding of the wall during the later stages of the tests. Damage was concentrated in the lower part of the

wall and was characterized by either crushing on the extreme compression fibers at the wall base and vertical splitting cracks in the wall boundary regions (Specimens S1, S6 and S9) or extensive concrete crushing in the wall web (Specimen S4). None of the RC specimens exhibited a diagonal tension failure.

2) HPFRC walls reinforced with either a 1.5% volume fraction of regular-strength hooked steel fibers or a 2% volume fraction of Spectra fibers and subjected to moderate shear stress demands (in the range of ($4.4\sqrt{f_c'}$ to $6.5\sqrt{f_c'}$, psi) showed a stable hysteretic behavior despite the elimination of the confinement reinforcement in the wall boundary regions. These walls exhibited drift capacities ranging from 2.1% to 3.0%. In addition, the use of a self-consolidating HPFRC material with a 1.5% volume fraction of high-strength hooked steel fibers allowed a significant relaxation in the confinement reinforcement in walls tested under high shear stress reversals (in the range of $6.4\sqrt{f_c'}$ to $8.6\sqrt{f_c'}$ psi), without compromising wall deformation capacity (drift capacities ranged between 1.5% and 2.2%). For the HPFRC walls tested under high shear stress reversals, the confining reinforcing ratio in the wall boundary regions was one-fourth of that in the companion RC specimens.

3) The RC walls subjected to shear stress demands in the range $5.9\sqrt{f_c'}$ to $6.7\sqrt{f_c'}$(psi) showed a concentration of damage in the lower part of the wall for drifts larger than 1.3%. The RC walls tested under high shear stress reversals ($8\sqrt{f_c'}$ to $9.4\sqrt{f_c'}$(psi)), on the other hand, exhibited significant shear-related damage at drifts of approximately 1.2%, while concrete spalling initiated during the cycles at drifts ranging from 1.3% to 1.5%. Compared to the companion RC walls, the HPFRC wall specimens showed a much denser array of cracks of smaller widths. Only minor shear-related damage was evident in the walls constructed with an HPFRC material at drifts below 1.3% and concrete spalling, if any, was not substantial, even at drifts in the order of 2.0%. The HPFRC specimens therefore exhibited superior damage tolerance compared to the companion RC specimens.

4) Horizontal sliding along the cold joint at the wall base was significant during the later stages of the test for all the RC walls. However, the wall-foundation interface was particularly critical in the HPFRC low-rise walls because no fibers bridged that section, making it susceptible to damage localization and potential sliding shear failure. This is exacerbated by the excellent bond between reinforcing bars and HPFRC. The need for reinforcement to strengthen the HPFRC wall-base interface was clearly demonstrated by the hysteretic behavior of HPFRC Specimen S2, without any additional reinforcement at the wall base. Despite the low aspect ratio of the wall (shear span-to-length ratio of 1.2), the concentrated flexural deformations at the wall base were large enough (approximately equal to 0.008 rad and larger than 0.01 rad at a drift of 2.3% and 3.0%, respectively) to result in an excessive loss of stiffness and a subsequent sliding shear failure. Thus, the use of dowel reinforcement is recommended to strengthen the cold joint at the base of HPFRC low-rise walls in order to force inelastic deformations to occur within the walls and avoid a premature sliding shear failure.

5) RC walls tested under moderated shear stress reversals ($5.9\sqrt{f_c'}$ to $6.7\sqrt{f_c'}$, psi) sustained drifts that exceeded 2.0%, whereas the increase in the shear stress demand to stresses above $8\sqrt{f_c'}$ (psi) limited their drift capacity to approximately 1.5%. On the other hand, the HPFRC low-rise walls exhibited drift capacities equal to or larger than those of the companion RC specimens. In addition, the variation of wall shear span-to-length ratio from 1.2 to 1.5 did not seem to have a strong effect on wall deformation capacity in the case of both RC and HPFRC walls.

6) Moderate shear related damage in RC walls was associated with shear strains varying between 0.005 rad and 0.007 rad. Only minor shear related damage was evident in the HPFRC walls at shear distortions of about 0.01 rad and diagonal crack opening was evident at shear strains greater than 0.015 rad. Specimens S7 and S8, which failed in diagonal tension, exhibited shear strains of 0.02 rad prior to failure. Based on the experimental results, the shear distortion capacity of low-rise HPFRC walls can be conservatively taken as 0.015 rad.

7) All the HPFRC specimens had a higher peak-to-peak displacement secant stiffness, normalized by the specimen secant stiffness at 0.15% drift, compared to the normalized stiffness of the companion RC specimens at the same drift level. The stiffness values of the RC and HPFRC walls for the second loading cycle at the same drift were very close to the first drift cycle values. It was also observed that shear stress level had an adverse effect on stiffness retention because the RC and HPFRC specimens tested under moderate shear stress levels ($4.4\sqrt{f_c'}$ to $6.7\sqrt{f_c'}$, psi) exhibited a more gradual loss of stiffness compared to the walls subjected to higher shear stress demands ($8\sqrt{f_c'}$to $9.4\sqrt{f_c'}$, psi).

8) In the RC walls tested under high shear stress reversals (Specimens S4 and S9) the contribution of rotations (elastic and inelastic) to the total drift was approximately 60% for cycles up to 1% drift. For larger drifts, however, the contribution from flexural rotations decreased as the slip at the wall base increased (a contribution that ranged from 30% to 40% of the total drift). For the HPFRC specimens subjected to high shear stress demands (Specimens S5 and S10), the contribution of shear distortions to the applied drift increased from 25% for drifts below 1% to 80% and 40% in the cycles leading to failure for Specimens S5 and S10, respectively. Rotations, mostly concentrated at the wall base, contributed close to 70% of the total drift at the end of the test for the HPFRC specimen that failed by sliding shear at the wall base (Specimen S2), whereas this contribution was approximately 50% in the companion RC specimen (Specimen S1).

9) The plastic hinge length for the RC walls tested under high shear stress reversals (Specimens S4 and S9) was found to be in the range of $0.10h$ to $0.15h$, where h refers to the wall height (excluding the top block). The HPFRC specimens designed for the same shear stress demands (Specimens S5 and S10) exhibited a longer plastic hinge length (in the range of $0.15h\ to\ 0.2h$). The equation proposed by Pauley and Priestley (1993) for low-rise walls resulted in longer plastic hinge lengths for these walls compared to the experimentally estimated values.

10) The test results revealed a nearly linear increase in wall shear strength with an increase in the area of vertical reinforcement, which can be described by the following equation:

$$v_{max} = 0.25 \times \left(\frac{A_{vf} f_y}{A_{cv}}\right) + 180$$

where A_{vf} (in.^{2}) is the area of vertical reinforcement in the wall (wall main and web vertical reinforcement) and A_{cv} (in.^{2}) is the wall cross-sectional area. The lower limit of $6.0\sqrt{f_c'}$ (psi) for the shear strength of low-rise walls proposed by Wood (1990) was found to be consistent with the test results, expect for the HPFRC specimen that failed prematurely by sliding shear (Specimen S2) because of the lack of dowel reinforcement strengthening the wall-foundation interface.

11) In all the RC wall specimens in which damage concentrated at the wall corners close to the base (Specimens S1, S6 and S9), the maximum value for the rotation at $0.1h$ from the wall base (where *h* is the wall height excluding the top block) was found to be approximately equal to 0.005 rad, regardless of wall shear span-to-length ratio or shear stress demand.

12) For HPFRC Specimens S7 and S8 that failed by diagonal shear, the ratio of shear distortion to rotation, γ/θ, increased gradually and remained below 1.2 for shear stress levels of up to $5.0\sqrt{f_c'}$ (psi). For larger shear stresses, this ratio increased at a substantially faster rate, indicating a rapid deterioration in shear stiffness and a degradation of the shear resisting mechanisms. For Specimen S7 and S8, the HPFRC contribution to the wall shear resistance was estimated to be $4.5\sqrt{f_c'}$ (psi), for the drift cycle at which the peak shear stress was reached.

Further experimental research, coupled with analytical studies, is needed in the following areas:

1) Evaluation of the behavior of HPFRC walls with shear span-to-length ratios well below 1.2 when subjected to displacement reversals. In this research, the HPFRC low-rise walls tested had shear span-to-length aspect ratios of 1.2 and 1.5 and as a result, the conclusions from this study may not be applicable to walls with much lower aspect ratios.

2) In this research, only HPFRC materials with either 1.5% or 2% volume fraction of fibers (hooked steel fibers and Spectra fibers) were evaluated for use in low-rise structural walls. Thus, the behavior of low-rise walls with lower fiber volume fractions should be investigated, given the increase in cost associated with the addition of fibers to the concrete.

3) The results from this study demonstrated the potential for a substantial relaxation in the confinement reinforcement in the boundary regions of low-rise walls through the use of HPFRC materials. Further experimental studies, however, are necessary to determine the minimum amount of required confinement to ensure adequate wall behavior, based on parameters such as shear stress, wall aspect ratio, and drift demand.

Table 2-1 Summary of Tests of Rectangular Low-Rise Reinforced Concrete Structural Walls

Researchers	Label	Type of loading	Wall Thickness (in.)	Shear Span-to-Length Ratio	Peak Shear Stress, in $\sqrt{f'_c}$ (psi)	Ultimate Drift [1] (%)	Failure Mode
Synge et al. (1980)	Wall 1	Cyclic	4	0.6	6.2	0.85	Sliding shear
	Wall 2		4	0.6	6.8	0.80	Buckling of diagonal bars
Cardenas et al. (1980)	SW-7	Monotonic	3	1.1	6.6	1.1	Diagonal tension
	SW-8		3	1.1	7.2	1.5	
	SW-9		3	1.1	8.6	0.6	Diagonal compression
	SW-10		3	1.1	4.0	0.7	Diagonal tension
	SW-11		3	1.1	8.2	1.4	Diagonal tension [2]
	SW-12		3	1.1	8.8	1.9	
	SW-13	Cyclic	3	1.1	8.0	0.5	Diagonal compression
Wiradinata and Saatcioglu (1986)	Wall 1	Cyclic	4	0.6	6.9	1.75	Diagonal tension
	Wall 2		4	0.3	8.9	2.6	Sliding shear
Lefas et al. (1990)	SW11	Monotonic	2.8	1.1	8.2	1.0	Vertical splitting of boundary region
	SW12		2.8	1.1	10.7	1.1	
	SW13		2.8	1.1	11.9	1.1	
	SW14		2.8	1.1	9.4	1.4	
	SW15		2.8	1.1	11.2	1.0	
	SW16		2.8	1.1	11.3	0.7	
	SW17		2.8	2.1	8.2	1.3	
	SW21		2.8	2.1	5.5	1.5	
	SW22		2.8	2.1	6.0	1.0	
	SW23		2.8	2.1	7.4	1.0	
	SW24		2.8	2.1	4.9	1.3	
	SW25		2.8	2.1	6.4	0.6	
	SW26		2.8	2.1	6.4	1.5	

Maier (1992)	S4	Monotonic	4	1.2	7.0	1.0	Diagonal compression
	S9		4	1.2	6.5	0.9	Diagonal tension
	S10		4	1.2	12.3	1.1	Diagonal compression
Salonikios et al. (1999; 2000)	MSW1	Cyclic	4	1.5 [3]	3.9	1.5	Buckling of longitudinal bars
	MSW2		4	1.5 [3]	2.4	1.9	Sliding shear
	MSW3		4	1.5 [3]	3.6	1.4	
	MSW4		4	1.5 [3]	3.2	1.5	
	MSW5		4	1.5 [3]	4.0	1.4	
	MSW6		4	1.5 [3]	3.9	1.5	
	LSW1		4	1.0 [3]	5.6	0.9	
	LSW2		4	1.0 [3]	4.1	0.9	
	LSW3		4	1.0 [3]	5.5	1.3	
	LSW4		4	1.0 [3]	4.8	0.8	
	LSW5		4	1.0 [3]	5.1	1.3	
Lopes (2000[a]; 2000[b])	SW13	Cyclic	1.8	1.1	9.3	1.1	Web crushing
	SW16		1.8	1.1	7.2	0.94	Diagonal tension
	SW17		1.8	1.1	7.4	0.94	
	SW18		1.8	1.1	8.9	0.96	

Hidalgo et al. (2002)	1	Cyclic	4.8	1.0	4.5	0.93	Diagonal tension
	2		4.8	1.0	6.1	1.31	
	4		4.8	1.0	7.4	1.21	
	6		4.8	0.7	5.7	0.95	
	7		4.8	0.7	6.6	1.11	
	8		4.8	0.7	7.3	1.13	
	9		4.0	0.7	5.7	1.01	
	10		3.2	0.7	5.4	0.86	
	11		4.0	0.5	5.0	0.74	
	12		4.0	0.5	6.3	0.70	
	13		4.0	0.5	5.8	0.74	
	14		3.2	0.35	5.5	0.38	
	15		3.2	0.35	7.5	0.53	
	16		3.2	0.35	7.4	0.51	
	21		4.0	0.7	4.9	NA [3]	
	22		4.0	0.7	5.0	0.28	
	23		4.0	0.7	6.3	0.78	
	24		4.0	0.7	6.1	0.23	
	25		4.0	0.5	6.2	0.51	
	26		4.0	0.5	5.4	0.48	
	27		4.0	0.5	8.6	0.83	
	28		4.0	0.5	4.6	0.36	
	29		3.2	0.35	8.3	NA[3]	
	30		3.2	0.35	8.5	0.57	
	31		3.2	0.35	8.2	NA[3]	
	32		3.2	0.35	7.2	NA[3]	

Choi (2006)	SWR1	Cyclic	4.0	0.75	6.1	NA [4]	Sliding shear
	SWR2		4.0	0.75	6.3	NA [4]	Web crushing/Buckling of diagonal reinforcement

[1] Drift is defined as the ratio of the reported displacement at ultimate condition to the wall shear span
[2] Inadequate anchorage development of the straight vertical reinforcement in the upper part of the wall was also reported for the specimen
[3] The shear span value was not given in the publication; thus the wall height-to-length ratio is given here
[4] No data were reported for this specimen

Table 2-2 Summary of Tests of Barbell and Flanged Low-Rise Reinforced Concrete Structural Walls

Researchers	Label	Type of loading	Wall Thickness (in.)	Shear Span-to-Length Ratio	Peak Shear Stress , $\sqrt{f'_c}$ (psi)	Ultimate Drift (%)	Failure Mode
Barda et al. (1977)	B1-2	Monotonic	4	0.5	14.0	0.6	Diagonal tension
	B2-1		4	0.5	15.1	0.7	
	B3-2	Cyclic	4	0.5	13.3	0.6	
	B4-3		4	0.5	14.5	0.5	
	B5-4		4	0.5	8.1	0.5	
	B6-4		4	0.5	11.8	0.6	
	B7-5		4	0.3	13.9	0.8	
	B8-5		4	1.0	11.4	0.6	
Synge et al. (1980)	Wall 3	Cyclic	4	0.6	6.2	0.35	Sliding shear
	Wall 4		4	0.6	6.3	0.60	Buckling of diag. bars
Maier (1992)	S1	Monotonic	4	1.2	11.4	2.1	Diagonal Compression
	S2		4	1.2	16.1	1.1	
	S3		4	1.2	16.5	1.1	
	S5	Cyclic	4	1.2	11.4	1.5	
	S6	Monotonic	4	1.2	11.4	1.7	
	S7	Cyclic	4	1.2	15.0	0.7	
	S8	Monotonic	4	1.2	9.2	1.1	
Sittipunt et al. (2001)	W1	Cyclic	4	1.4	6.5	1.8	Web crushing
	W2		4	1.4	8.2	1.5	
	W3		4	1.4	7.4	1.7	Crushing of flanges
	W4		4	1.4	8.2	1.8	
Choi (2006)	SW4	Cyclic	4	0.75	9.1	NA[(1)]	Diagonal tension
	SW5		4	0.75	11.3	NA[(1)]	
	SW6		4	0.75	9.1	NA[(1)]	Sliding shear
	SW7		4	0.75	10.2	NA[(1)]	Web crushing

[(1)] It was not possible to obtain the ultimate drift from the publication.

Table 3-1 Main Features of Test Specimens

Specimen	$t_w \times \ell_w$ [1] (in. × in.)	h_w [2] (in.)	a/ℓ_w [3]	Target Shear Stress Level (psi)	Mixture Description
S1	40 × 40	40	1.2	$5-6\sqrt{f_c'}$	Regular Concrete
S2	40 × 40	40	1.2	$5-6\sqrt{f_c'}$	Mortar with 2.0% volume fraction of Dramix ZP 305 [5]
S4	40 × 40	40	1.2	$8.5-9.5\sqrt{f_c'}$	Regular Concrete
S5	40 × 40	40	1.2	$8.5-9.5\sqrt{f_c'}$	Concrete with 1.5% volume fraction of Dramix RC-80/30-BP [6]
S6	40 × 40	52	1.5	$6.5-7.5\sqrt{f_c'}$	Regular Concrete
S7 [4]	40 × 40	52	1.5	$6.5-7.5\sqrt{f_c'}$	Mortar with 2.0% volume fraction of Dramix ZP 305
S8 [4]	40 × 40	52	1.5	$6.5-7.5\sqrt{f_c'}$	Mortar with 1.5% volume fraction of Spectra Fibers [7]
S9	40 × 40	52	1.5	$8.5-9.5\sqrt{f_c'}$	Regular Concrete
S10	40 × 40	52	1.5	$8.5-9.5\sqrt{f_c'}$	Regular Concrete

[1] t_w: wall thickness; ℓ_w: wall length
[2] h_w: wall height (excluding top block)
[3] a/ℓ_w: shear span-to-wall length ratio
[4] Specimen tested by Kim and Parra (2003)
[5] Dramix ZP 305 fibers: length 1.2 in.; diameter 0.022 in.; tensile strength 160-200 ksi
[6] Dramix RC-80/30-BP: length 1.2 in.; diameter 0.015 in.; tensile strength 335 ksi
[7] Spectra fibers: length 1.5 in.; diameter 0.0015 in.; tensile strength 375 ksi

Table 3-2 Maximum Wall Shear and Calculated Shear Strength of Test Specimens

Specimen	Shear Demand		Nominal Shear Strength		Nominal "Concrete" Contribution		Nominal "Steel" Contribution		"Concrete" Contribution Demand	
	V_{max} (kips)	$v_{max}/\sqrt{f'_c}$	V_n [(1)] (kips)	$v_n/\sqrt{f'_c}$	V_c (kips)	$v_c/\sqrt{f'_c}$	V_s (kips)	$v_s/\sqrt{f'_c}$	$V_{max}-V_s$ (kips)	$\frac{(v_{max}-v_s)}{\sqrt{f'_c}}$
S1	70.6	6.2	102	9.0	34.0	3.0	68.0	6.0	2.6	0.2
S2	56.9	5.0	86.6	7.6	56.6	5.0 [(2)]	30	2.6	26.9	2.4
S4	105	9.3	134	11.8	34.0	3.0	100	8.8	5.00	0.5
S5	101	8.9	132	11.7	56.5	5.0 [(2)]	75.6	6.7	25.4	2.2
S6	87.0	7.7	102	9.0	34.0	3.0	68.0	6.0	19.0	1.7
S7	86.0	7.6	69.0	6.1	56.5	5.0 [(2)]	12.5	1.1	73.5	6.5
S8	86.0	7.6	69.0	6.1	56.5	5.0 [(2)]	12.5	1.1	73.5	6.5
S9	108	9.6	114	10.1	34.0	3.0	80.4	7.1	27.6	2.5
S10	96.0	8.5	117	10.3	56.5	5.0 [(2)]	60.0	5.3	36.0	3.2

[(1)] Nominal shear strength provided by "concrete" contribution and "shear reinforcement" contribution, i.e. horizontal web reinforcement
[(2)] Assumed contribution based on previous research (see Section 3.2.2)

Table 3-3 Nominal Shear Strength for Shear-Transfer at the Wall Base of Test Specimens

Specimen	$A_{vf}f_y\mu$ [(1)] (kips)	V_n [(2)] (kips)	V_{max} [(3)] (kips)
S1	93.6	93.6	70.6
S2	72.0	72.0	56.9
S4	143	128 [(4)]	105
S5	174	128 [(4)]	101
S6	143	128 [(4)]	87
S7	185	128 [(4)]	86
S8	185	128 [(4)]	86
S9	181	128 [(4)]	116
S10	216	128 [(4)]	97

[(1)] A_{vf} refers to total vertical reinforcement in the wall, including dowel bars, if any, nominal f_y was taken equal to 60,000 psi for all types of vertical reinforcement, and the shear coefficient, μ, was taken as 0.6
[(2)] Nominal shear strength for shear transfer at the wall cold joint
[(3)] Maximum expected base shear (see Table 3-2)
[(4)] Limit of $800A_c = 128\ kips$ governed the nominal shear strength for shear transfer

Table 3-4 Extreme Fiber Compressive Stress Corresponding to Maximum Moment for Evaluating Need for Confinement in Boundary Elements According to 2005 ACI Code.

Specimen	Stress (psi) [(1)]
S1	3180
S2	2560
S4	4725
S5	4545
S6	5220
S7	5160
S8	5160
S9	6480
S10	5760

[(1)] The limit of $0.2f_c'$ for the compressive stress is equal to 1000 psi for the design value of f_c' equal to 5000 psi

Table 3-5 Wall Reinforcement Details

Specimen	Vertical Reinforcement (Boundary Region)			Vertical Reinforcement (web region)		Horizontal Reinforcement		Confinement Reinforcement (Boundary Region)	Dowel Reinforcement
	Bars	ρ_{boubd}[(1)]	ρ[(2)]	Bars	ρ_v[(3)]	Bars	ρ_h[(4)]		
S1	4No.4	5.0	0.53	No.2@3.5 in.	0.71	No.2@3.5 in.	0.71	Ø0.162 @ 1.0 in.	-
S2	4No.4	5.0	0.53	No.2@8.0 in.	0.31	No.2@8.0 in.	0.31	-	-
S4	2No.6+2No.5	9.4	1.0	D5@3.0 in.	0.83	D5@3.0 in.	0.83	Ø0.162 @ 1.0 in	-
S5	4No.5	7.6	0.82	D5@4.0 in.	0.63	D5@4.0 in.	0.63	Ø0.162 @ 1.0 in	4No.4
S6	2No.6+2No.5	9.4	0.98	No.2@3.5 in.	0.71	No.2@3.5 in.	0.71	Ø0.162 @ 4.0 in	-
S7	3No.7	7.5	1.1	No.2@6.0 in.	0.21	No.2@10 in.[(5)]	0.13	-	2No.5
S8	3No.7	7.5	1.1	No.2@6.0 in.	0.21	No.2@10 in.[(5)]	0.13	-	2No.5
S9	2No.7+2No.6	13.0	1.4	D4@3.0 in.	0.67	D4@3.0 in.	0.67	Ø0.162 @ 1.0 in	-
S10	4No.6	11.0	1.2	D4@4.0 in.	0.50	D4@4.0 in.	0.50	Ø0.162 @ 4.0 in	4No.4

(1) ρ_{boubd}: Boundary region reinforcing ratio
(2) ρ: Longitudinal reinforcement in the boundary elements as a tension reinforcement ratio
(3) ρ_v: Vertical reinforcement ratio
(4) ρ_h: Horizontal reinforcement ratio
(5) One layer of reinforcement

Table 3-6 Mixture Proportions (by Weight) for Regular Concrete and HPFRC Mixtures

Mixture Designation	Portland Cement	Sand	Coarse Aggregate	Water	Fly Ash	SP[(1)]	VMA[(2)]	Fiber Type	V_f [(3)]
RC	1	1.55	1.45	0.48	-	-	-	-	-
HPFRC-SH	1	2	-	0.48	0.20	-	-	Dramix ZP305	2.0%
HPFRC-PE	1	1	-		0.5	0.15	-	Spectra [(4)]	1.5%
Self-Consolidating HPFRC	1	2.2	1.2	0.8	0.88	0.005	0.038	Dramix RC-80/30-BP	1.5%

[(1)] Superplasticizer
[(2)] Viscosity Modifying Agent
[(3)] Volume fraction of fibers
[(4)] Ultra high molecular weight polyethylene fibers

Table 3-7 Properties of Fibers

Fiber	Dramix ZP305	Dramix RC-80/30-BP	Spectra
Length (in.)	1.2	1.2	1.5
Diameter (in.)	0.022	0.015	0.0015
Tensile strength (ksi)	160 to 200	335	375
Modulus of elasticity (ksi)	29,000	29,000	17,000

Table 3-8 Average Concrete Cylinder Compressive Strength at Test Day (ksi)

Specimen	Wall		Beams	
	Material	Average Strength	Bottom	Top
S1	Regular concrete	6.7	5.7	6.2
S2	Mortar with 2.0% volume fraction of Dramix ZP 305 fibers	7.0	6.2	6.9
S4	Regular concrete	6.7	5.5	5.1
S5	Concrete with 1.5% volume fraction of Dramix RC-80/30-BP	5.7	3.8	3.7
S6	Regular Concrete	6.8	4.0	6.3
S7	Mortar with 2.0% volume fraction of Dramix ZP 305 fibers	6.8 [(1)]	N/A	N/A
S8	Mortar with 1.5% volume fraction of Spectra fibers	6.3 [(1)]	N/A	N/A
S9	Regular concrete	6.2	3.8	3.9
S10	Concrete with 1.5% volume fraction of Dramix RC-80/30-BP	5.5	2.9[(2)]	5.9

[(1)]) Compressive strength obtained from 3×6 in. cylinders
[(2)] Lower compressive strength due to an error of the ready-mix concrete supplier (see Section 3.3.1.1)

Table 3-9 ASTM 1609 Beam Test Results [(1)]

Specimen	First Peak		Second Peak		P150,0.75[(2)] (kips)	P150,3.0[(3)] (kips)
	Load (kips)	Deflection (in.)	Load (kips)	Deflection (in.)		
S5	11.2	0.0045	14.4	0.022	13.7	6.6
S10	8.8	0.0053	9.8	0.018	7.9	5.2

[(1)] All tests conducted on $6 \times 6 \times 20$ in. beams
[(2)] P150, 0.75: Load at 0.03 in. (0.75 mm) deflection
[(3)]P150, 3.0: Load at 1.2 in. (3 mm) deflection

Table 3-10 Steel Strength (ksi)

Specimen	Reinforcement Type	Average Yield Stress[(1)]	Average Ultimate Stress
S1&S2	No.2	95.8	99.7
	No.4	74.3	108
S4&S5	D5	91.8	94.6
	No.4	66.1	106
	No.5	64.4	97.2
	No.6	65.8	109
S6	No.2	97.3	98.4
	No.5	69.8	103
	No.6	71.3	108
S7&S8	No.2	N/A	N/A
	No.5	70.1	89.3
	No.7	72.3	98.3
S9&S10	D4	90.2	95.2
	No.4	70.1	99.7
	No.6	69.3	106
	No.7	67.2	101

[(1)] The yield stress for the No.2 bars, and the D4 and D5 wire was determined using the 0.2% offset method.

Table 4-1 Summary of Test Results

Specimen	S1		S2		S4		S5		S6		S7		S8		S9		S10	
Peak Load [1] (kips)	81.5	72.7	55.0	62.4	101	107	79.5	77.0	87.9	88.3	82.0	80.3	81.8	82.4	119	116	105	97
Peak Shear Stress [1] (psi)	510	454	343	390	630	669	495	481	549	552	512	502	511	515	746	726	658	605
Peak Shear Stress [1] (in $\sqrt{f_c'}$, psi)	6.2	5.5	4.1	4.7	7.7	8.2	6.5	6.3	6.7	6.7	6.2	6.1	6.4	6.5	9.5	9.3	8.9	8.2
Drift at Peak Load [1] (%)	2.0	2.2	1.5	1.7	0.6	0.9	0.9	0.8	1.3	1.6	1.32	1.8	1.8	1.8	1.5	1.0	1.1	0.9
Drift Capacity [2] (%)	2.4		3.0		1.5		1.5		2.1		2.1		2.2		1.5		2.2	
Final drift [1] (%)	2.3	2.5	3.0	2.9	2.3	2.1	2.3	2.4	2.1	2.2	2.5	2.0	2.3	2.3	2.2	2.1	2.4	2.0

[1] Values correspond to the positive and negative loading directions

[2] Drift Capacity (%) is defined as the maximum drift at which at least 80% of the peak load was sustained in both loading directions. For Specimens S1, S2, S6 and S10 there was no significant loss of strength so the drift capacity listed in the table is the peak average drift applied during the test

Table 4-2 Probable Shear Demand Associated with Flexural Failure and Nominal Shear Strength

Specimen	Probable Shear Demand, V_{pr} [(1)] (kips)	Nominal Shear Strength, V_n [(2)] (kips)
S1	72.1	149
S2	57.2	107 [(3)]
S4	108	161
S5	91	150 [(3)]
S6	88.6	150
S7	87.0	78.1 [(3)]
S8	87.0	78.1 [(3)]
S9	109	135
S10	90.4	131 [(3)]

[(1)] Shear demand corresponding to moment capacity at the wall base, calculated based on actual material properties and nonlinear section analysis

[(2)] Nominal shear strength calculated using actual steel yield strength and concrete strength, based on the modified truss analogy

[(3)] HPFRC concrete contribution to shear strength assumed equal to $5\sqrt{f_c'}$ (psi) (see Section 3.2.2)

Table 4-3 Load-Displacement History for Specimen S1

Cycle	Load (kips)	Drift (%)
1	-15.1	-0.14
	10.2	0.02
2	-8.3	-0.09
	10.2	0.02
3	-14.4	-0.17
	17.2	0.08
4	-14.9	-0.17
	14.4	0.06
5	-32.4	-0.34
	28.3	0.23
6	-27.6	-0.33
	28.5	0.23
7	-38.3	-0.51
	42.3	0.36
8	-37.6	-0.57
	43.3	0.35
9	-43.4	-0.75
	55.6	0.52
10	-43.5	-0.79
	55.7	0.52
11	-52.1	-0.92
	72.1	0.73
12	-49.1	-0.93
	64.7	0.73
13	-63.3	-1.21
	76.6	0.95
14	-61.9	-1.2
	74.7	0.99
15	-68.4	-1.5
	79.5	1.2
16	-63.1	-1.4
	77.1	1.2
17	-69.6	-1.7
	80.5	1.5
18	-68.0	-1.7
	76.4	1.4
19	-70.4	-1.9
	81.0	1.8
20	-72.7	-2.2
	81.5	2.0
21	-63.0	-2.5
	60.00	2.3

Table 4-4 Load-Displacement History for Specimen S2

Cycle	Load (kips)	Drift (%)
1	-9.8	-0.12
	7.8	0.07
2	-3.8	-0.07
	9.3	0.12
3	-12.9	-0.15
	15.2	0.21
4	-13.2	-0.19
	12.2	0.20
5	-35.6	-0.47
	25.3	0.46
6	-34.4	-0.48
	20.7	0.44
7	-48.1	-0.66
	33.1	0.64
8	-47.1	-0.71
	30.9	0.69
9	-55.2	-0.91
	45.9	0.95
10	-47.2	-0.87
	46.6	1.0
11	-59.1	-1.2
	53.1	1.3
12	-56.2	-1.2
	49.8	1.3
13	-60.3	-1.4
	55.0	1.5
14	-58.8	-1.5
	49.7	1.5
15	-62.4	-1.7
	53.5	1.7
16	-52.0	-1.7
	48.0	1.7
17	-62.2	-2.0
	49.3	2.0
18	-58.1	-1.9
	41.1	1.9
19	-60.9	-2.2
	43.0	2.3
20	-60.5	-2.9
	46.3	3.0

Table 4-5 Load-Displacement History for Specimen S4

Cycle	Load (kips)	Drift (%)
1	11.1	0.04
	-9.9	0.00
2	10.2	0.05
	-9.5	0.01
3	20.9	0.23
	-25.1	0.23
4	20.8	-0.08
	-18.9	-0.02
5	40.0	0.23
	-37.6	-0.08
6	39.7	0.24
	-36.8	-0.08
7	60.8	0.34
	-58.5	-0.19
8	63.8	0.36
	-61.5	-0.22
9	81.8	0.44
	-85.9	-0.37
10	80.9	0.45
	-85.5	-0.38
11	98.3	0.56
	-95.2	-0.55
12	89.1	0.58
	-99.9	-0.59
13	97.2	0.77
	-102	-0.92
14	90.1	0.87
	-94.7	-0.83
15	92.9	1.0
	-95.4	-1.0
16	85.4	1.0
	-94.5	-1.0
17	95.6	1.3
	-95.2	-1.3
18	84.9	1.3
	-88.5	-1.3
19	87.3	1.5
	-83.5	-1.6
20	65.4	1.9
	-53.9	-2.1
21	26.4	2.3

Table 4-6 Load-Displacement History for Specimen S5

Cycle	Load (kips)	Drift (%)
1	10.6	0.04
	-9.9	-0.04
2	7.1	0.04
	-7.1	-0.03
3	15.2	0.10
	-15.4	-0.06
4	15.6	0.11
	-15.4	-0.05
5	27.4	0.24
	-32.6	-0.17
6	32.4	0.29
	-30.4	-0.14
7	39.3	0.36
	-43.8	-0.29
8	41.3	0.37
	-44.0	-0.28
9	53.4	0.50
	-55.3	-0.43
10	49.9	0.45
	-53.3	-0.44
11	69.1	0.63
	-71.4	-0.62
12	68.2	0.63
	-68.0	-0.61
13	73.2	0.86
	-76.1	-0.79
14	77.8	1.1
	-73.2	-0.84
15	70.5	1.1
	-74.4	-1.1
16	68.5	1.1
	-69.5	-1.1
17	68.0	1.4
	-67.7	-1.4
18	62.0	1.4
	-62.1	-1.4
19	59.1	1.6
	-58.4	-1.7
20	52.7	1.9
	-51.8	-2.0
21	42.3	2.3
	-40.6	-2.4

Table 4-7 Load-Displacement History for Specimen S6

Cycle	Load (kips)	Drift (%)
1	11.6	0.04
	-12.5	-0.08
2	12.7	0.05
	-12.8	-0.07
3	20.6	0.12
	-20.8	-0.15
4	23.8	0.14
	-22.0	-0.16
5	37.5	0.29
	-36.7	-0.31
6	41.7	0.29
	-39.6	-0.33
7	53.9	0.43
	-55.3	-0.51
8	54.5	0.44
	-54.6	-0.50
9	72.2	0.58
	-70.5	-0.70
10	69.2	0.59
	-71.2	-0.69
11	80.0	0.81
	-81.7	-0.95
12	76.5	0.83
	-80.7	-0.94
13	81.6	1.0
	-87.0	-1.2
14	79.5	1.1
	-83.7	-1.2
15	81.8	1.3
	-88.4	-1.4
16	80.2	1.3
	-79.2	-1.4
17	81.1	1.6
	-86.3	-1.6
18	77.6	1.6
	-75.6	-1.6
19	77.9	1.8
	-86.0	-1.9
20	74.1	2.1
	-77.3	-2.2

Table 4-8 Load-Displacement History for Specimen S7

Cycle	Load (kips)	Drift (%)
1	13.0	0.09
	-10.0	-0.08
2	13.0	0.09
	-10.4	-0.08
3	21.3	0.18
	-18.0	-0.21
4	22.4	0.18
	-17.3	-0.20
5	31.8	0.27
	-24.0	-0.29
6	31.0	0.27
	-23.4	-0.29
7	43.1	0.39
	-31.0	-0.41
8	41.4	0.39
	-29.6	-0.40
9	61.3	0.57
	-44.0	-0.61
10	60.1	0.57
	-44.3	-0.62
11	75.8	0.77
	-57.0	-0.84
12	73.6	0.81
	-65.1	-0.92
13	75.3	1.1
	-69.0	-1.1
14	74.9	1.0
	-70.3	-1.1
15	77.8	1.3
	-73.3	-1.3
16	73.9	1.3
	-72.9	-1.3
17	76.6	1.5
	-75.8	-1.5
18	75.2	1.6
	-75.0	-1.5
19	75.1	1.8
	-76.4	-1.8
20	72.2	1.8
	-75.4	-1.8
21	64.8	2.1
	-75.4	-2.0
22	39.9	2.4

Table 4-9 Load-Displacement History for Specimen S8

Cycle	Load (kips)	Drift (%)
1	14.0	0.11
	-12.1	-0.07
2	13.2	0.11
	-12.3	-0.08
3	20.3	0.20
	-19.7	-0.18
4	20.4	0.20
	-19.5	-0.18
5	28.2	0.29
	-272	-0.26
6	27.6	0.30
	-26.4	-0.26
7	33.6	0.41
	-32.8	-0.36
8	35.2	0.40
	-32.8	-0.36
9	46.9	0.61
	-44.0	-0.55
10	48.9	0.61
	-44.1	-0.56
11	63.4	0.84
	-57.3	-0.78
12	64.7	0.81
	-58.6	-0.84
13	74.8	1.07
	-64.5	-0.98
14	72.2	1.1
	-66.4	-1.0
15	75.1	1.0
	-68.8	-1.1
16	74.5	1.3
	-70.3	-1.2
17	75.5	1.3
	-71.2	-1.2
18	76.3	1.6
	-82.4	-1.8
19	76.2	1.5
	-62.0	-1.5
20	75.6	1.8
	-69.6	-1.8
21	77.2	1.82
	-70.	-1.8
22	75.9	2.0
	-69.8	-2.0
23	74.3	2.3
	-50.8	-2.3

Table 4-10 Load-Displacement History for Specimen S9

Cycle	Load (kips)	Drift (%)
1	-12.6	-0.01
	15.1	0.02
2	-14.4	-0.01
	16.1	0.02
3	-20.9	-0.02
	26.8	0.05
4	-28.3	-0.03
	26.4	0.05
5	-53.5	-0.11
	49.2	0.12
6	-50.4	-0.12
	51.2	0.14
7	-81.3	-0.22
	66.1	0.21
8	-77.9	-0.22
	65.1	0.21
9	-99.3	-0.30
	91.9	0.32
10	-96.0	-0.31
	85.8	0.31
11	-109	-0.49
	103	0.39
12	-108	-0.49
	103	0.40
13	-111	-0.70
	113	0.67
14	-106	-0.72
	109	0.66
15	-109	-0.98
	113	0.91
16	-103	-0.97
	108	0.94
17	-106	-1.2
	110	1.3
18	-96.7	-1.2
	94.4	1.3
19	-95.7	-1.5
	94.9	1.5
20	-84.0	-1.8
	87.5	1.9
21	-70.4	-2.1
	72.2	2.2

Table 4-11 Load-Displacement History for Specimen S10

Cycle	Load (kips)	Drift (%)
1	-11.9	-0.11
	10.9	0.03
2	-11.7	-0.03
	9.8	0.03
3	-17.7	-0.06
	20.5	0.07
4	-19.0	-0.07
	29.0	0.09
5	-32.0	-0.15
	43.3	0.18
6	-32.1	-0.15
	42.3	0.17
7	-48.1	-0.25
	59.0	0.29
8	-48.9	-0.25
	60.2	0.30
9	-65.9	-0.35
	74.6	0.41
10	-70.3	-0.36
	74.1	0.42
11	-84.6	-0.43
	88.5	0.66
12	-82.1	-0.47
	87.6	0.61
13	-88.7	-0.62
	91.7	0.80
14	-84.7	-0.63
	90.7	0.76
15	-90.3	-0.90
	98.5	1.1
16	-93.1	-1.1
	93.7	1.1
17	-86.5	-1.0
	94.8	1.2
18	-88.7	-1.1
	93.7	1.2
19	-90.0	-1.3
	97.3	1.5
20	-89.8	-1.5
	94.3	1.8
21	-87.8	-1.8
	95.7	2.1
22	-87.0	-2.0
	90.3	2.4

Table 4-12 Initial Values for Secant Peak-to-Peak Displacement Stiffness and Corresponding Drifts

Specimen	Stiffness (kip/in.)	Drift [1] (%)
S1	260	0.10
S2	160	0.14
S4	530	0.13
S5	310	0.14
S6	260	0.10
S7	170	0.15
S8	180	0.15
S9	720	0.10
S10	480	0.14

[1] The drift value listed refers to the average drift in the cycle for which the secant stiffness was calculated

Table 5-1 Theoretical Yield Curvature Based on Section Modeling

Specimen	ϕ_y (rad/in.)
S4	9.8×10^{-5}
S5	9.9×10^{-5}
S9	8.5×10^{-5}
S10	9.1×10^{-5}

Table 5-2 Plastic Hinge Length

Specimen	Plastic Hinge Length, ℓ_p			
	Pauley and Priestley (1993)		Experimental	
	(in.)	$\left(\ell_p/h\right)^{(1)}$	(in.)	$\left(\ell_p/h\right)^{(1)}$
S4 (RC)	9.8	0.25	6.6	0.16
S5 (HPFRC)			8.7	0.22
S9 (RC)	10.3	0.20	5.8	0.11
S10 (HPFRC)			7.9	0.15

(1) h is the wall height (in.) excluding the top block

Table 5-3 Stress-Strain Values for Modeling of Regular Concrete (Specimens S4 and S9) and HPFRC (Specimens S5 and S10) Tensile Behavior

Matrix	σ_{t1}	ε_{t1}	σ_{t2}	ε_{t2}	σ_{t3}	ε_{t3}	σ_{t4}	ε_{t4}
Regular Concrete	450	0.00008	0	0.00008	-	-	-	-
HPFRC	400	0.0001	500	0.005	200	0.015	100	0.02

Table 5-4 Compression Stress-Strain Model for Regular Concrete (Specimens S4 and S9) and HPFRC (Specimens S5 and S10) Matrix

Matrix	f'_c (psi)	ε_o	Z	ε_{cu}
Regular concrete	6300	0.003	150	0.008
HPFRC	5600	0.006	100	0.01

Table 5-5 Compressive Strains at Wall Edge in RC Specimens

Compressive Strain [1]	Specimen S4			Specimen S9		
	1.0% drift	1.5% drift [5]	2.0% drift	1.0% drift	1.5% drift [5]	2.0% drift
ε_1 [2]	0.0043	0.0055	0.0061	0.0028	0.0039	0.0085 [6]
ε_2 [3]	0.001	0.0018	0.0026 [7]	0.0016	0.0028 [7]	N/A [8]
ε_3 [4]	0.00036	0.00040	0.00048 [7]	0.0040	0.00029	0.00026

[1] Strain refers to the average compression strain calculated for the positive and negative loading direction, unless otherwise noted
[2] Average compressive strain measured at wall edge from 0 in. to 4 in. from the wall base
[3] Average compressive strain measured at wall edge from 4 in. to 9 in. from the wall base
[4] Average compressive strain measured at wall edge from 9 in. to 14 in. from the wall base
[5] For Specimens S4 and S9, the wall drift capacity was 1.5%
[6] Strain refers only to the positive loading direction
[7] Strain refers only to the negative loading direction
[8] Concrete spalling at the wall edge affected the readings of some Optotrak markers and a reasonable estimated for the compressive strain could not be obtained

Table 5-6 Friction Coefficient Values Based on Test Results

Specimen	Calculated Shear Friction Coefficient, μ
S1	0.52
S2	0.52
S4	0.42
S5	0.39
S6	0.37
S7	0.35
S8	0.35
S9	0.39
S10	0.41

Table 5-7 Elastic Sliding Stiffness Normalized by Shear Friction Strength (μ = 1)

Specimen	Normalized Elastic Sliding Stiffness $(1/in.)$
S4	8.9
S5	7.1
S6	8.2
S9	7.8
S10	7.5

Table 5-8 Comparison of test results with other studies [1]

Researcher	Specimen	a/ℓ_w [4]	ρ_v [5] (%)	ρ_h [6] (%)	ρ_{conf} [7] (%)	v_{max} in $\sqrt{f'_c}$ (psi)	Drift capacity (%)
Cardenas et al. (1980)	SW-7 [2]	1.1	1.0	0.27	-	6.6	1.1
	SW-8 [2]	1.1	2.8	0.27	-	7.2	1.5
	SW-9 [2]	1.1	2.8	1.0	-	8.6	0.6
	SW-10 [2]	1.1	-	-	-	4.0	0.7
	SW-11 [2]	1.1	-	0.75	-	8.2	1.4
	SW-12 [2]	1.1	-	1.0	-	8.8	1.9
	SW-13 [3]	1.1	2.8	1.0	-	8.0	0.5
Lefas et al. (1990)	SW11 [2]	1.1	2.4	1.1	0.67 [8]	8.2	1.0
	SW14 [2]	1.1	2.4	1.1	0.67 [8]	9.4	1.4
	SW17 [2]	1.1	2.4	1.1	0.67 [8]	8.2	1.3
Maier (1992)	S4 [2]	1.2	1.0	1.0	-	7.0	1.0
	S9 [2]	1.2	1.0	-	-	6.5	1.4
	S10 [2]	1.2	1.0	0.98	-	12	1.3
Salonikios et al. (1999)	MSW1 [3]	1.5	0.57	0.57	1.0 [9]	3.9	1.5
	MSW2 [3]	1.5	0.28	0.28	1.0 [9]	2.4	1.9
	MSW6 [3]	1.5	0.57	0.57	1.7 [9]	3.9	1.6
	LSW1 [3]	1.0	0.57	0.57	1.7 [9]	5.6	0.9
	LSW2 [3]	1.0	0.28	0.28	1.7 [9]	4.1	0.9
This study	S1 [3]	1.2	0.71	0.71	1.0	5.9	2.4
	S2 [3]	1.2	0.31	0.31	-	4.4	3.0
	S4 [3]	1.2	0.83	0.83	1.0	7.9	1.5
	S5 [3]	1.2	0.63	0.63	0.25	6.4	1.5
	S6 [3]	1.5	0.71	0.71	1.0	6.7	2.1
	S7 [3]	1.5	0.21	0.13	-	6.2	2.1
	S8 [3]	1.5	0.21	0.13	-	6.5	2.2
	S9 [3]	1.5	0.67	0.67	1.0	9.4	1.5
	S10 [3]	1.5	0.50	0.50	0.25	8.6	2.2

[1] See also Tables 2-1 and 2-2 for more information on the test specimens
[2] Monotonic loading tests
[3] Cyclic loading tests
[4] a/ℓ_w: wall shear span-to-length
[5] ρ_v: web vertical reinforcement ratio
[6] ρ_h: web horizontal reinforcement ratio
[7] ρ_{conf}: ratio of volume of confinement reinforcement to volume of concrete core in wall boundary elements
[8] Approximate value of confinement reinforcing ratio as exact information could not be obtained from the publication (does not comply with 2005 ACI Code provisions for special boundary elements)
[9] Confinement in the boundary region followed the provisions of Eurocode EC8 but the detailing did not comply with Eurocode EC8 provisions
[10] Inadequate anchorage development of the straight vertical reinforcement in the upper part of the wall was also reported for the specimen

Fig. 1-1 Typical Reinforcement Detailing in the Boundary Regions of Reinforced Concrete Structural Walls (courtesy of Andres Lepage)

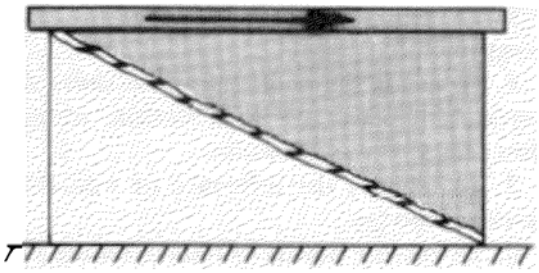

(a) Typical Diagonal Tension Failure

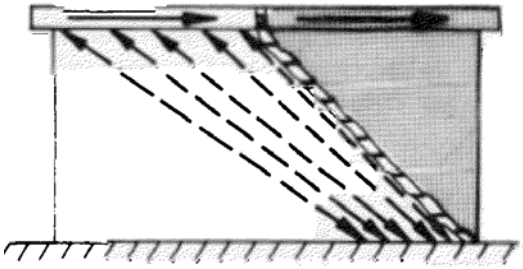

(b) Diagonal Tension in a Steep Failure Plane

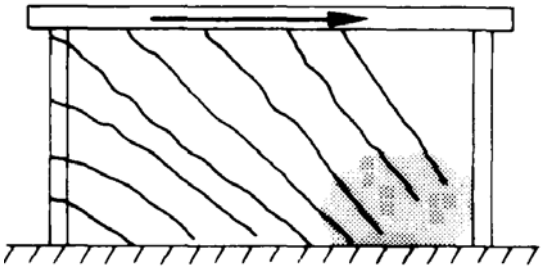

(c) Typical Diagonal Compression Failure

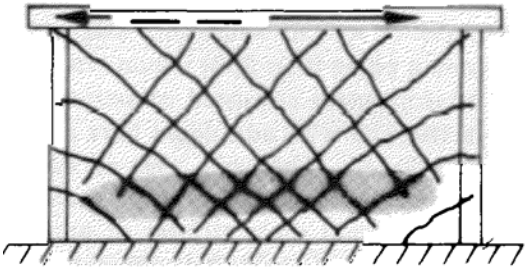

d) Concrete Crushing in the Wall Web

Fig. 2-1 Shear Failure Modes in RC Low-Rise Structural Walls (Paulay et al., 1982)

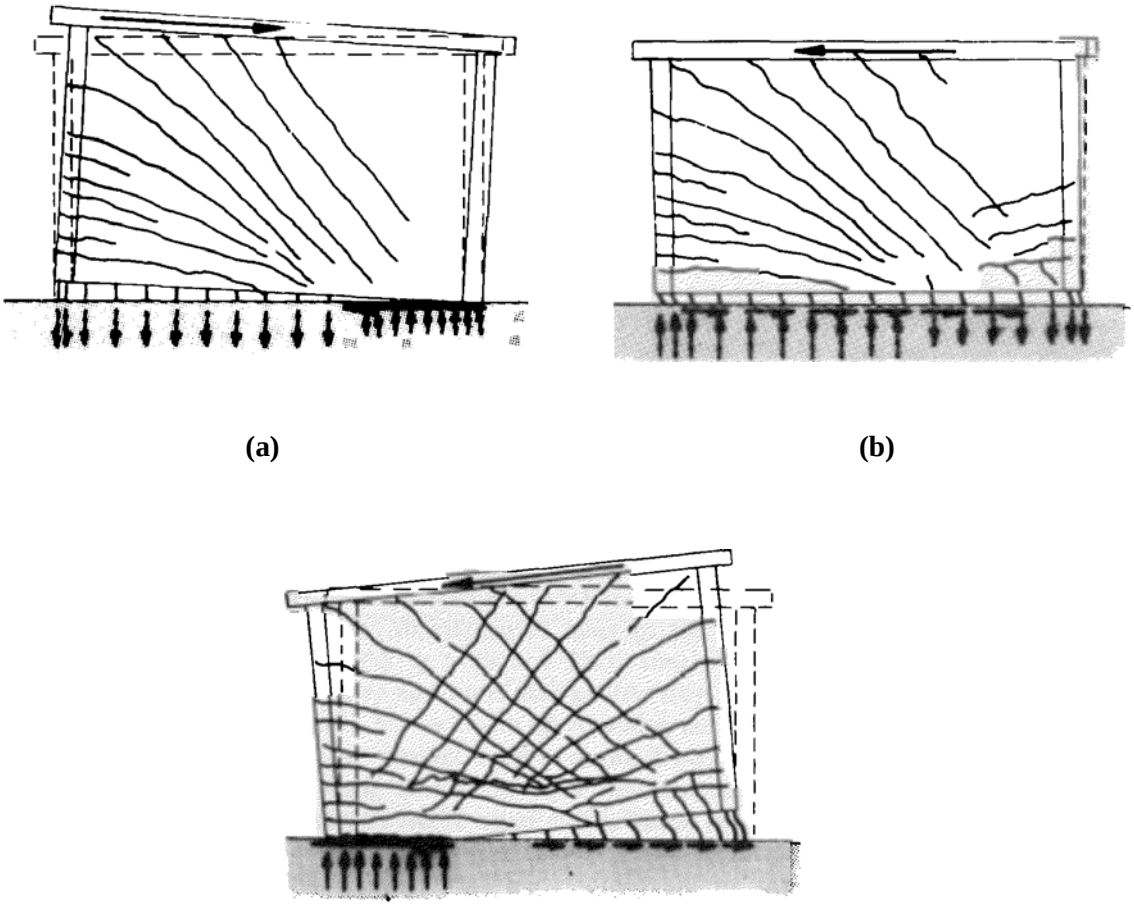

(a) **(b)**

(c)

Fig. 2-2 Development of Sliding Shear Mechanism in RC Low-Rise Walls (Paulay et al., 1982)

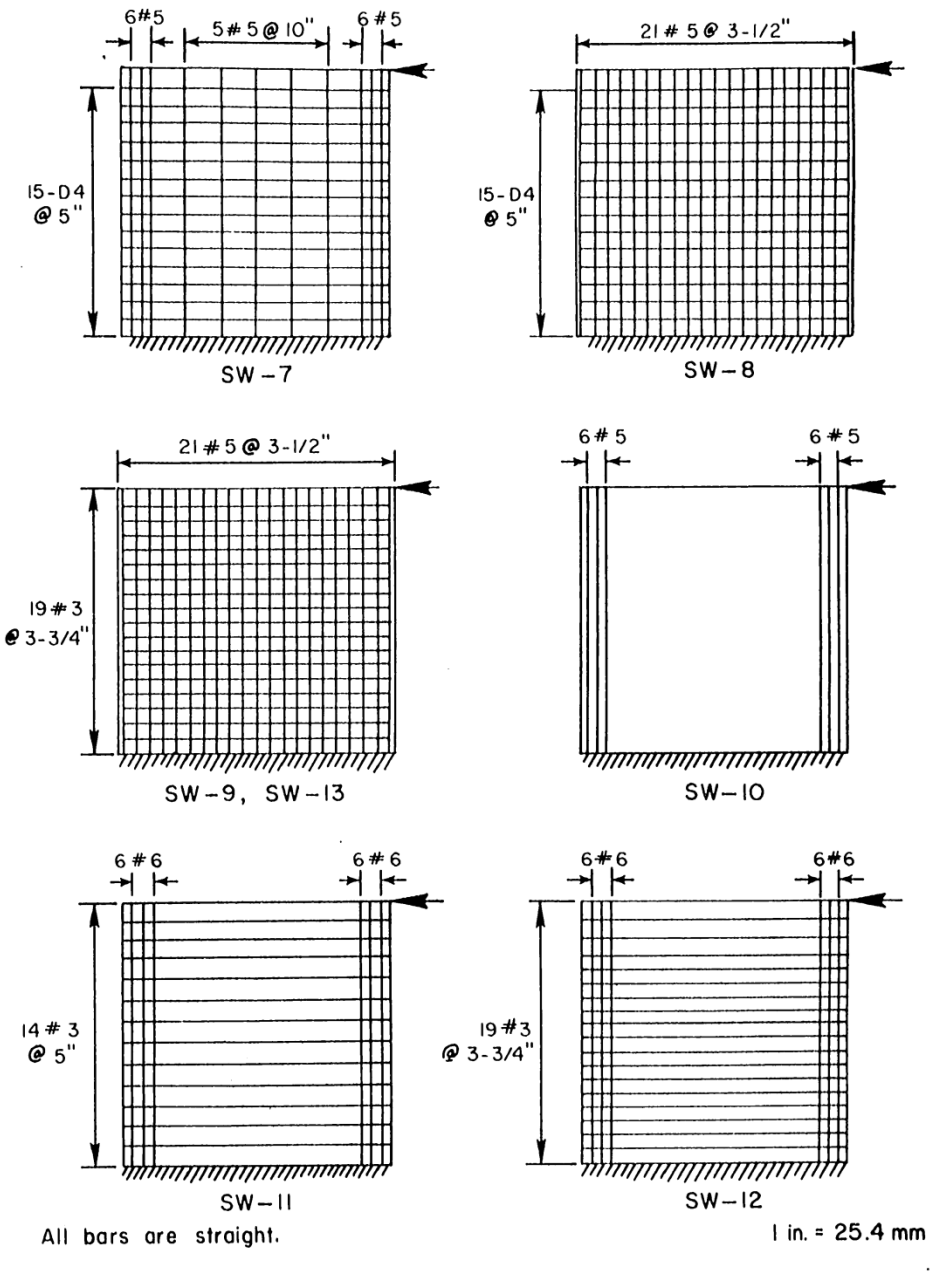

Fig. 2-3 Reinforcing Detailing for the Wall Specimens Tested by Cardenas et al. (1980)

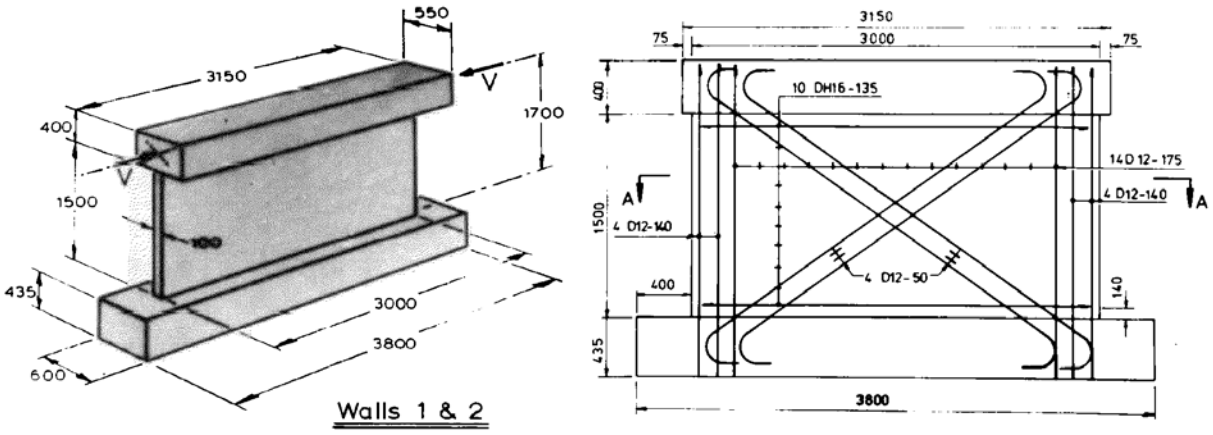

(a) Dimensions of Specimens (in mm) **(b) Diagonal Reinforcement Layout**

Fig. 2-4 Low-Rise Wall Specimen Details in the Study by Paulay et al. (1982)

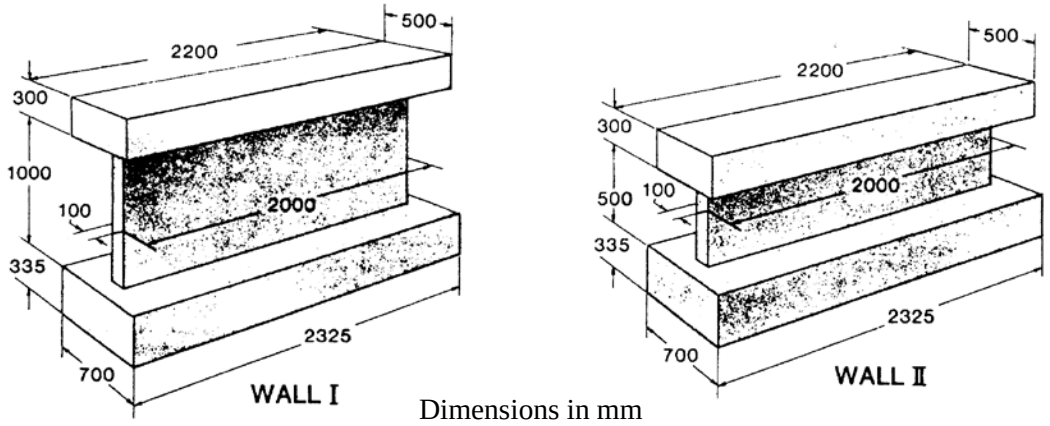

Dimensions in mm

Fig. 2-5 Geometry of Test Specimens by Wiradinata and Saatcioglu (1986)

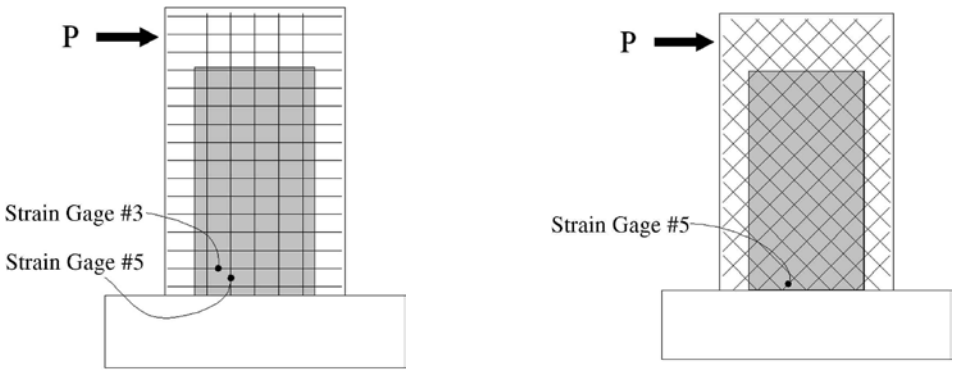

(a) Specimen W1 **(b) Specimen W3**

Fig. 2-6 Reinforcement Layout in the Wall Specimens Tested by Sittupunt et al. (2001)

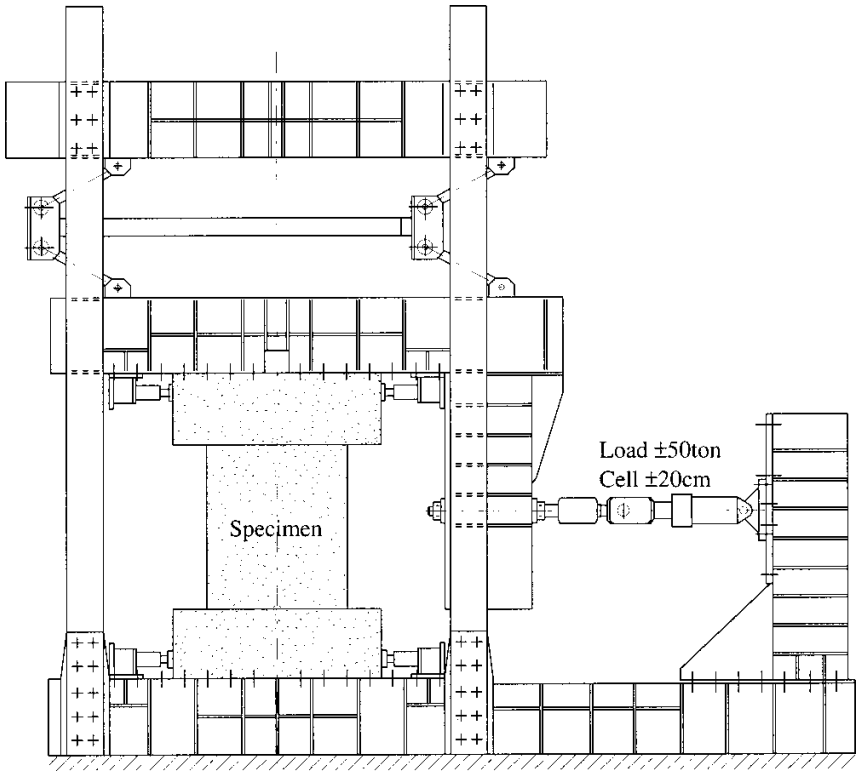

Fig. 2-7 Test Set-Up for Low-Rise Wall Specimens used by Hidalgo et al. (2002)

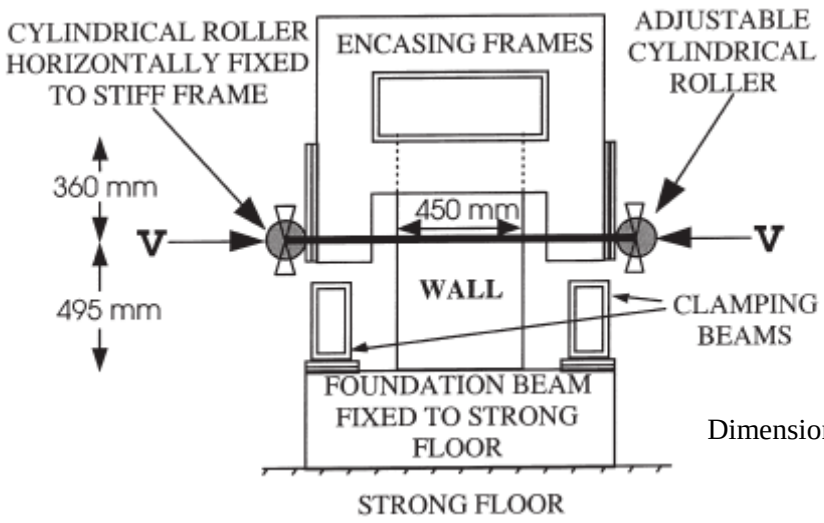

Fig. 2-8 Wall Test Set-Up by Lopes (2000[(a)])

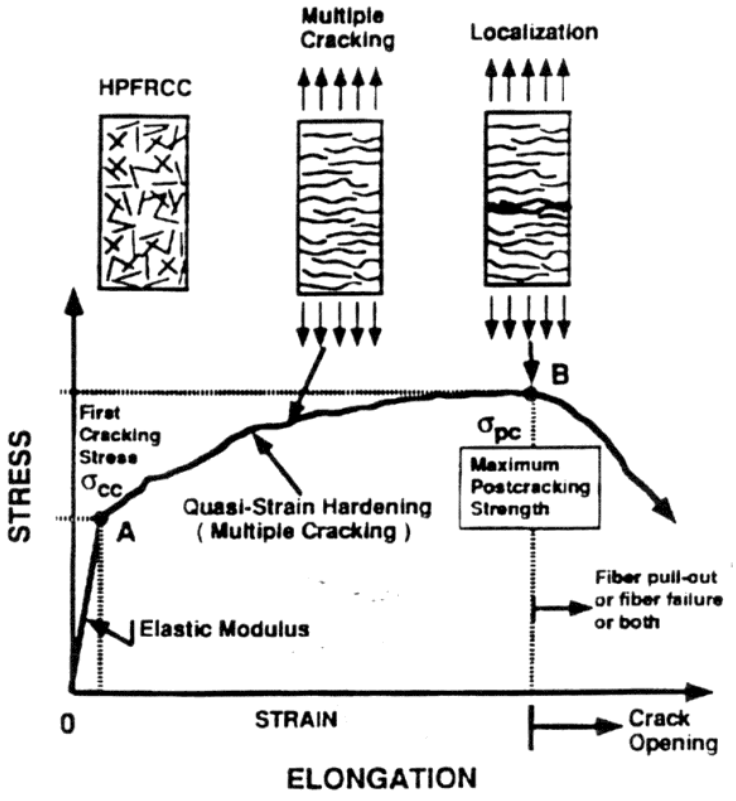

Fig. 2-9 Tensile Stress-Strain Behavior of HPFRCCs (Naaman, 1998)

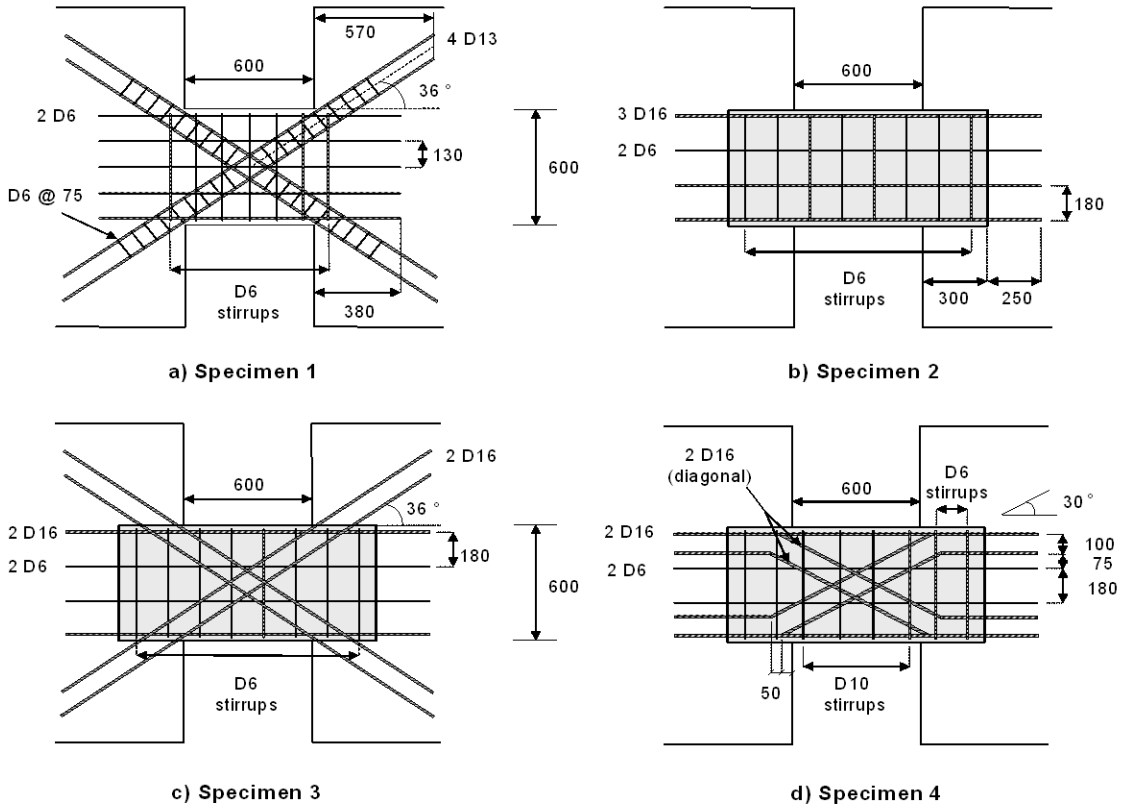

Fig. 2-10 Coupling Beam Specimens in the Study by Canbolat et al. (2005)

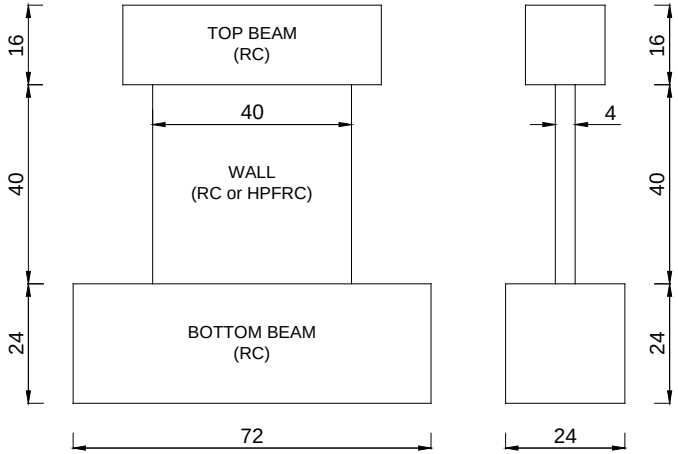

(a) Wall Height-to-Length Ratio of 1.0 (Shear Span-to-Length ratio of 1.2)

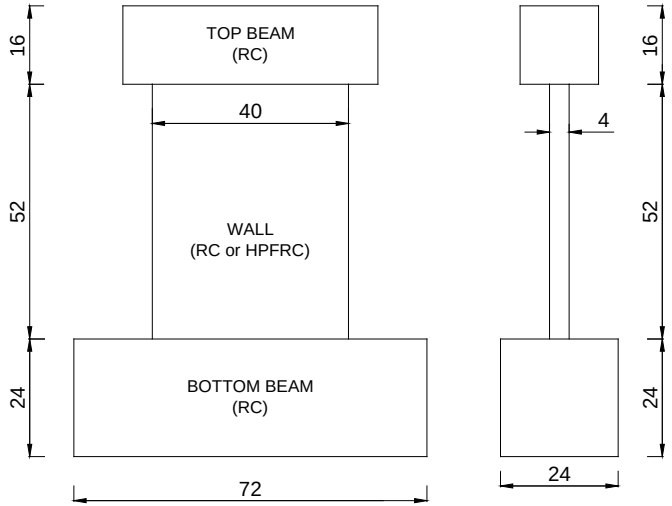

(b) Wall Height-to-Length Ratio of 1.3 (Shear Span-to-Length Ratio of 1.5)

Fig. 3-1 Dimensions of Test Specimens

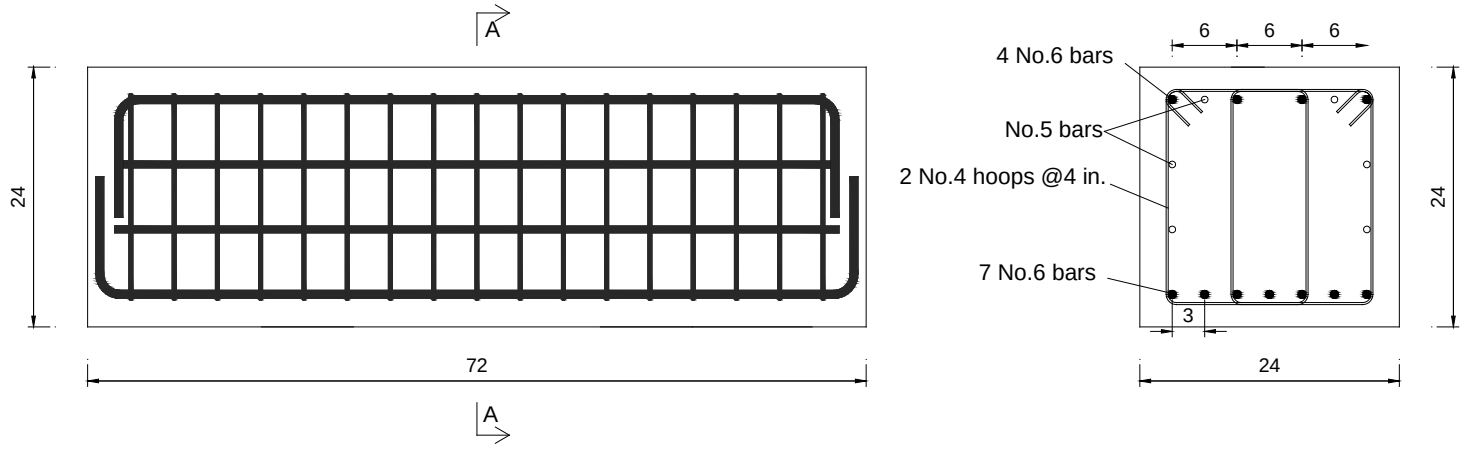

Fig. 3-2 Reinforcement Details for Bottom and Top Block in Specimens S1, S2, S6, S7 and S8

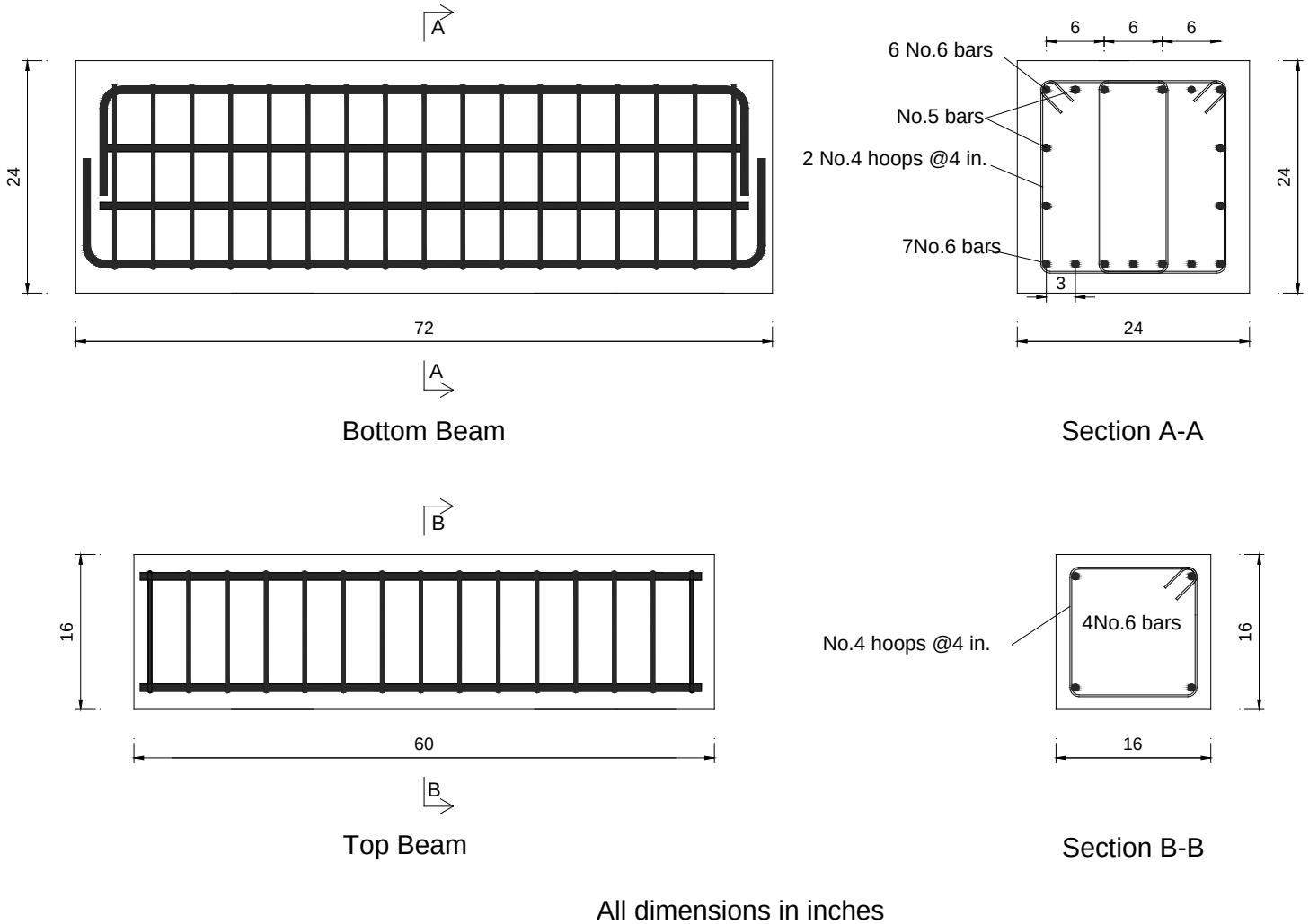

Fig. 3-3 Reinforcement Details for Bottom and Top Block in Specimens S4, S5, S9 and S10

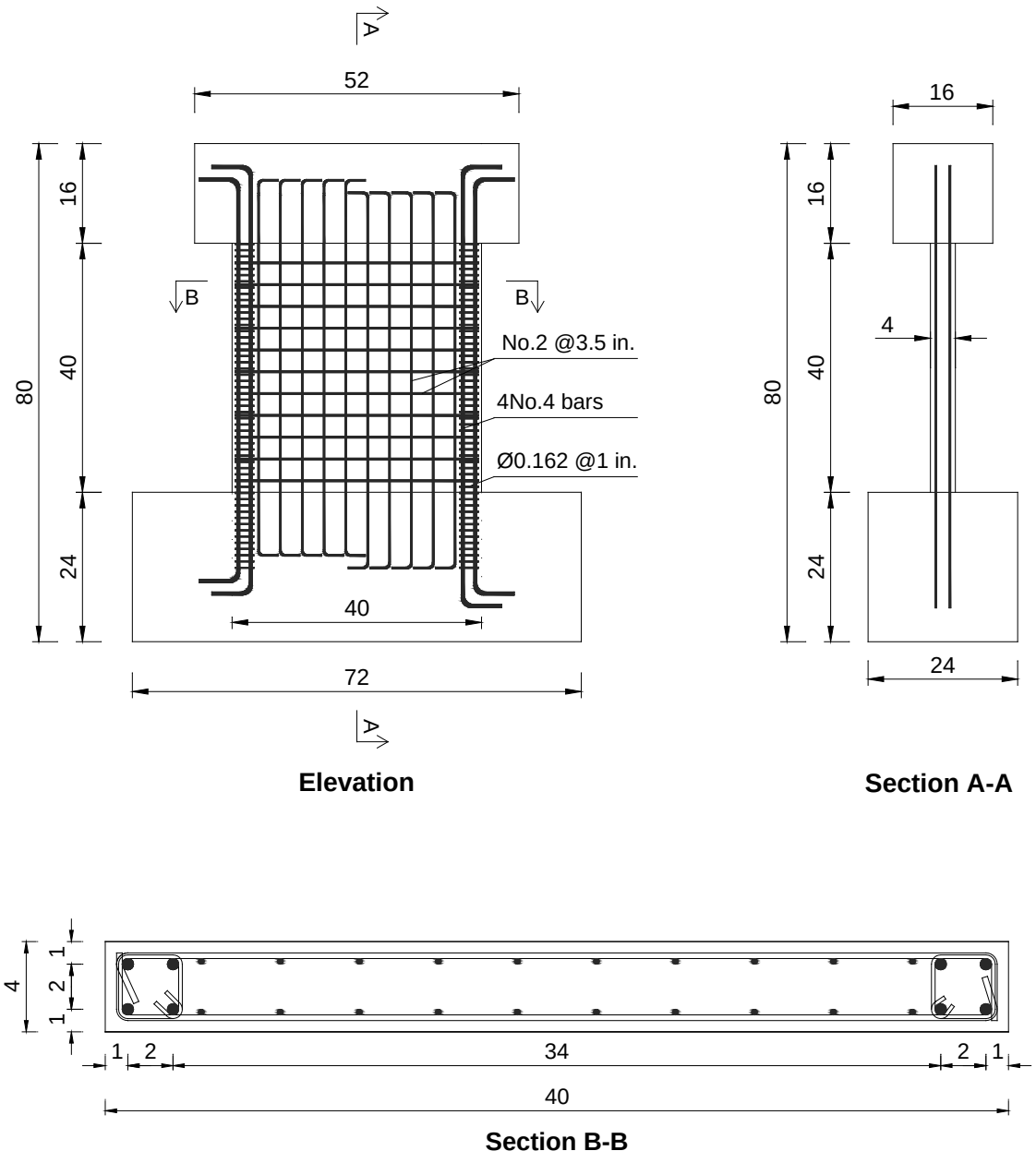

Fig. 3-4 Reinforcement Layout in Specimen S1

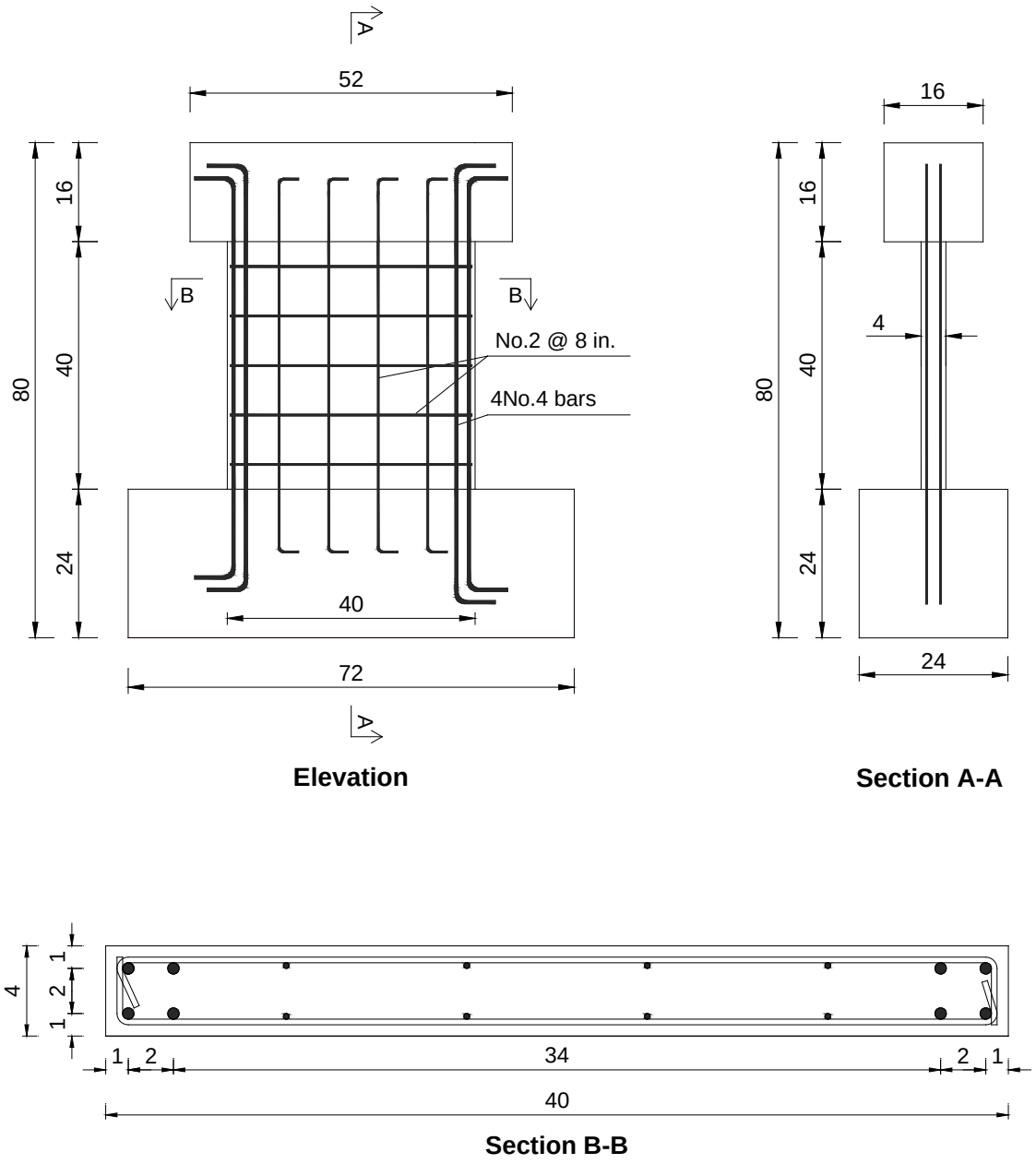

All dimensions in inches

Fig. 3-5 Reinforcement Layout in Specimen S2

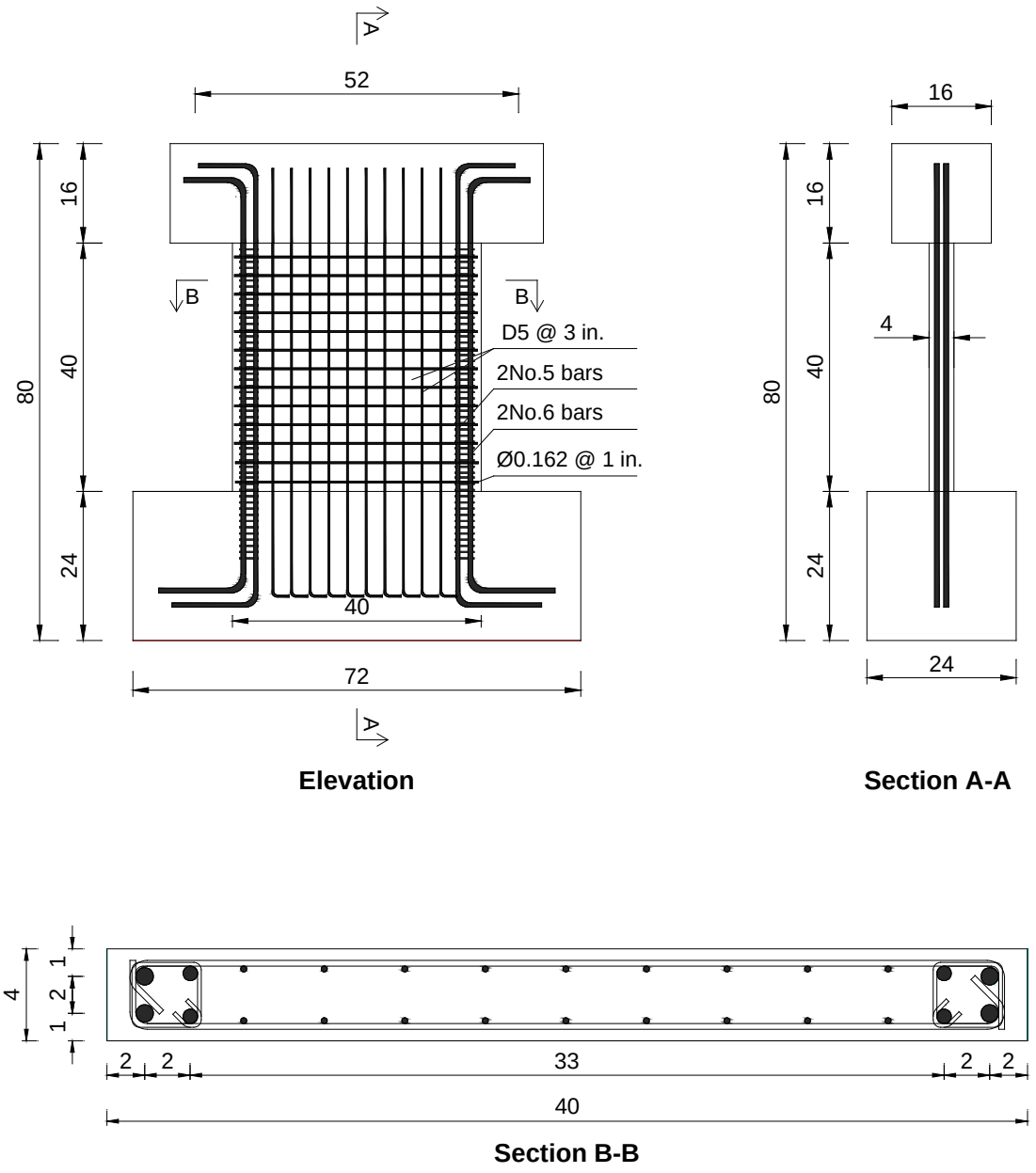

Fig. 3-6 Reinforcement Layout in Specimen S4

Fig. 3-7 Dowel Reinforcement in Specimen S5

Fig. 3-8 Sleeves in Dowel Reinforcement (Specimen S10)

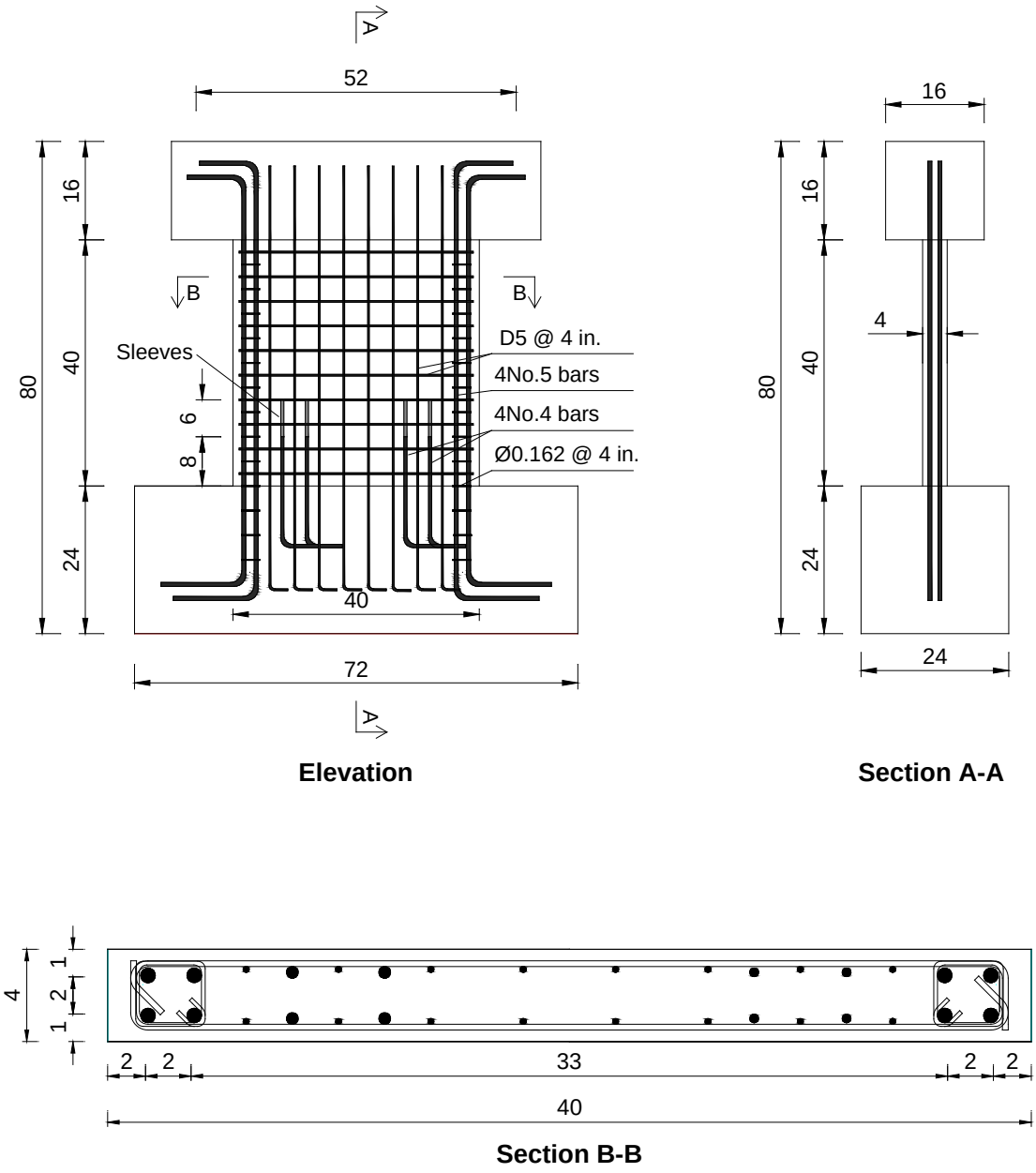

All dimensions in inches

Fig. 3-9 Reinforcement Layout in Specimen S5

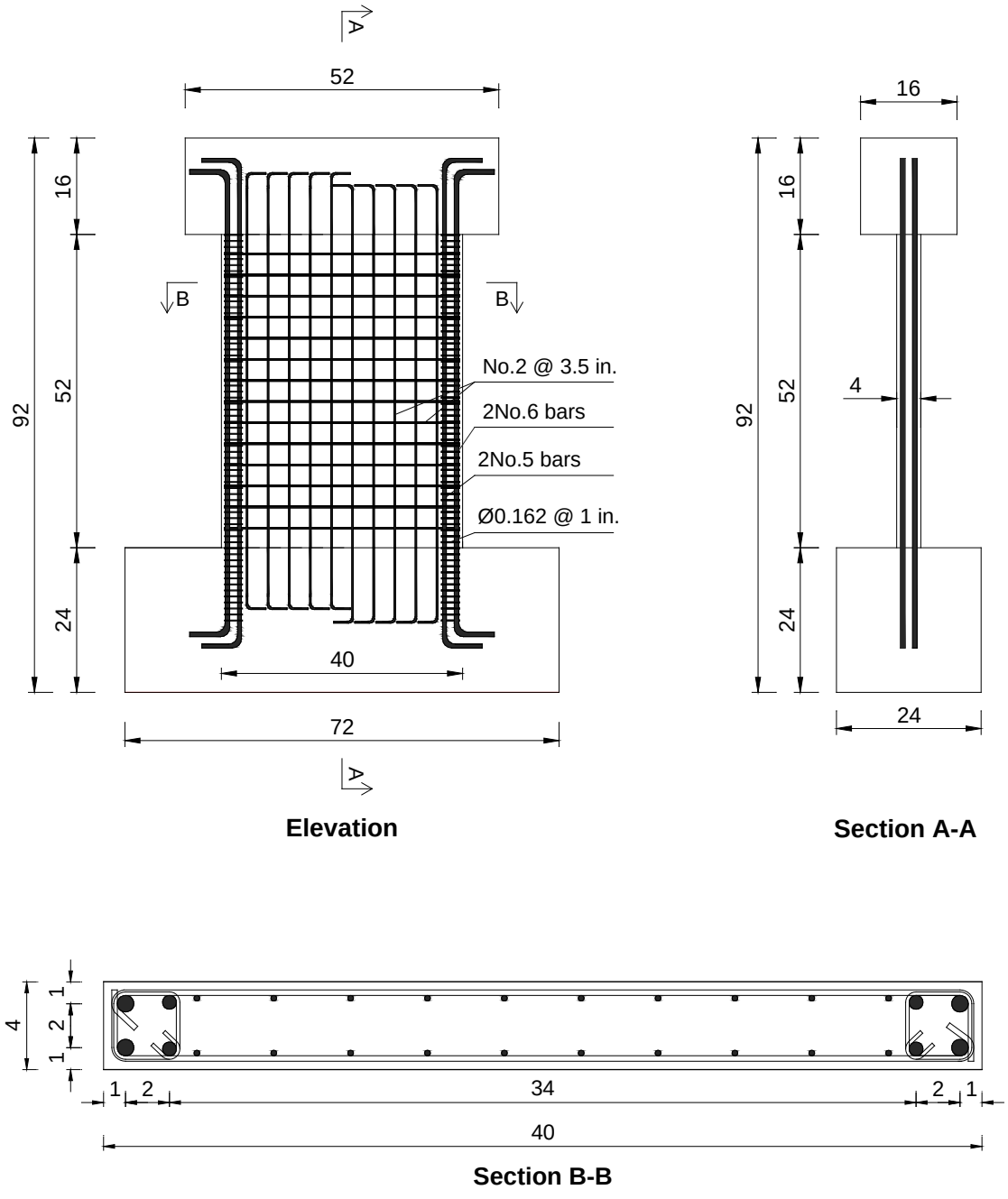

All dimensions in inches

Fig. 3-10 Reinforcement Layout in Specimen S6

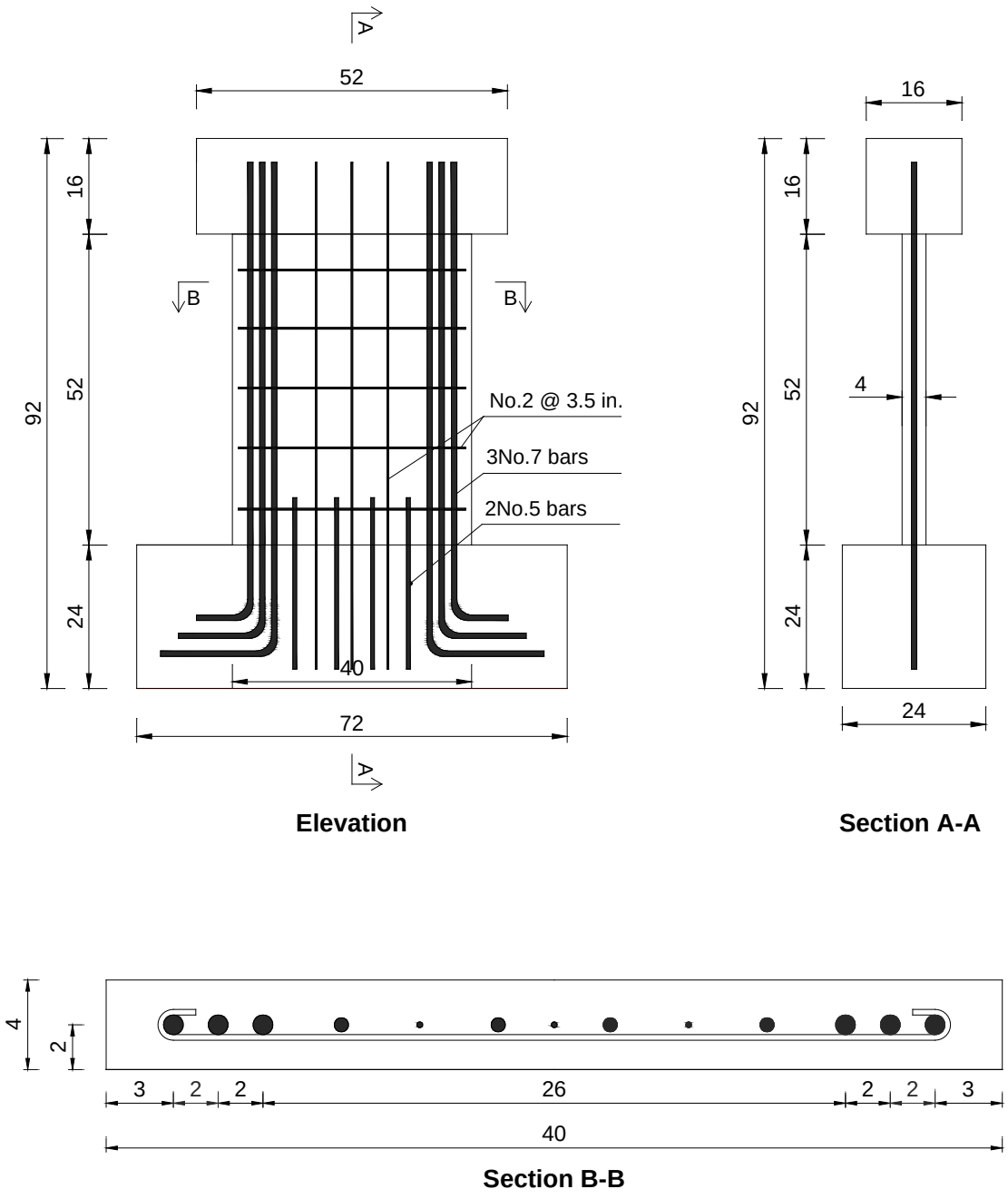

Fig. 3-11 Reinforcement Layout in Specimens S7 and S8

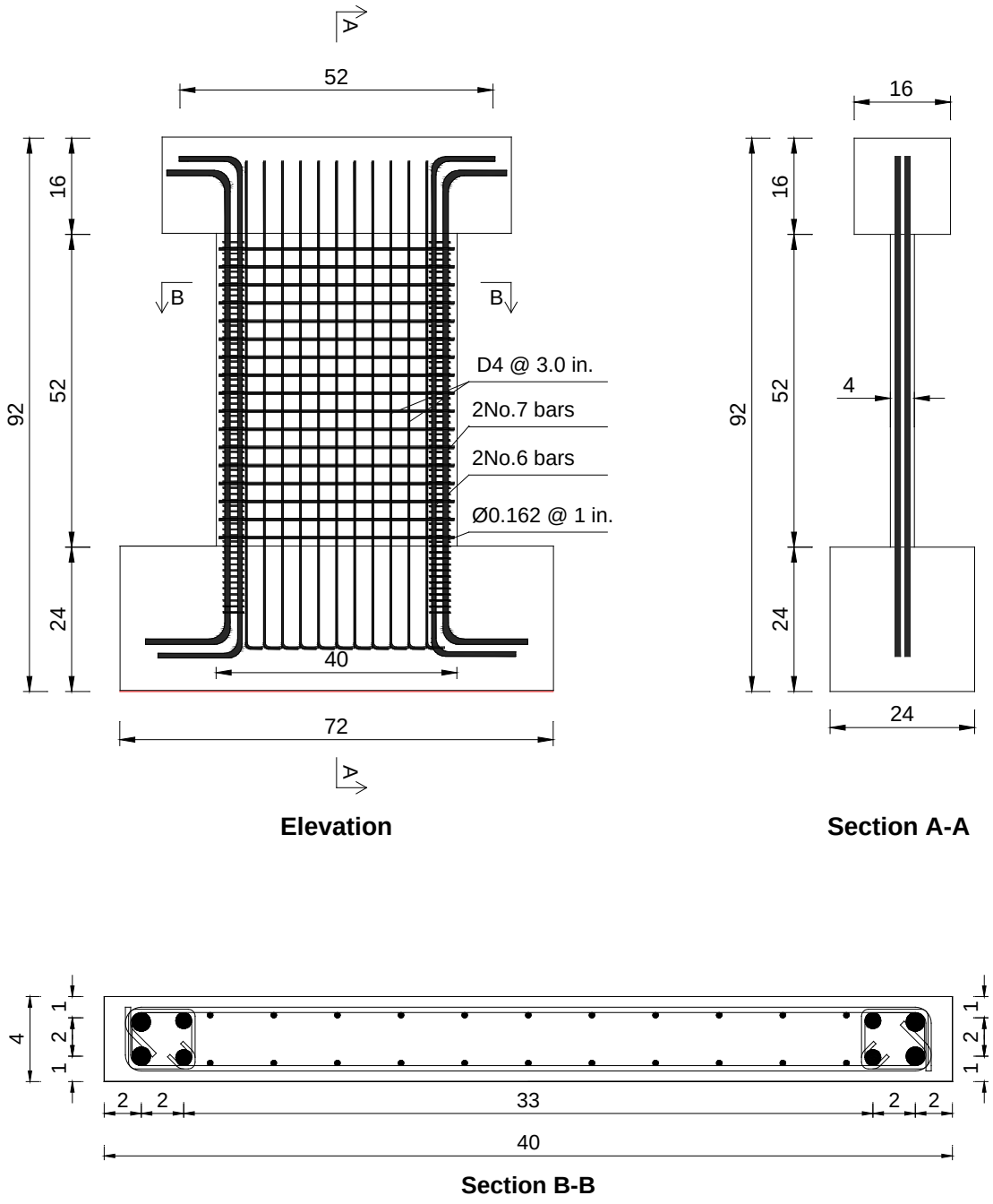

All dimensions in inches

Fig. 3-12 Reinforcement Layout in Specimen S9

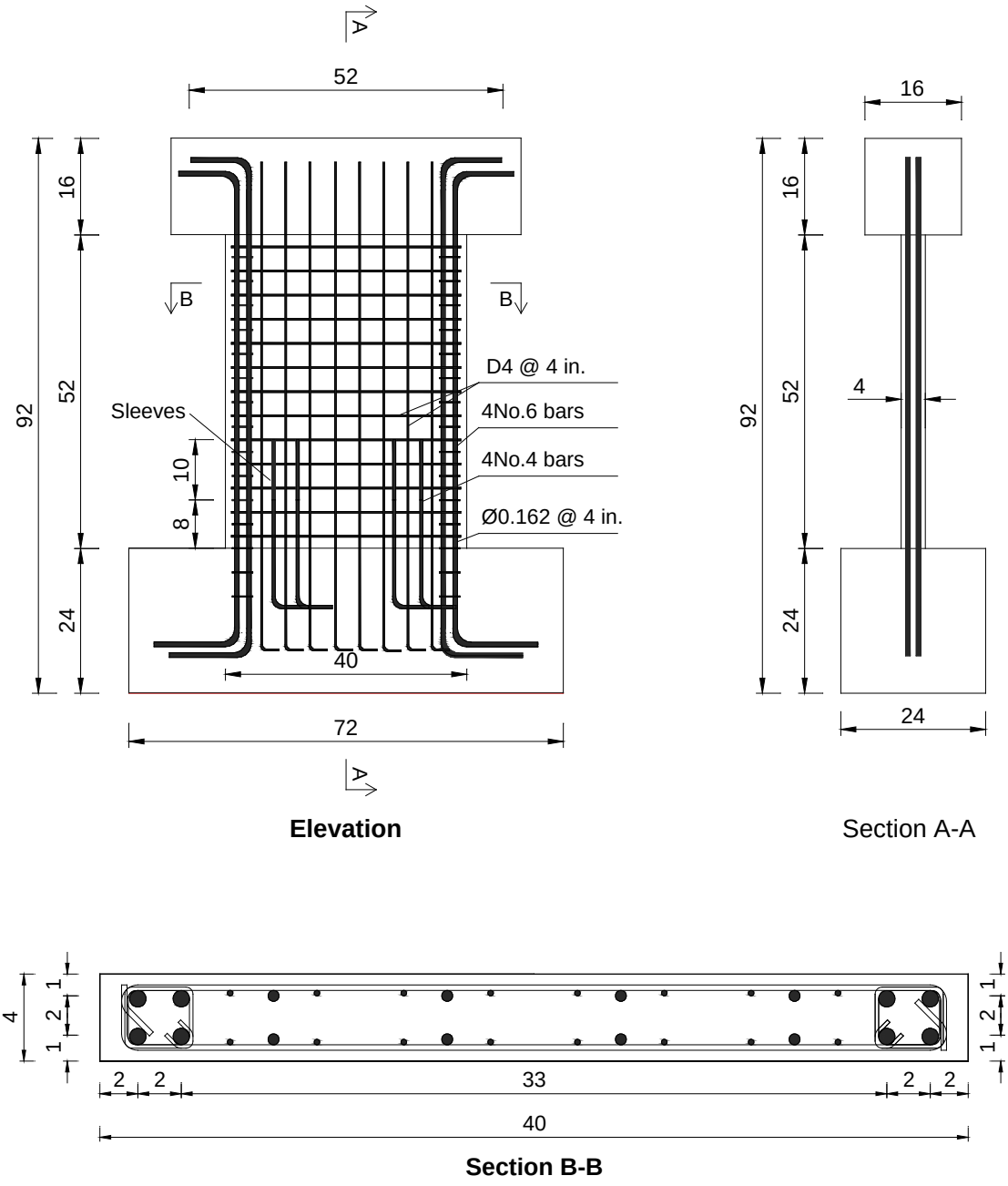

All dimensions in inches

Fig. 3-13 Reinforcement Layout in Specimen S10

(a) 5 Cubic Feet Mixer **(b) 1.5 Cubic Feet Mixer**

Fig. 3-14 Laboratory Concrete Mixers

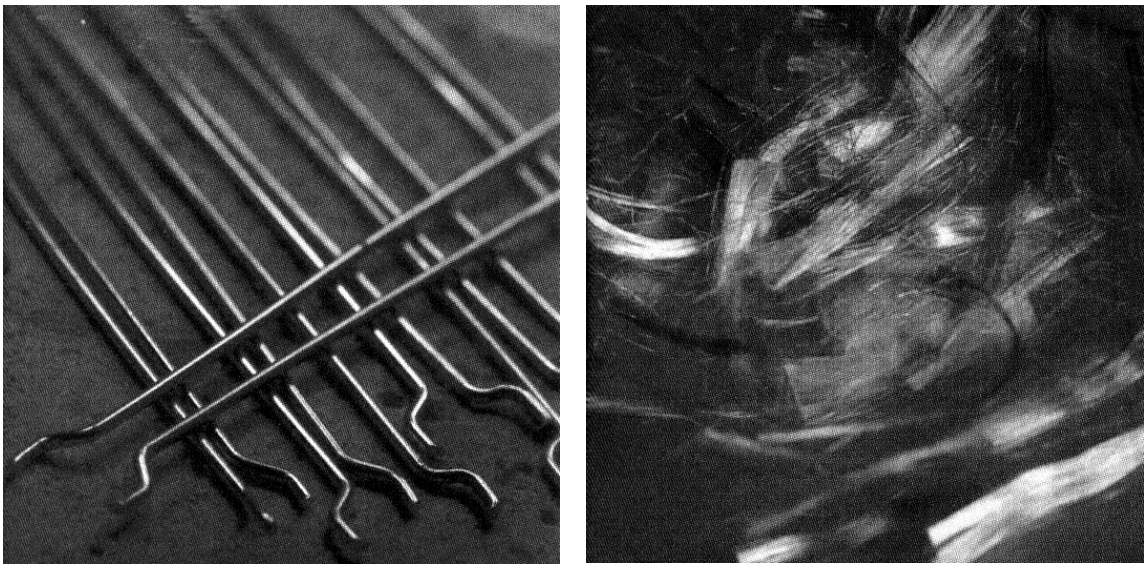

(a) Dramix Fiber **(b) Spectra (PE) Fiber**

Fig. 3-15 Fibers Used in this Study (Naaman, 1999)

(c) Crimped Wire (D4) **(d) Deformed Wire (D5)**

Fig. 3-16 Wire Used in Specimens S4, S5, S9 and S10

Fig. 3-17 ASTM 1609 Beam Test Set-Up

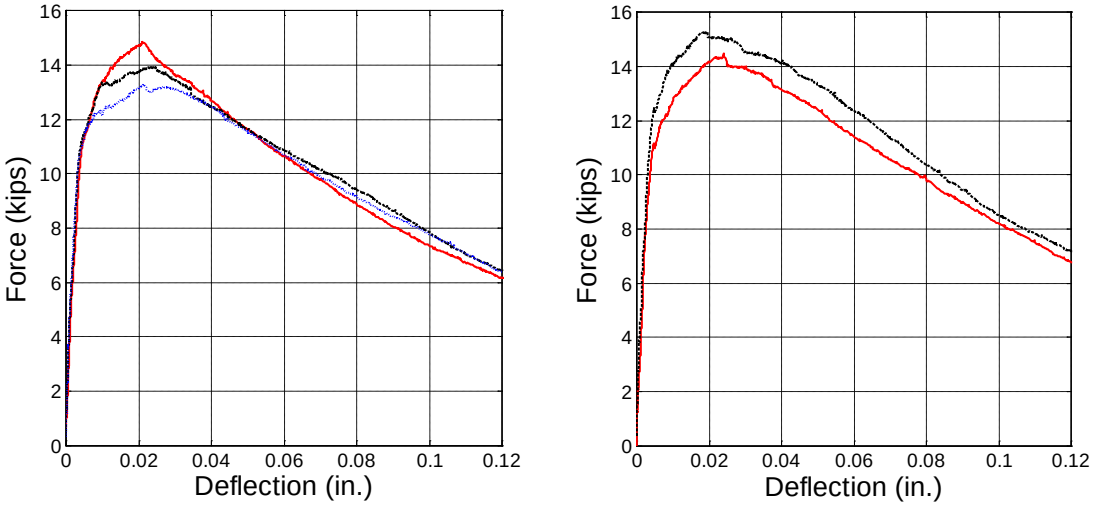

(a) Batch 1 **(b) Batch 2**

Fig. 3-18 Load versus Deflection Response for ASTM 1609 Beam Specimens (Specimen S5)

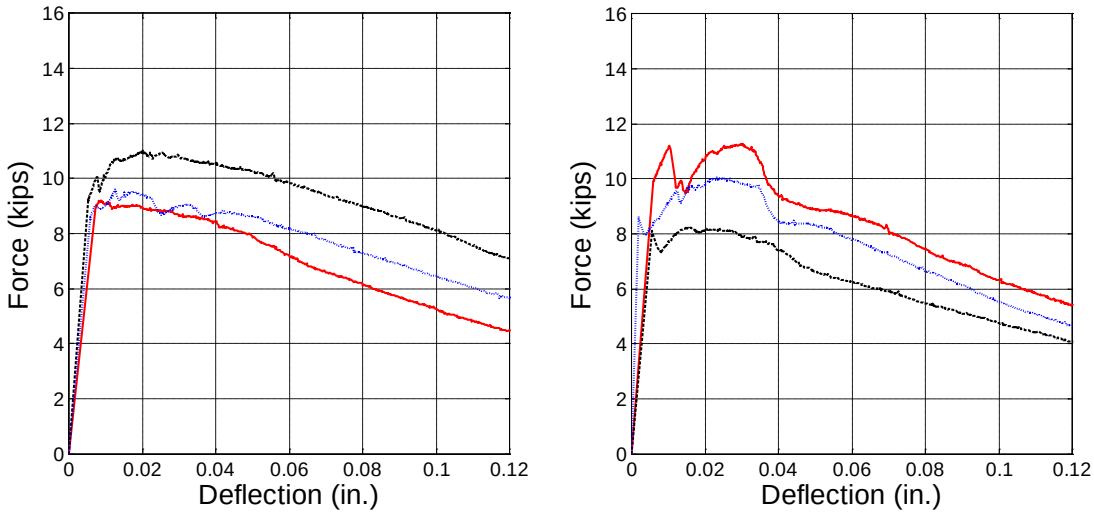

(a)Batch 1 **(b) Batch 2**

Fig. 3-19 Load versus Deflection Response for ASTM 1609 Beam Specimens (Specimen S10)

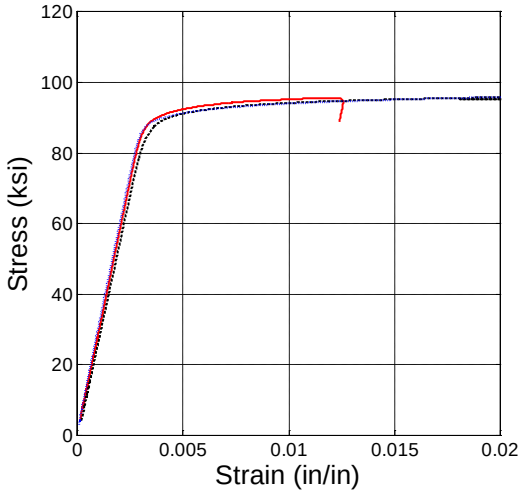

Fig. 3-20 Tensile Stress versus Strain Response for D4 Crimped Wire (Three Coupons)

Fig. 3-21 Base Block inside Formwork (Specimen S4)

Fig. 3-22 Base Block Ready for Casting (Specimen S10)

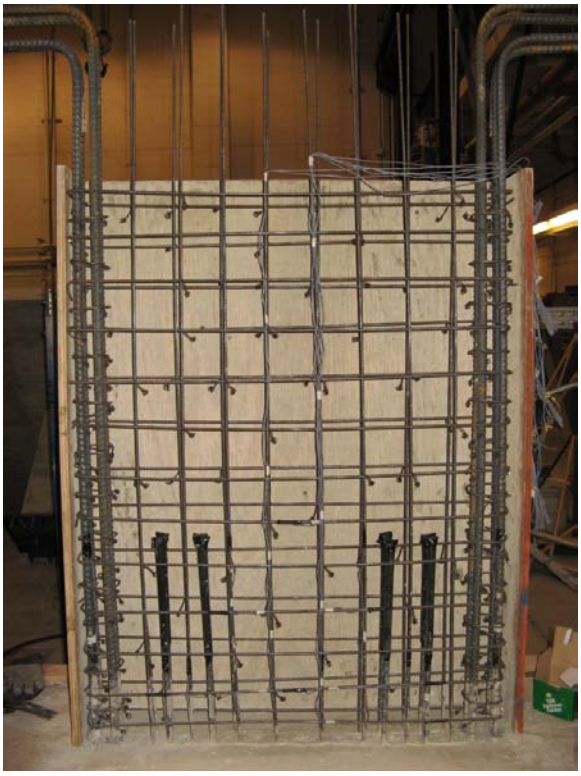

Fig. 3-23 Elevation View of Wall Reinforcement Layout (Specimen S10)

Fig. 3-24 Wall Ready for Casting (Specimen S10)

Fig. 3-25 Bottom Beam and Wall after Removal of Formwork (Specimen S4)

Fig. 3-26 View of Top Beam inside Formwork (Specimen S9)

Fig. 3-27 Completed Specimen (Specimen S6)

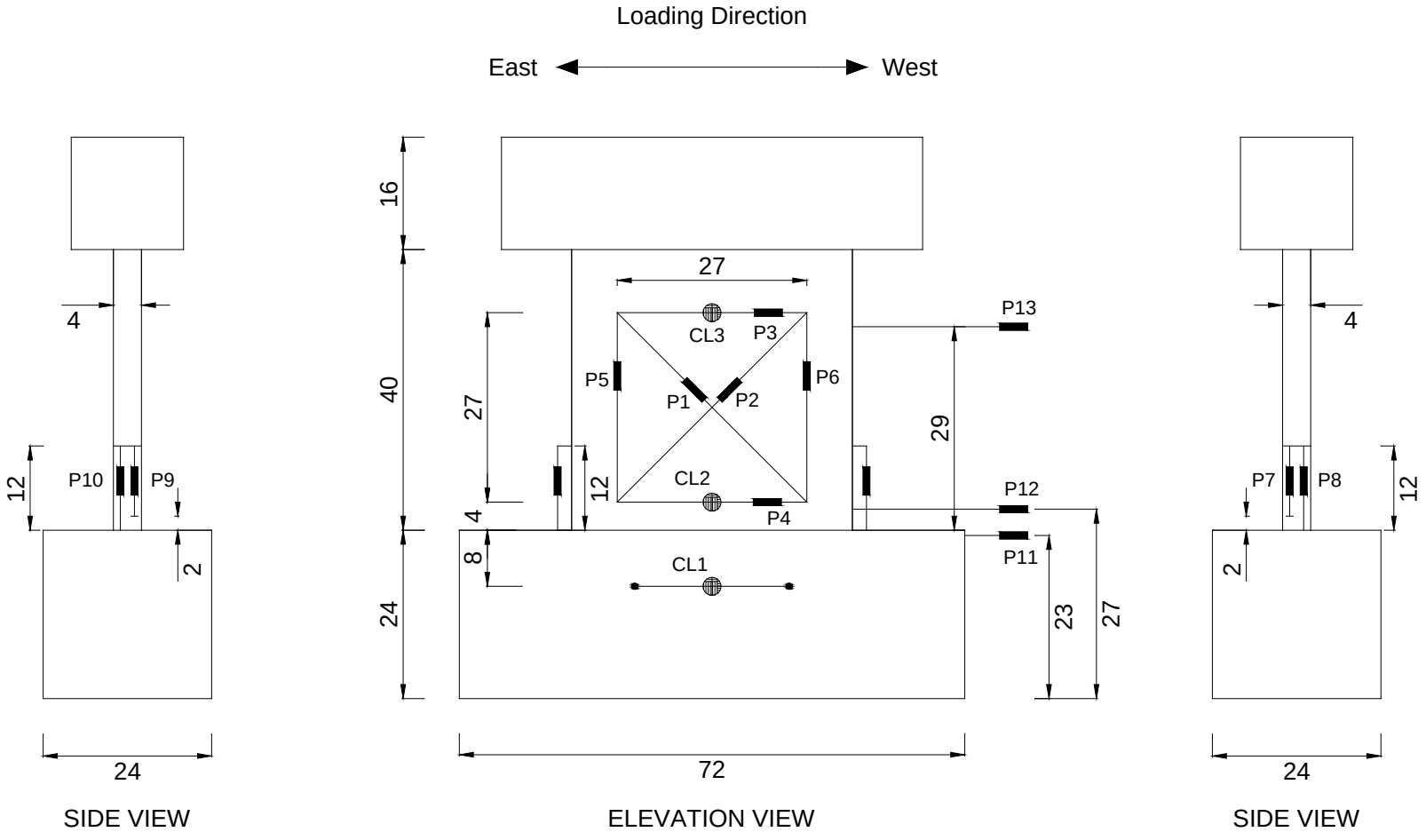

Fig. 3-28 Instrumentation Scheme for Specimens with Shear Span-to-Length Ratio of 1.2

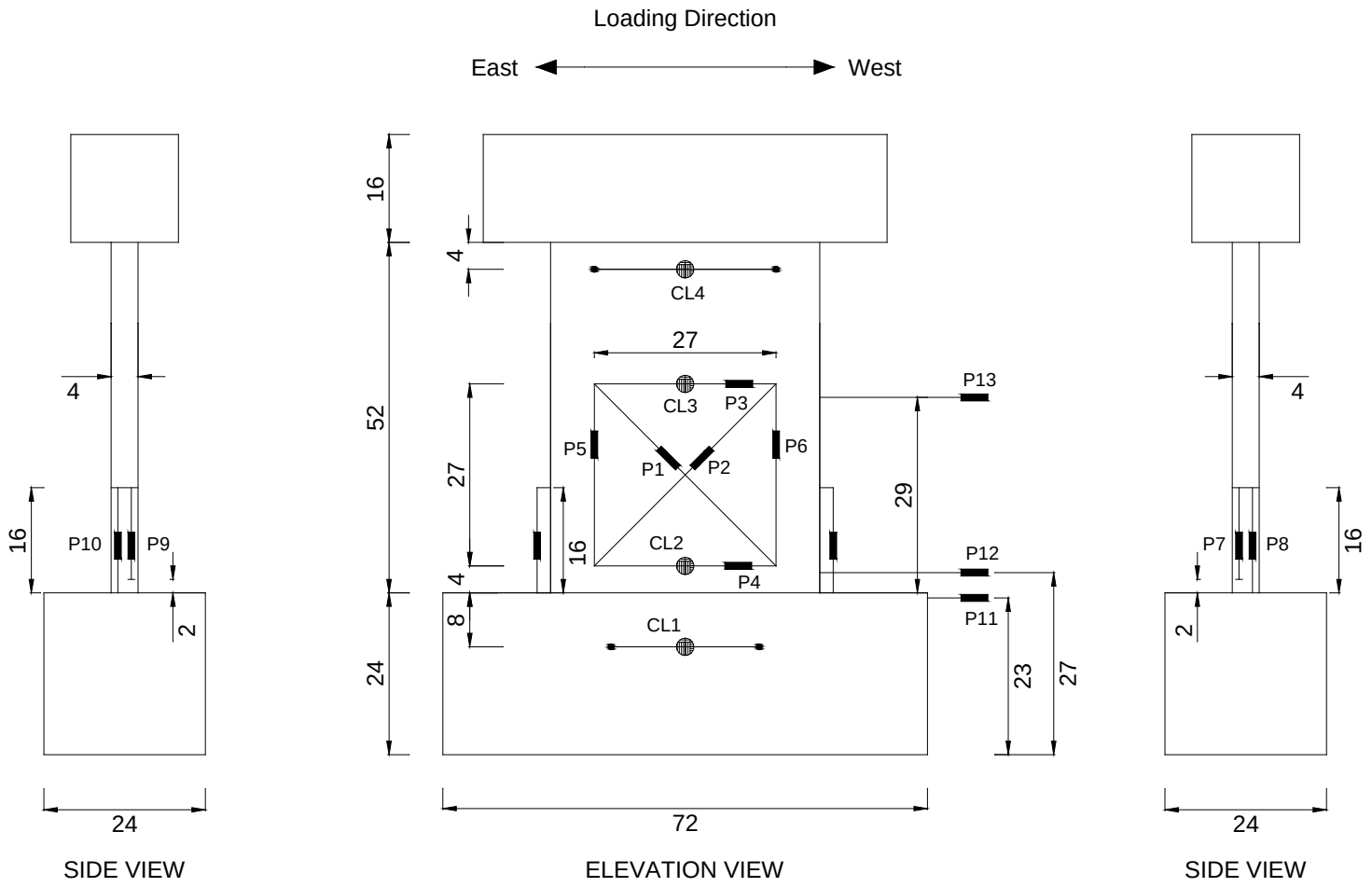

Fig. 3-29 Instrumentation Scheme for Specimens with Shear Span-to-Length Ratio of 1.5

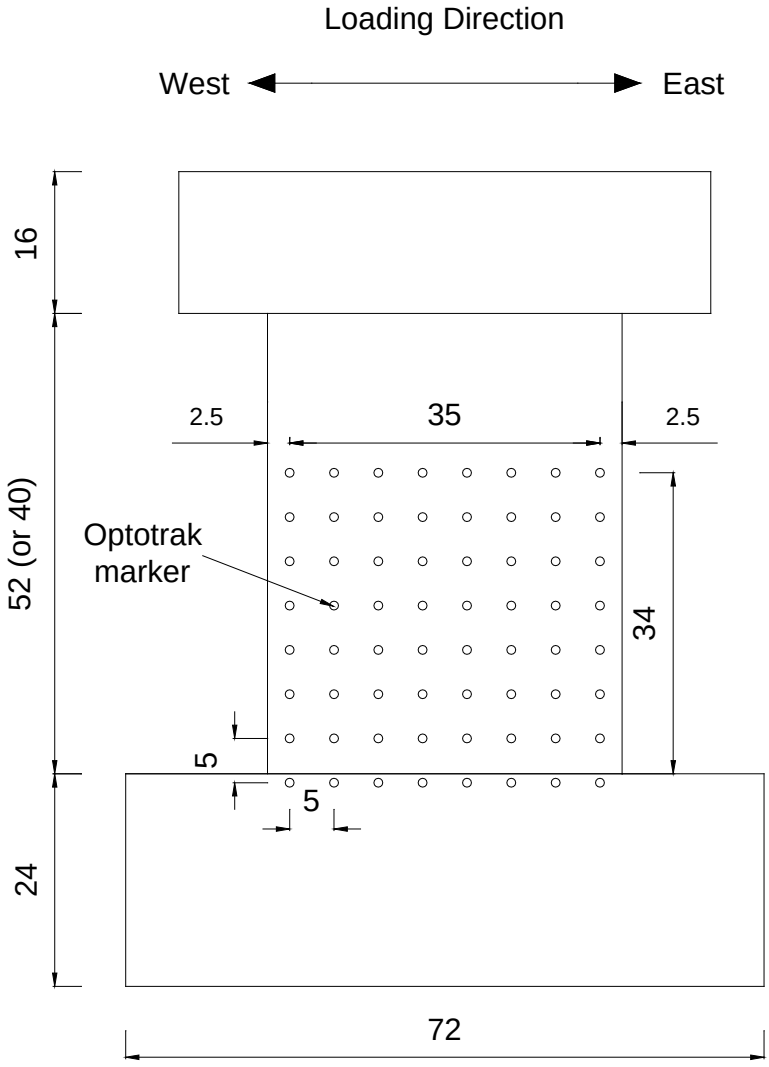

Fig. 3-30 Optotrak System Markers Grid

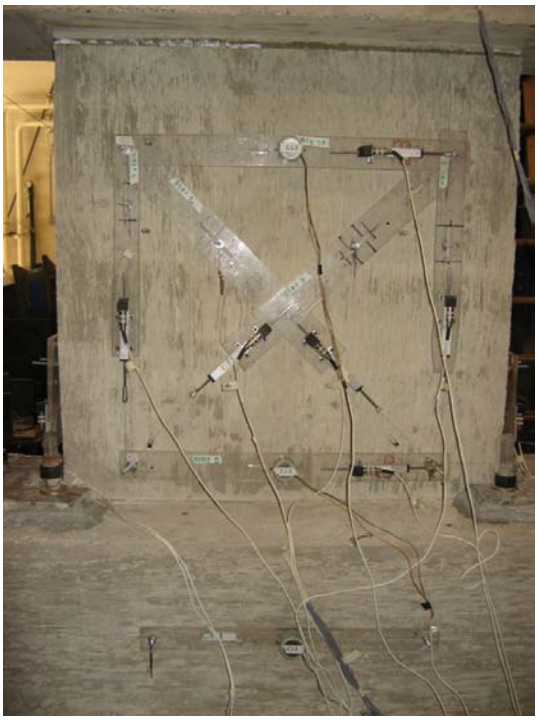

Fig. 3-31 Instrumentation Scheme with Potentiometers and Clinometers

Fig. 3-32 Optotrak Instrumentation Scheme

Fig. 3-33 Lateral Bracing Scheme (Specimen S10)

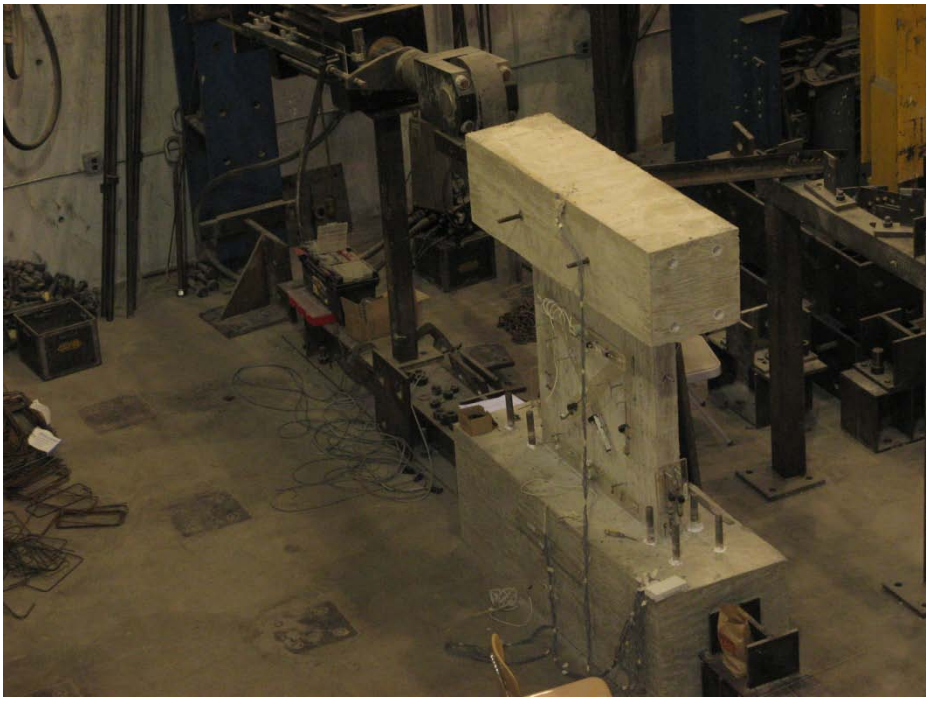

Fig. 3-34 Specimen S4 before Testing

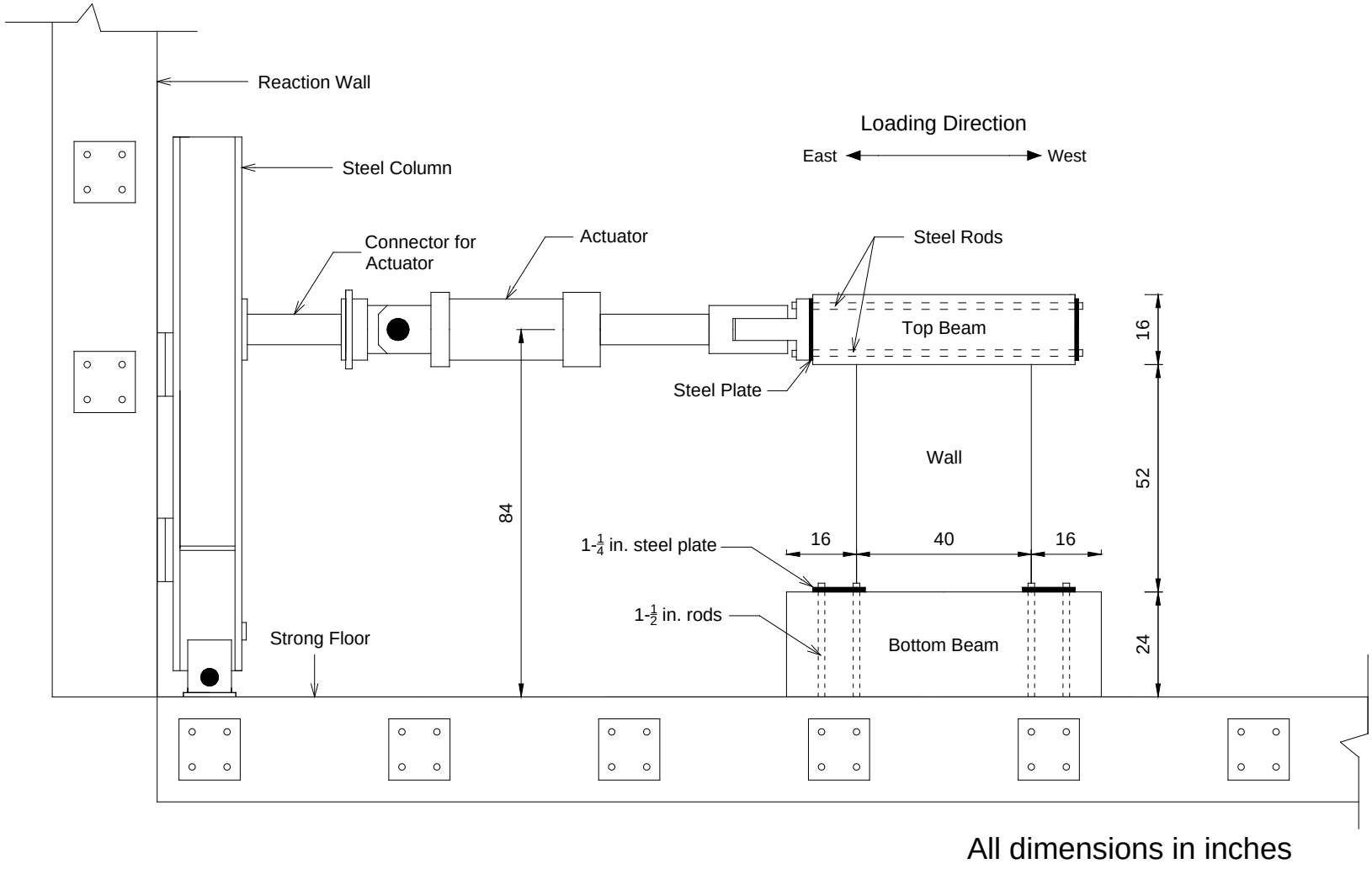

Fig. 3-35 Test Set-Up for Specimen S9

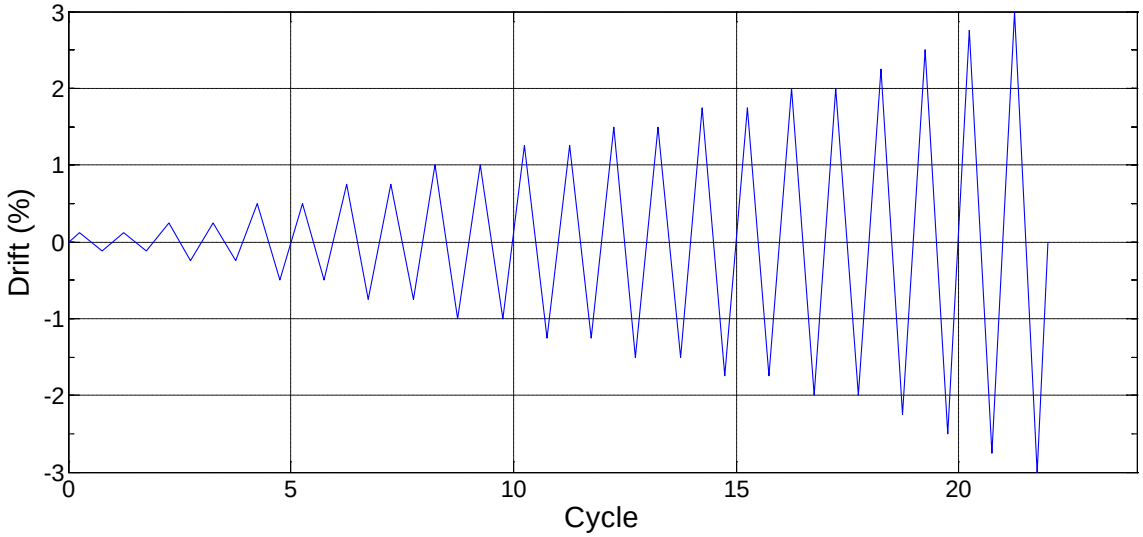

Fig. 3-36 Lateral Displacement History

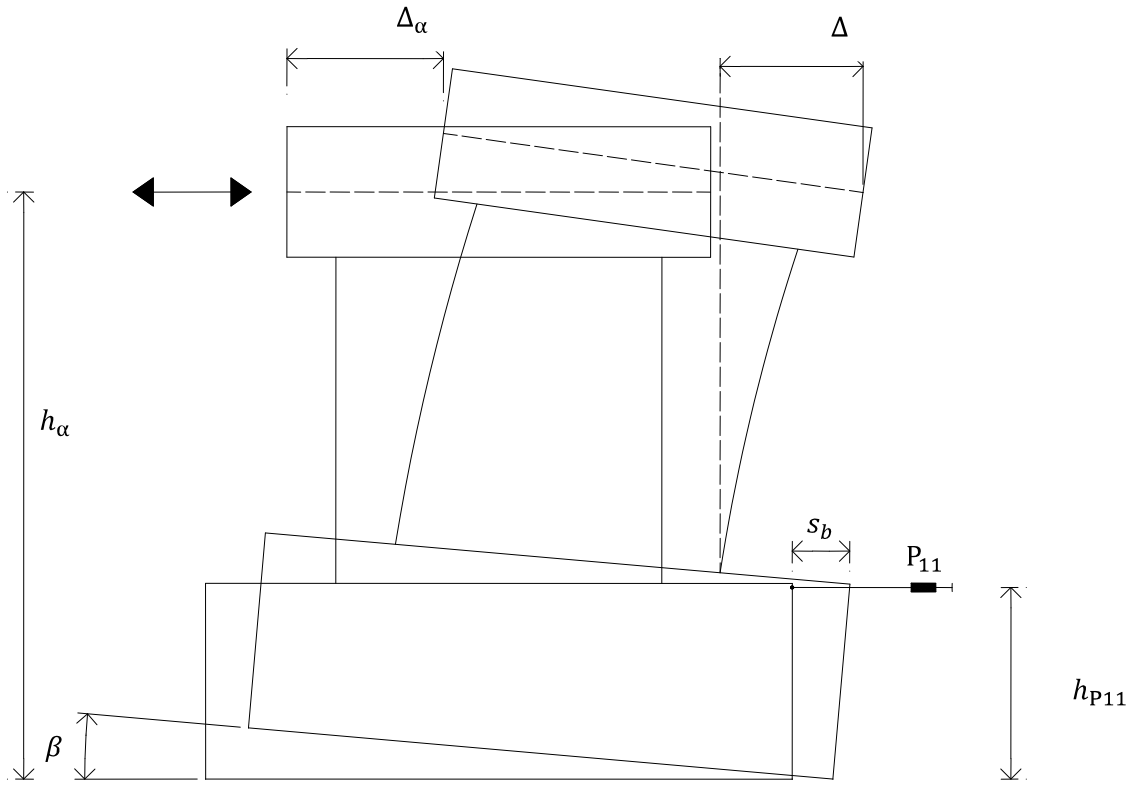

Fig. 4-1 Calculation of Wall Lateral Displacement

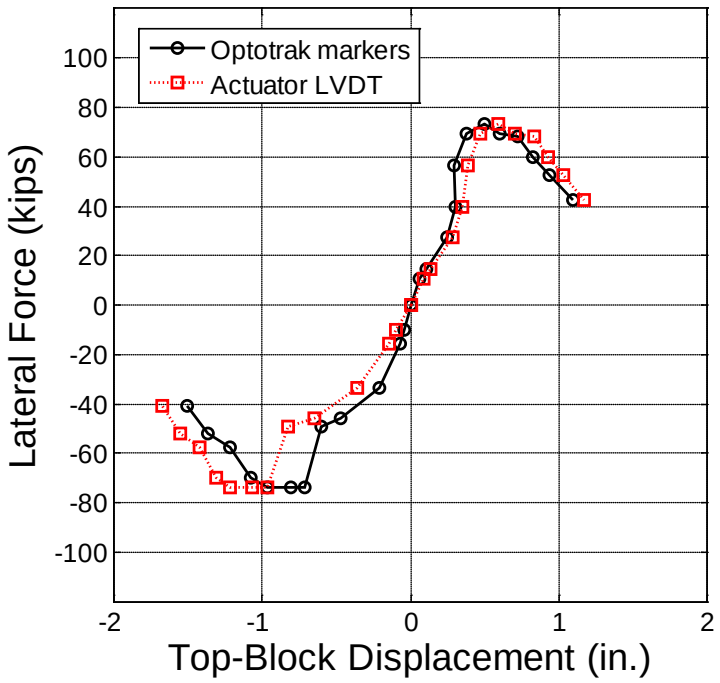

Fig. 4-2 Lateral Force versus Top-Block Displacement Envelope for Specimen S5

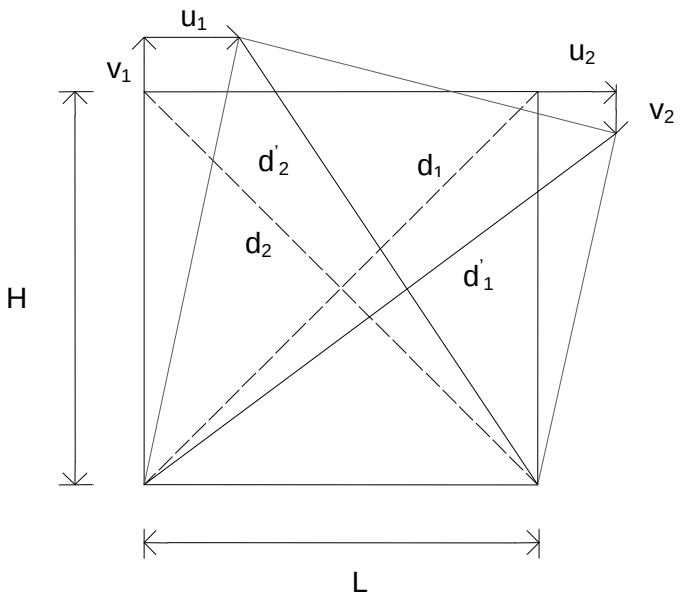

Fig. 4-3 Calculation of Shear Strain (adapted from Sittipunt and Wood, 1995)

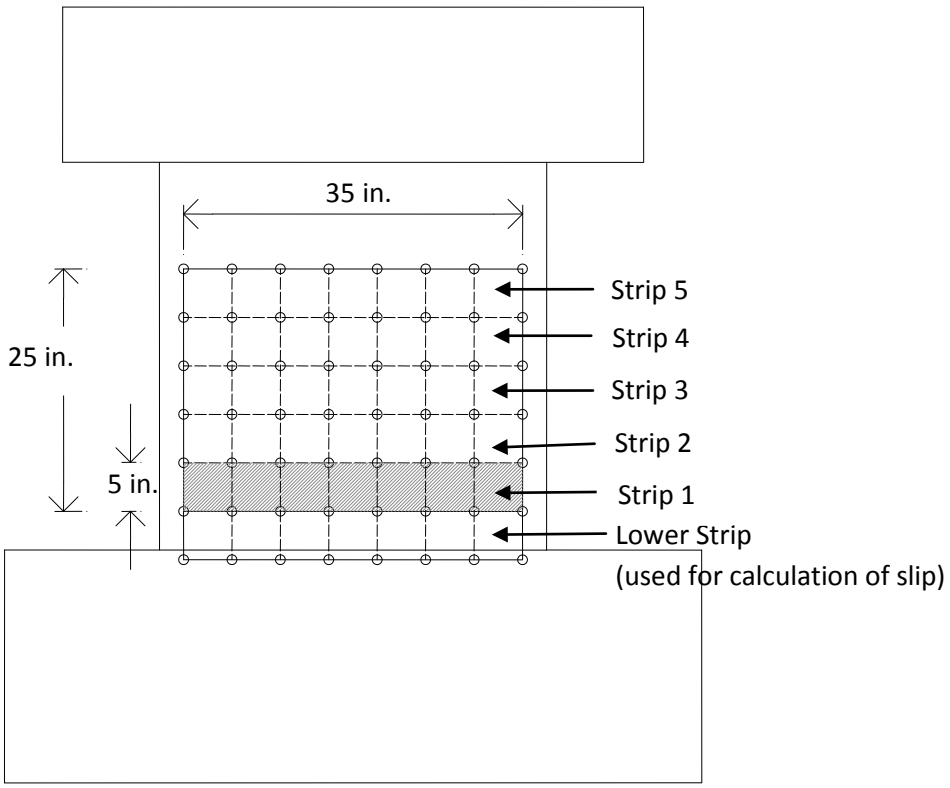

Fig. 4-4 Definition of "Longitudinal Strips" in Wall Specimen

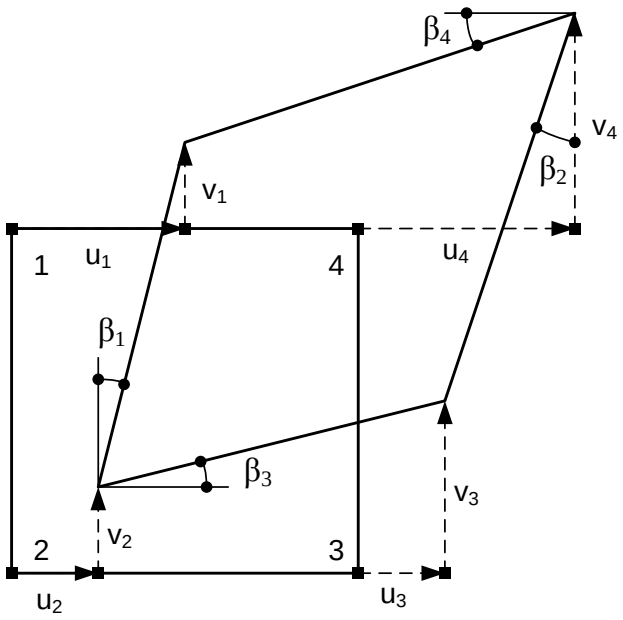

Fig. 4-5 Deformation of a Quadrilateral Element for Calculation of Average Strains

(a) 1.0% drift

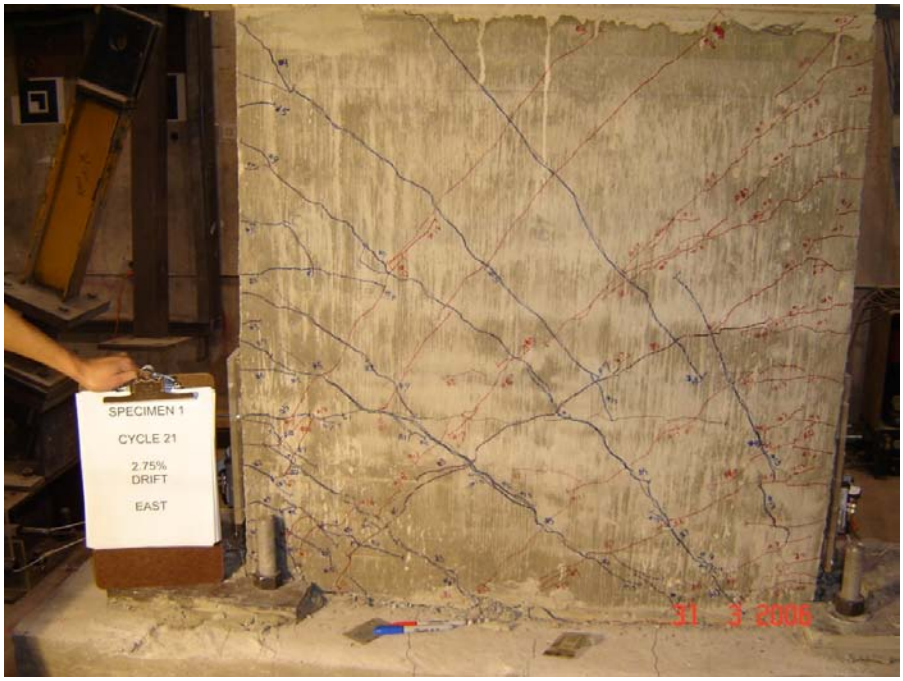

(b) 2.3% drift (end of test)

Fig. 4-6 Cracking Pattern in Specimen S1

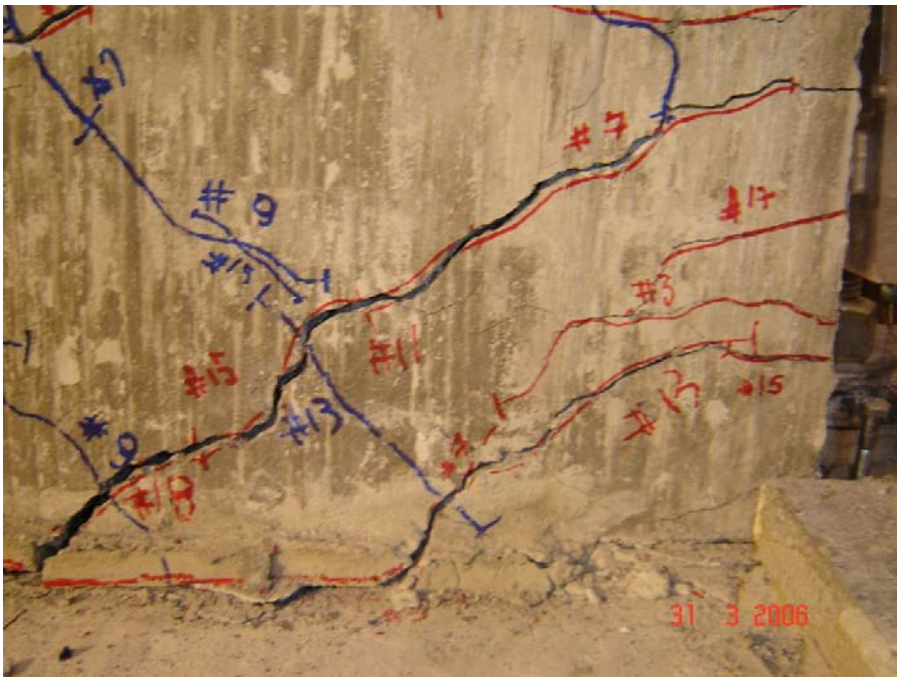

(c) close-up of damage in boundary region at the base of wall (2.3% drift)

Fig. 4-6 Cracking Pattern in Specimen S1

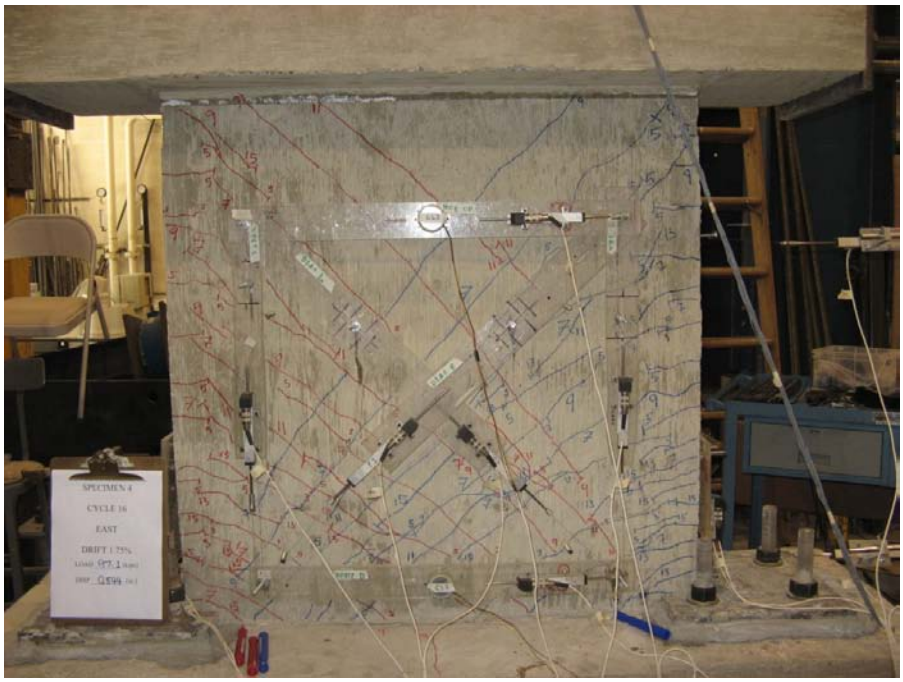

(a) 1.0% drift

Fig. 4-7 Cracking Pattern in Specimen S4

(b) 1.9% drift

(c) 2.4% drift (end of test)

Fig. 4-7 Cracking Pattern in Specimen S4

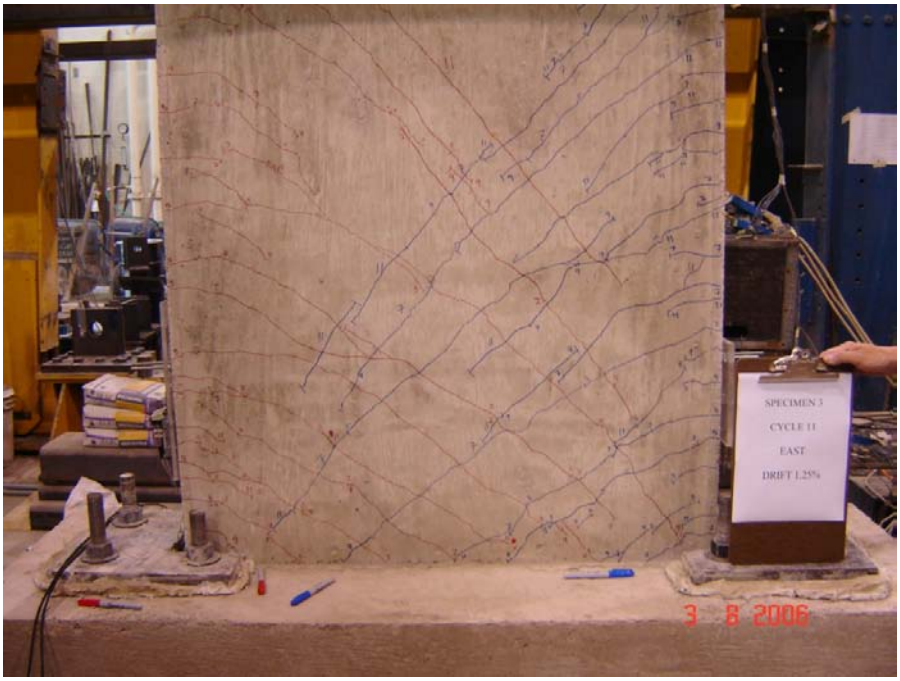

(a) 0.9% drift

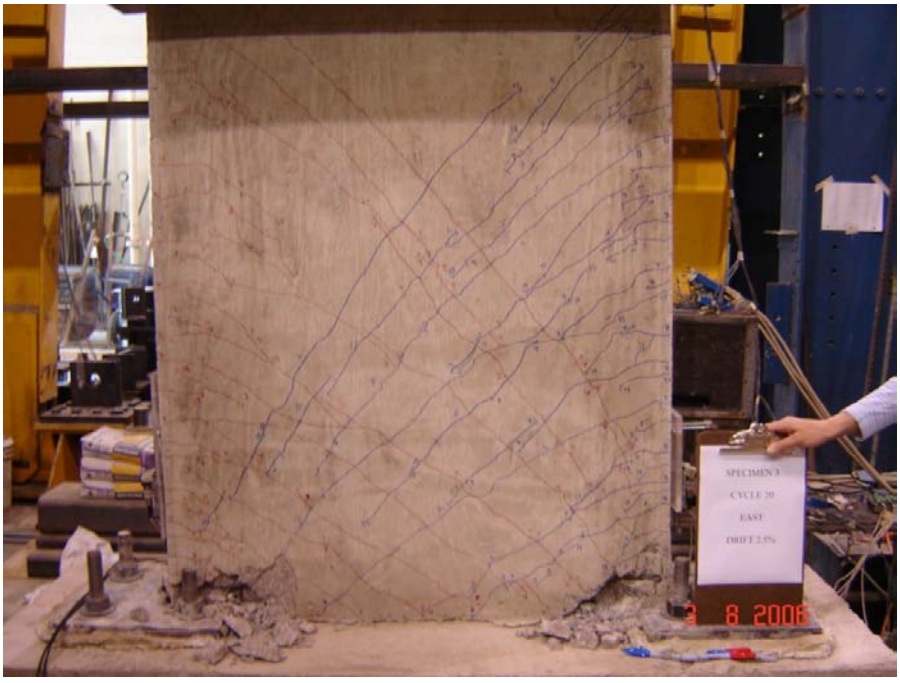

(b) 2.1% drift (end of test)

Fig. 4-8 Cracking Pattern in Specimen S6

(c) close-up of wall boundary region at end of test (2.1% drift)

Fig. 4-8 Cracking Pattern in Specimen S6

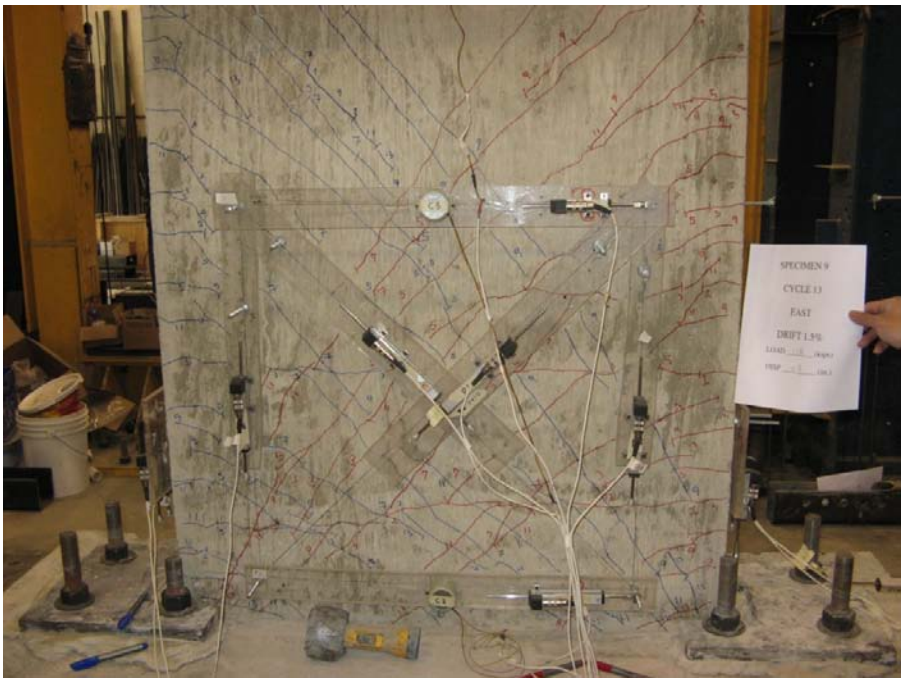

(a) 1.0% drift

Fig. 4-9 Cracking Pattern in Specimen S9

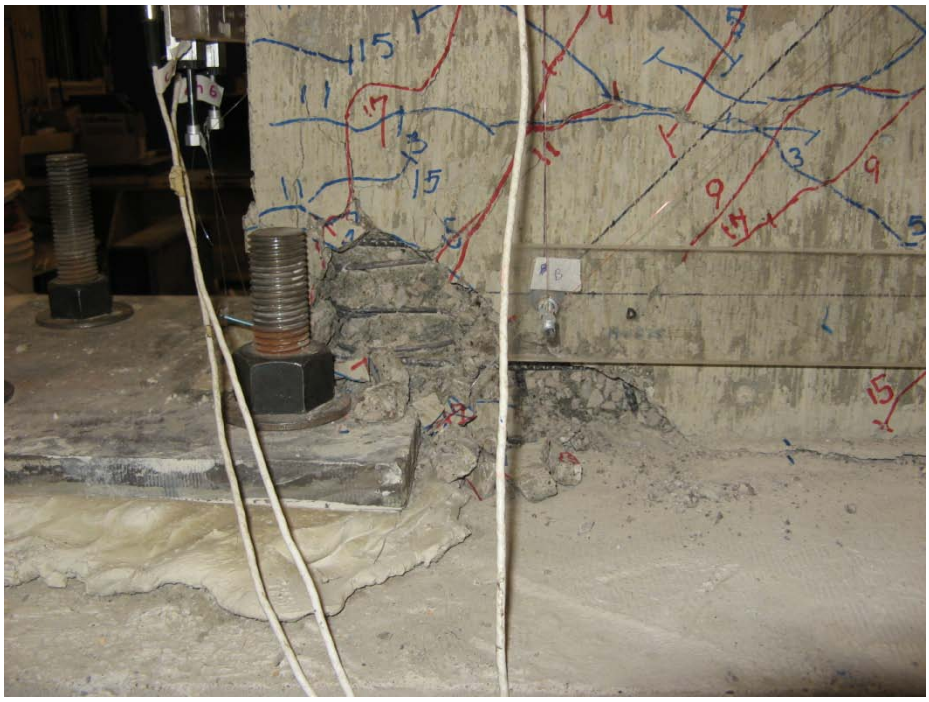

(b) state of damage in wall boundary region at 1.8% drift

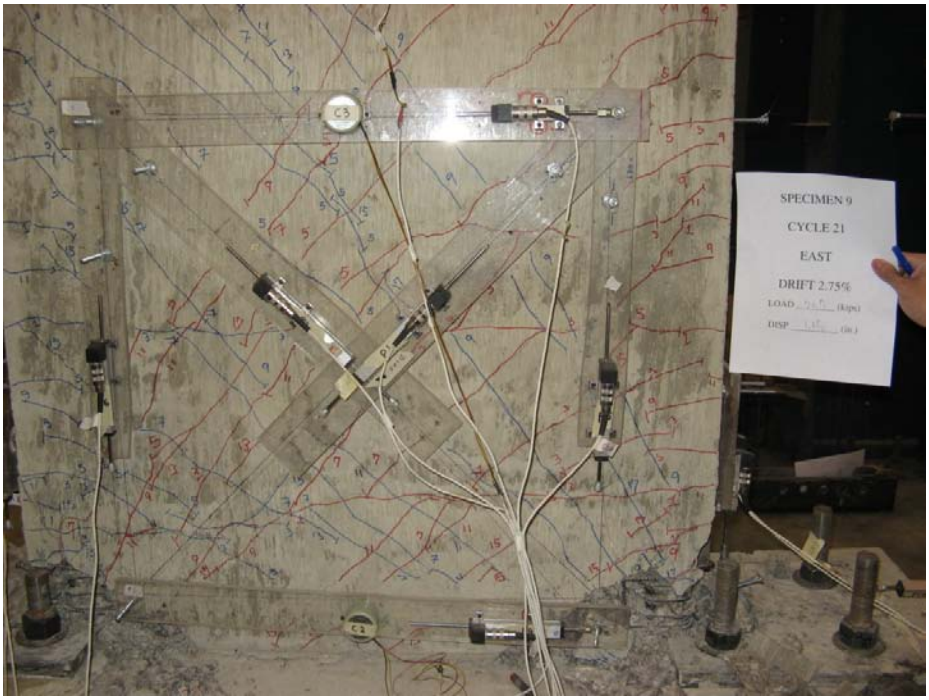

(c) 2.2% drift (end of test)

Fig. 4-9 Cracking Pattern in Specimen S9

(a) 1.2% drift

(b) first observed vertical splitting cracks at a drift of 1.5%

Fig. 4-10 Cracking Pattern in Specimen S2

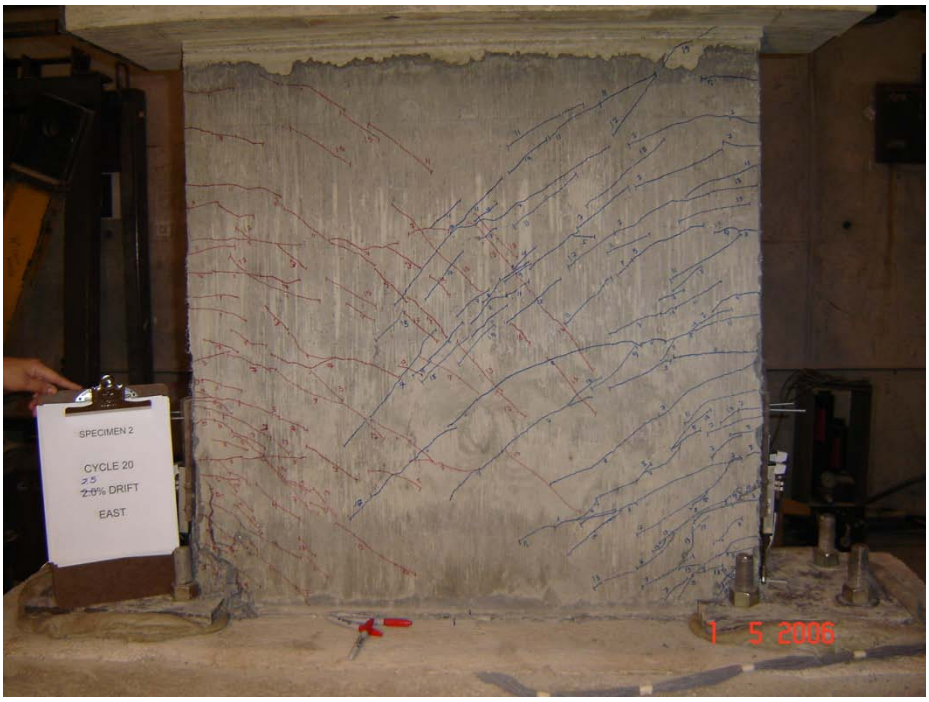

(c) 3.0% drift (end of test)

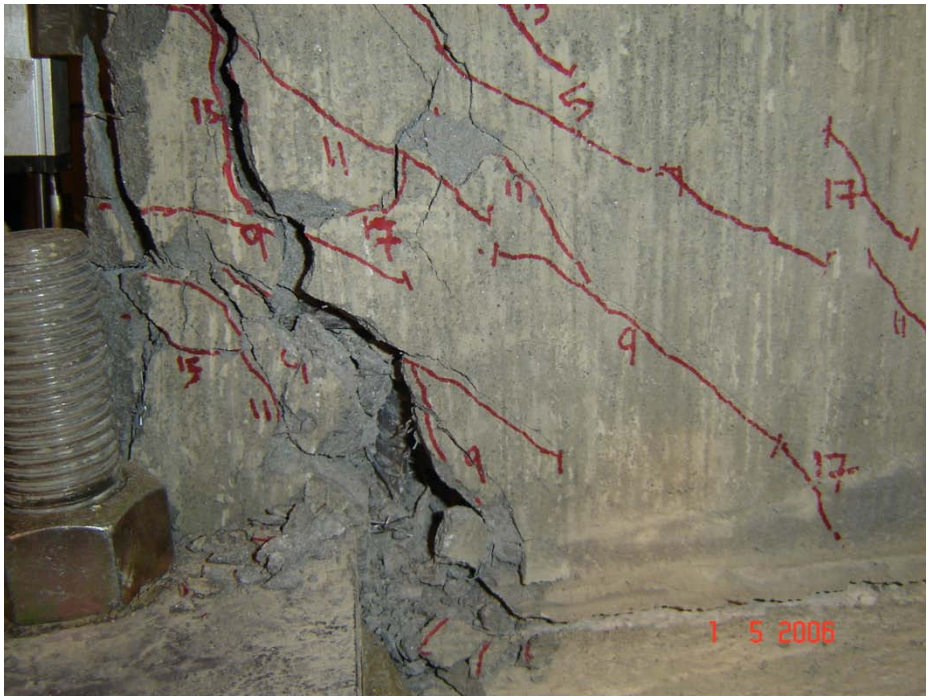

(d) close-up of boundary region after end of test (3.0% drift)

Fig. 4-10 Cracking Pattern in Specimen S2

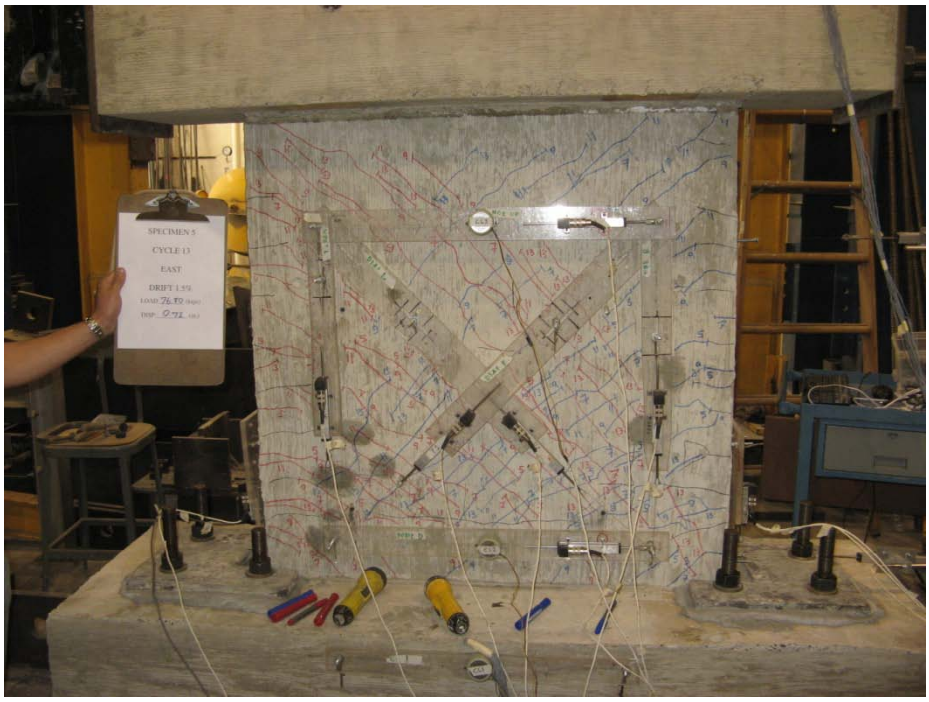

(a) 0.85% drift

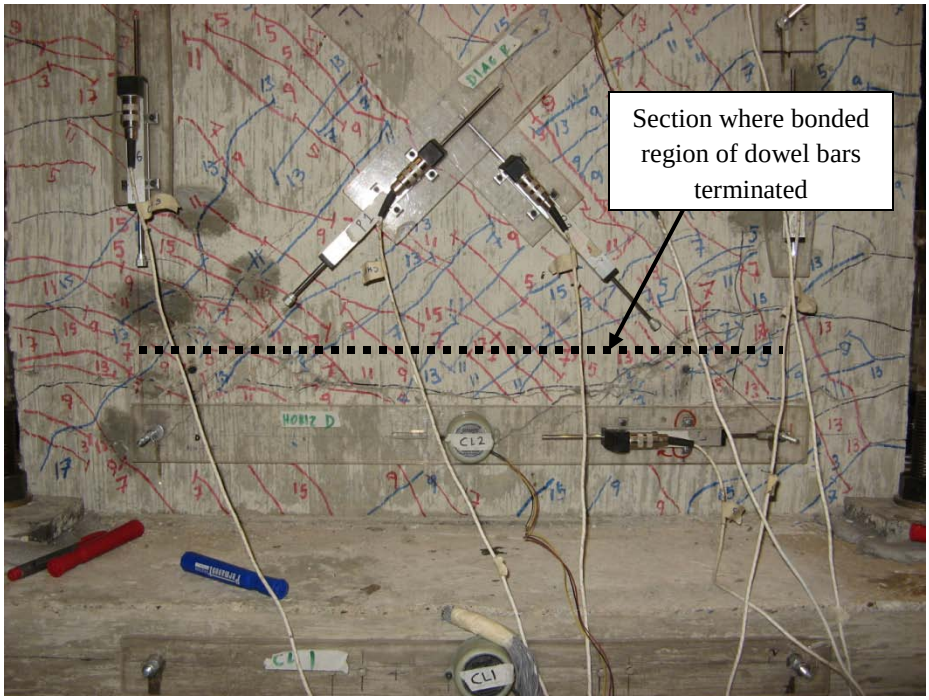

(b) 1.3% drift

Fig. 4-11 Cracking Pattern in Specimen S5

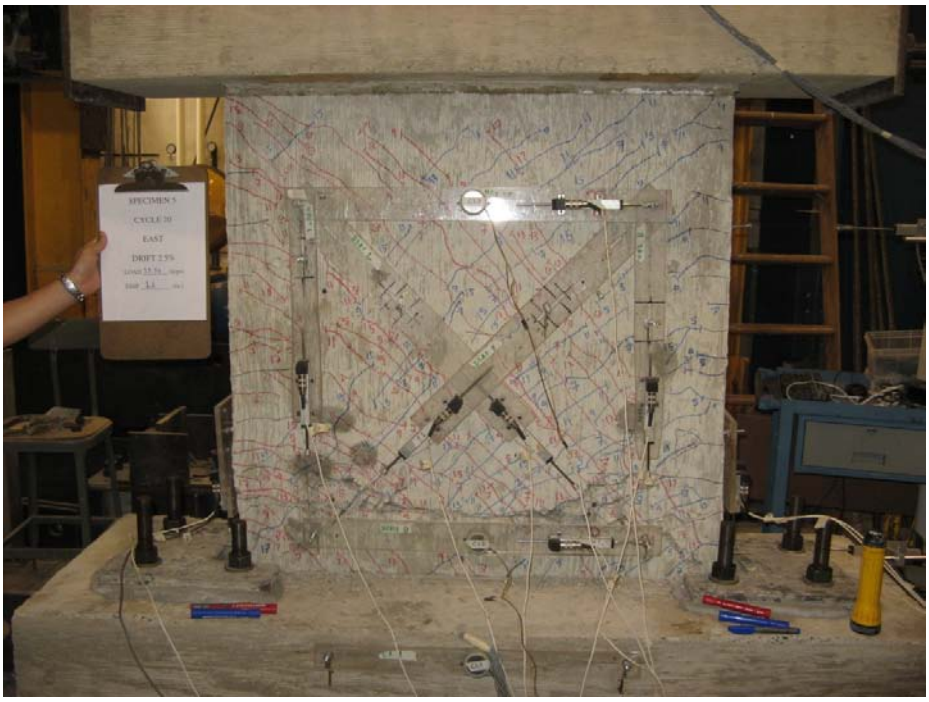

(c) 1.9% drift

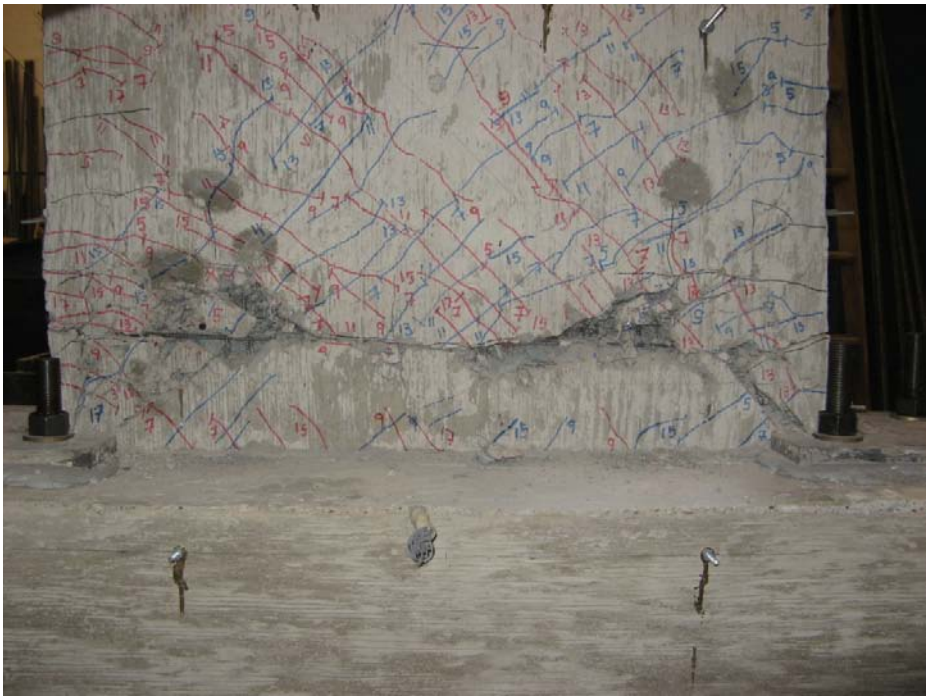

(d) 2.4% drift (end of test)

Fig. 4-11 Cracking Pattern in Specimen S5

(a) 1.0% drift

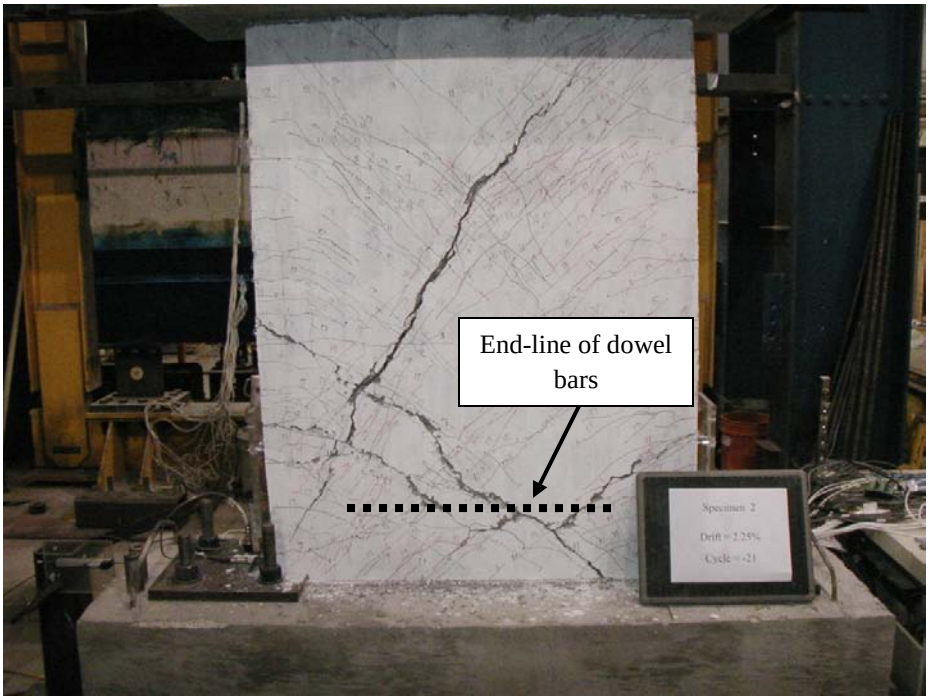

(b) 2.4% drift (end of test)

Fig. 4-12 Cracking Pattern in Specimen S7

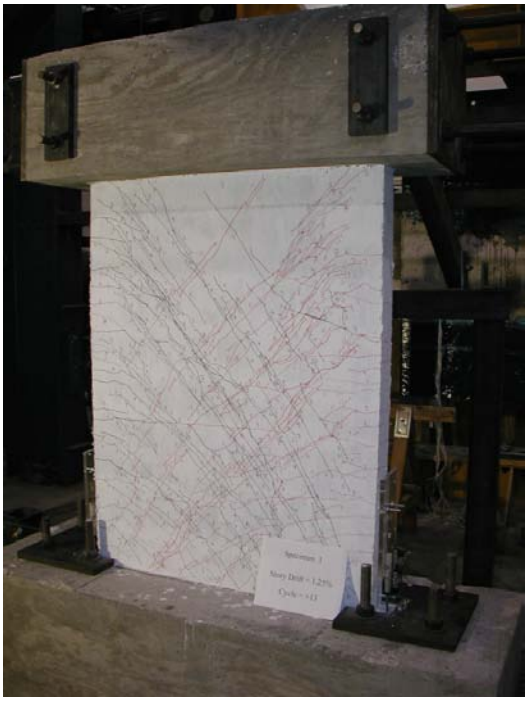

(a) 1.0% drift

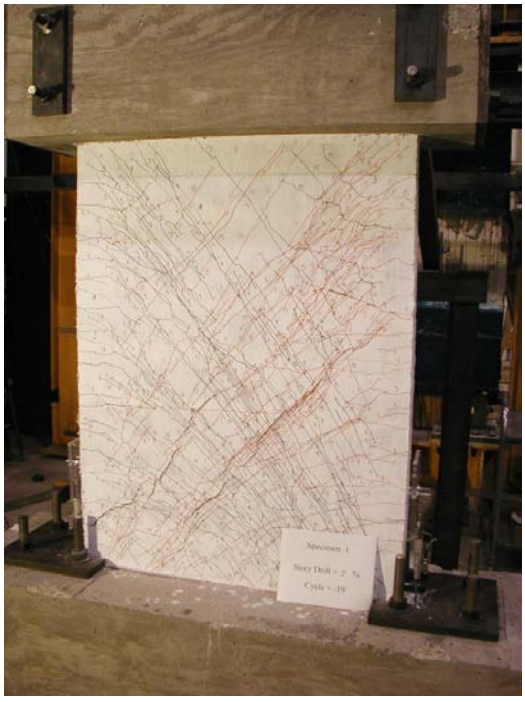

(b) 2.1% drift

Fig. 4-13 Cracking Pattern in Specimen S8

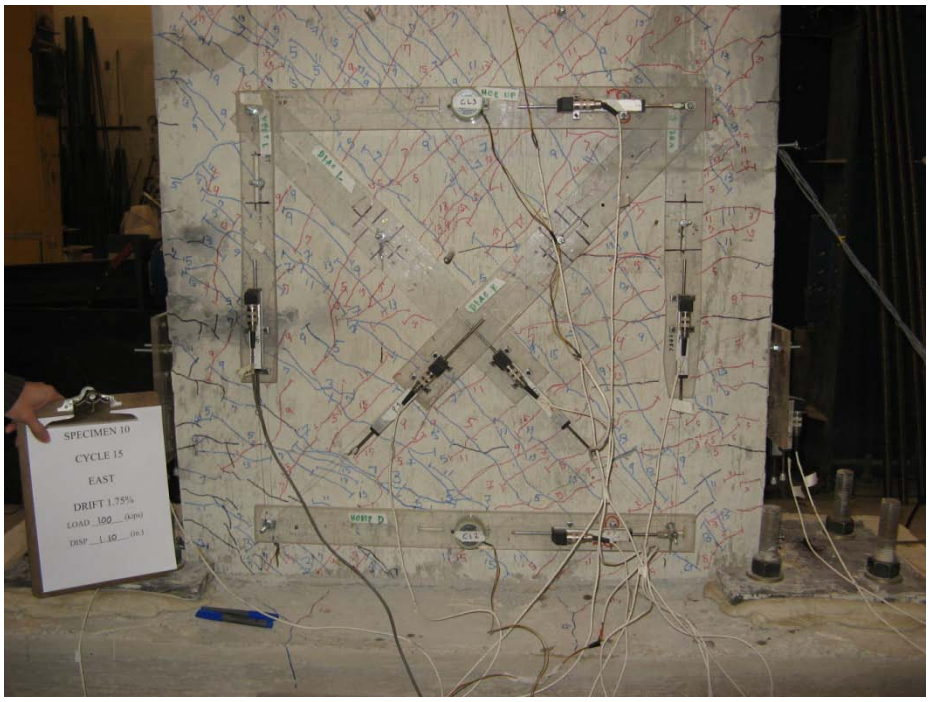

(a) 1.0% drift

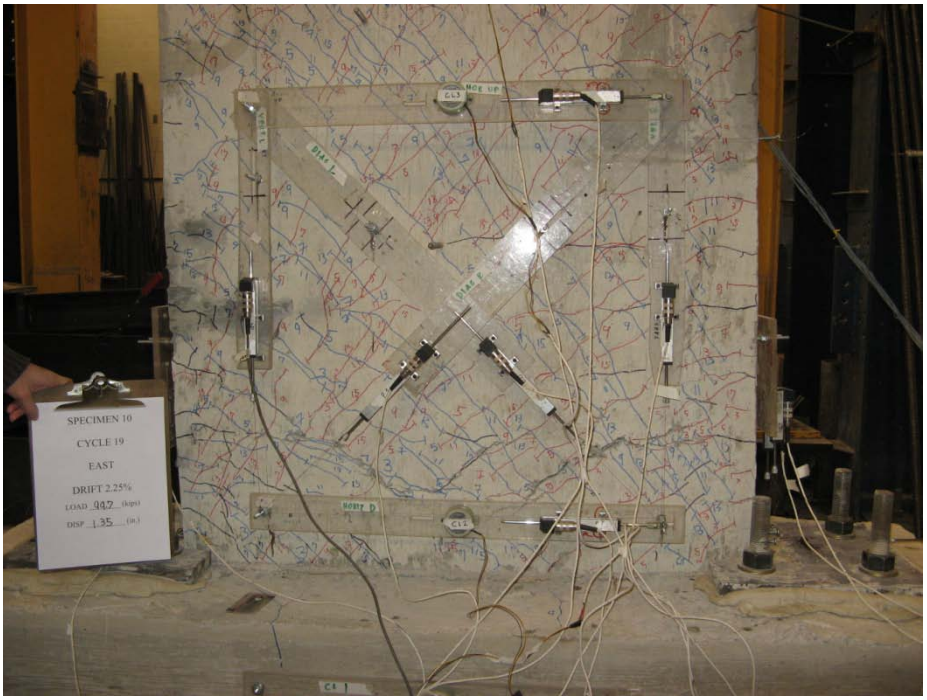

(b) 1.4% drift

Fig. 4-14 Cracking Pattern in Specimen S10

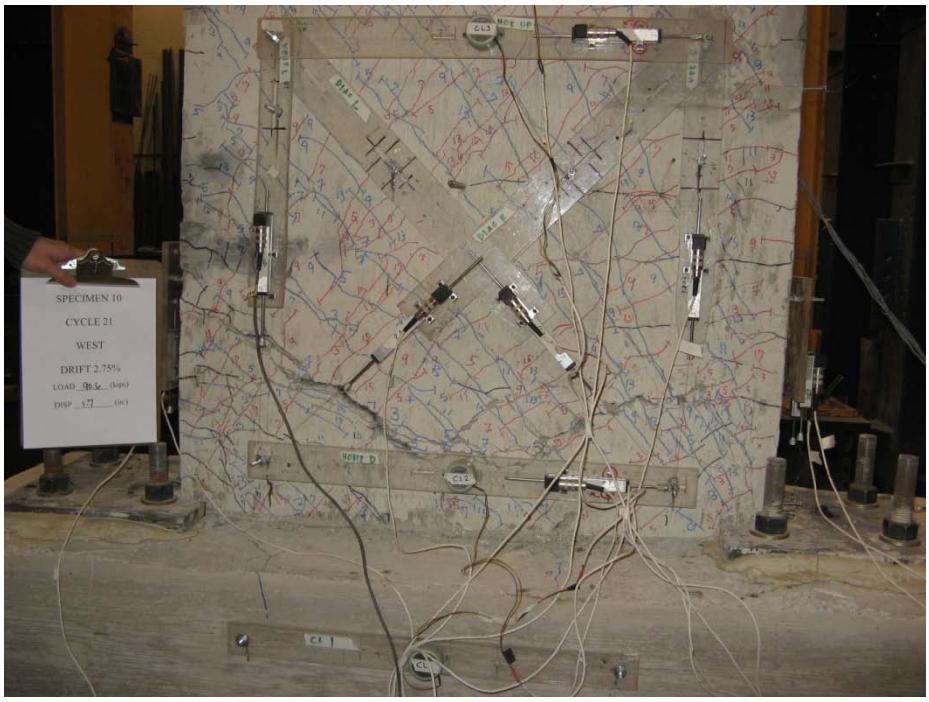

(c) 1.9% drift

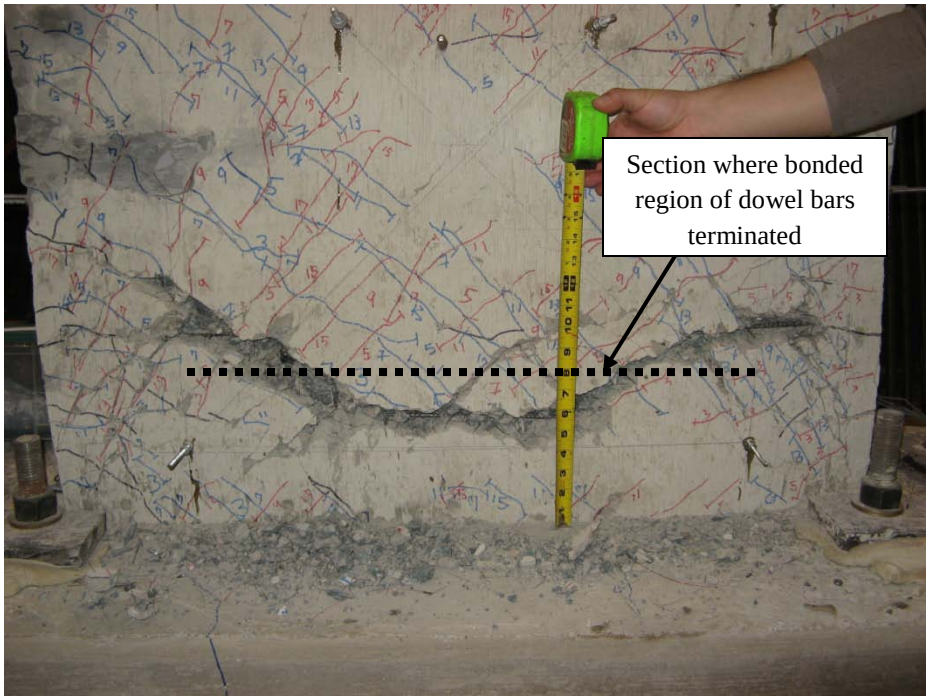

(d) 2.2 % drift (end of test)

Fig. 4-14 Cracking Pattern in Specimen S10

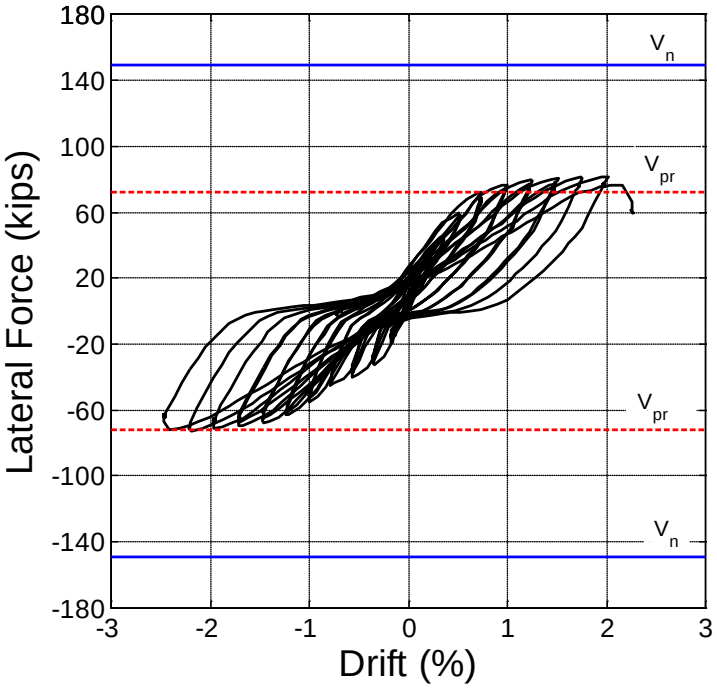

(a) Specimen S1

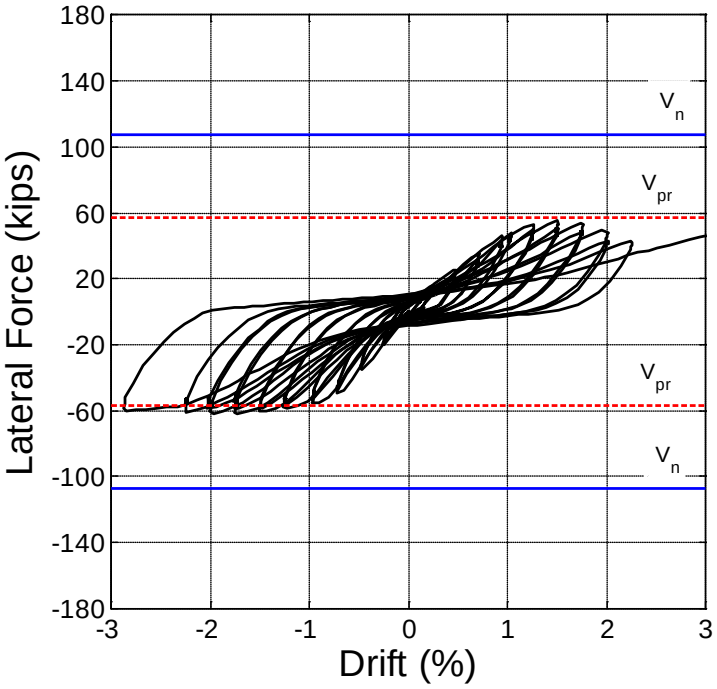

(b) Specimen S2

Fig. 4-15 Load versus Drift Response

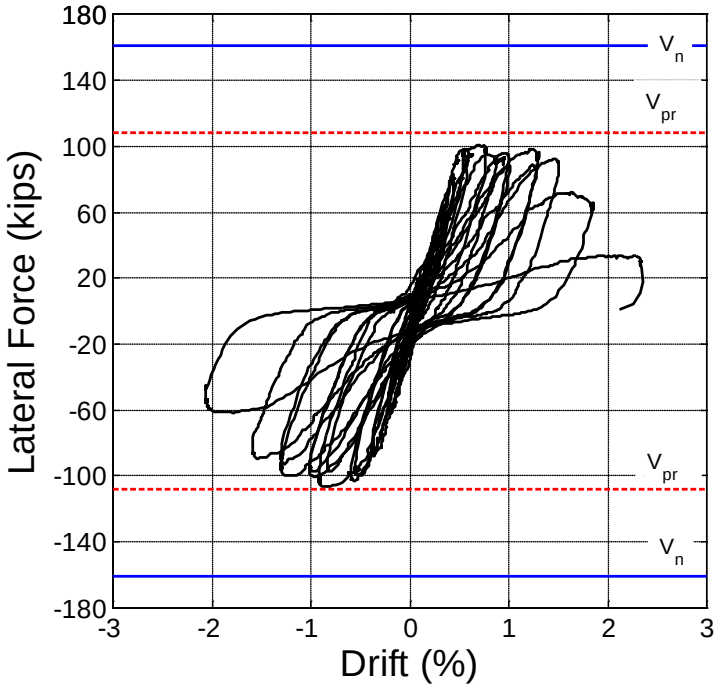

(c) Specimen S4

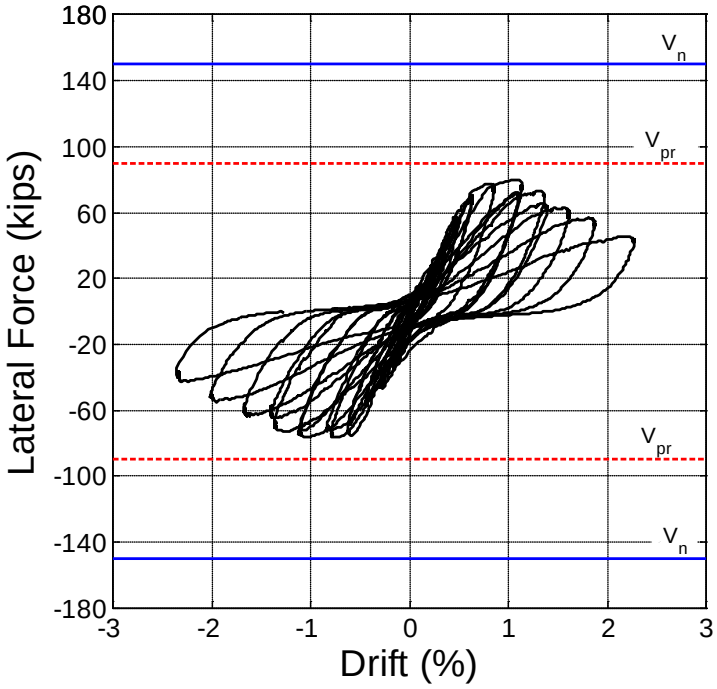

(d) Specimen S5

Fig. 4-15 Load versus Drift Response

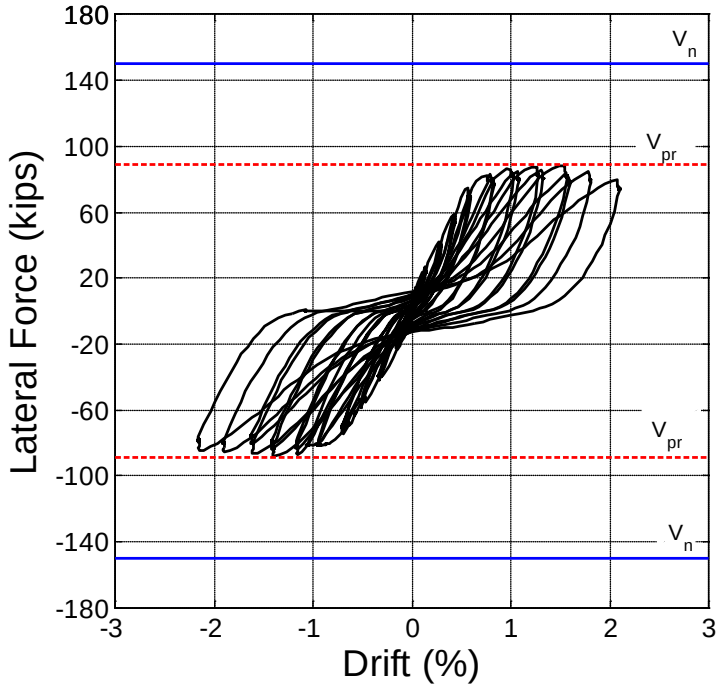

(e) Specimen S6

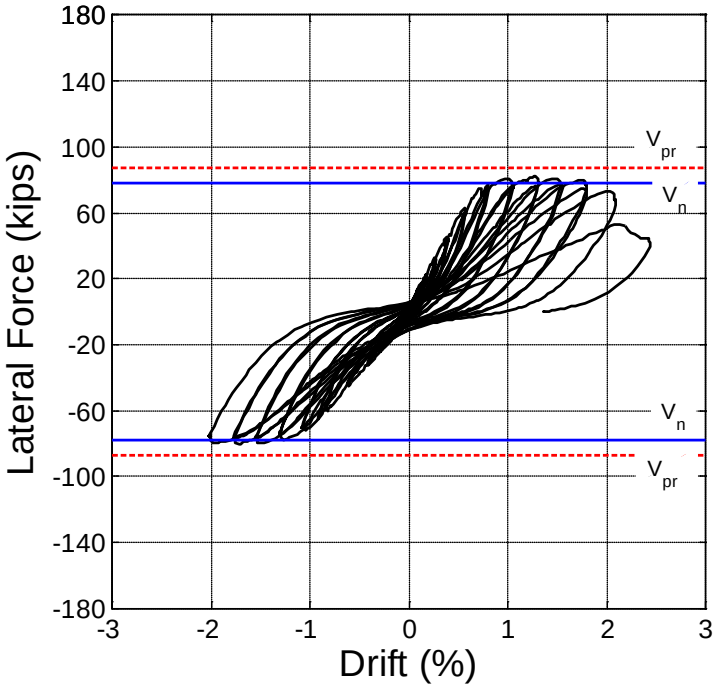

(f) Specimen S7

Fig. 4-15 Load versus Drift Response

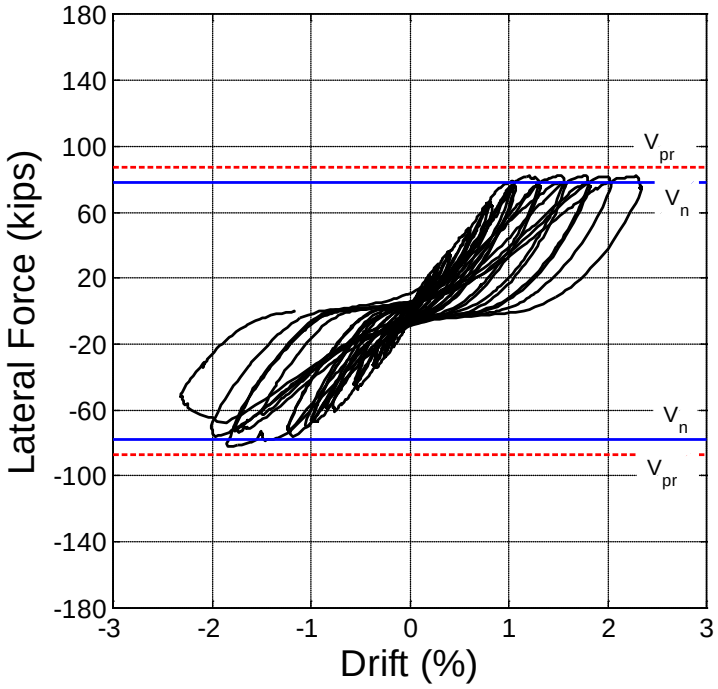

(g) Specimen S8

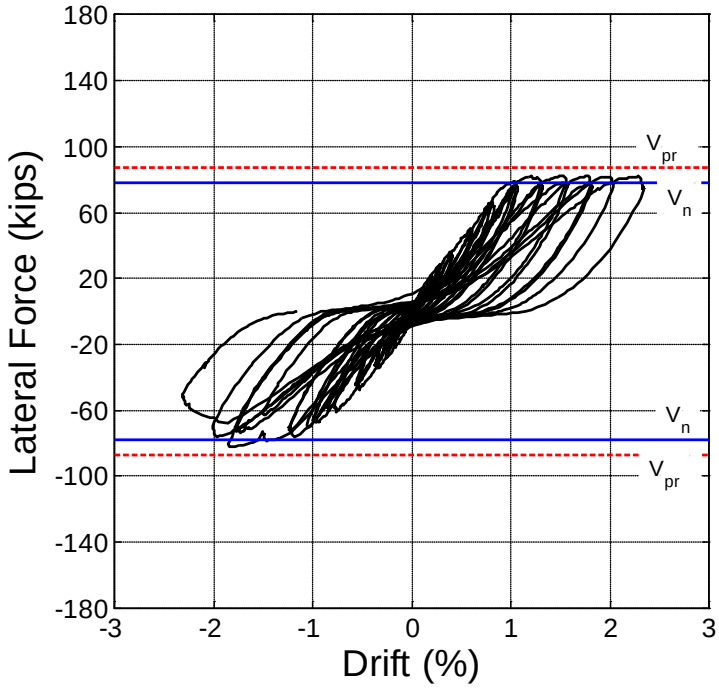

(h) Specimen S9

Fig. 4-15 Load versus Drift Response

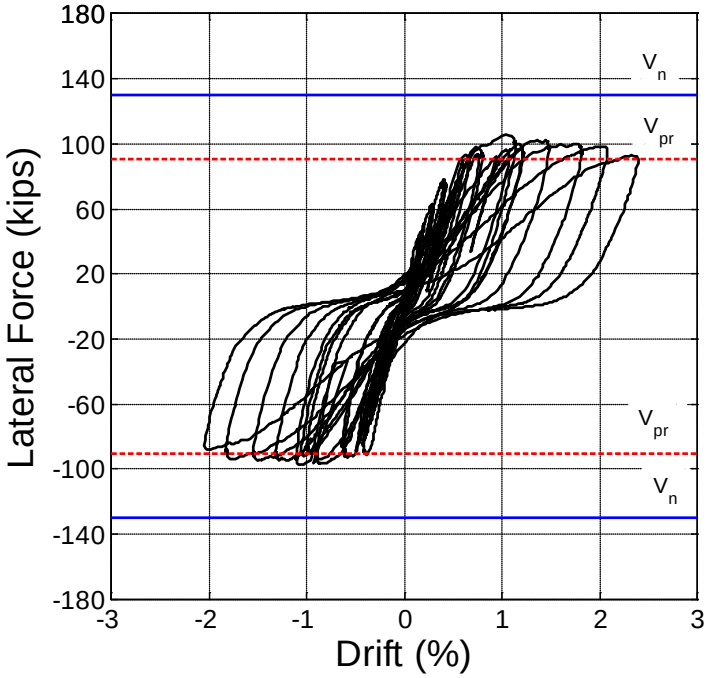

(i) Specimen S10

Fig. 4-15 Load versus Drift Response

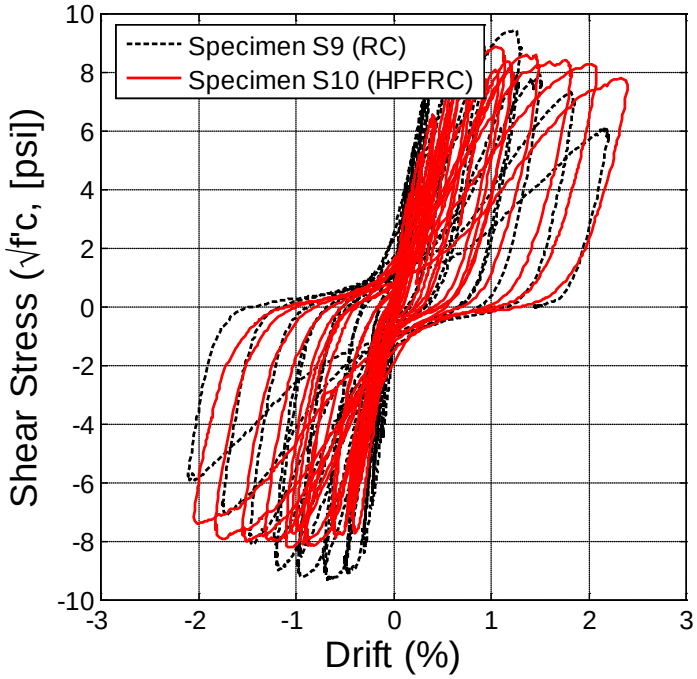

Fig. 4-16 Comparison of Shear Stress versus Drift Response for Specimens S9 and S10

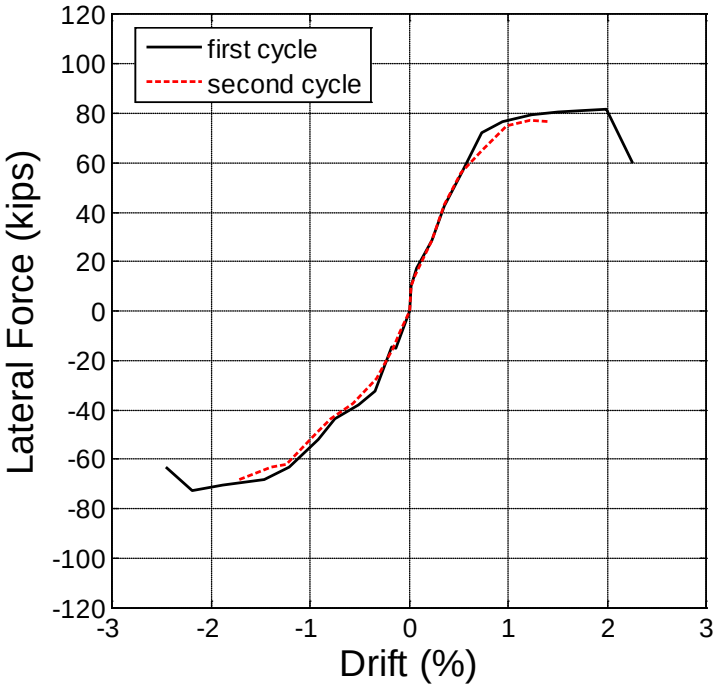

(a) Specimen S1

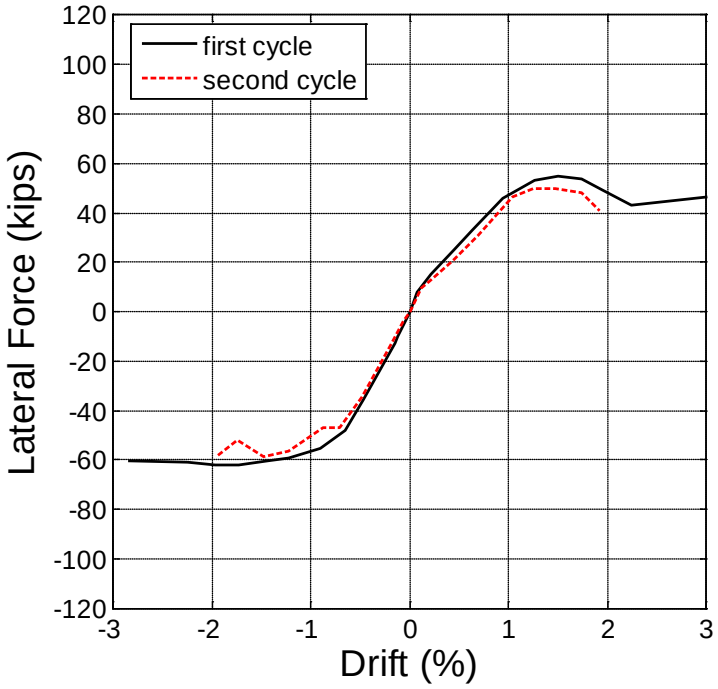

(b) Specimen S2

Fig. 4-17 Load versus Drift Envelope Response

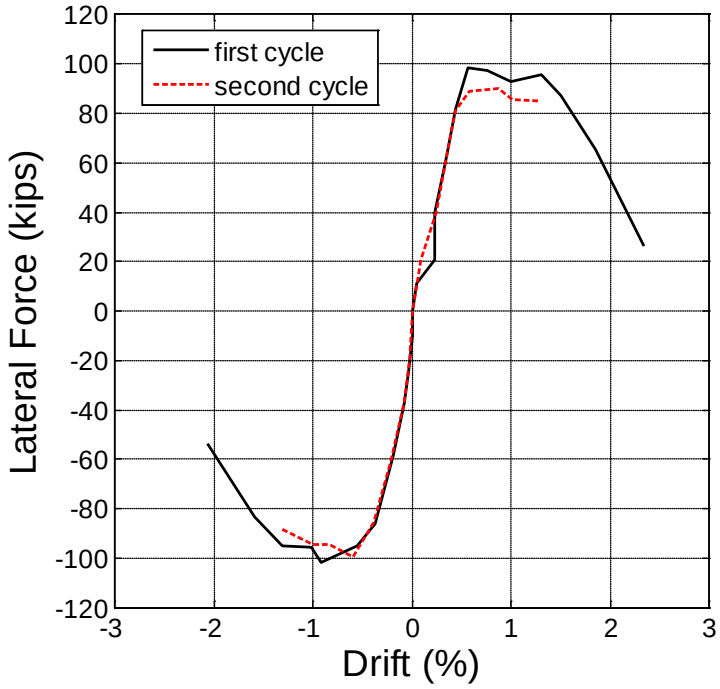

(c) Specimen S4

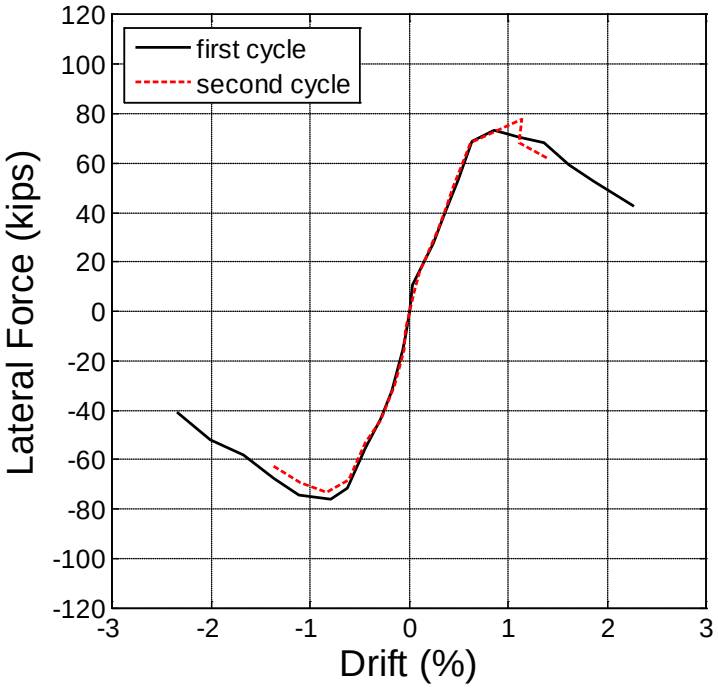

(c) Specimen S5

Fig. 4-17 Load versus Drift Envelope Response

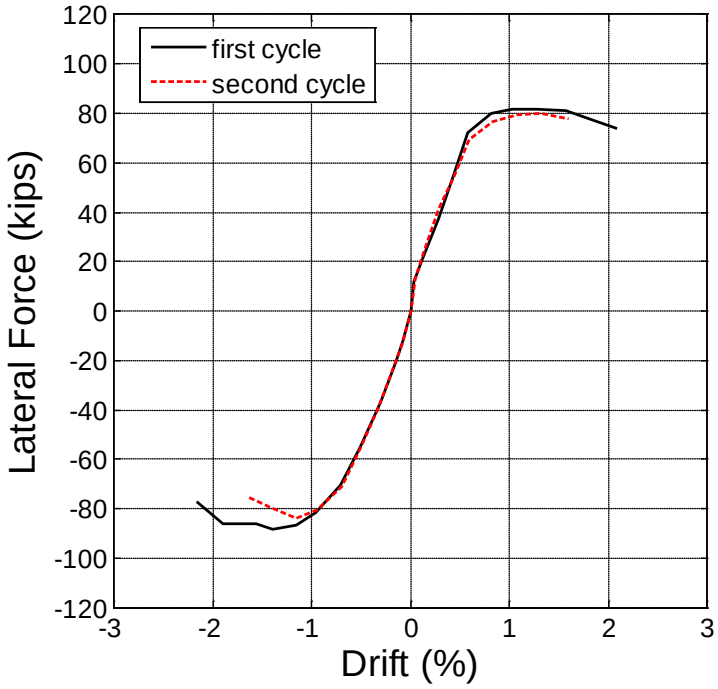

(e) Specimen S6

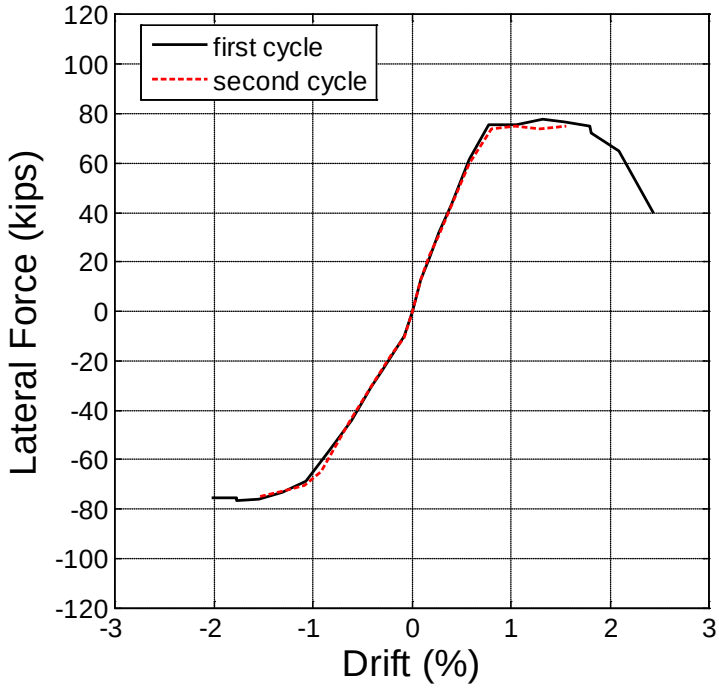

(f) Specimen S7

Fig. 4-17 Load versus Drift Envelope Response

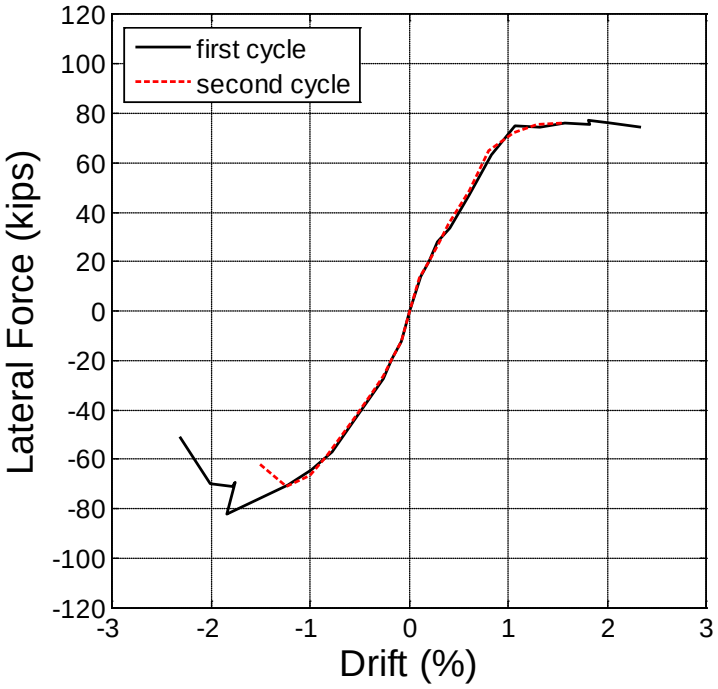

(g) Specimen S8

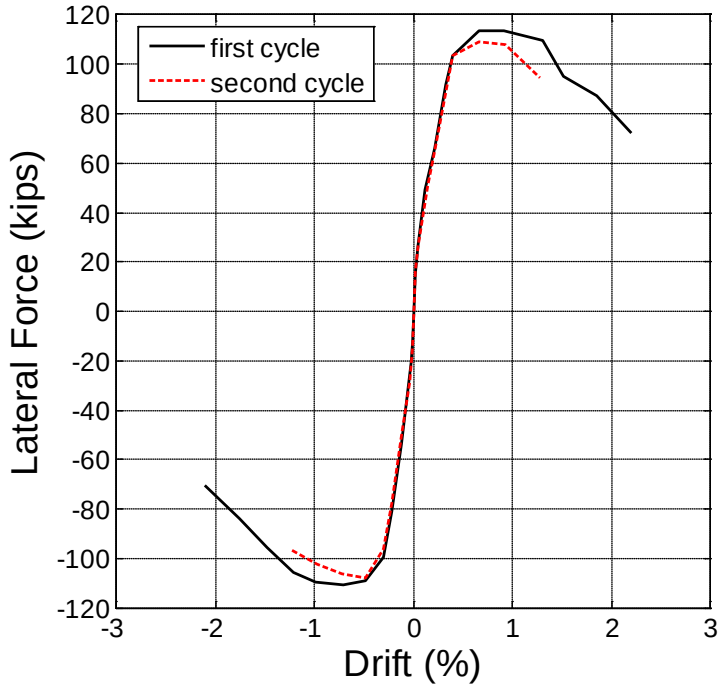

(h) Specimen S9

Fig. 4-17 Load versus Drift Envelope Response

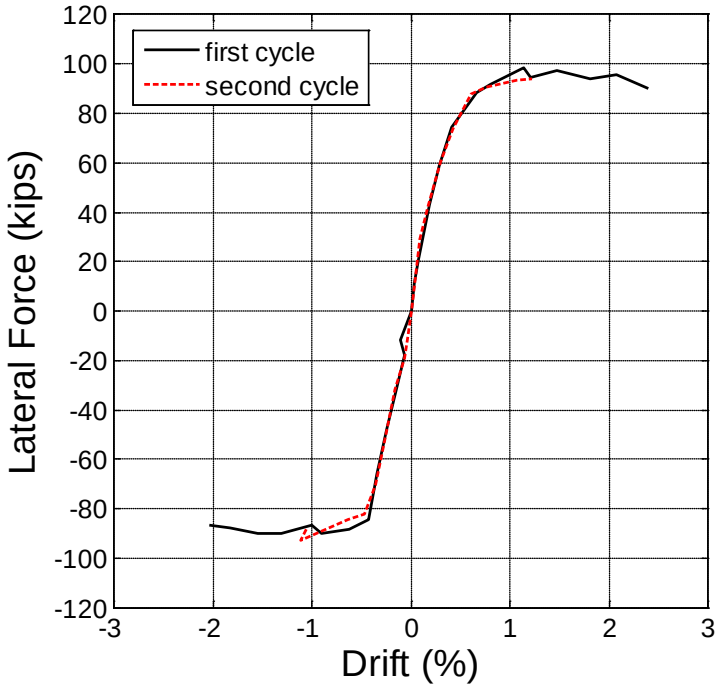

(i) Specimen S10

Fig. 4-17 Load versus Drift Envelope Response

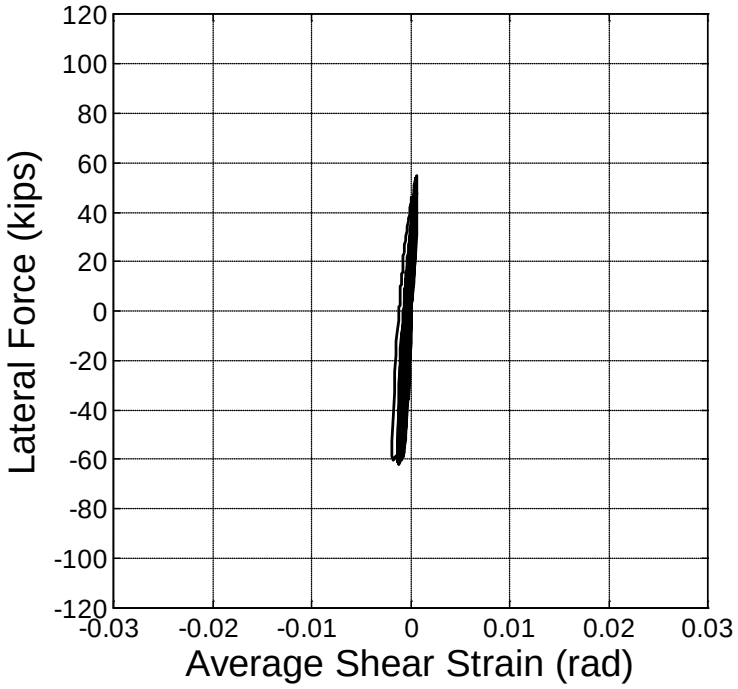

(a) Specimen S2

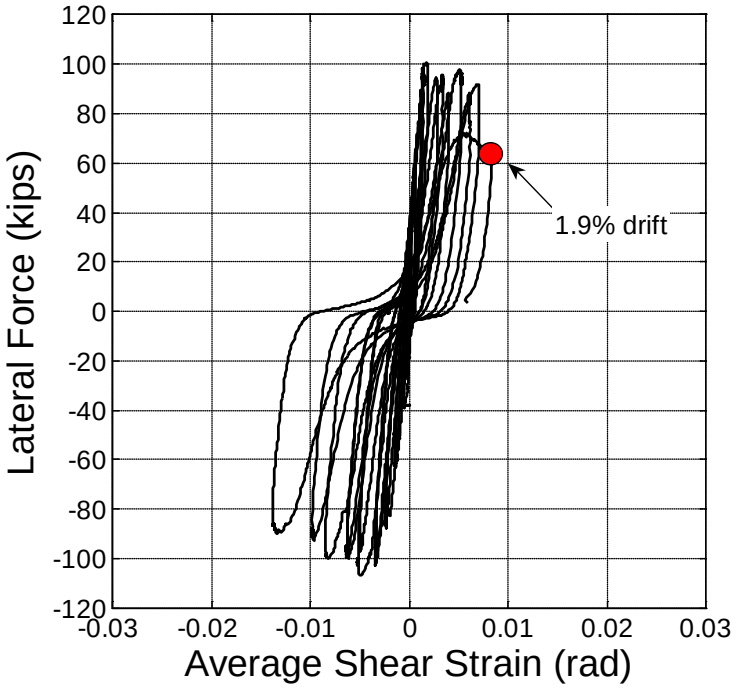

(b) Specimen S4

Fig. 4-18 Load versus Average Shear Strain Response

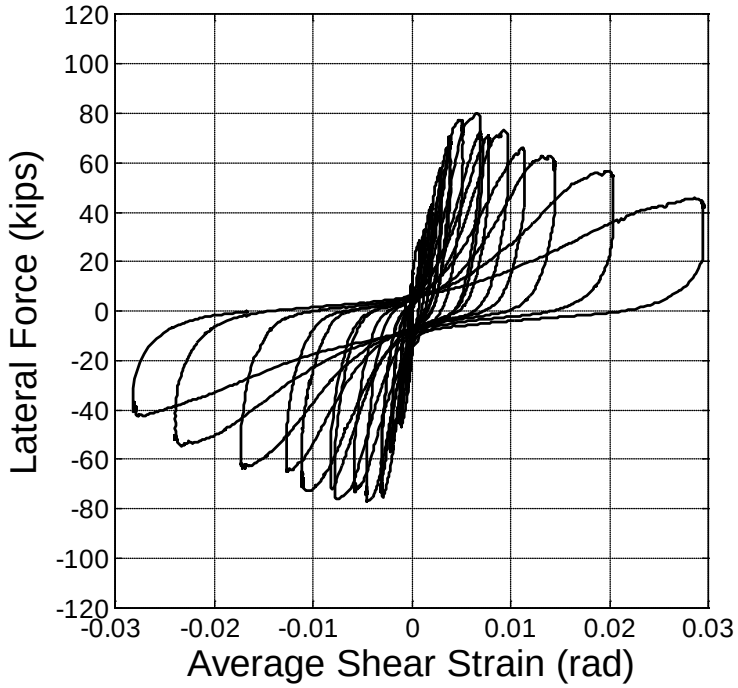

(c) Specimen S5

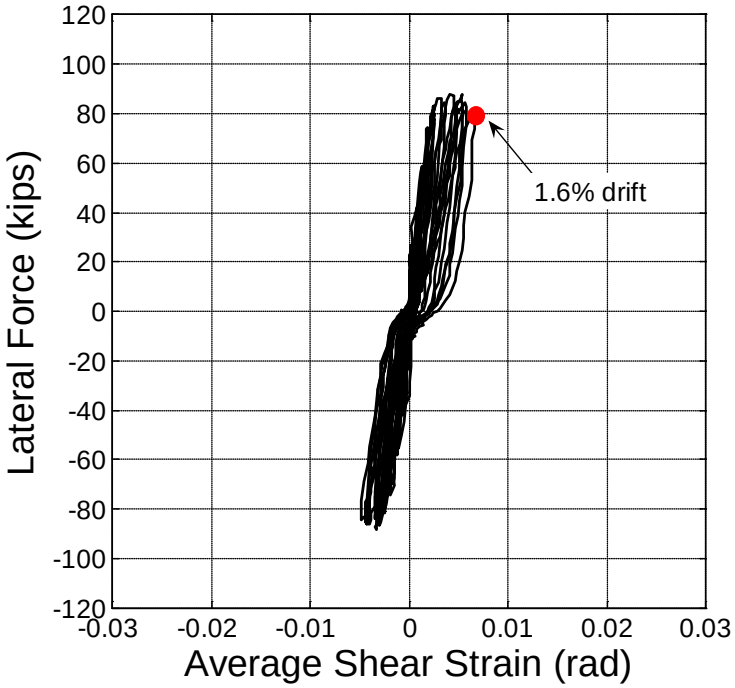

(d) Specimen S6

Fig. 4-18 Load versus Average Shear Strain Response

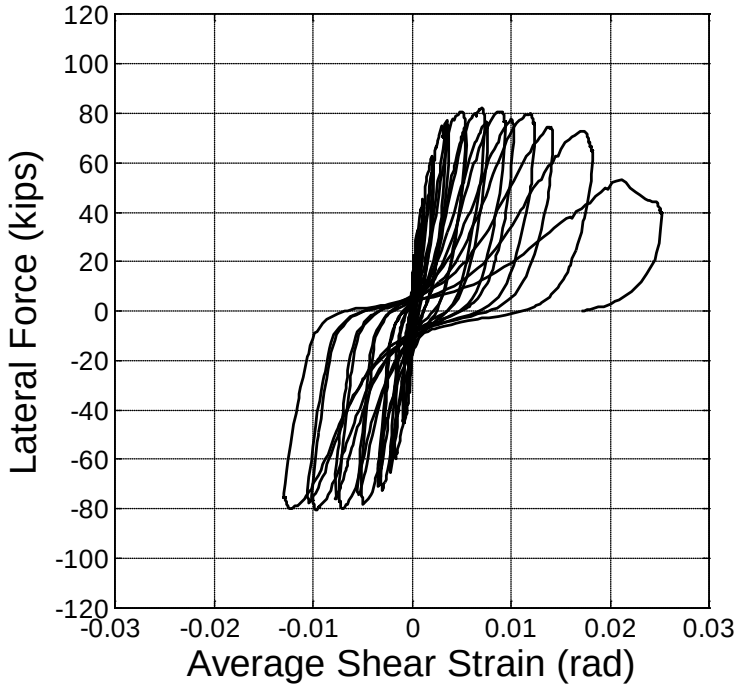

(e) Specimen S7

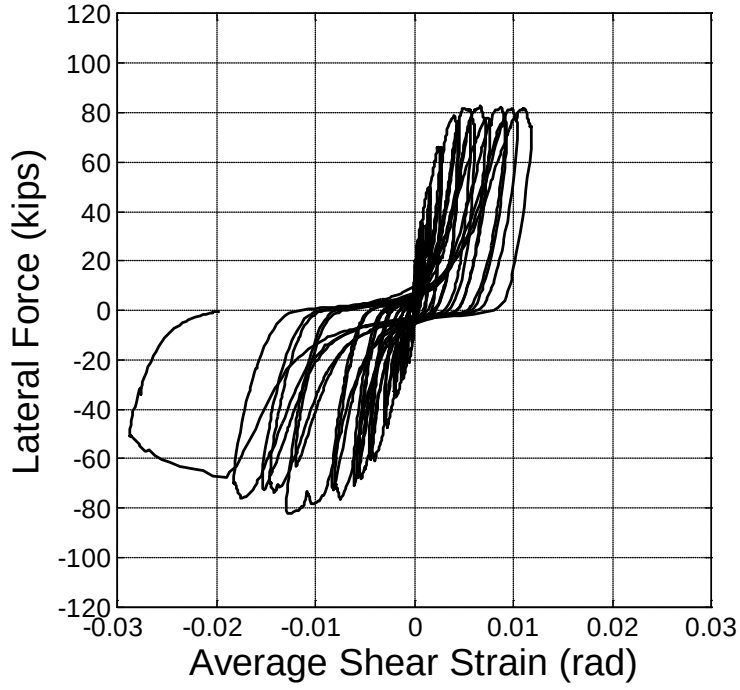

(f) Specimen S8

Fig. 4-18 Load versus Average Shear Strain Response

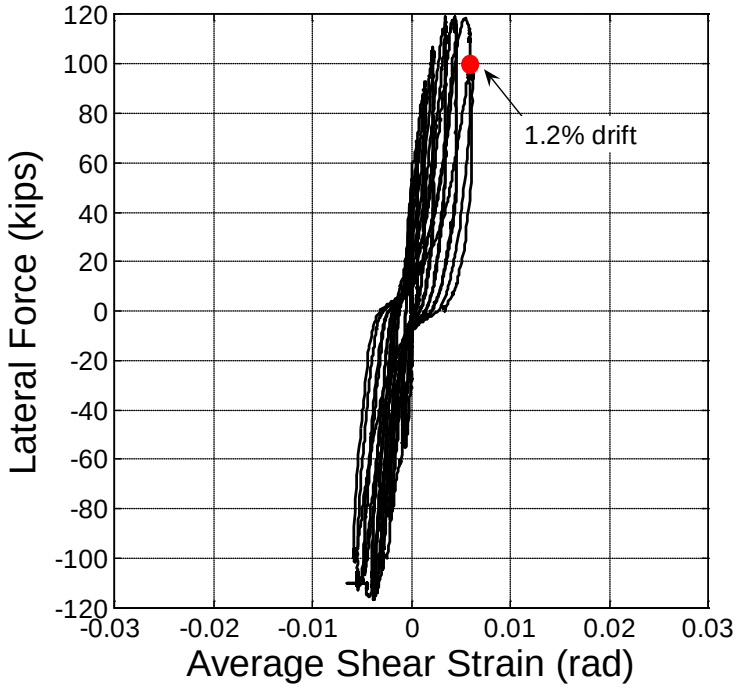

(g) Specimen S9

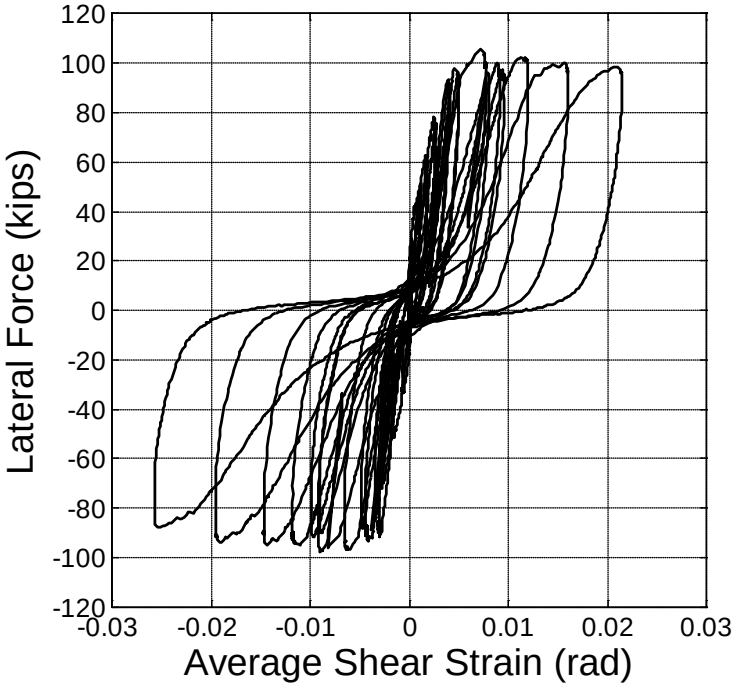

(h) Specimen S10

Fig. 4-18 Load versus Average Shear Strain Response

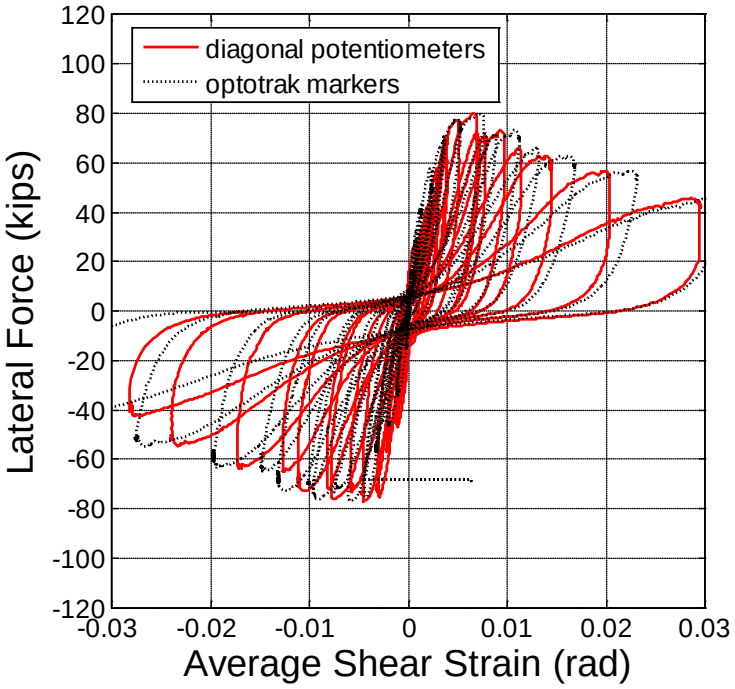

Fig. 4-19 Comparison of Shear Strain Response Calculated using Diagonal Potentiometers and Optotrak Markers for Specimen S5

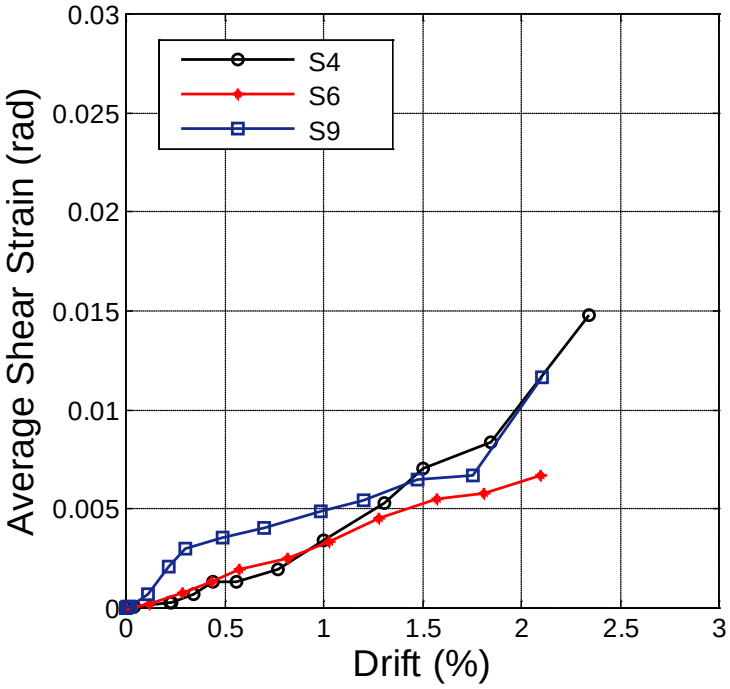

(a) RC Wall Specimens

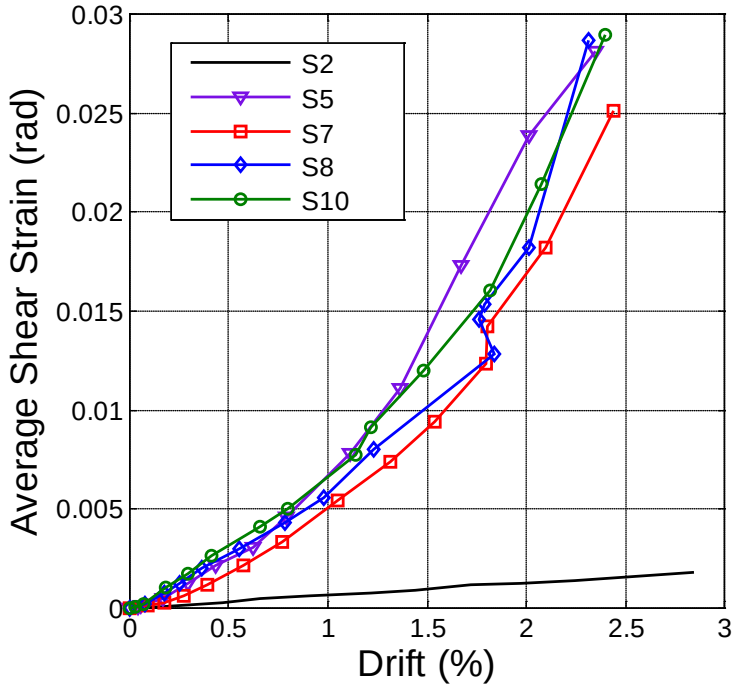

(b) HPFRC Wall Specimens

Fig. 4-20 Average Shear Strain versus Drift Envelope Response

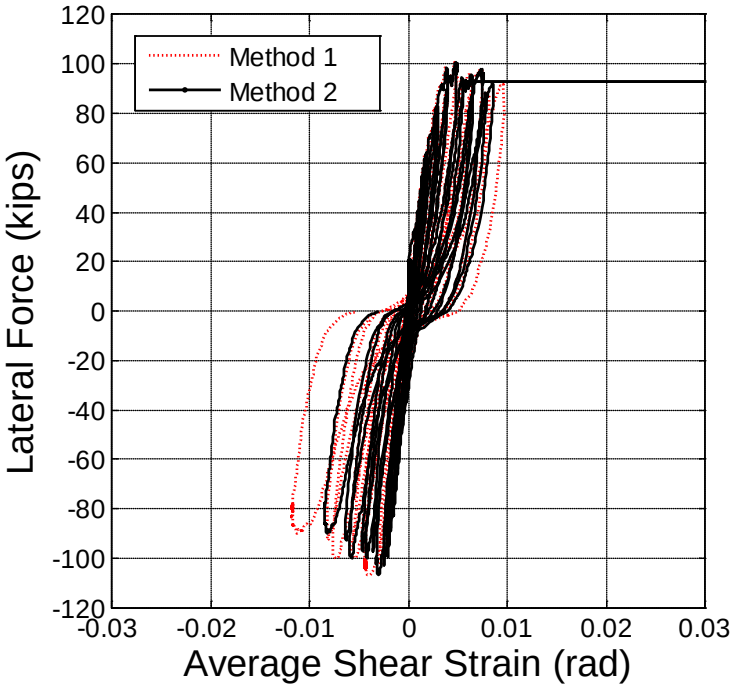

Fig. 4-21 Comparison of Shear Strain Response Calculated Using Method 1 (Eq. 4-4) and Method 2 (average of shear strain in strips) (Specimen S4)

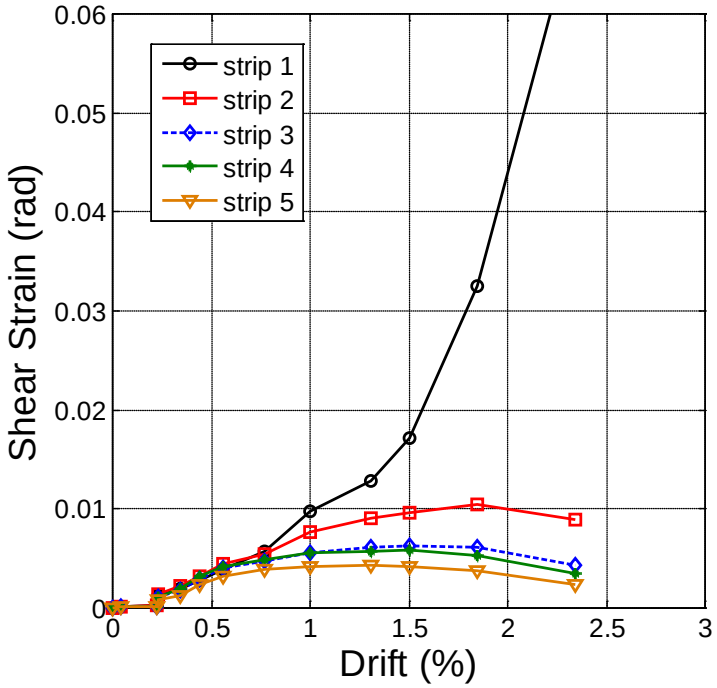

(a) Specimen S4

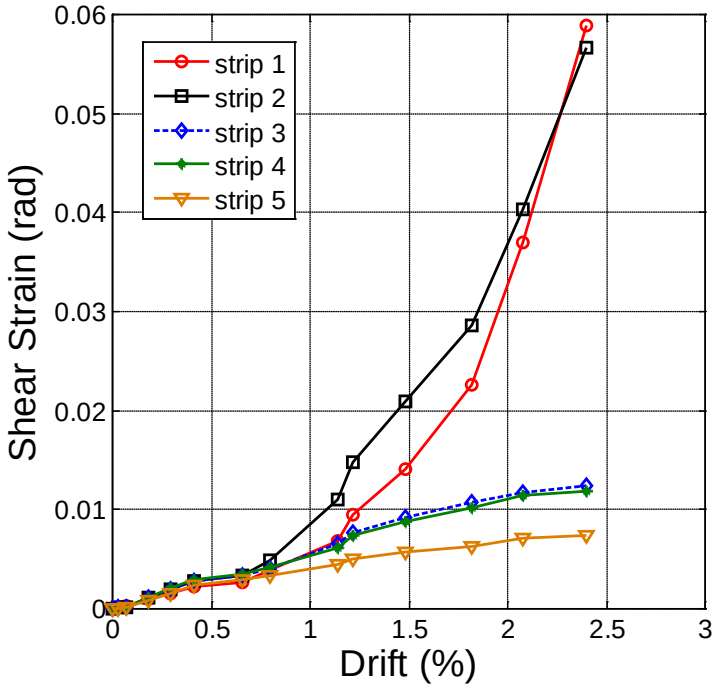

(b) Specimen S10

Fig. 4-22 Shear Strain versus Drift Envelope Response at Each Strip (Specimen S10)

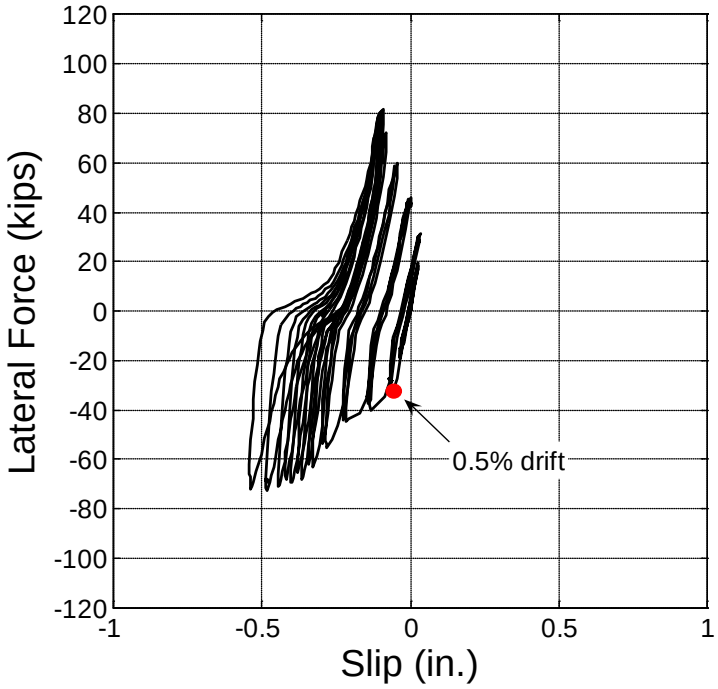

(a) Specimen S1

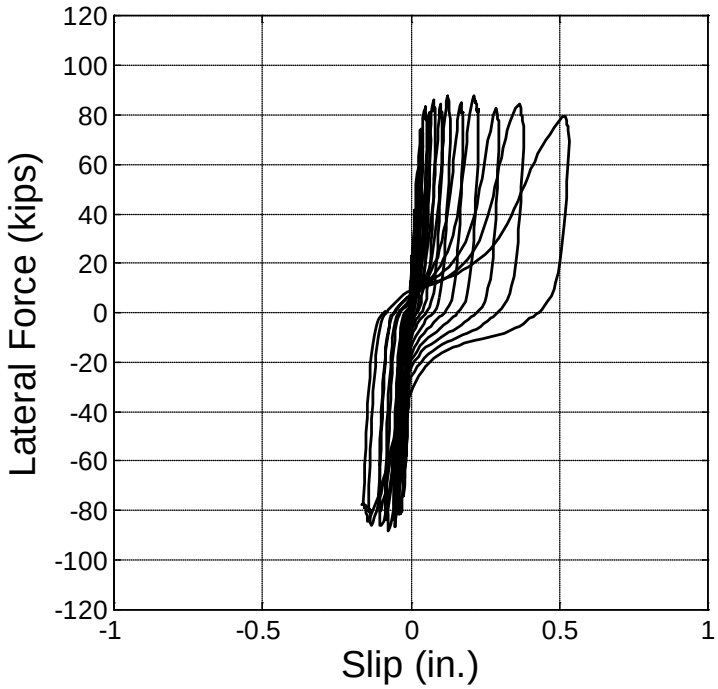

(b) Specimen S6

Fig. 4-23 Load versus Base Slip Response for RC Specimens

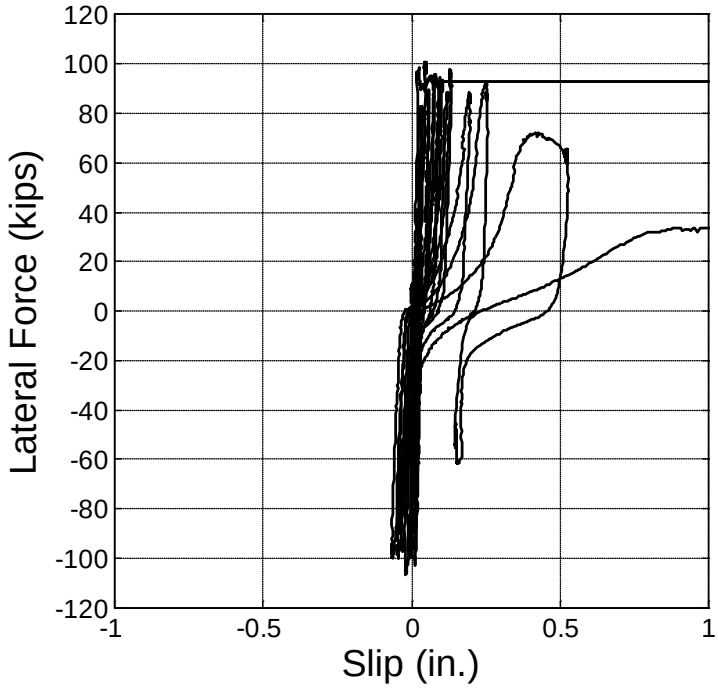

(c) Specimen S4

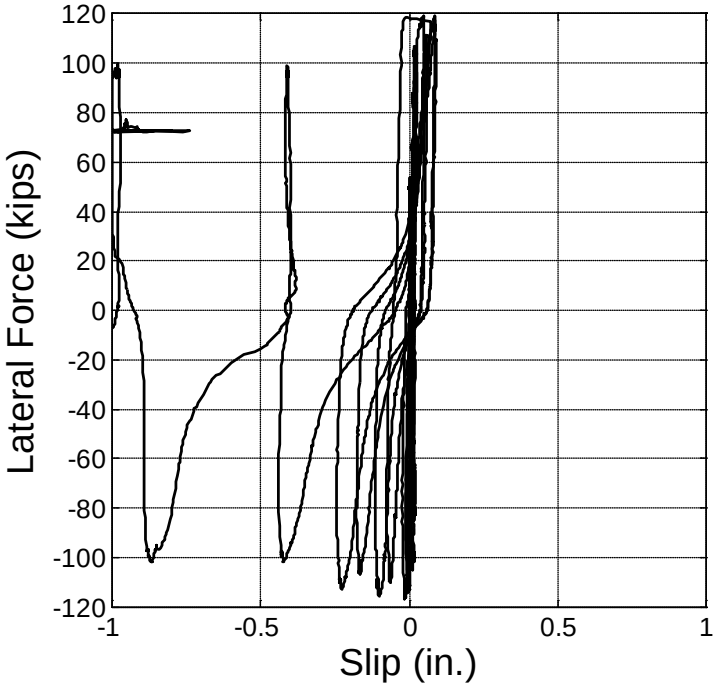

(d) Specimen S9

Fig. 4-23 Load versus Base Slip Response for RC Specimens

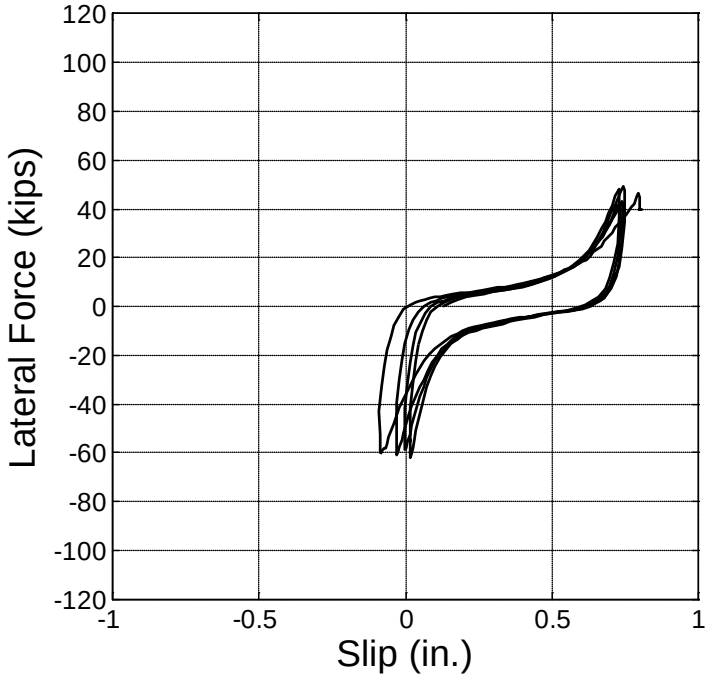

Fig. 4-24 Load versus Base Slip Response for HPFRC Specimen S2

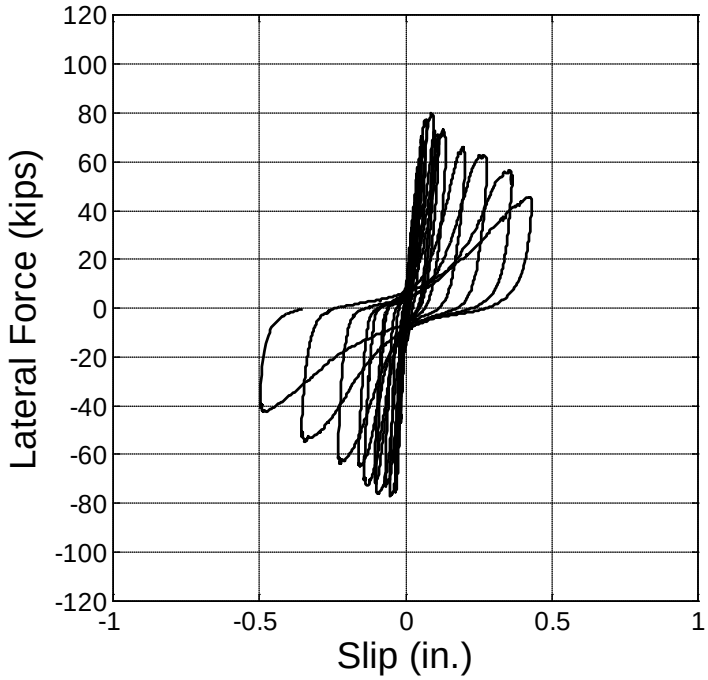

(a) Specimen S5

Fig. 4-25 Load versus Slip Response at Horizontal Crack for HPFRC Specimens with Dowel Bars at the Base

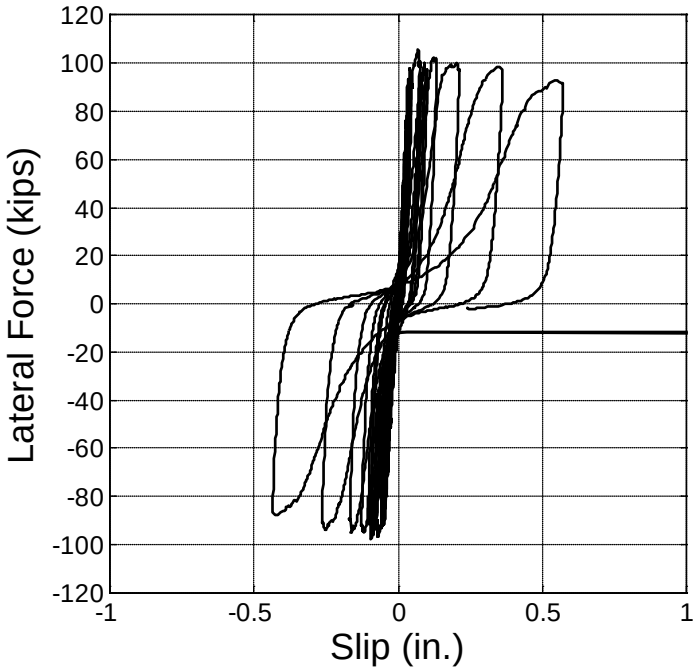

(b) Specimen S10

Fig. 4-25 Load versus Slip Response at Horizontal Crack for HPFRC Specimens with Dowel Bars at the Base

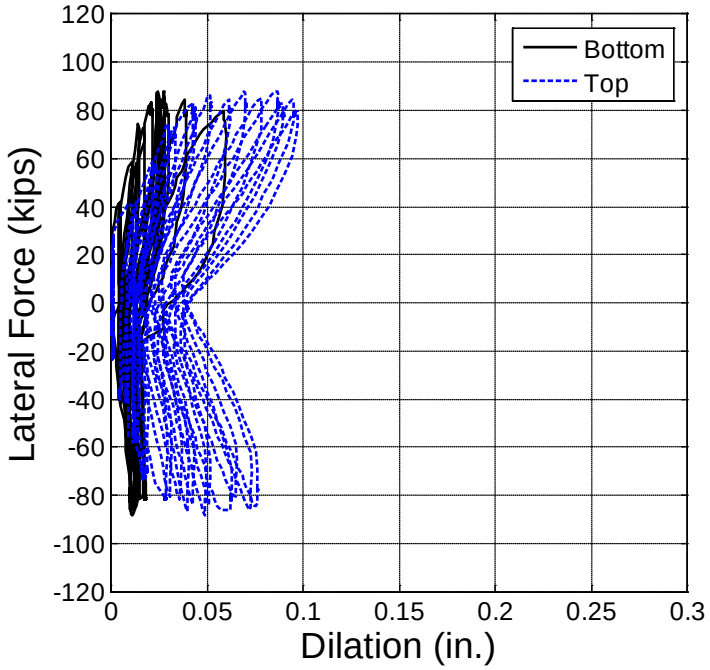

(a) Specimen S6

Fig. 4-26 Load versus Dilation Response for Specimens with a Shear Span-to-Length Ratio of 1.5

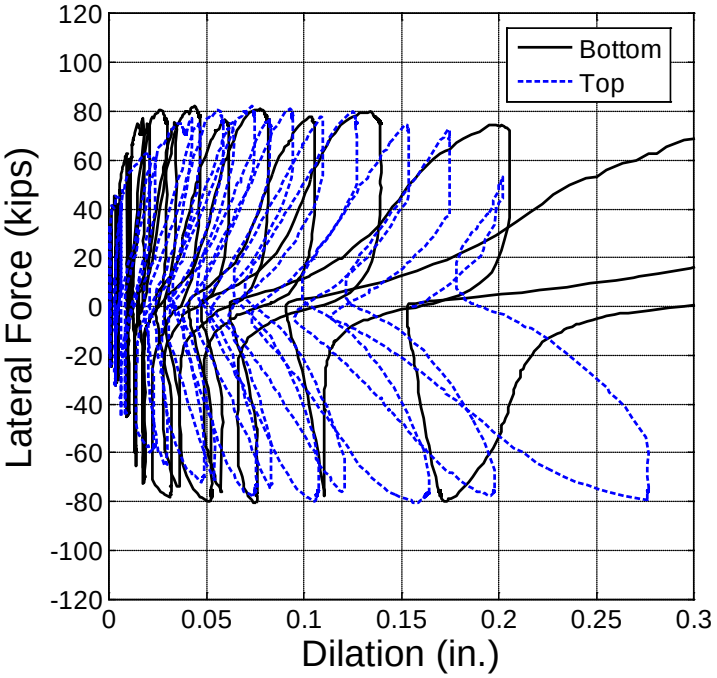

(b) Specimen S7

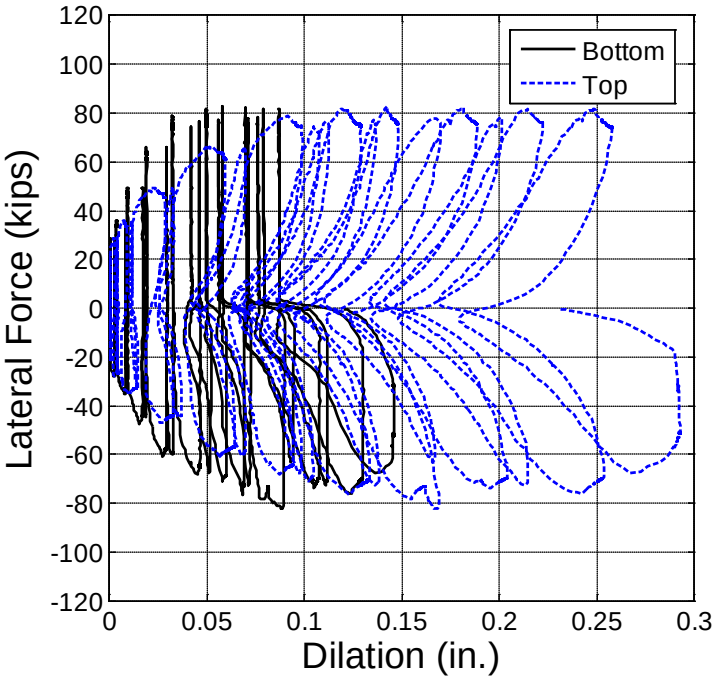

(c) Specimen S8

Fig. 4-26 Load versus Dilation Response for Specimens with a Shear Span-to-Length Ratio of 1.5

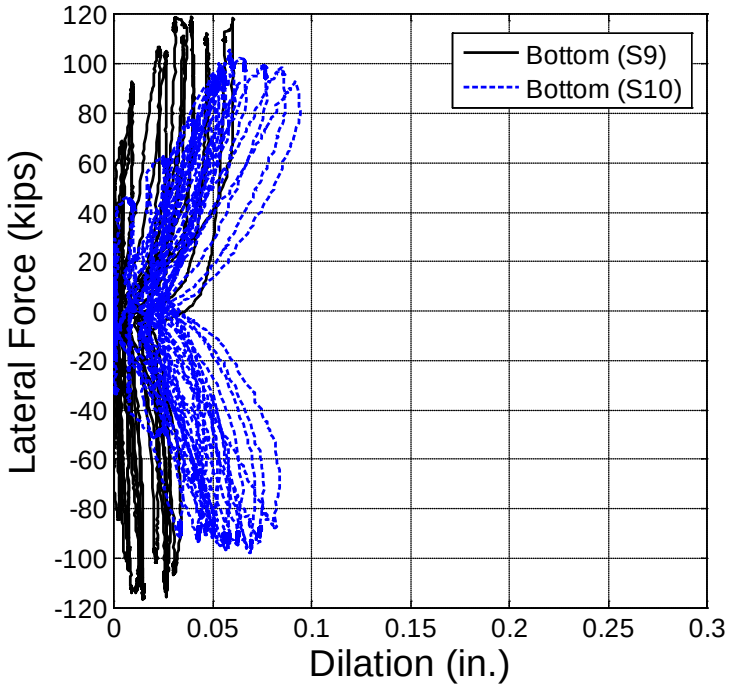

Fig. 4-27 Comparison of Dilation at Bottom of Wall for Specimens S9 and S10

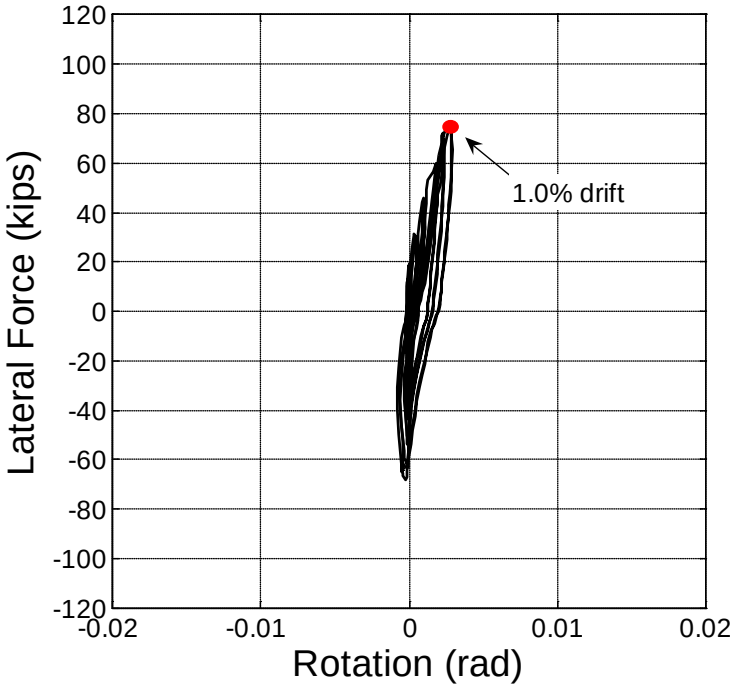

(a) Specimen S1

Fig. 4-28 Load versus Concentrated Rotation for Test Specimens

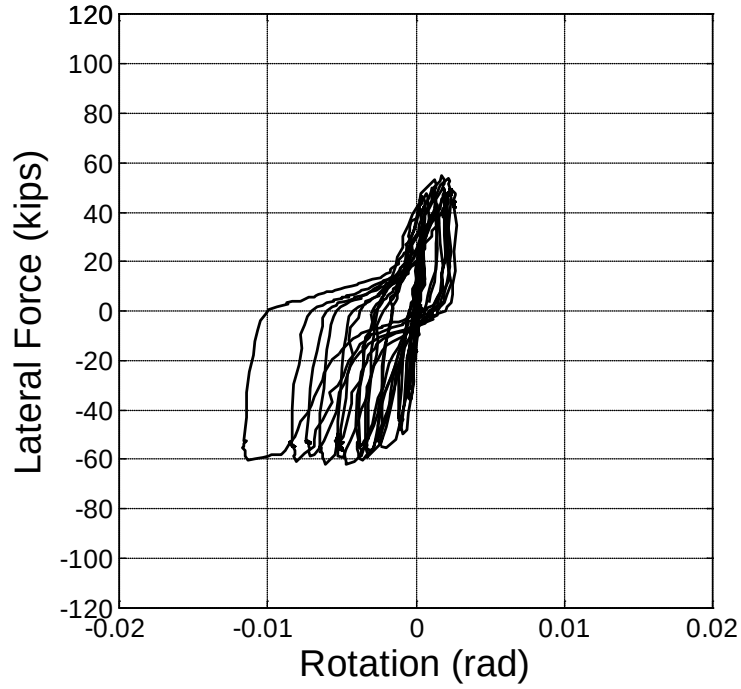

(b) Specimen S2

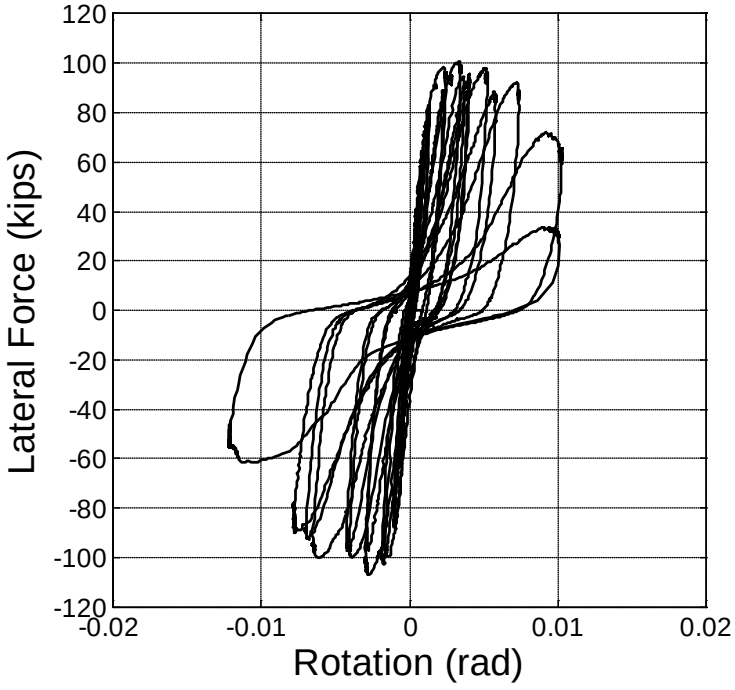

(c) Specimen S4

Fig. 4-28 Load versus Concentrated Rotation for Test Specimens

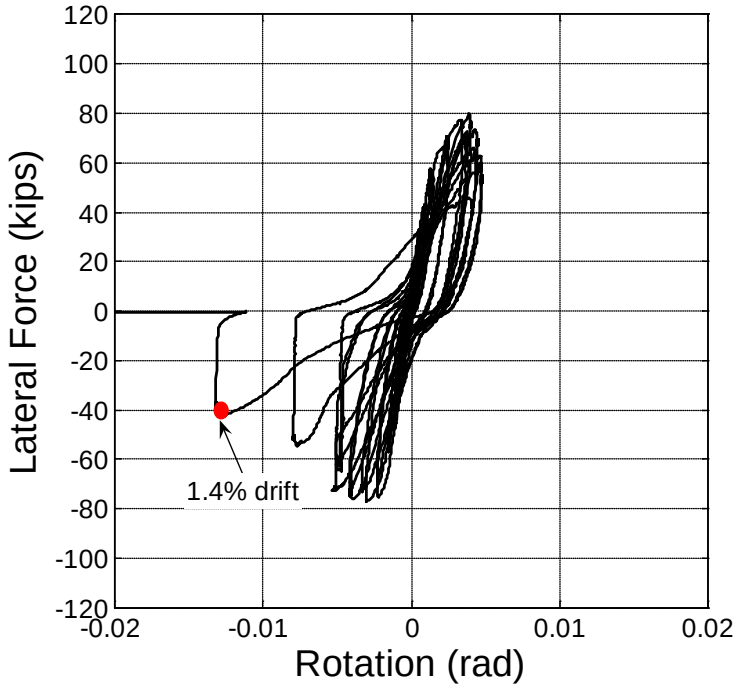

(d) Specimen S5

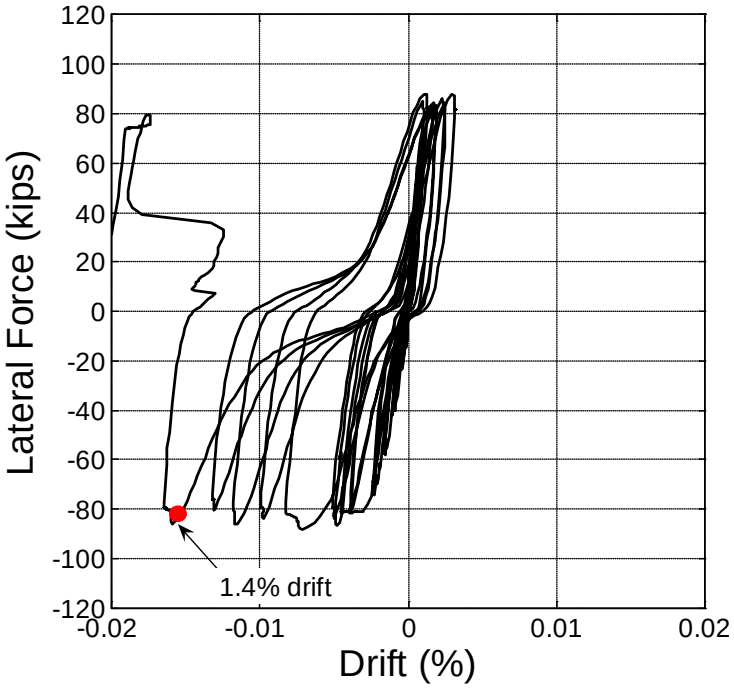

(e) Specimen S6

Fig. 4-28 Load versus Concentrated Rotation for Test Specimens

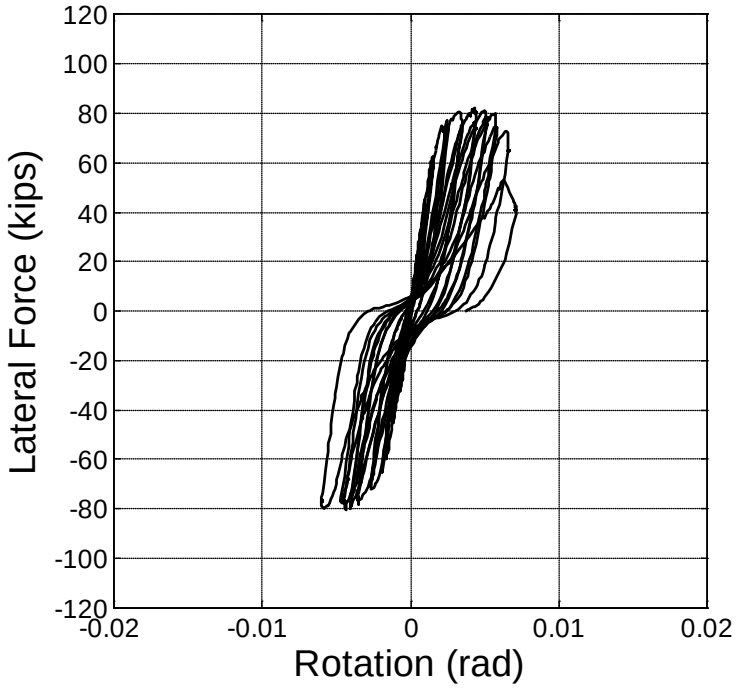

(f) Specimen S7

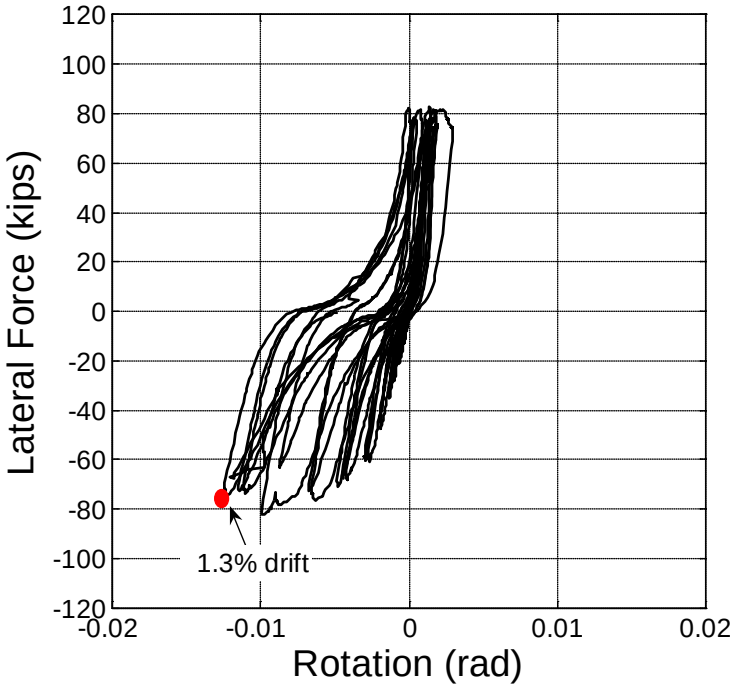

(g) Specimen S8

Fig. 4-28 Load versus Concentrated Rotation for Test Specimens

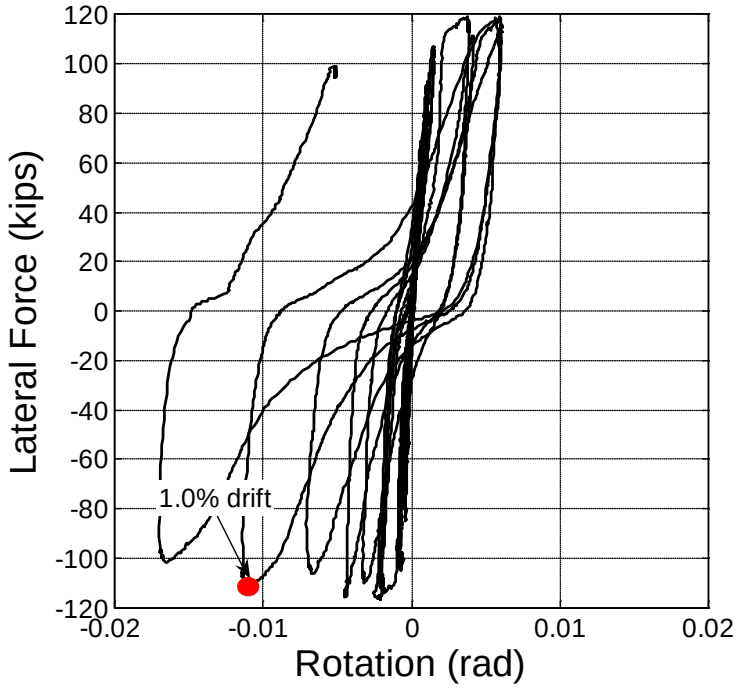

(h) Specimen S9

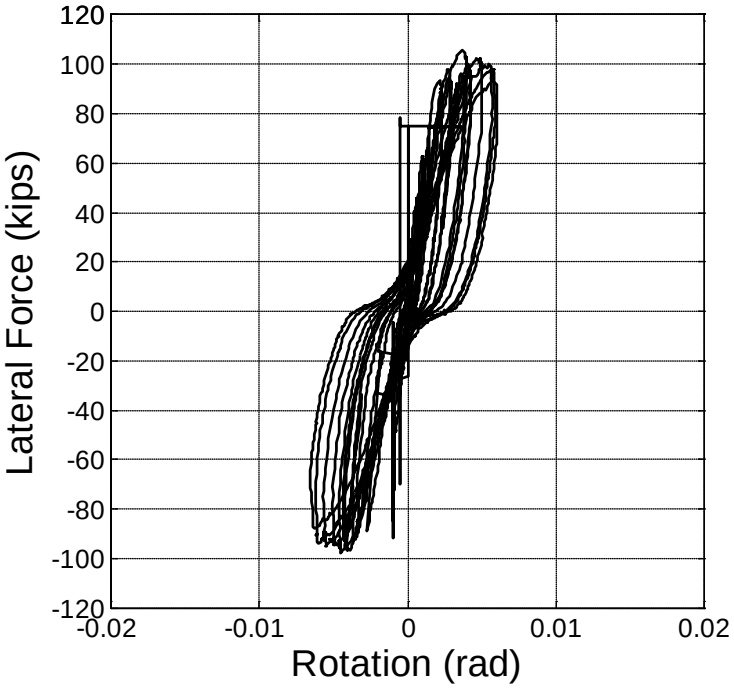

(i) Specimen S10

Fig. 4-28 Load versus Concentrated Rotation for Test Specimens

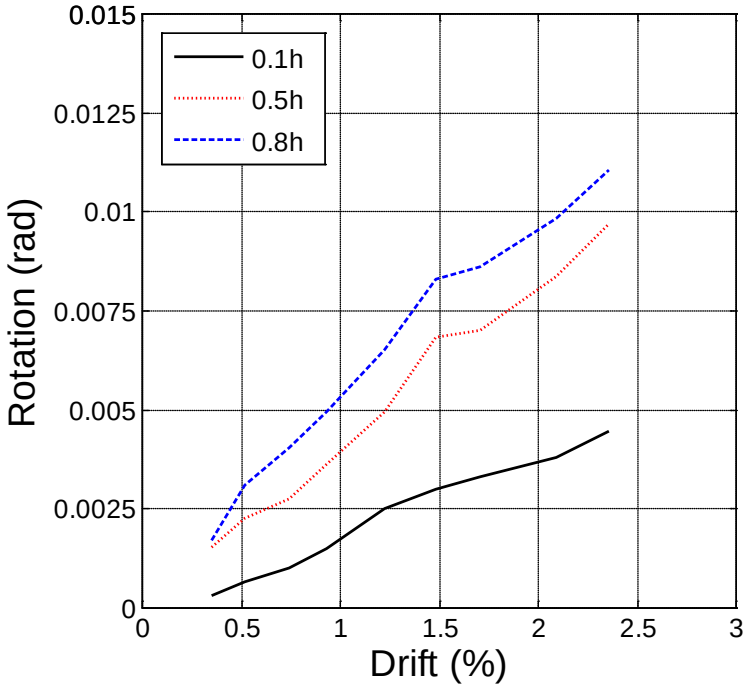

(a) Specimen S1

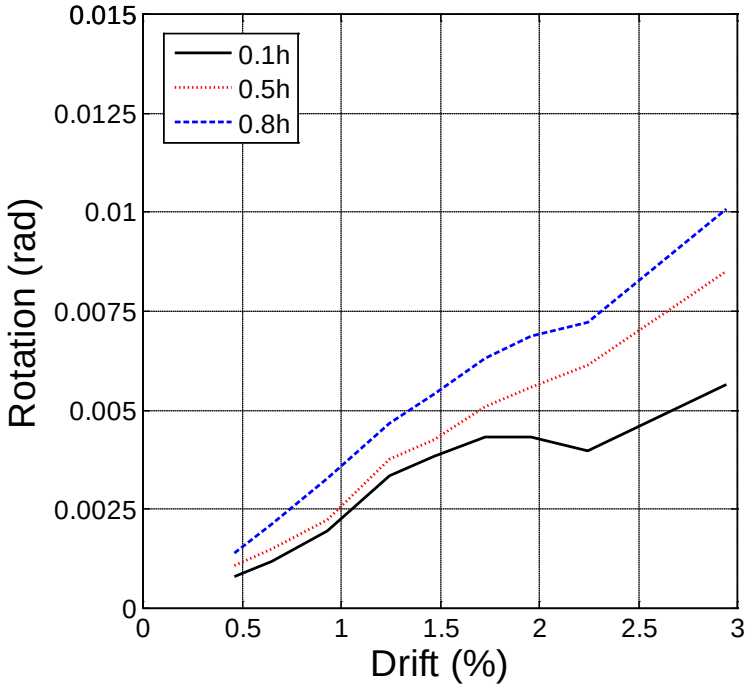

(b) Specimen S2

Fig. 4-29 Rotation versus Drift Envelope Response for Wall Specimens

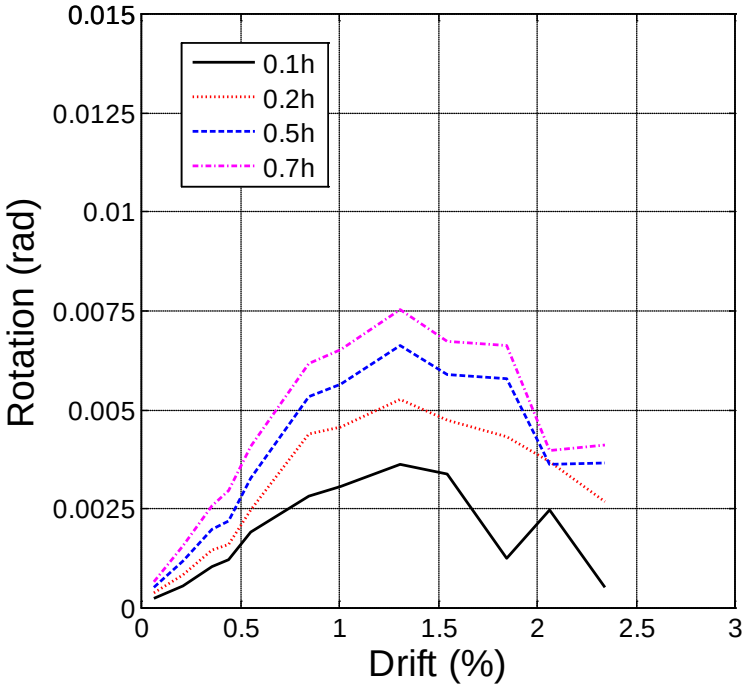

(c) Specimen S4

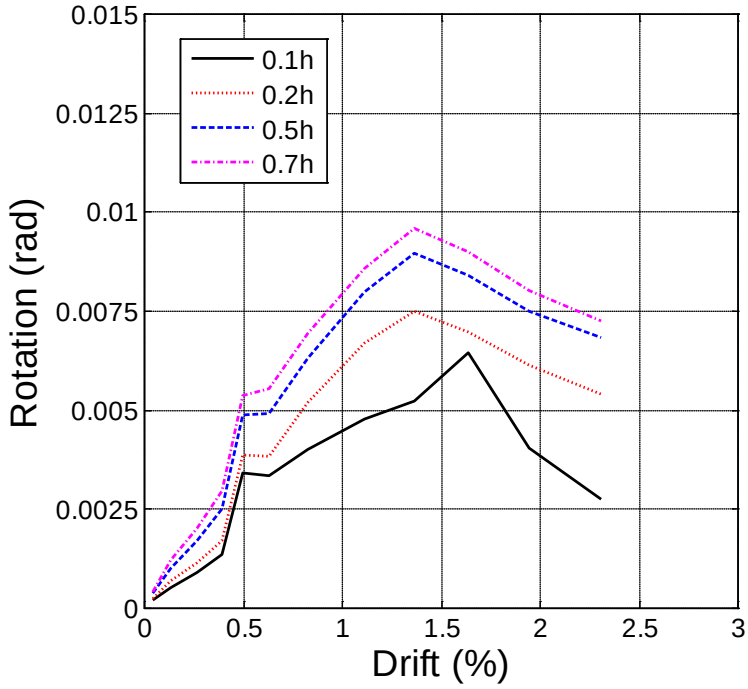

(d) Specimen S5

Fig. 4-29 Rotation versus Drift Envelope Response for Wall Specimens

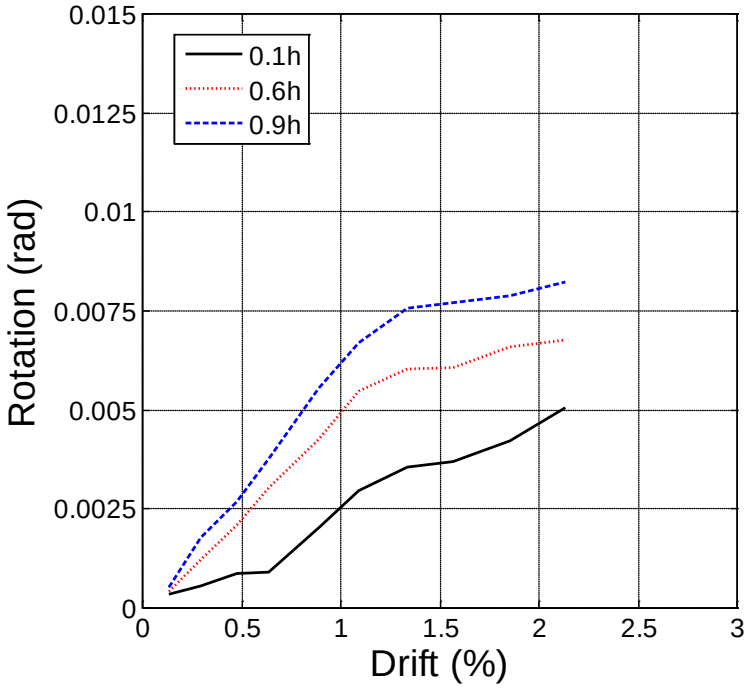

(e) Specimen S6

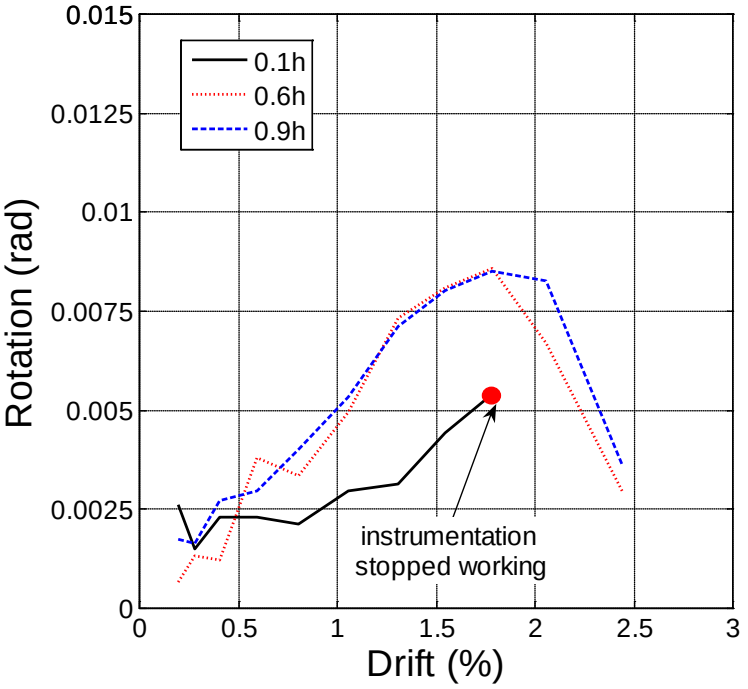

(f) Specimen S7

Fig. 4-29 Rotation versus Drift Envelope Response for Wall Specimens

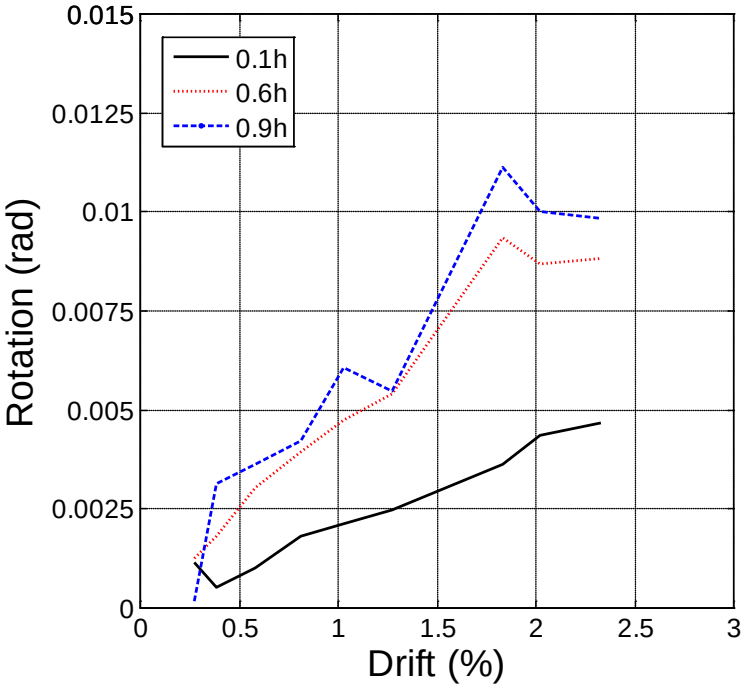

(g) Specimen S8

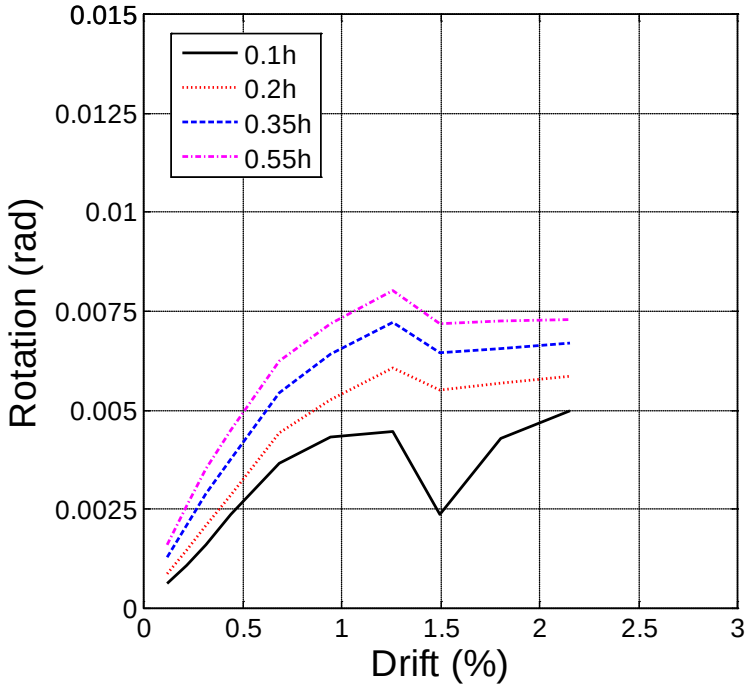

(h) Specimen S9

Fig. 4-29 Rotation versus Drift Envelope Response for Wall Specimens

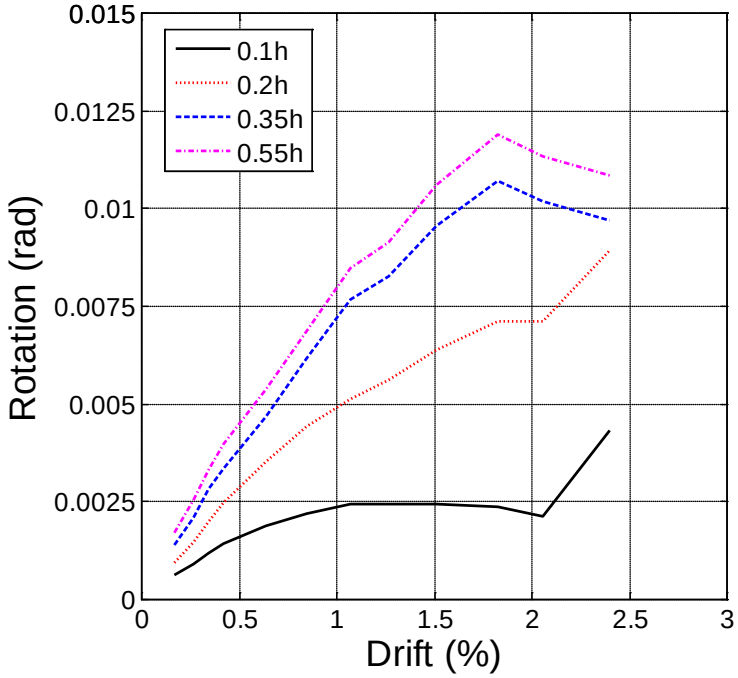

(i) Specimen S10

Fig. 4-29 Rotation versus Drift Envelope Response for Wall Specimens

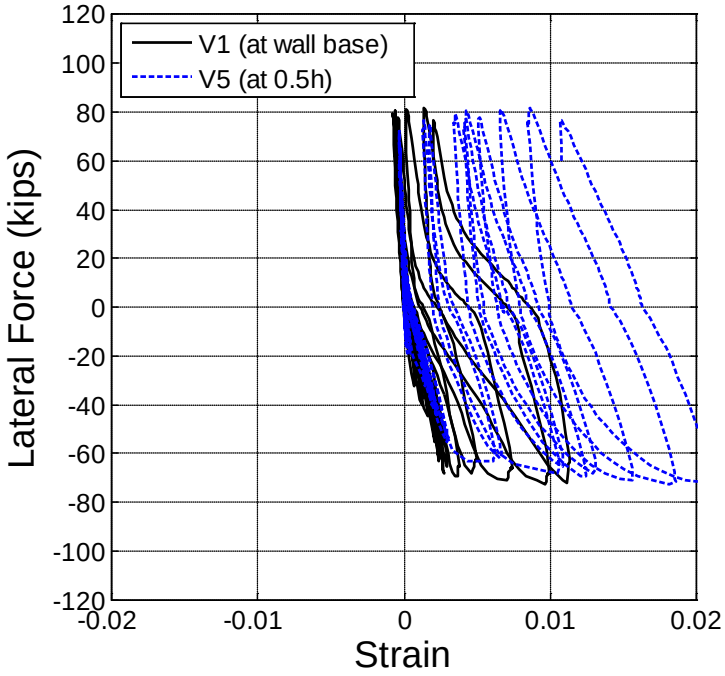

Fig. 4-30 Load versus Strain Response in Longitudinal Bar of Wall Boundary Element in Specimen S1

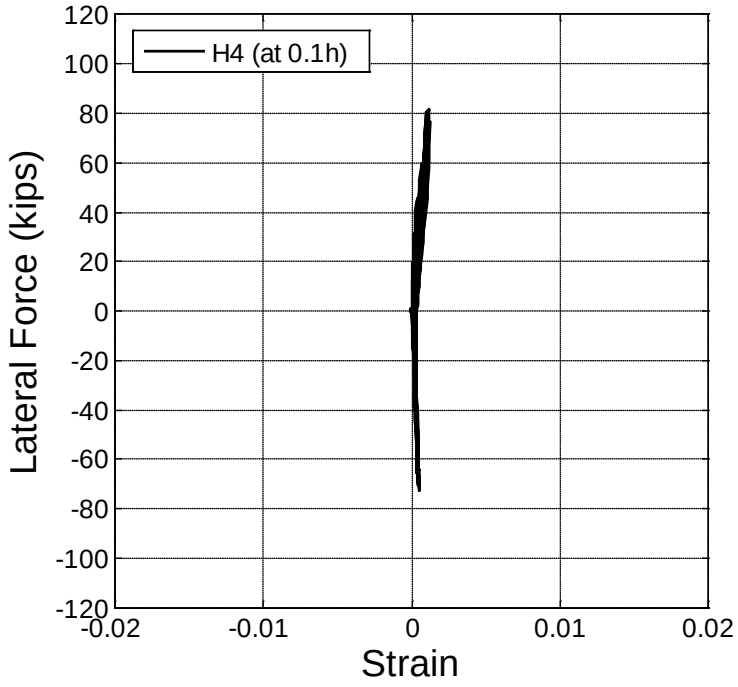

Fig. 4-31 Load versus Strain Response in a Horizontal Bar of Specimen S1

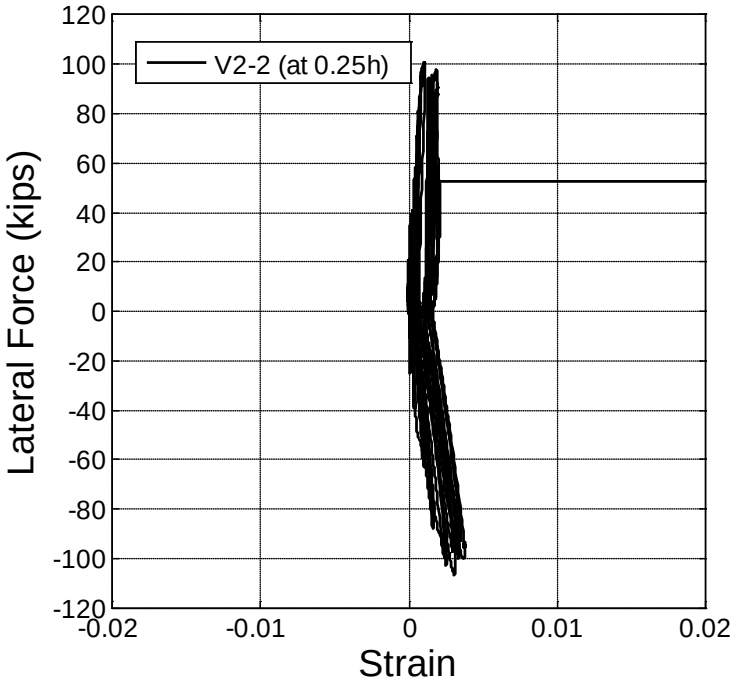

Fig. 4-32 Load versus Strain Response in a Vertical Bar of Specimen S4

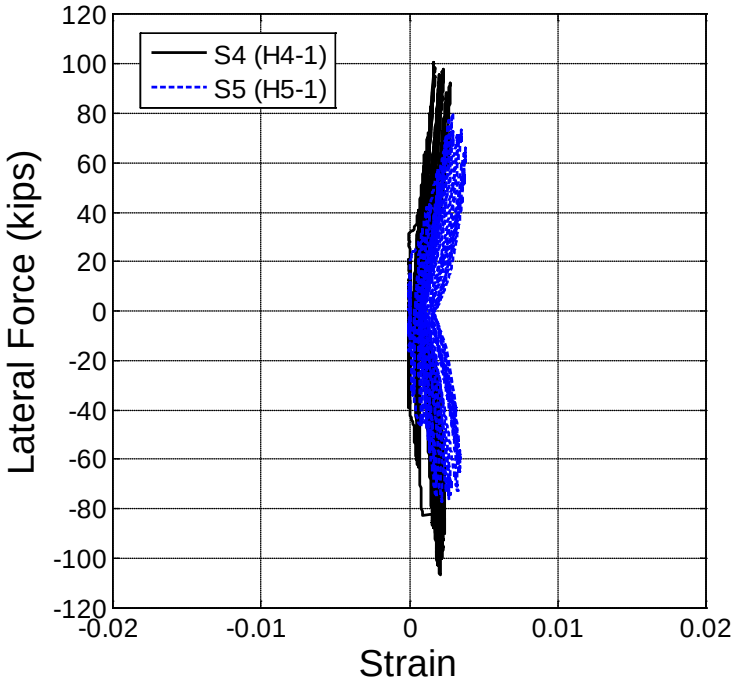

Fig. 4-33 Load versus Strain Response in a Horizontal Bars of Specimens S4 and S5

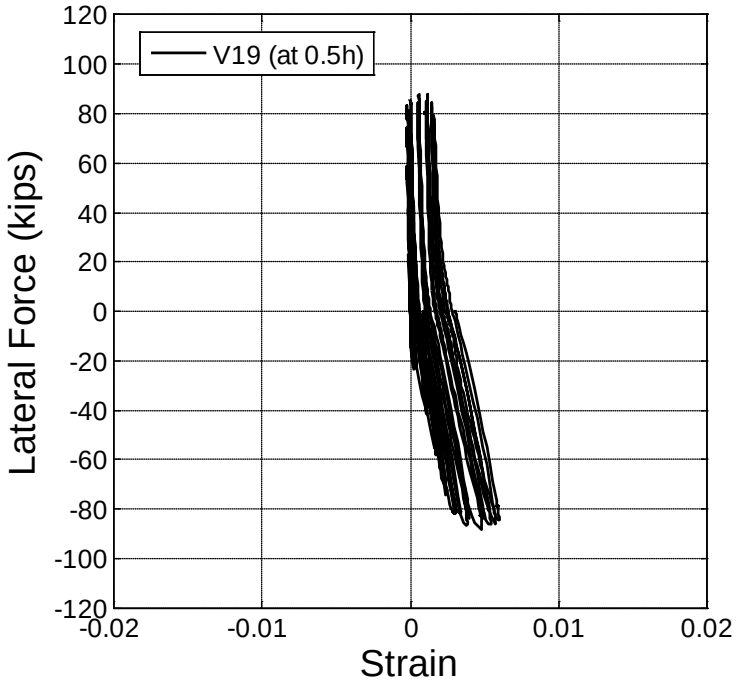

Fig. 4-34 Load versus Strain Response in Longitudinal Bar of Wall Boundary Element in Specimen S6

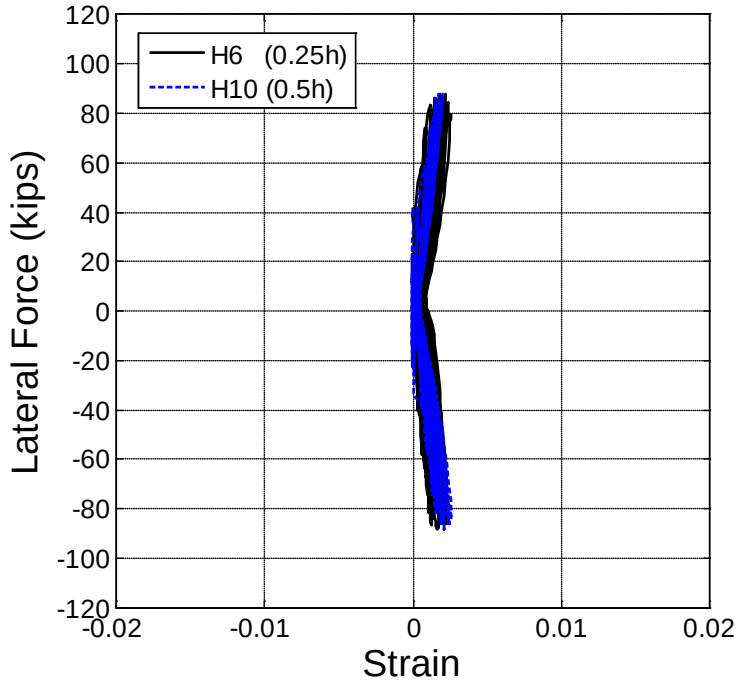

Fig. 4-35 Load versus Strain Response in Horizontal Bars of Specimen S6

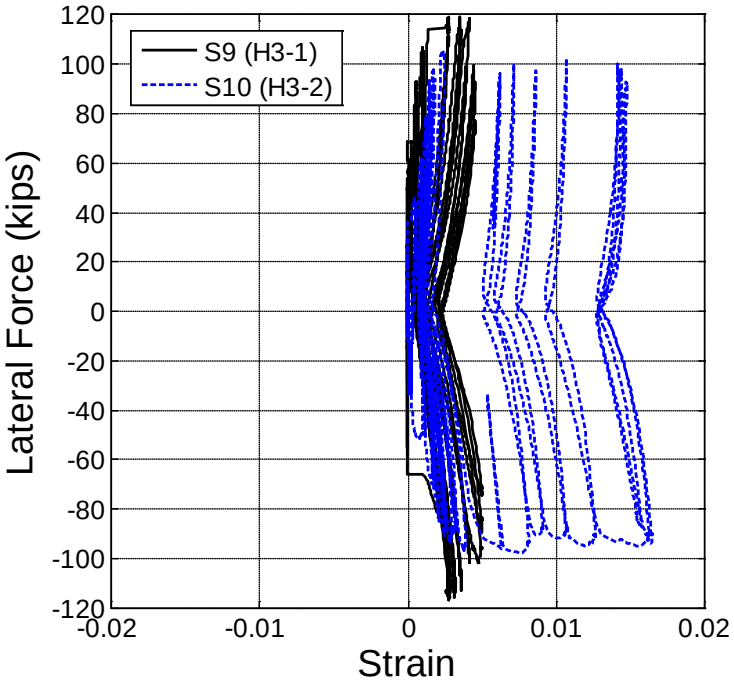

Fig. 4-36 Load versus Strain Response in Horizontal Bars at 0.3*h* for Specimens S9 and S10

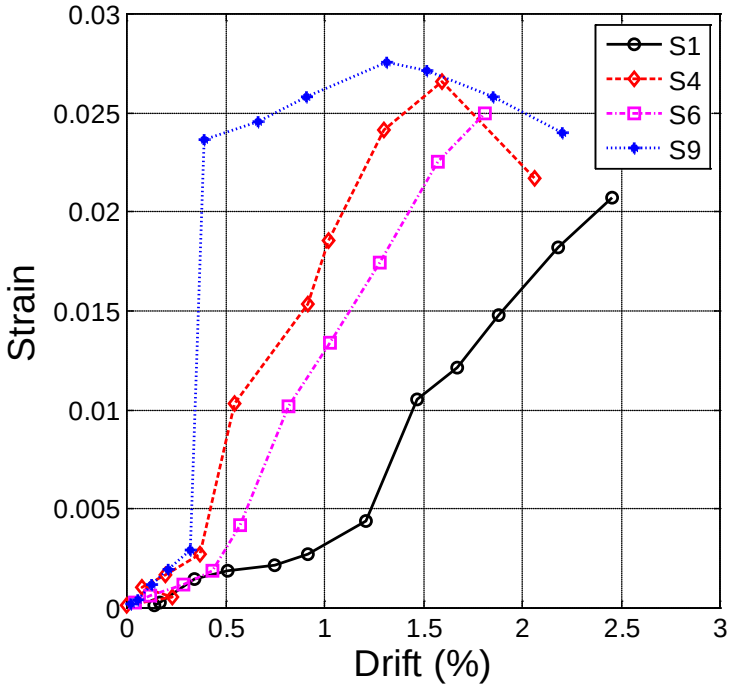

(a) RC Specimens

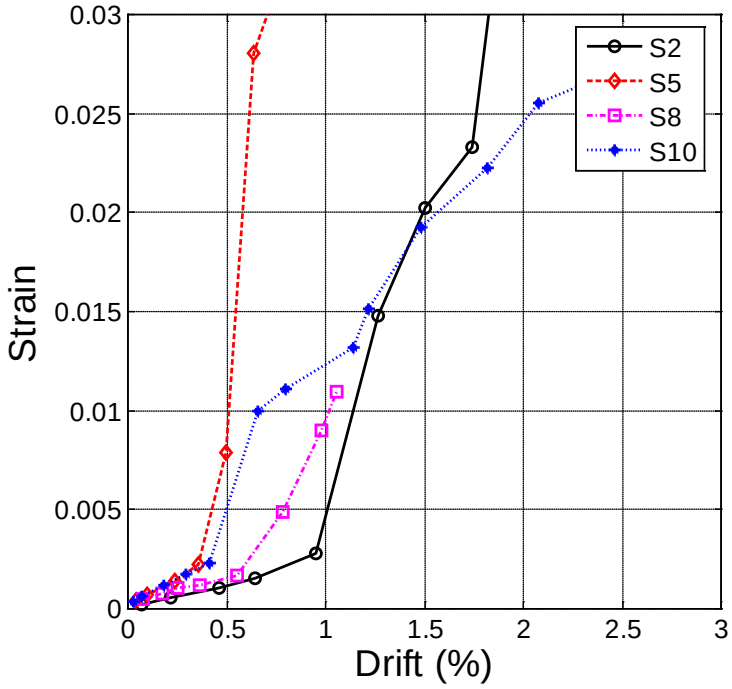

(b) HPFRC Specimens

Fig. 4-37 Drift versus Strain in Main Longitudinal Bars at 1 in. from Wall Base

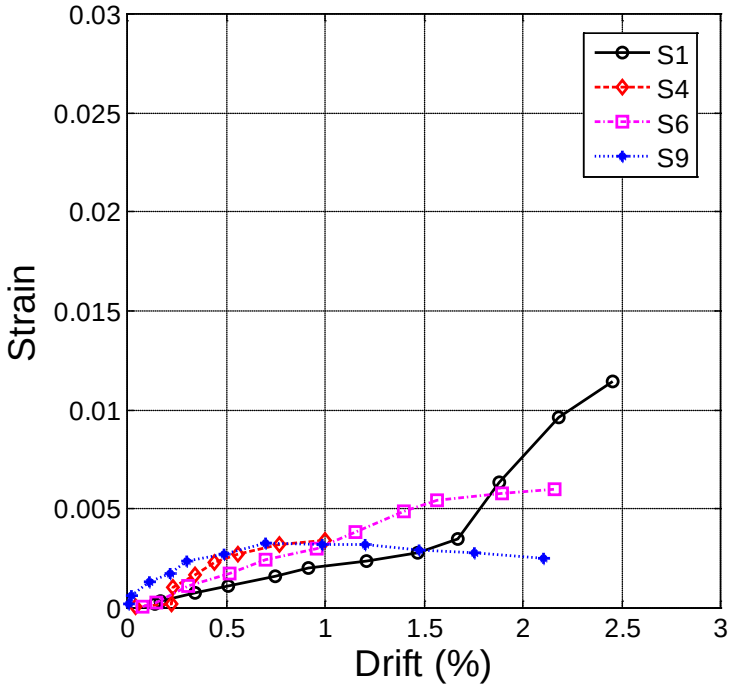

(a) RC Specimens

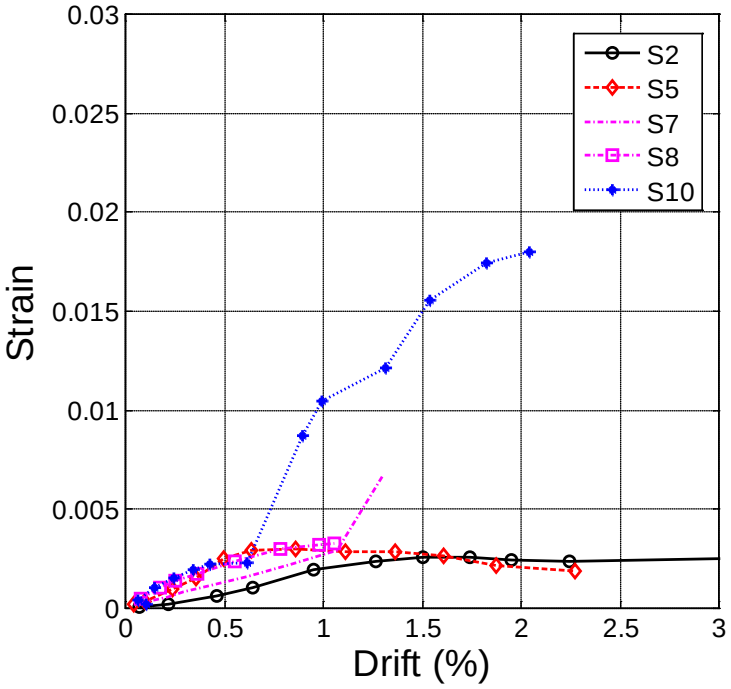

(b) HPFRC Specimens

Fig. 4-38 Drift versus Strain in Main Longitudinal Bars at Wall Mid-Height

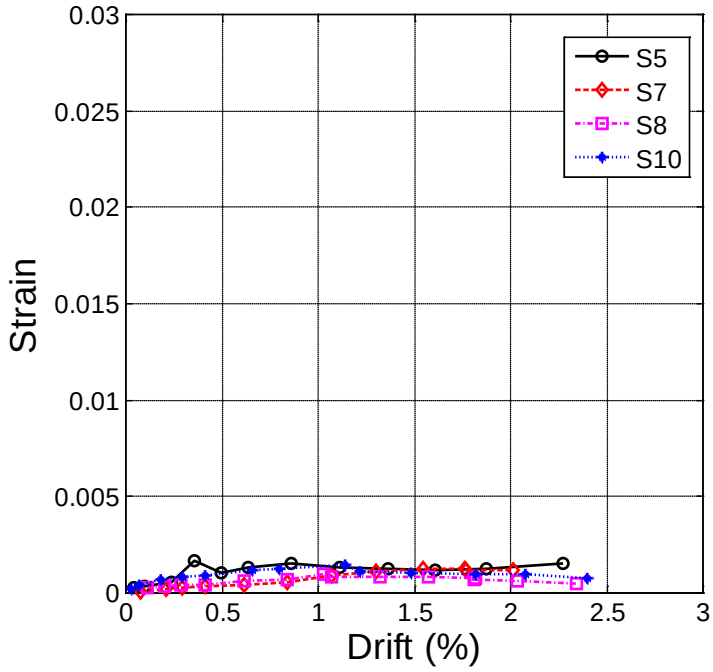

Fig. 4-39 Drift versus Strain in Dowel Bars at 1 in. from Wall Base in HPFRC Specimens

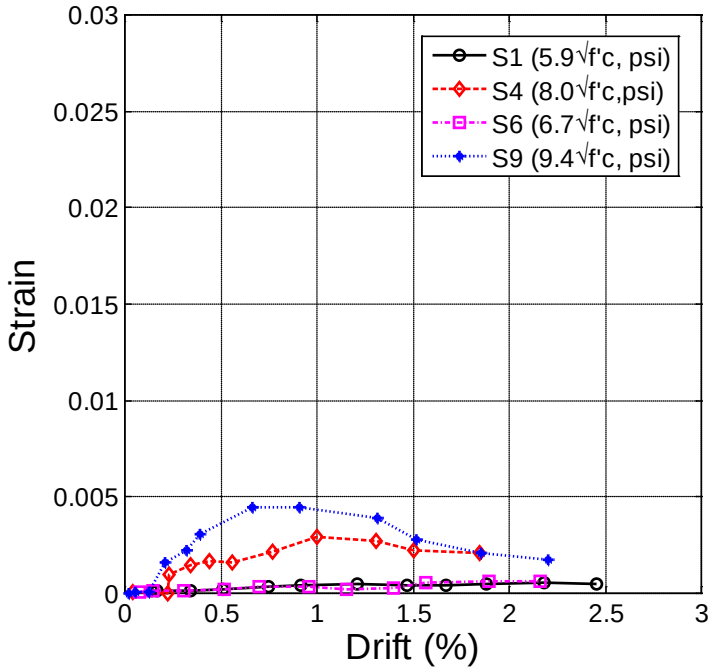

(a) RC Specimens

Fig. 4-40 Drift versus Strain at a Horizontal Bar at a Height of 0.1*h*

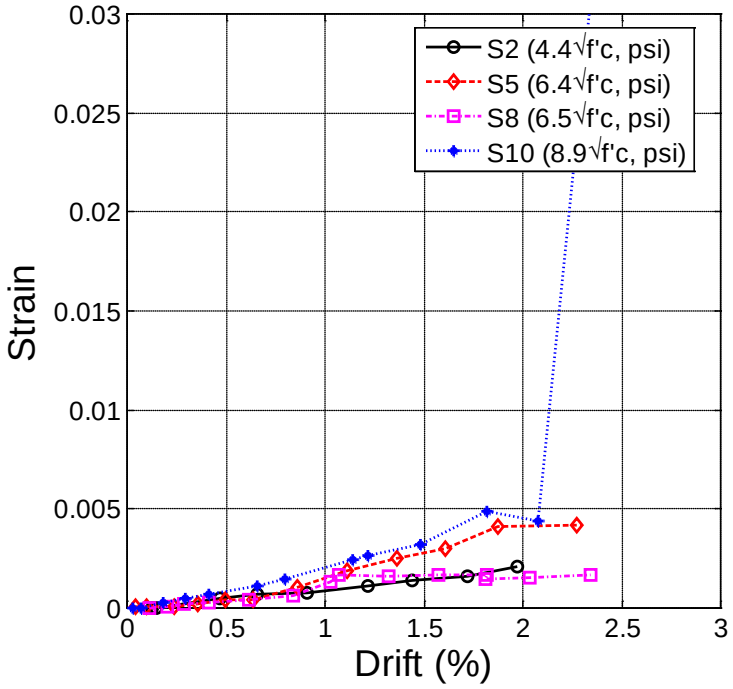

(b) HPFRC Specimens

Fig. 4-40 Drift versus Strain at a Horizontal Bar at a Height of 0.1*h*

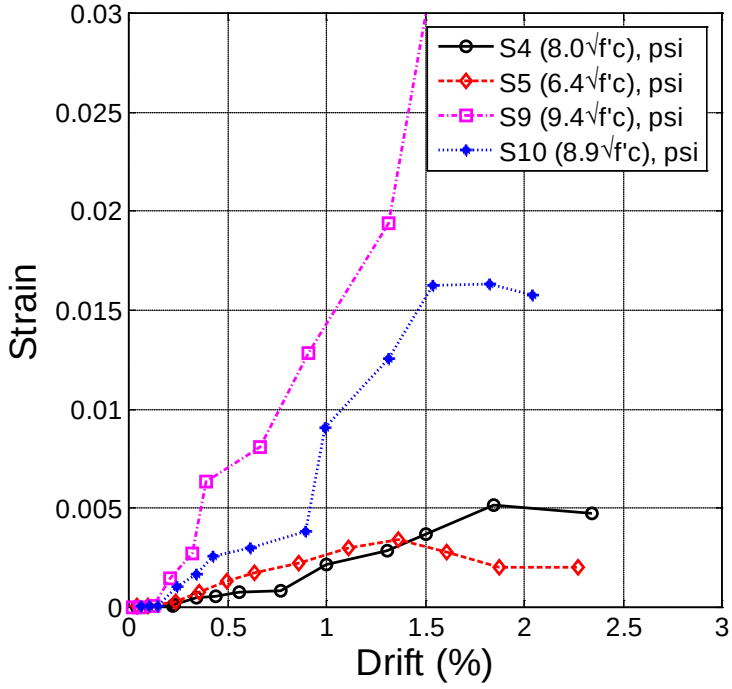

Fig. 4-41 Drift versus Strain at a Horizontal Bar at a Height of 0.25*h*

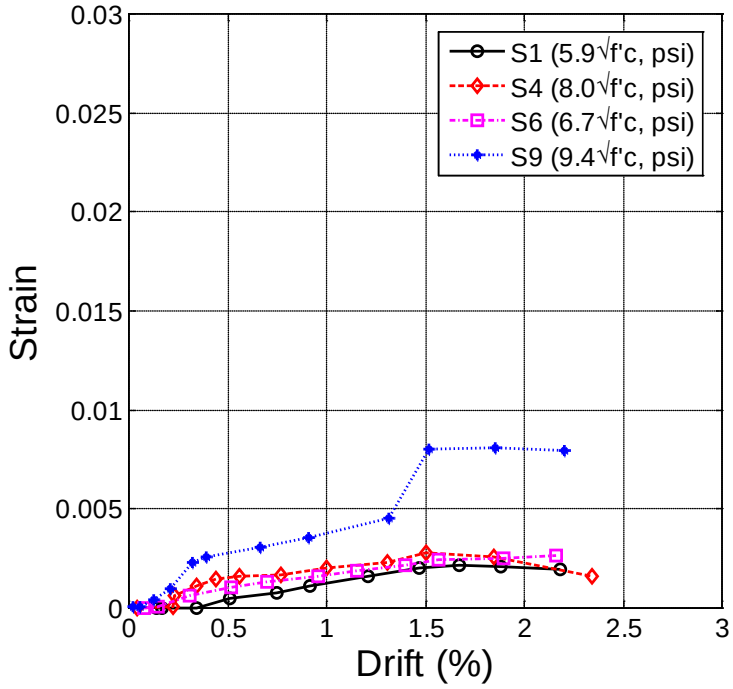

(a) RC Specimens

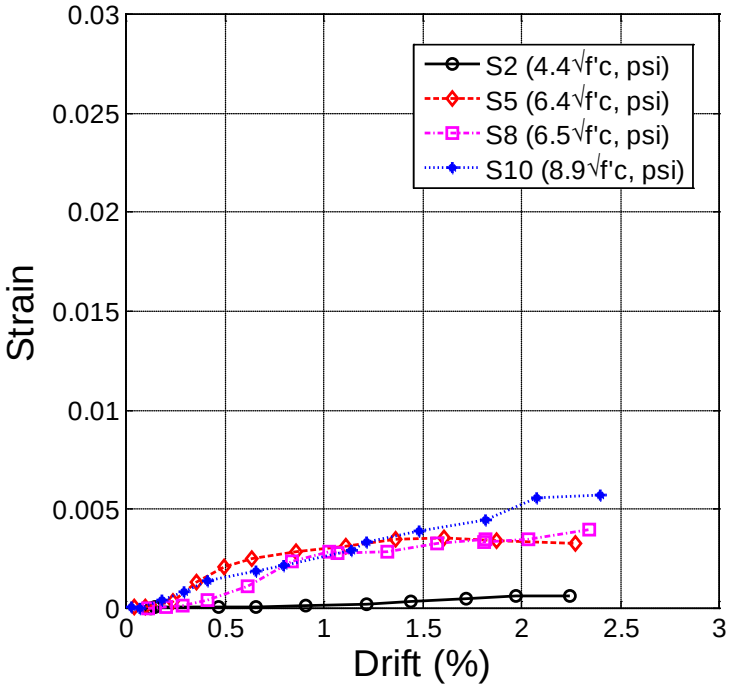

(b) HPFRC Specimens

Fig. 4-42 Drift versus Strain at a Horizontal Bar at a Height of 0.5*h*

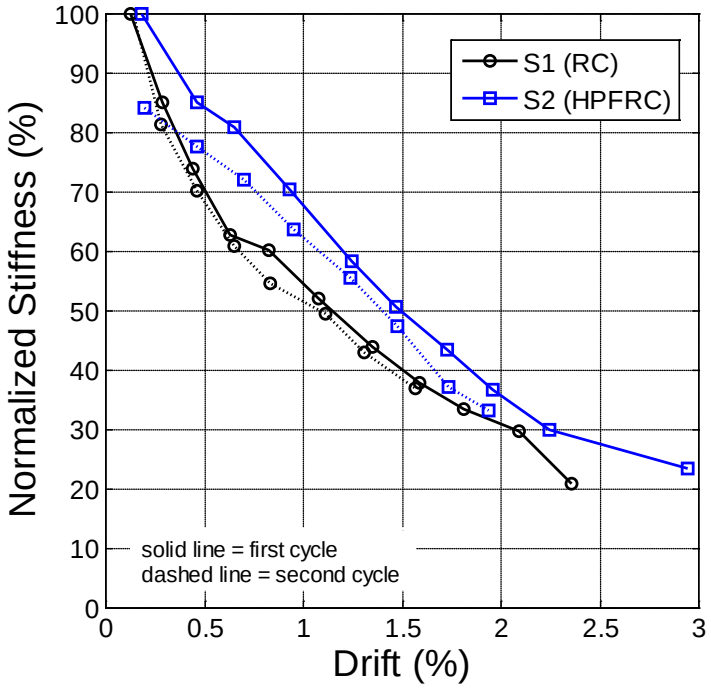

(a) Specimens S1 and S2

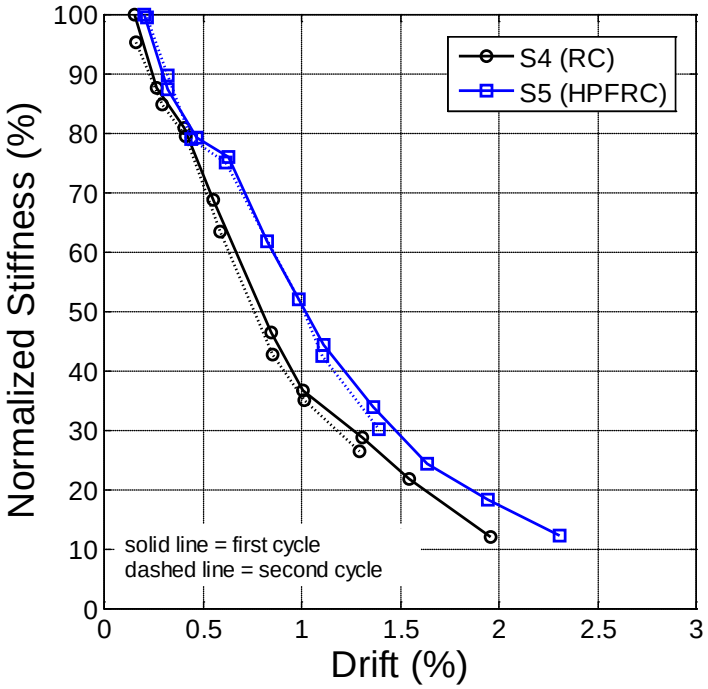

(b) Specimens S4 and S5

Fig. 4-43 Normalized Peak-to Peak Stiffness versus Drift for Wall Specimens

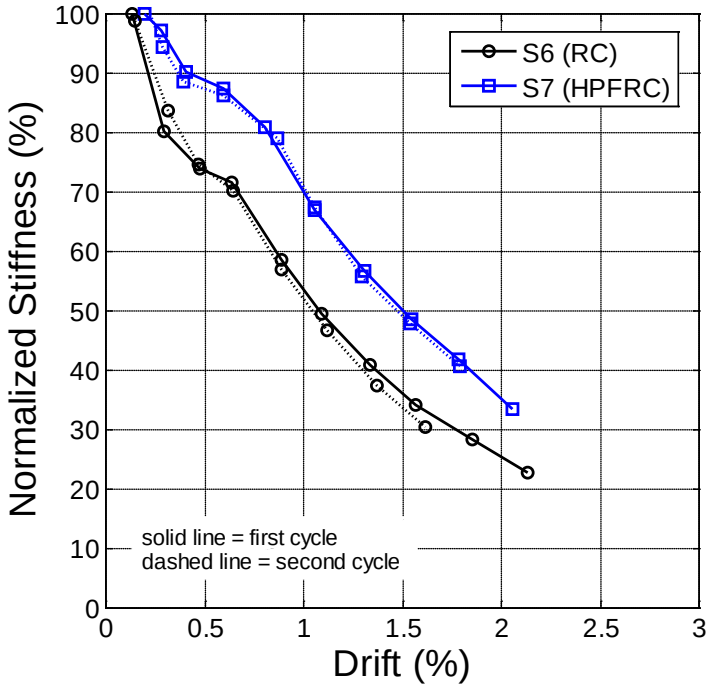

(c) Specimens S6 and S7

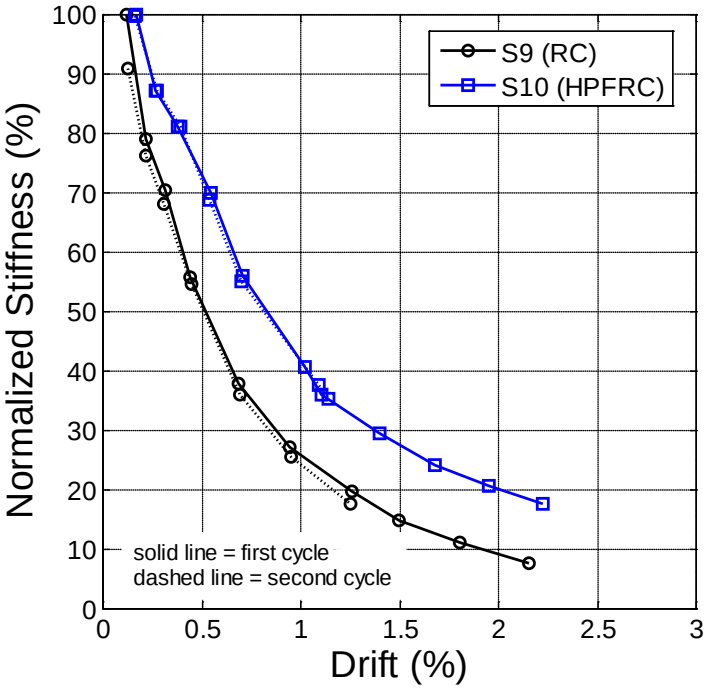

(d) Specimens S9 and S10

Fig. 4-43 Normalized Peak-to Peak Stiffness versus Drift for Wall Specimens

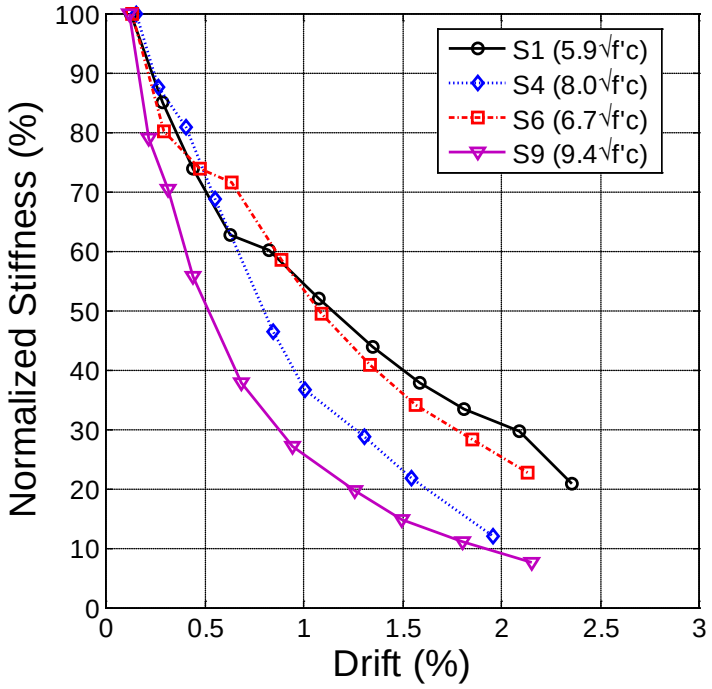

Fig.4-44 Comparison of Normalized Stiffness for RC Wall Specimens

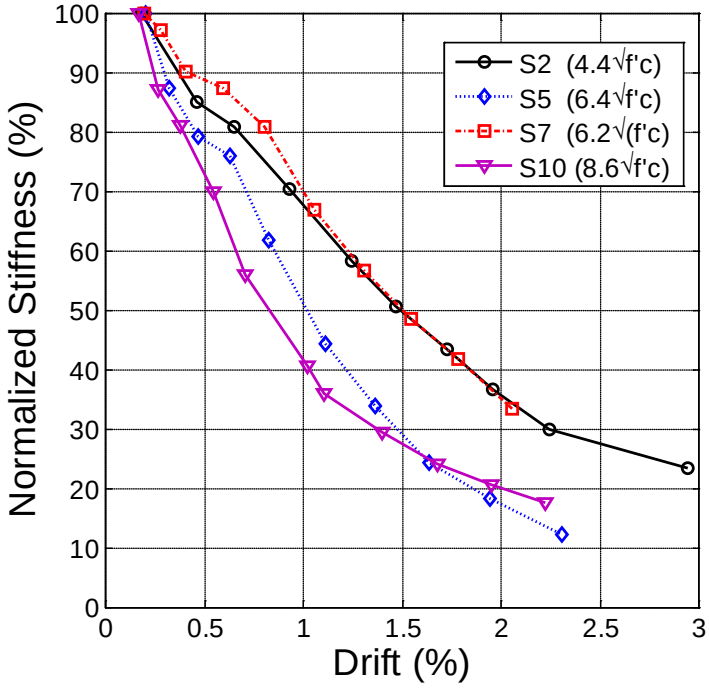

Fig.4-45 Comparison of Normalized Stiffness for HPFRC Wall Specimens

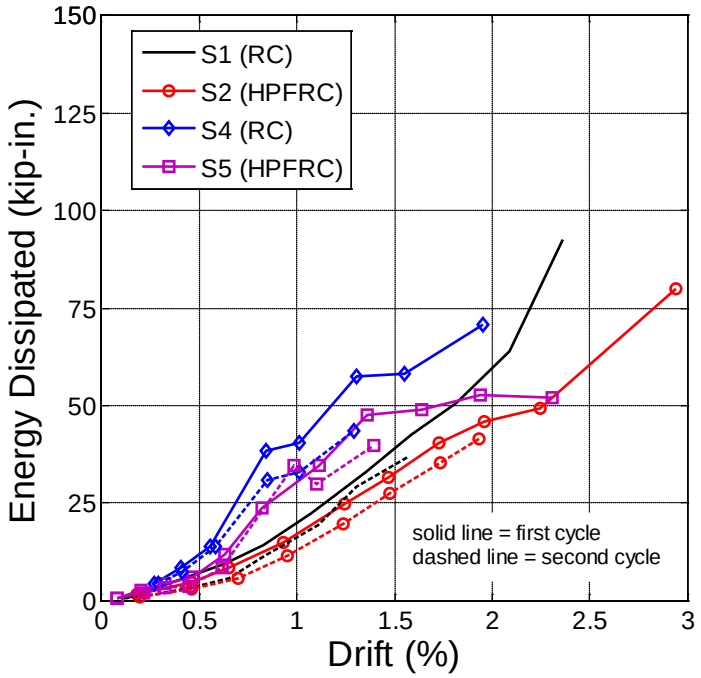

(a) Specimens with $a/\ell_w = 1.2$

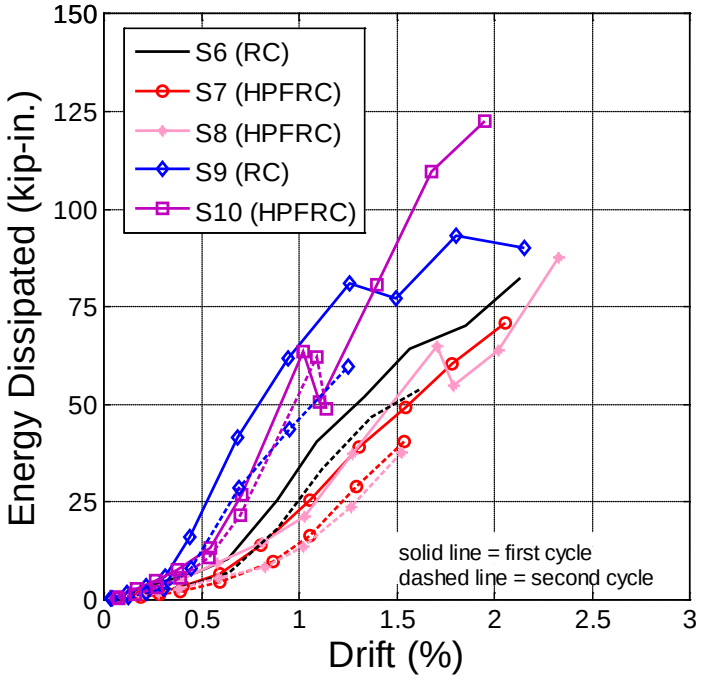

(b) Specimens with $a/\ell_w = 1.5$

Fig. 4-46 Energy Dissipated versus Drift for Wall Specimens

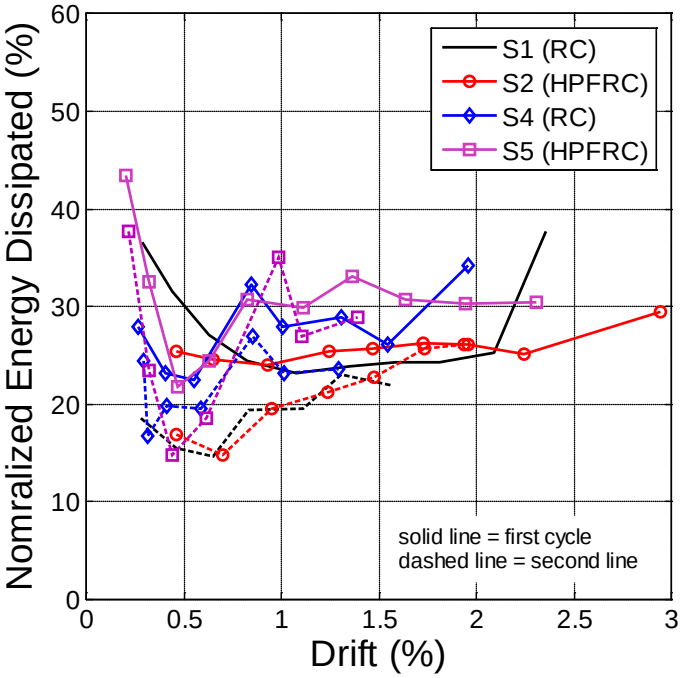

(a) Specimens with $a/\ell_w = 1.2$

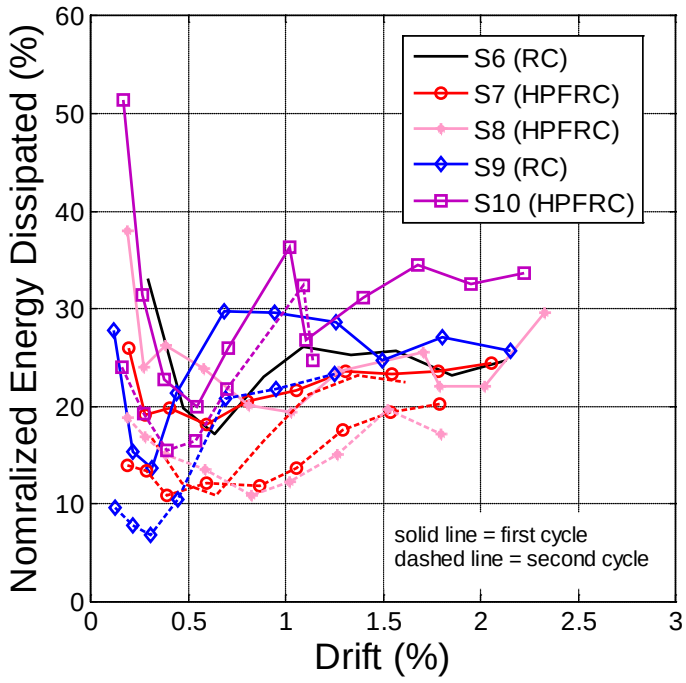

(b) Specimens with $a/\ell_w = 1.5$

Fig. 4-47 Normalized Energy Dissipated versus Drift for Wall Specimens

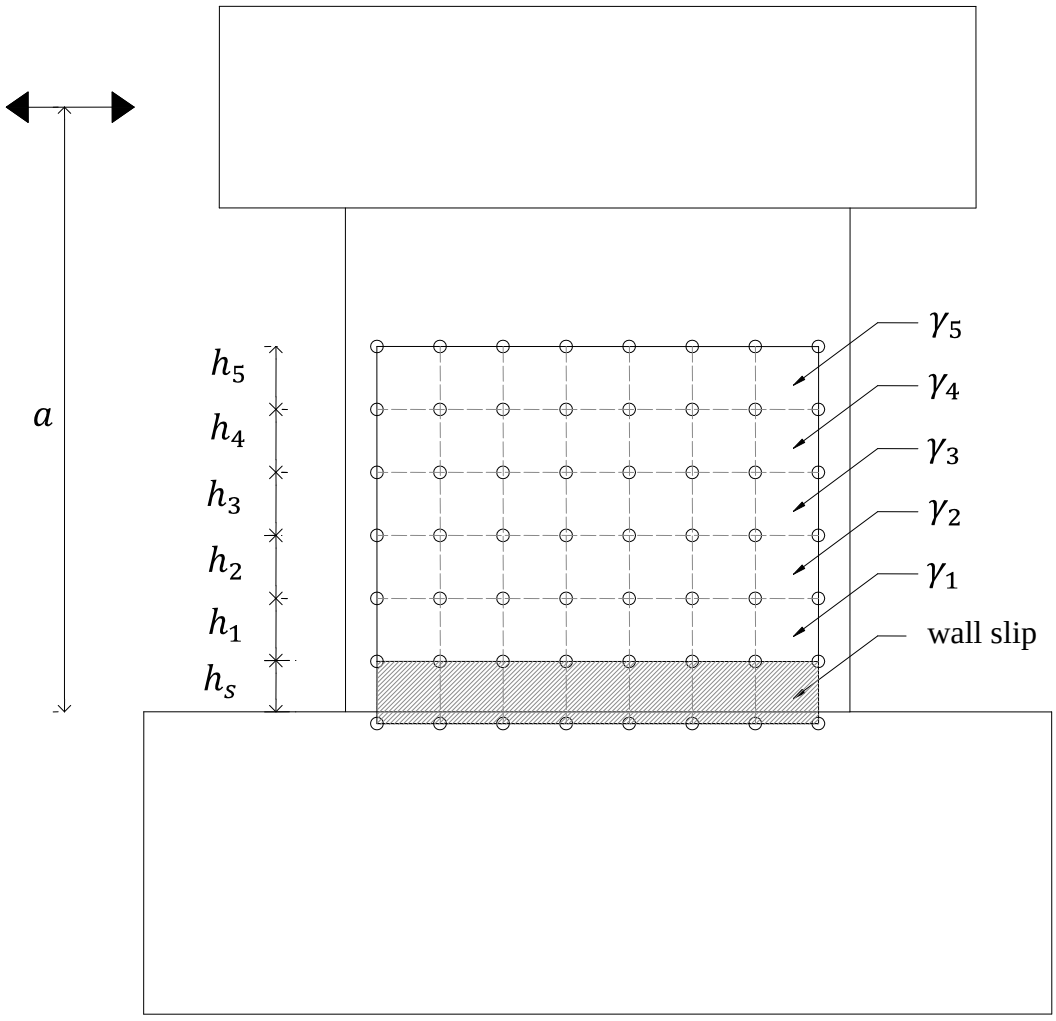

Fig. 5-1 Definition of Shear Strain for the Calculation of Wall Deformation Components

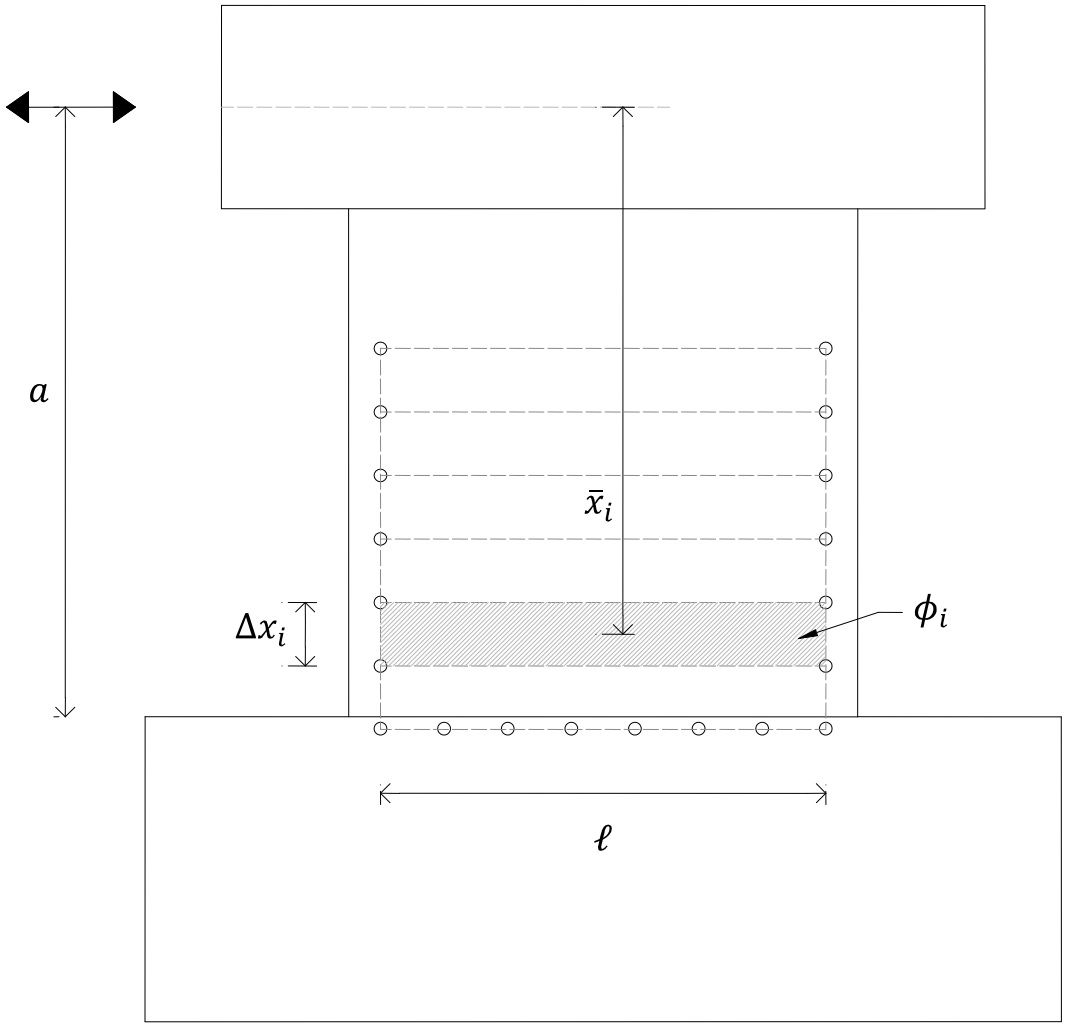

Fig. 5-2 Calculation of Curvature over the Wall Height

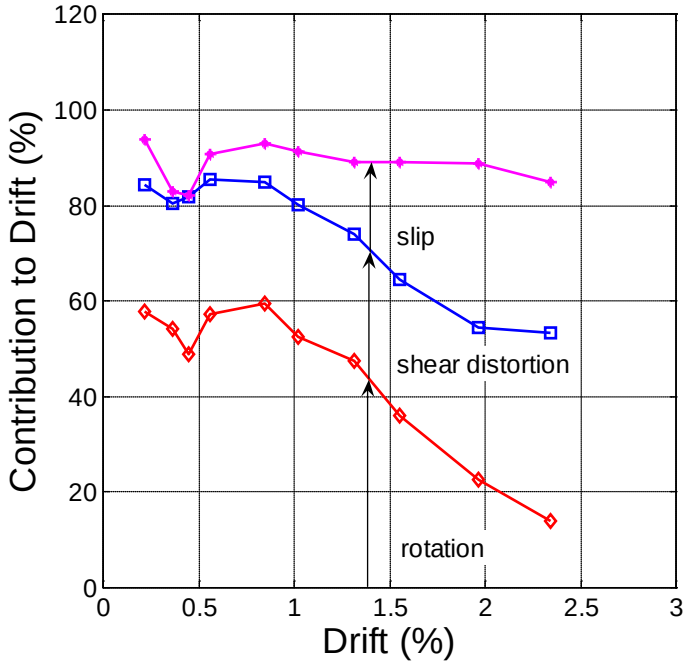

(a) RC Specimen S4

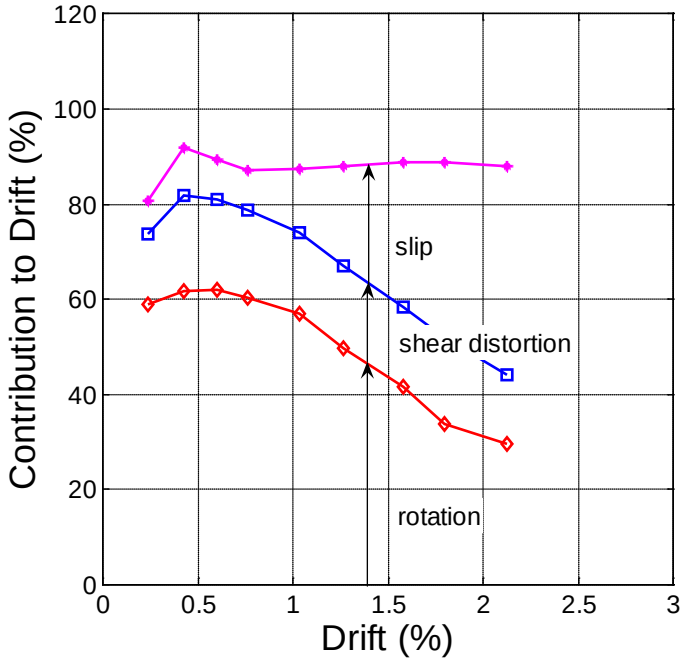

(b) RC Specimen S9

Fig. 5-3 Contribution of Deformation Components to Drift

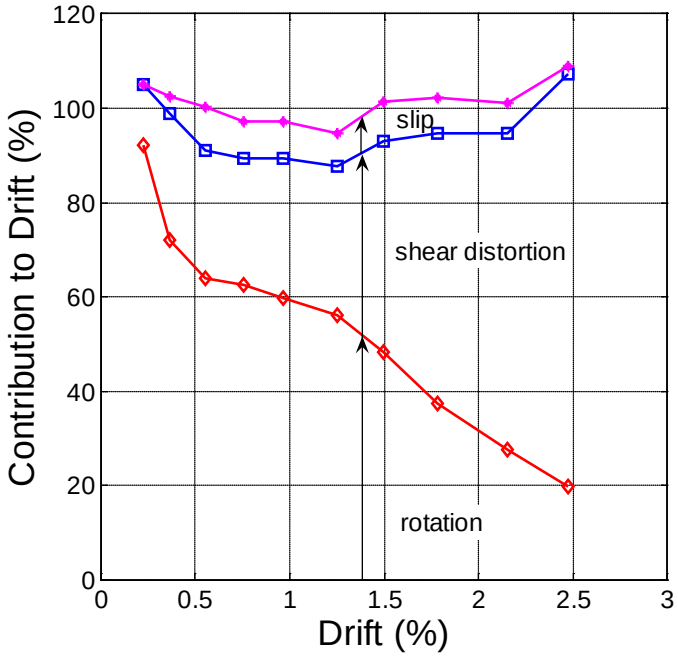

(c) HPFRC Specimen S5

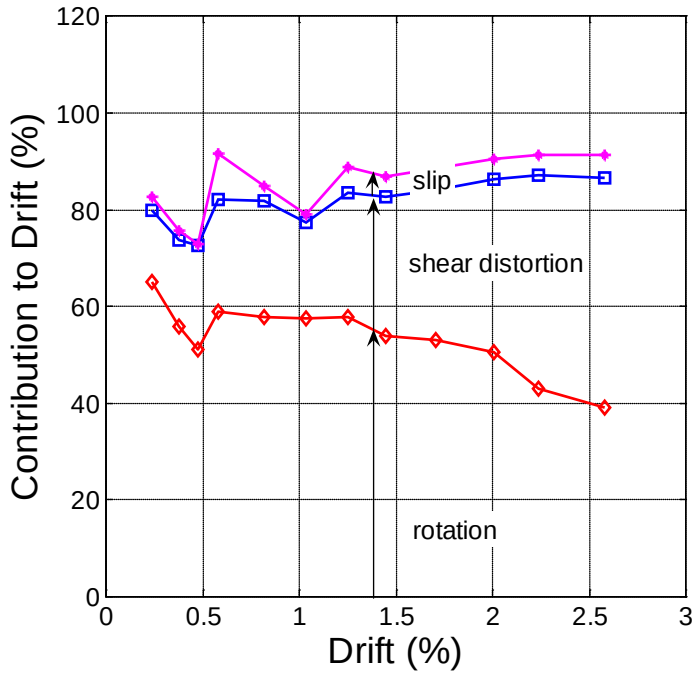

(d) HPFRC Specimen S10

Fig. 5-3 Contribution of Deformation Components to Drift

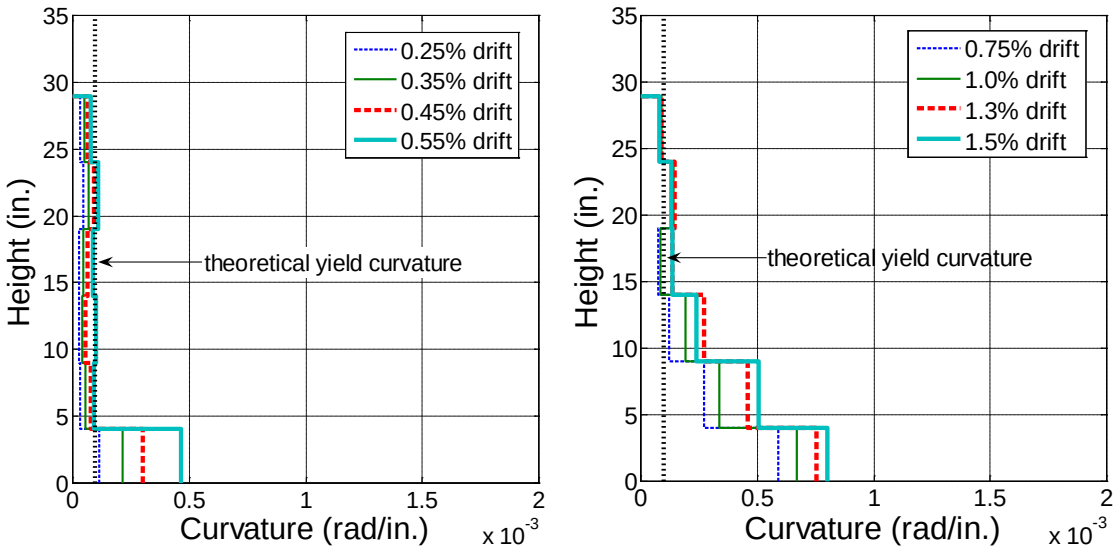

(a) Positive loading direction

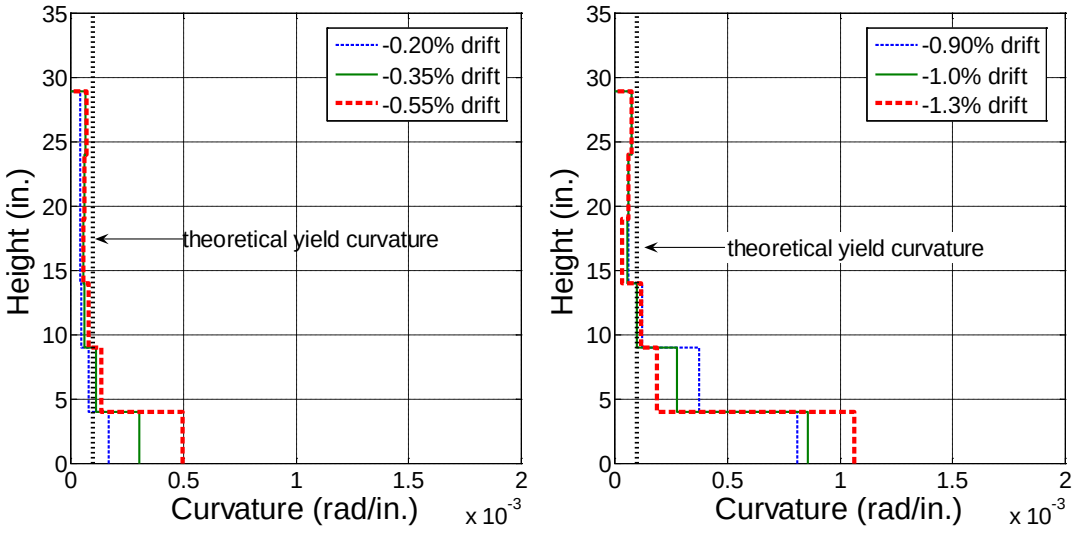

b) Negative loading direction

Fig. 5-4 Curvature Distribution for RC Specimen S4

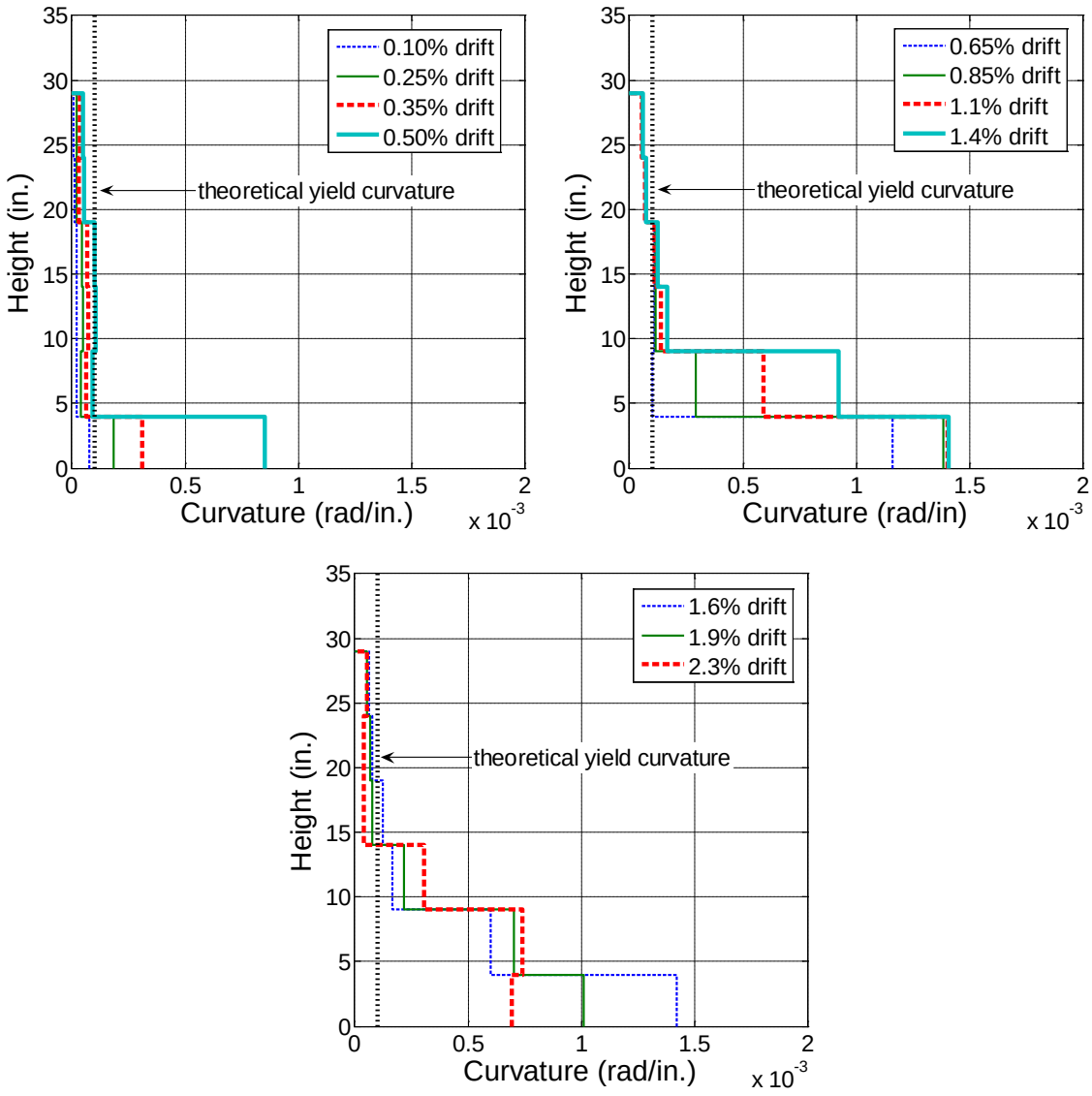

a) Positive loading direction

Fig. 5-5 Curvature Distribution for HPFRC Specimen S5

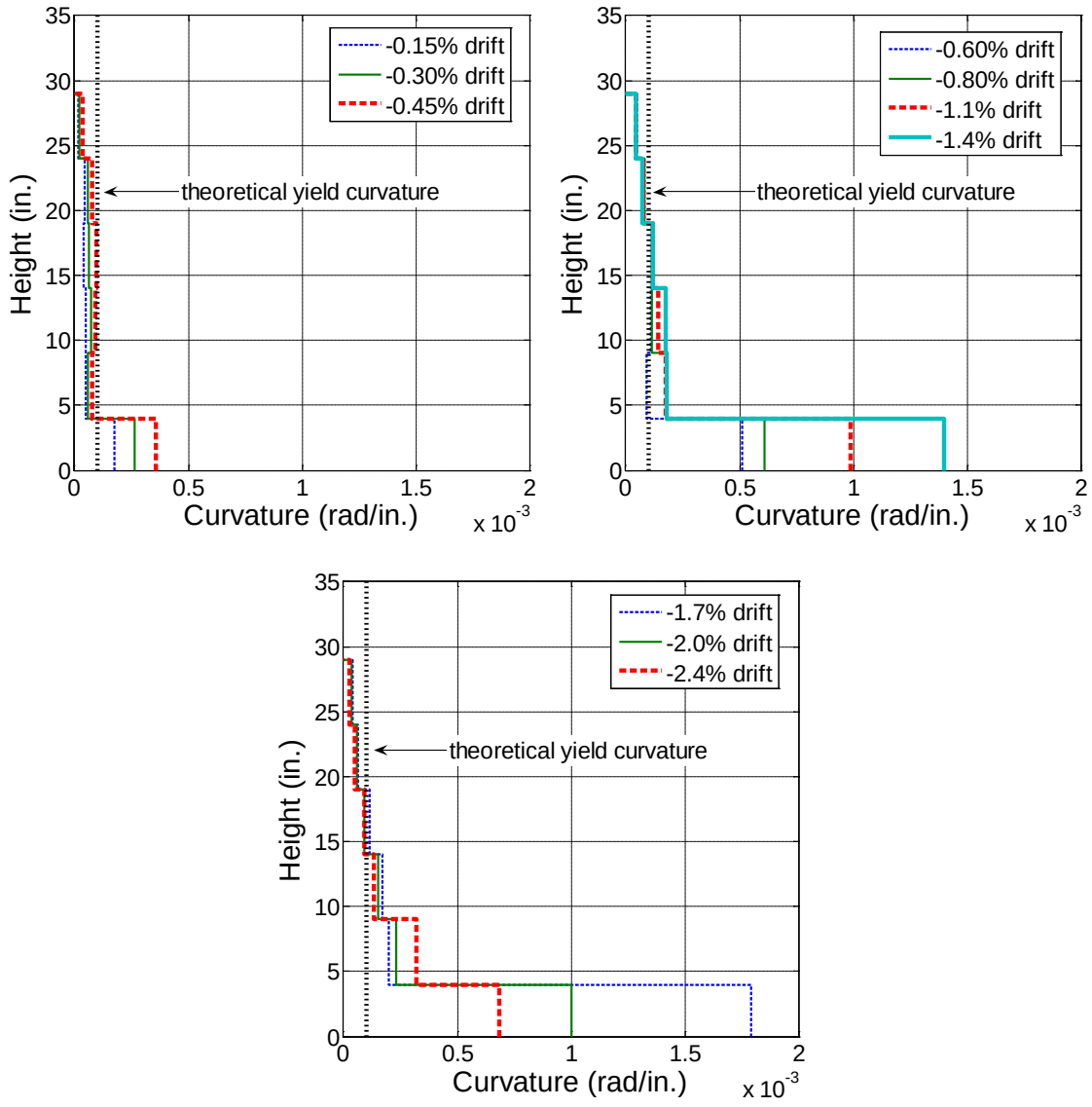

b) Negative loading direction

Fig. 5-5 Curvature Distribution for HPFRC Specimen S5

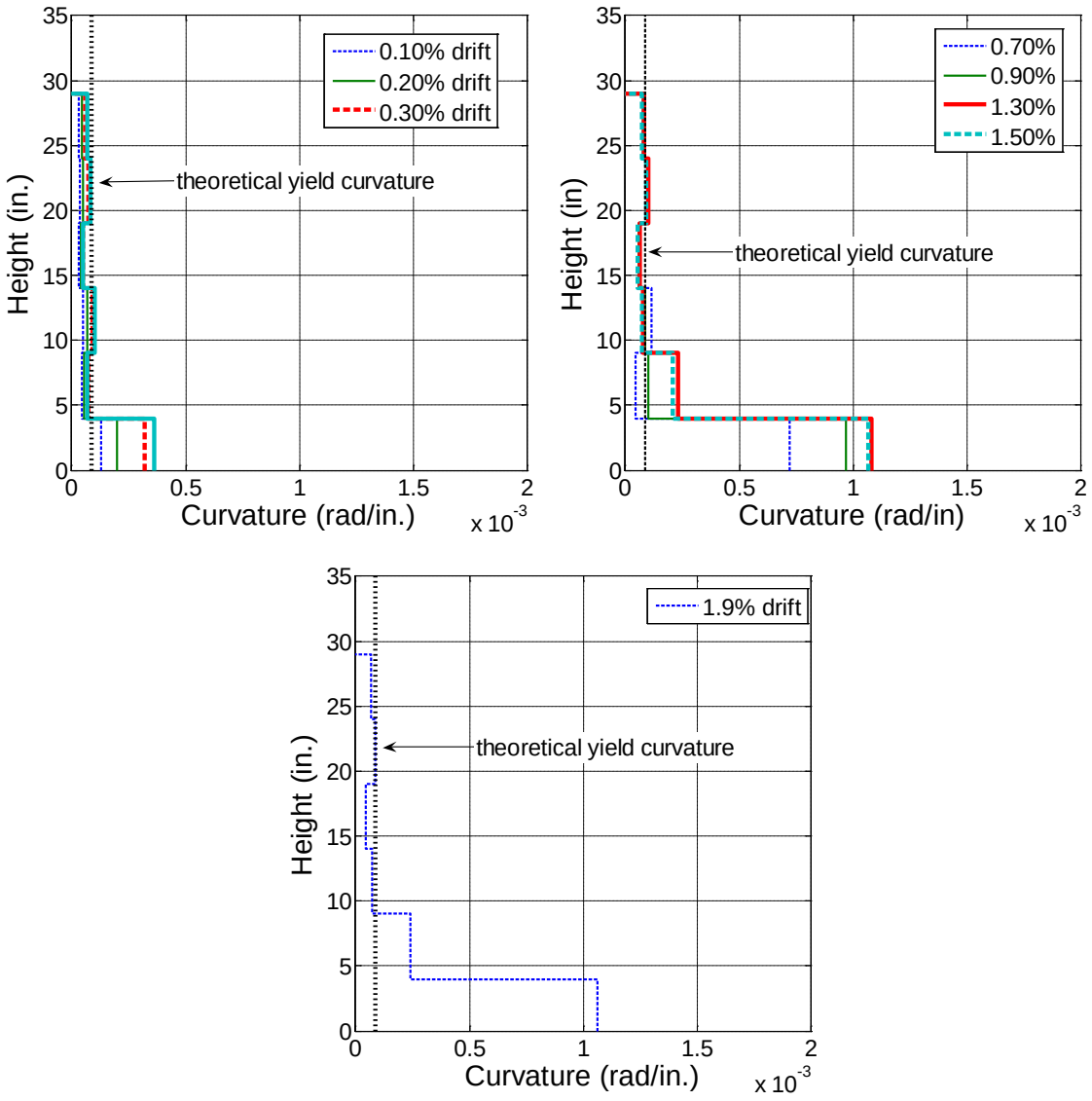

a) Positive loading direction

Fig. 5-6 Curvature Distribution for RC Specimen S9

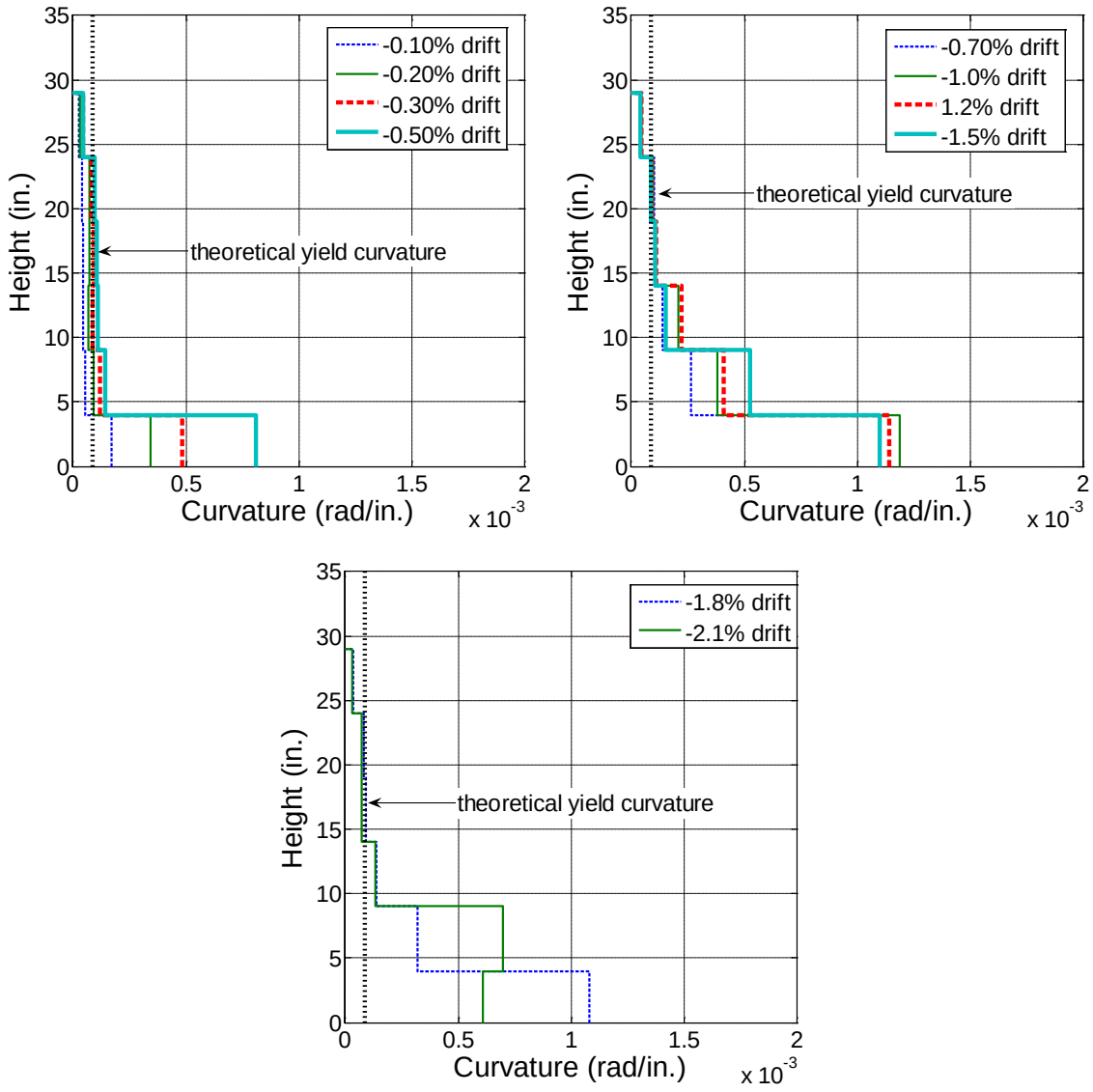

b) Negative loading direction

Fig. 5-6 Curvature Distribution for RC Specimen S9

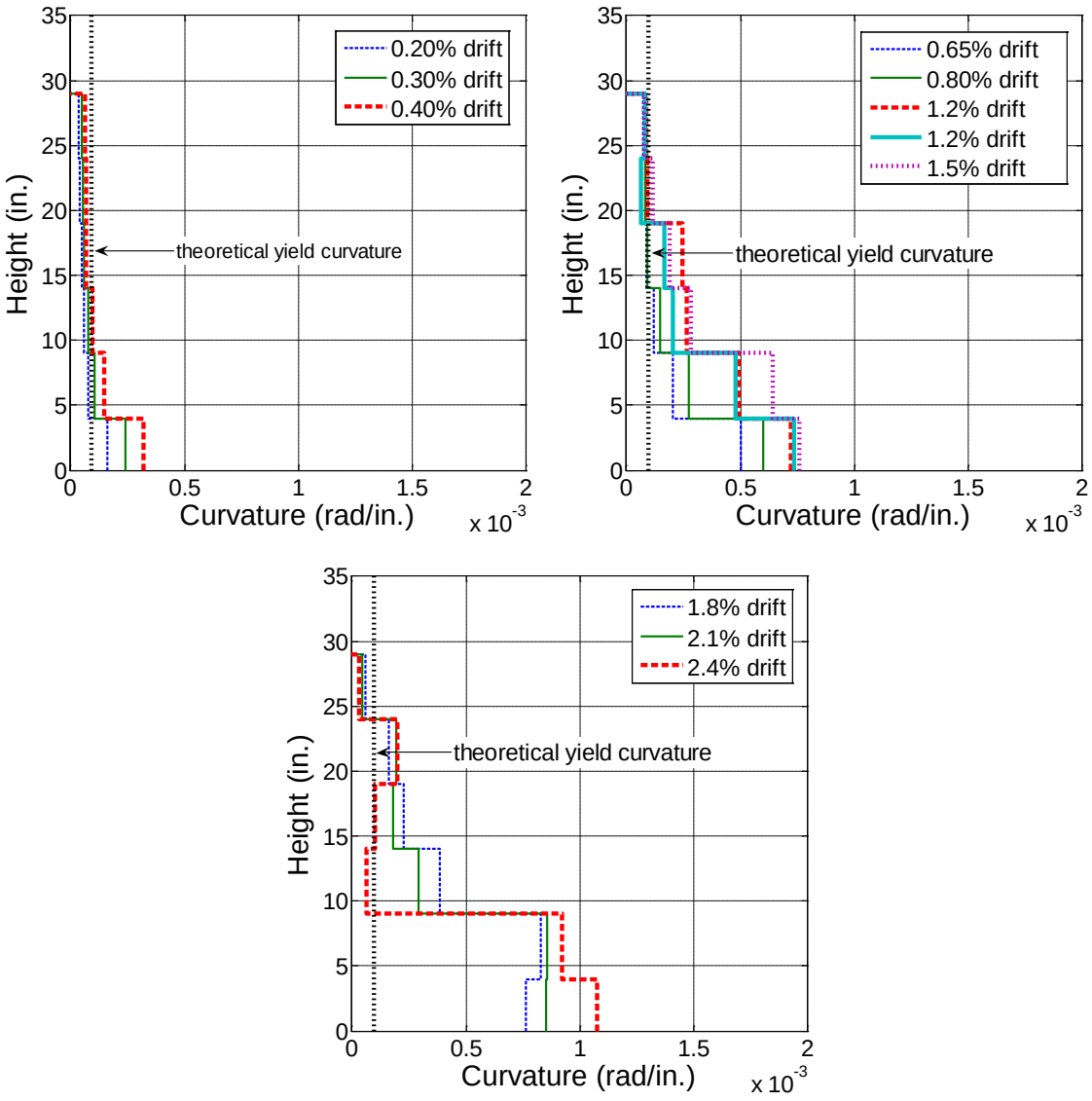

a) Positive loading direction

Fig. 5-7 Curvature Distribution for HPFRC Specimen S10

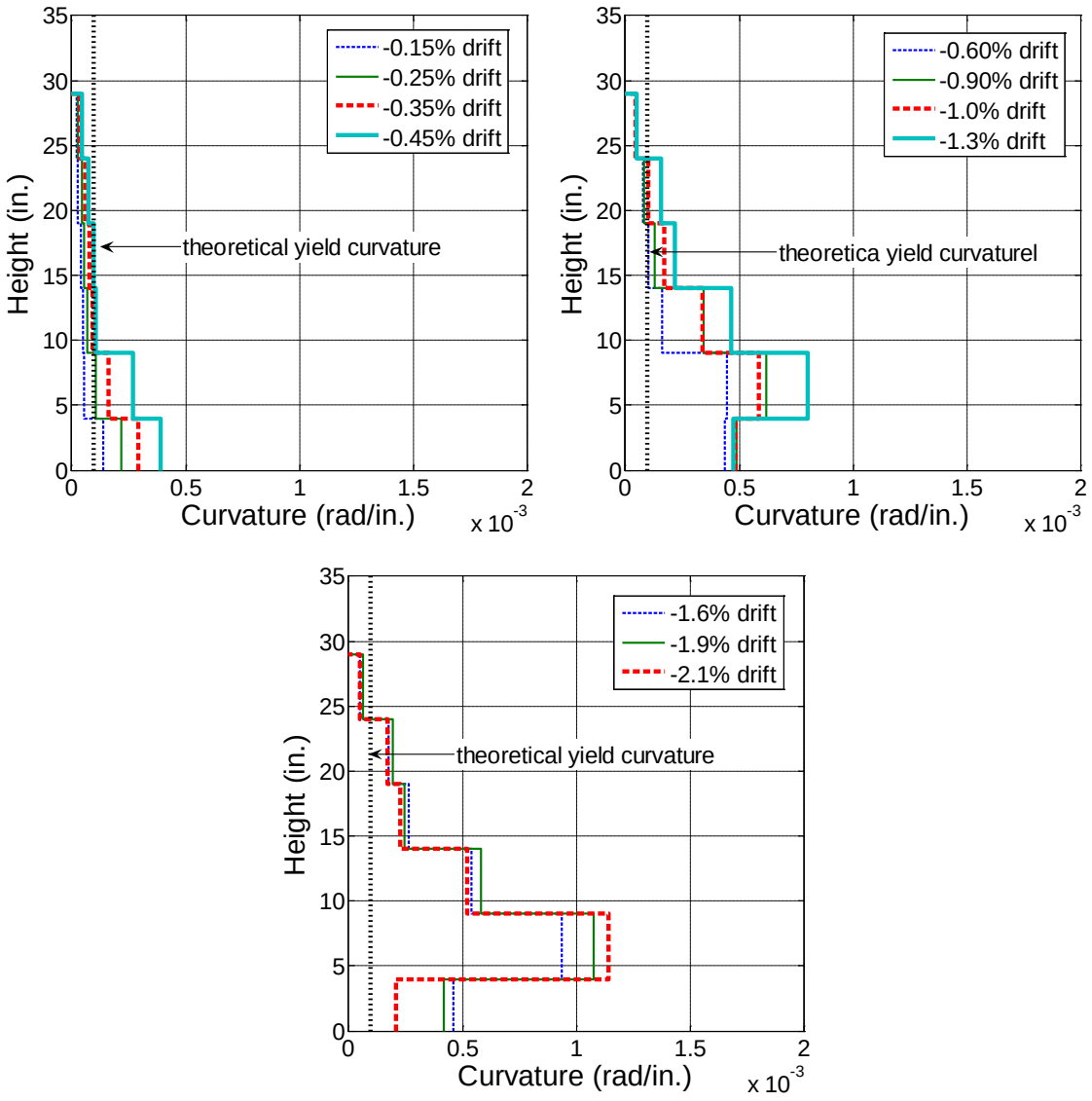

b) Negative loading direction

Fig. 5-7 Curvature Distribution for HPFRC Specimen S10

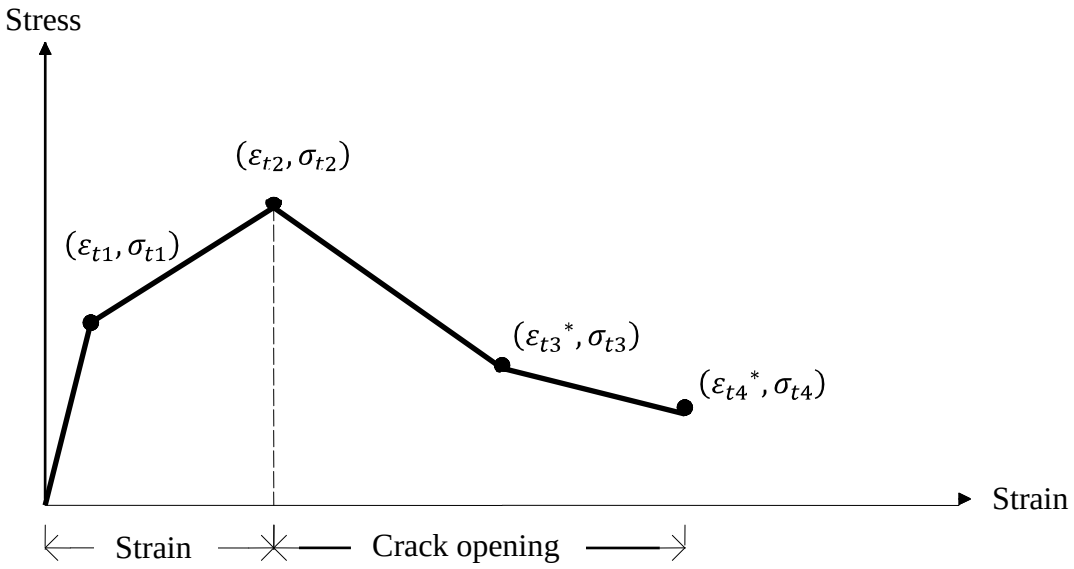

* Effective Strain

Fig. 5-8 Tensile Stress-Strain Model for HPFRC Matrix

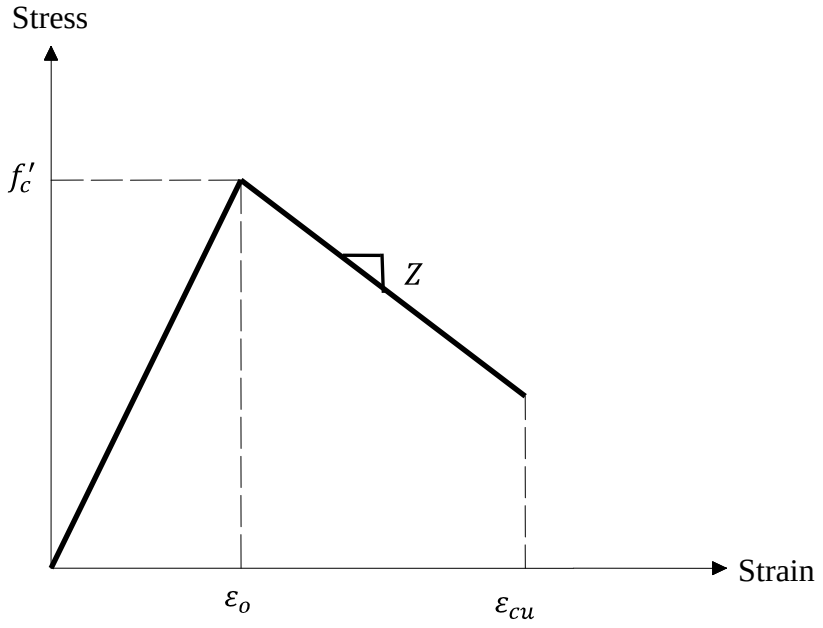

Fig. 5-9 Compression Stress-Strain Model for Regular Concrete and HPFRC Matrix

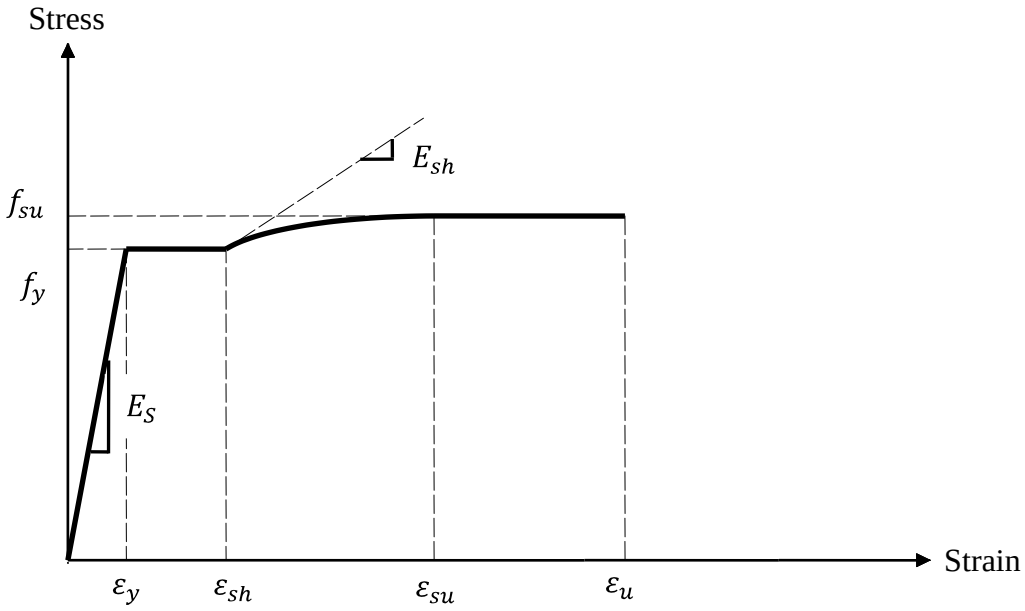

Fig. 5-10 Tensile Stress-Strain Model for Steel Reinforcement

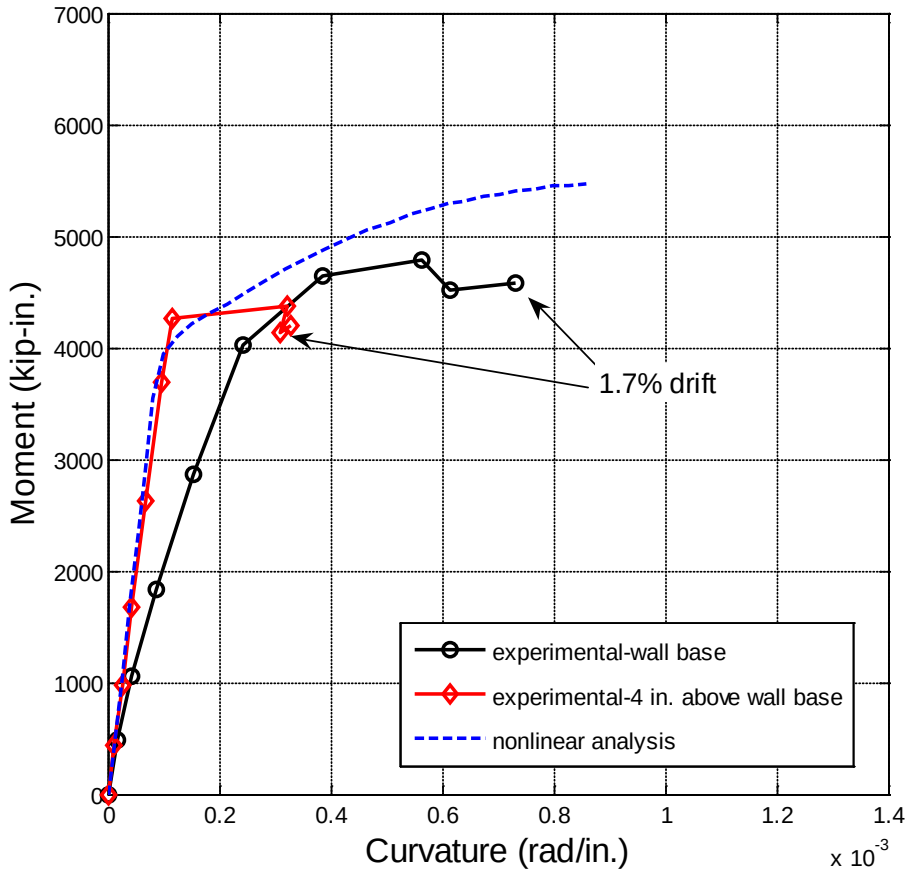

Fig. 5-11 Moment versus Curvature Response for RC Specimen S4

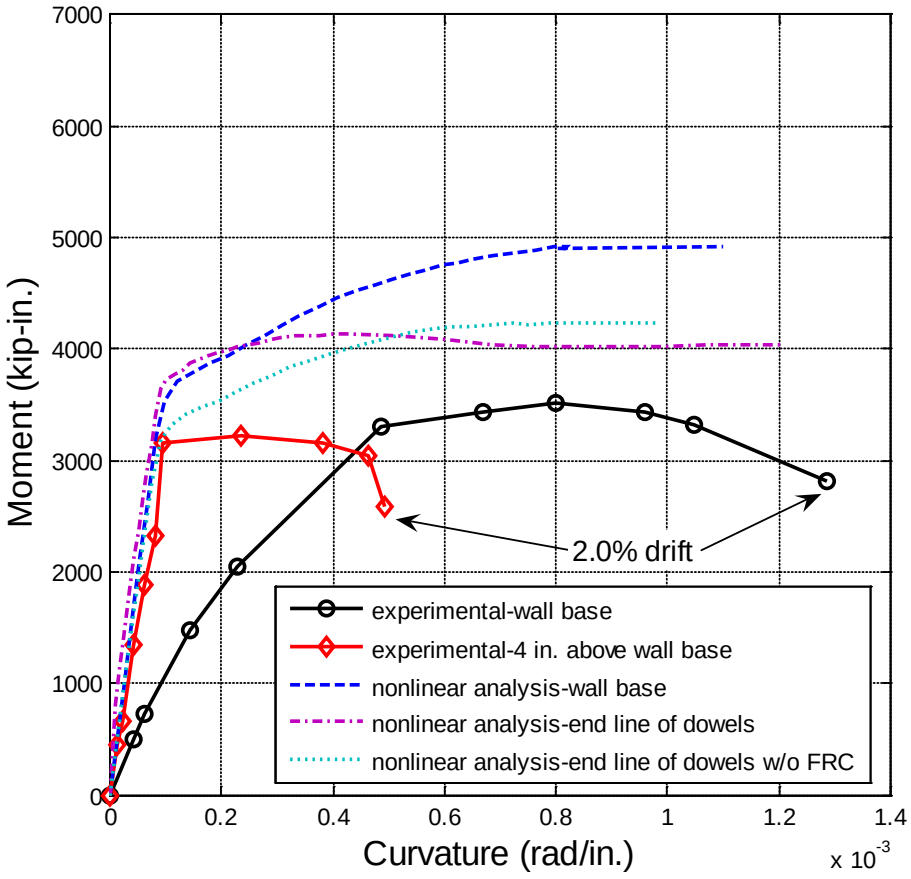

Fig. 5-12 Moment versus Curvature Response for HPFRC Specimen S5

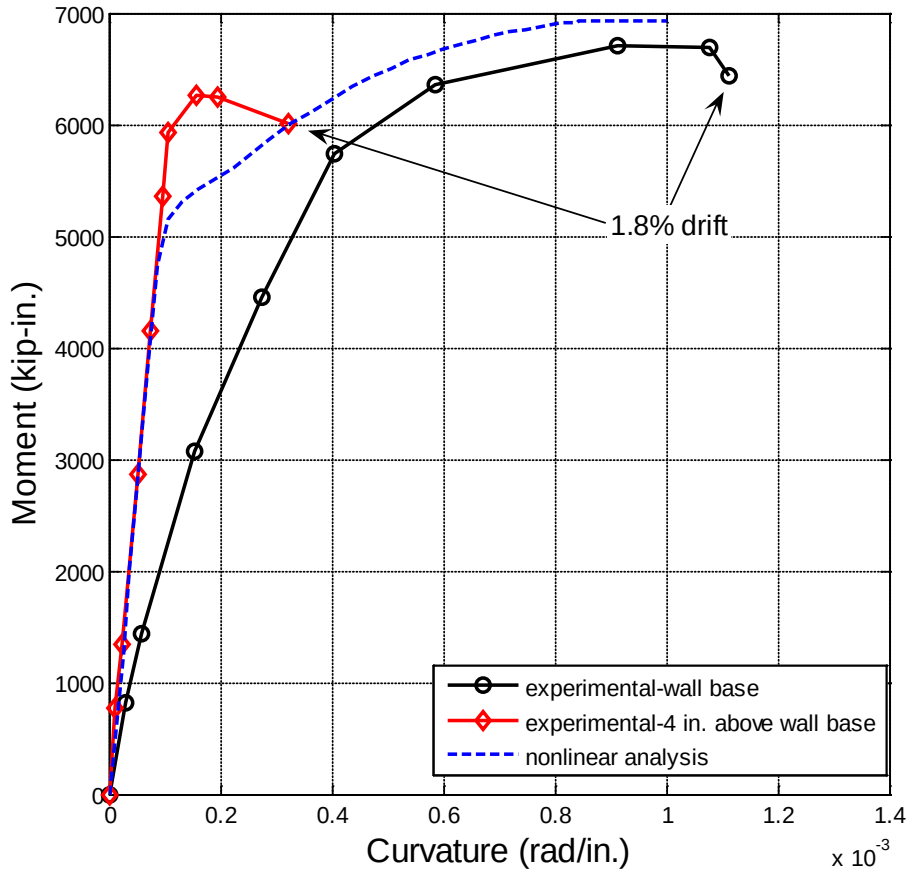

Fig. 5-13 Moment versus Curvature Response for RC Specimen S9

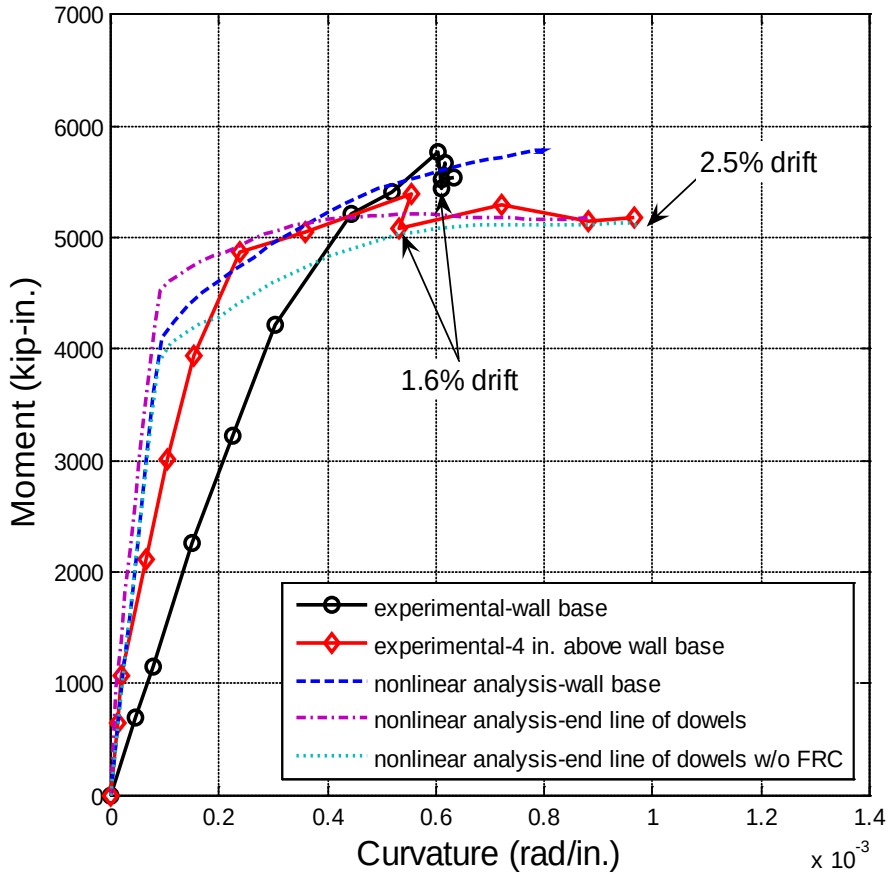

Fig. 5-14 Moment versus Curvature Response for HPFRC Specimen S10

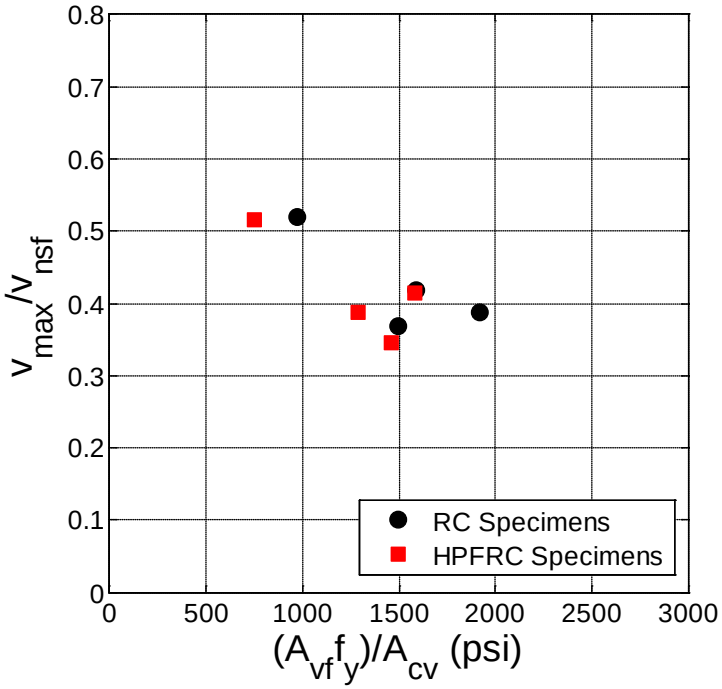

Fig. 5-15 Ratio of Measured Shear Strength to Shear Strength Calculated Using the Shear Friction Analogy ($\mu = 1.0$) versus Shear Friction Strength ($\mu = 1.0$)

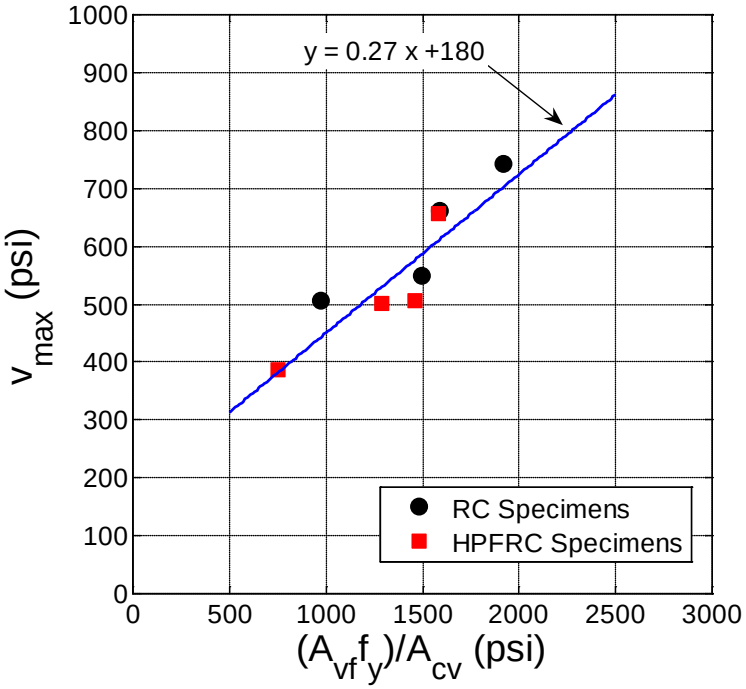

Fig. 5-16 Measured Shear Strength versus Shear Friction Capacity ($\mu = 1.0$)

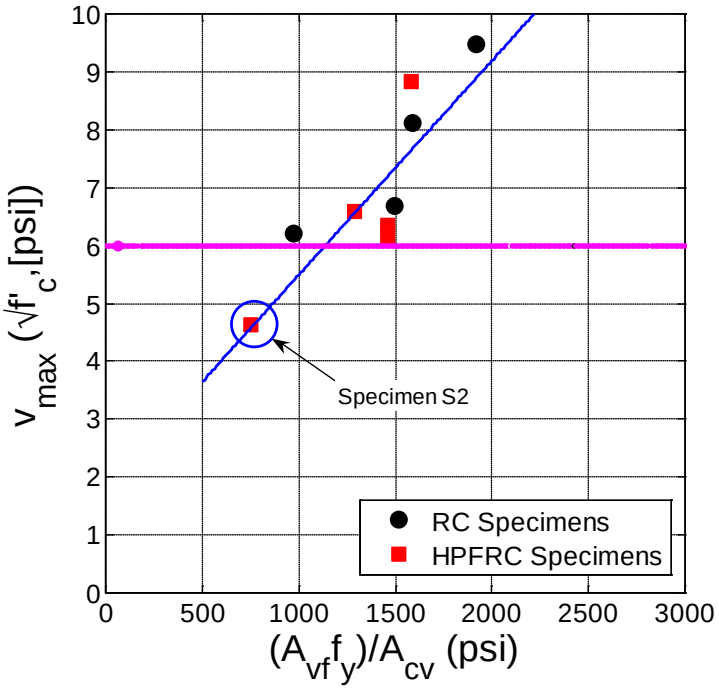

Fig. 5-17 Measured Normalized Shear Strength versus Shear Friction Strength ($\mu = 1.0$)

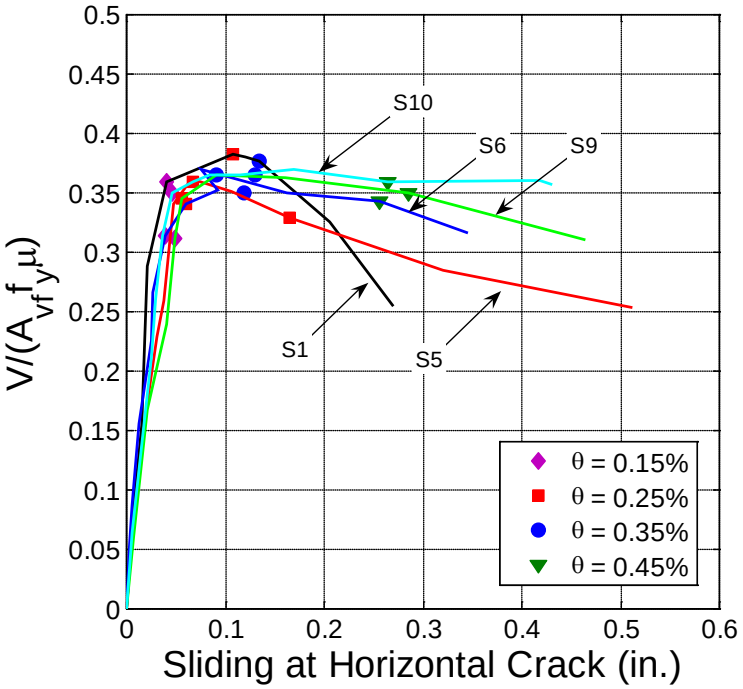

Fig. 5-18 Shear Force Normalized by Shear Friction Strength ($\mu = 1$) versus Horizontal Sliding Envelope Response

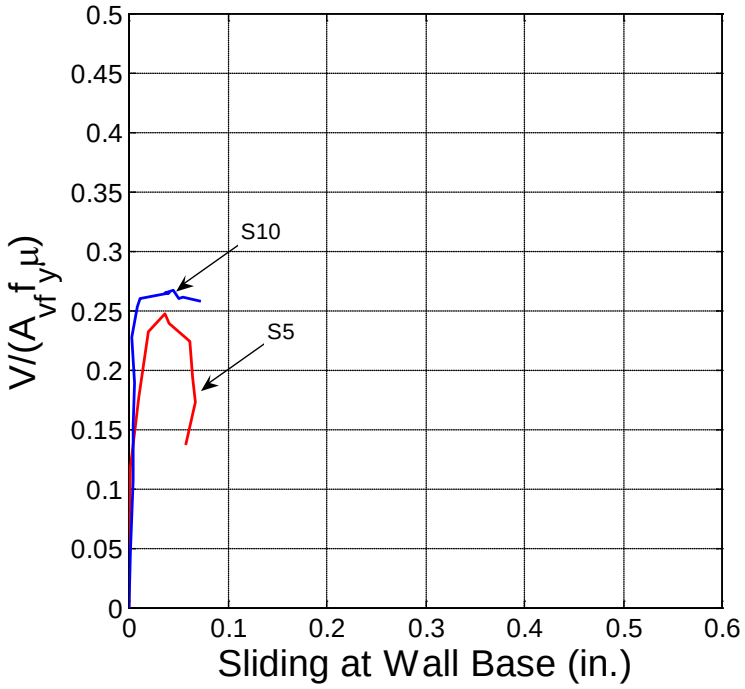

Fig. 5-19 Shear Force Normalized by Shear Friction Strength ($\mu = 1$) versus Horizontal Sliding Envelope Response for HPFRC Specimens S5 and S10 at the Wall Base (Cold Joint)

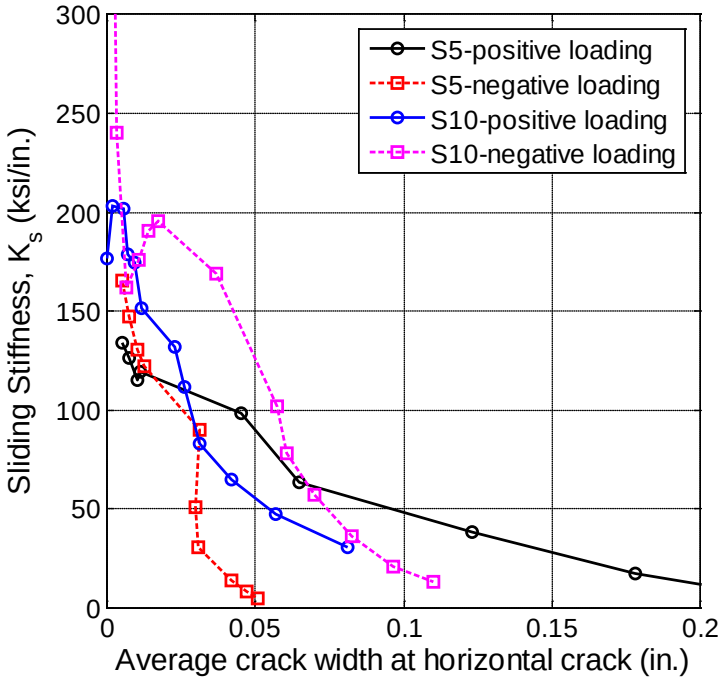

Fig. 5-20 Sliding Stiffness versus Average Horizontal Crack Width

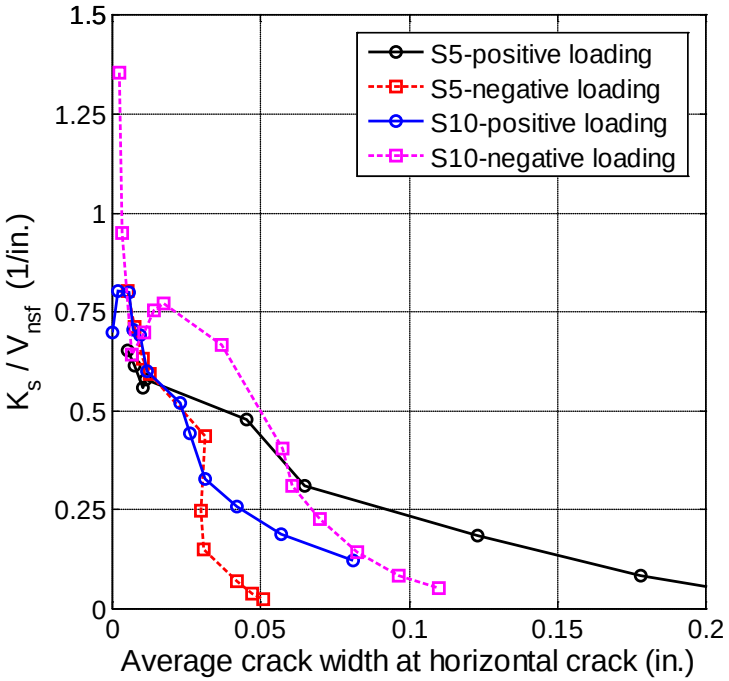

Fig. 5-21 Sliding Stiffness Normalized by Shear Friction Capacity ($\mu = 1.0$) versus Average Horizontal Crack Width

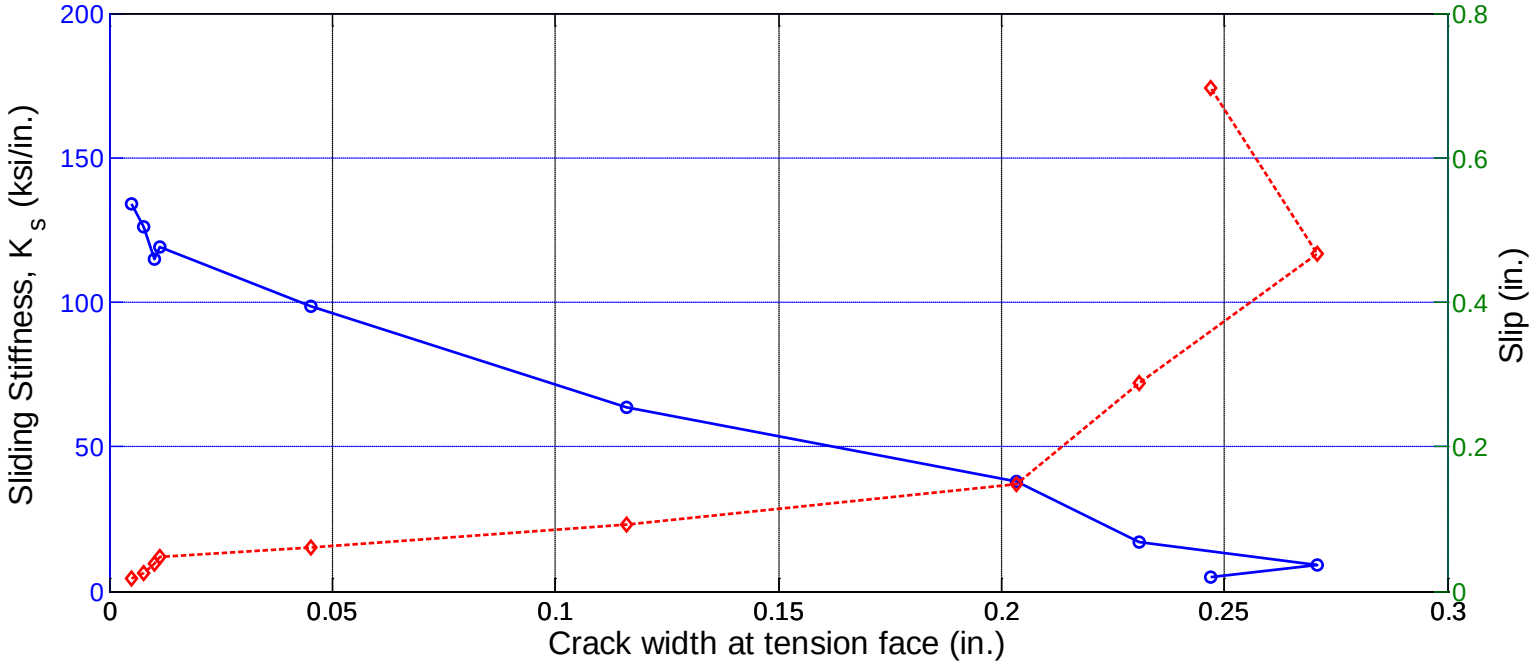

a) Positive Loading Direction

Fig. 5-22 Sliding Stiffness and Slip versus Crack Width on Tension Face of Horizontal Crack for HPFRC Specimen S5

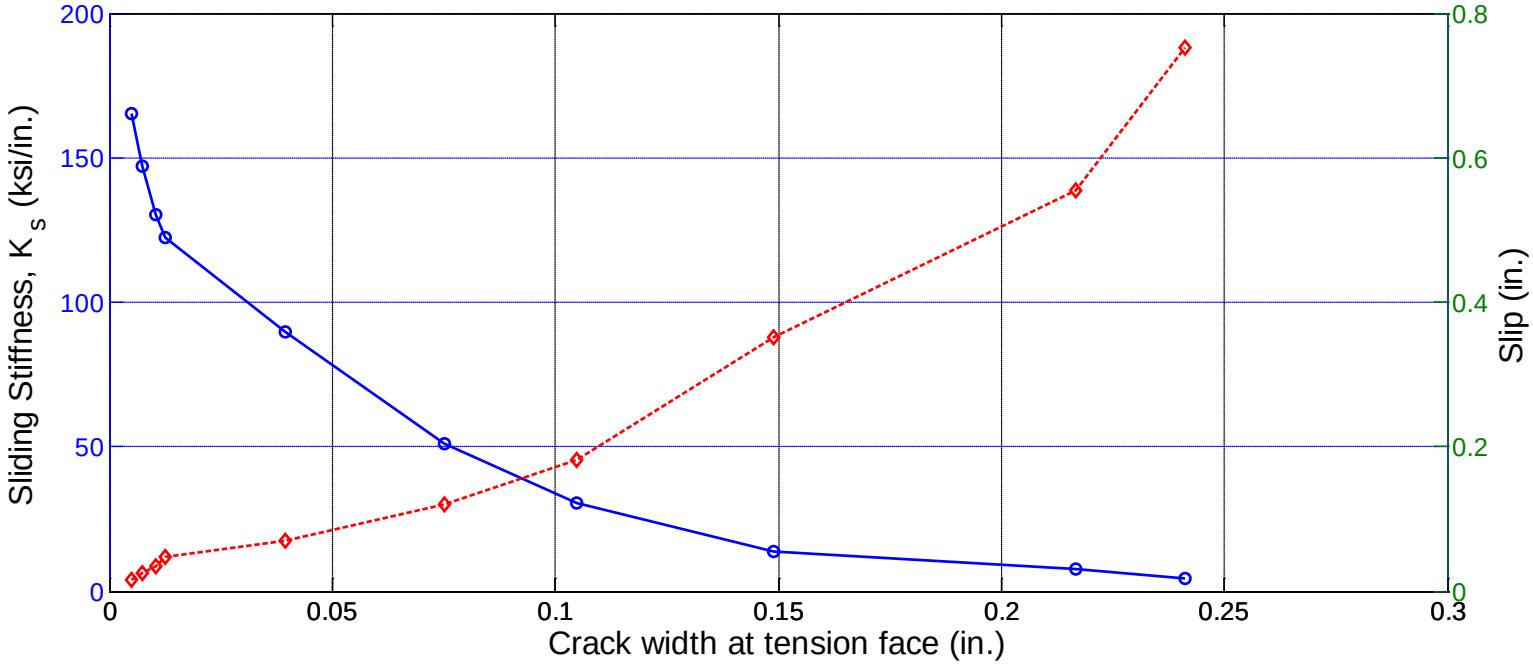

b) Negative Loading Direction

Fig. 5-22 Sliding Stiffness and Slip versus Crack Width on Tension Face of Horizontal Crack for HPFRC Specimen S5

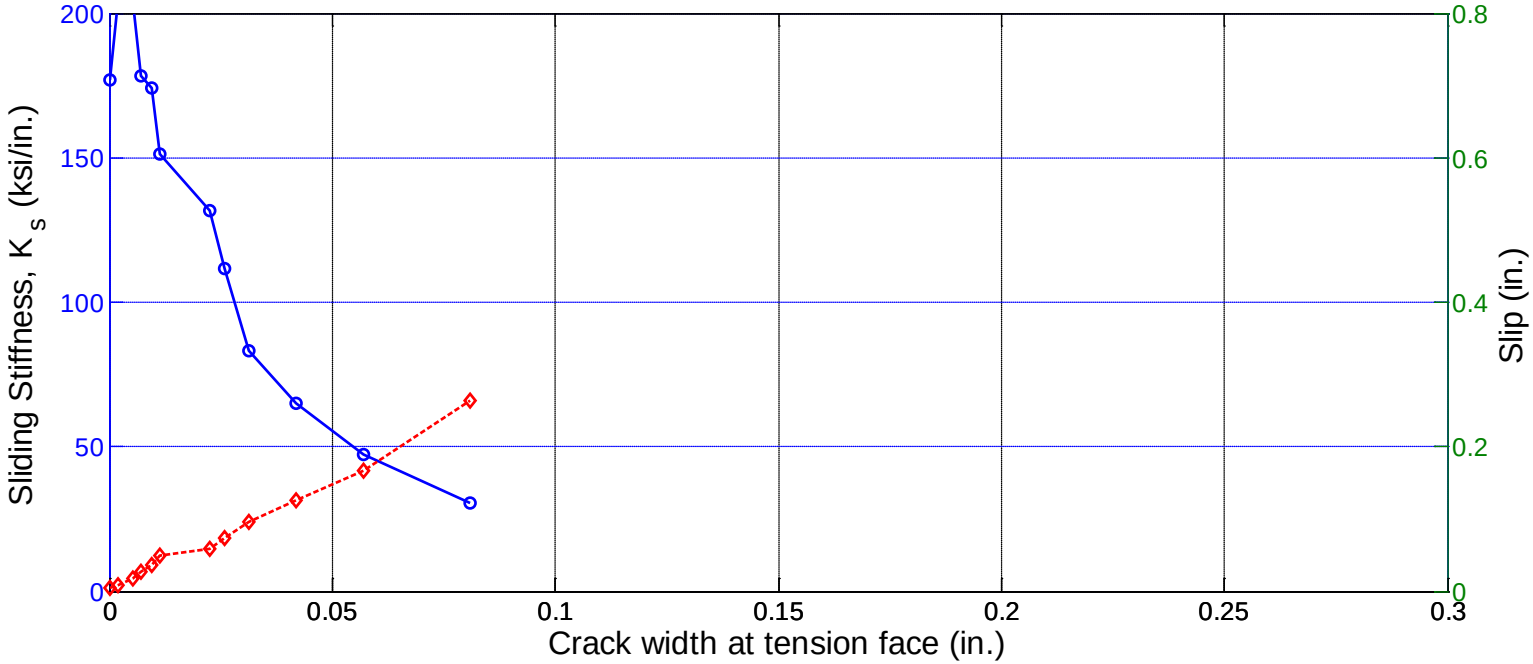

a) Positive Loading Direction

Fig. 5-23 Sliding Stiffness and Slip versus Crack Width on Tension Face of Horizontal Crack for HPFRC Specimen S10

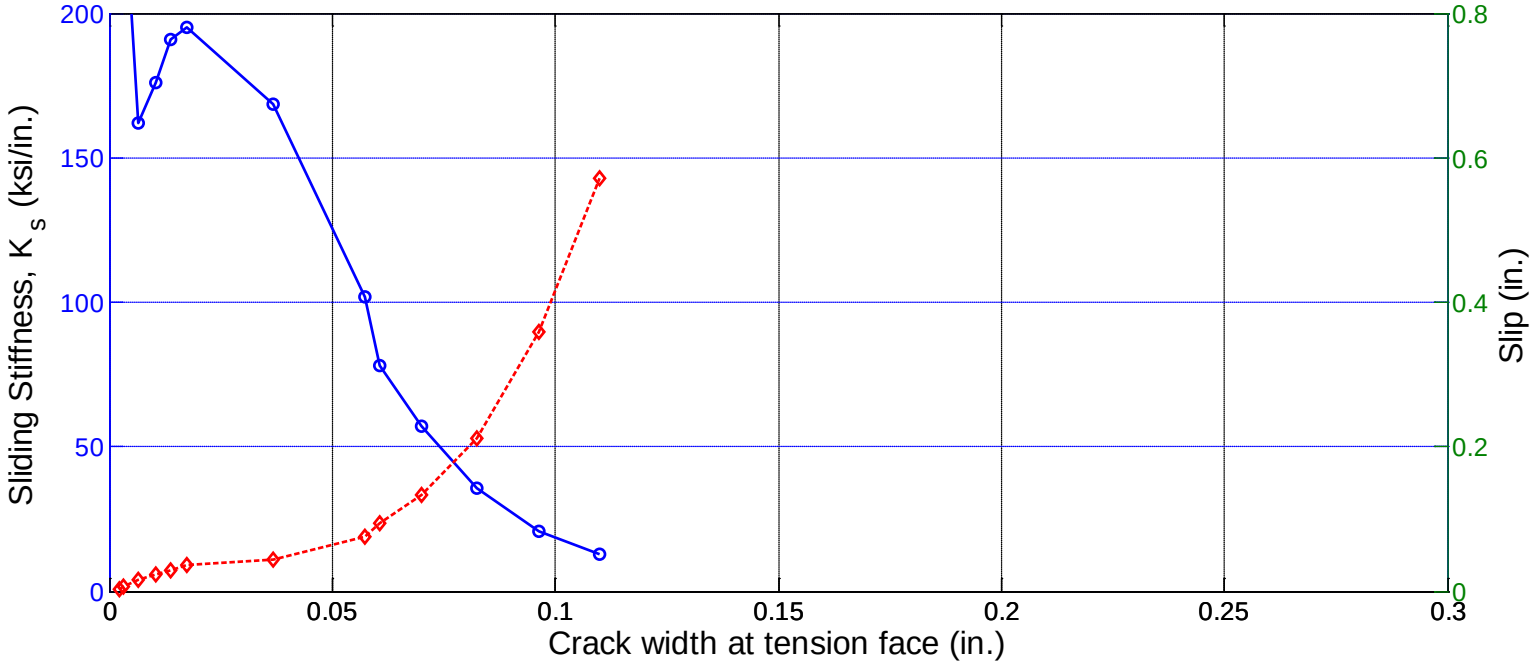

b) Negative Loading Direction

Fig. 5-23 Sliding Stiffness and Slip versus Crack Width on Tension Face of Horizontal Crack for HPFRC Specimen S10

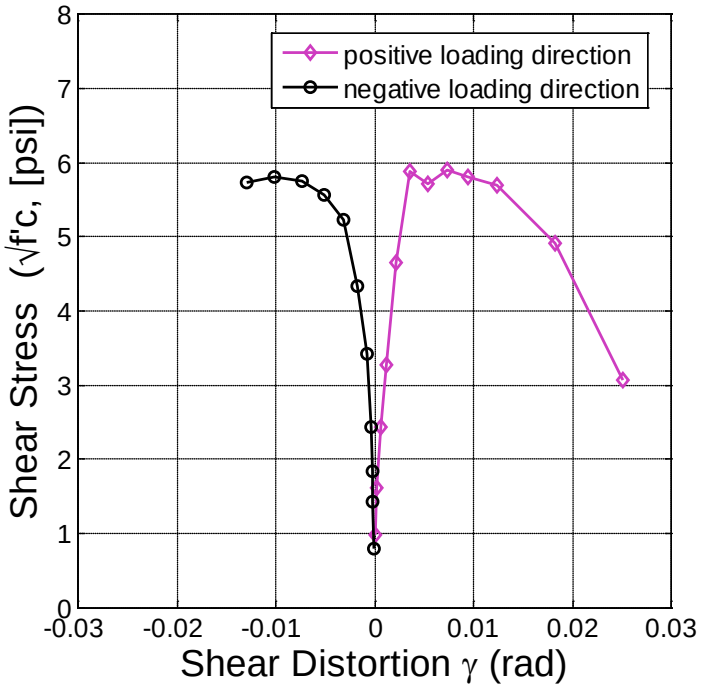

a) HPFRC Specimen S7

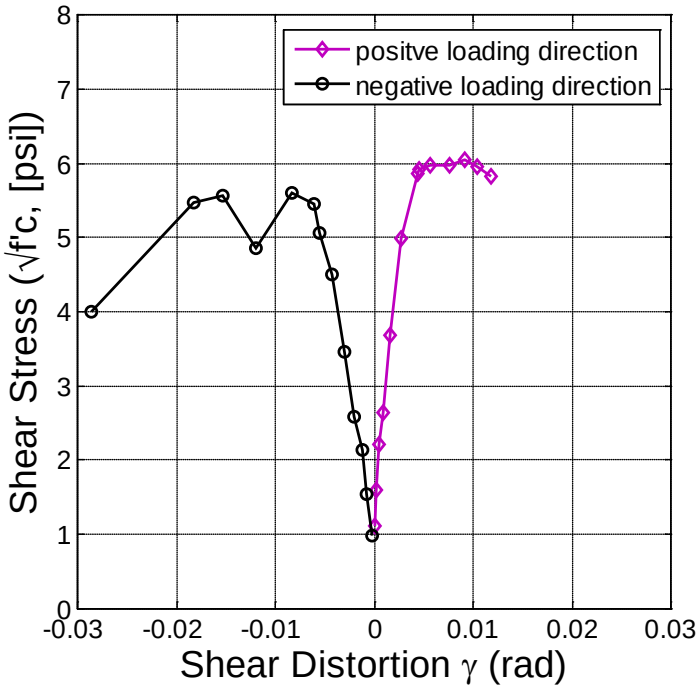

b) HPFRC Specimen S8

Fig. 5-24 Shear Stress versus Shear Distortion in HPFRC Specimens S7 and S8

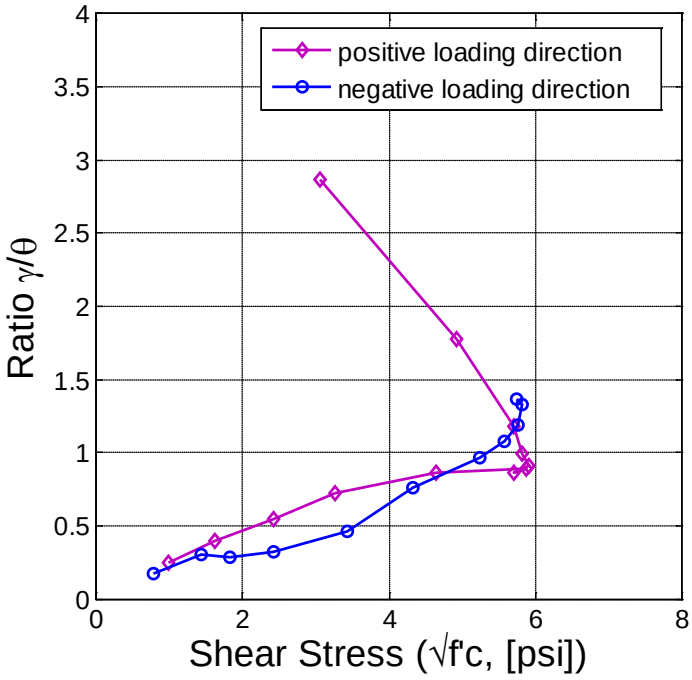

a) HPFRC Specimen S7

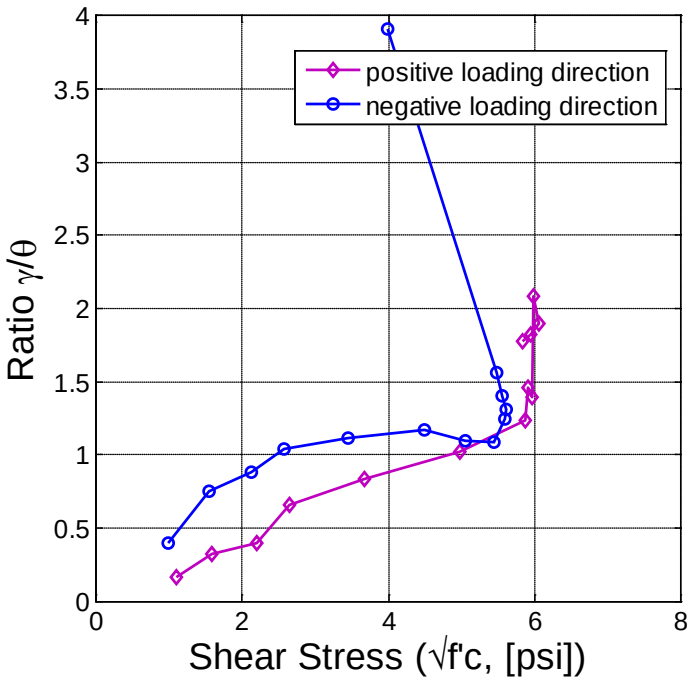

b) HPFRC Specimen S8

Fig. 5-25 Shear Strain to Rotation Ratio versus Shear Stress for Specimens S7 and S8

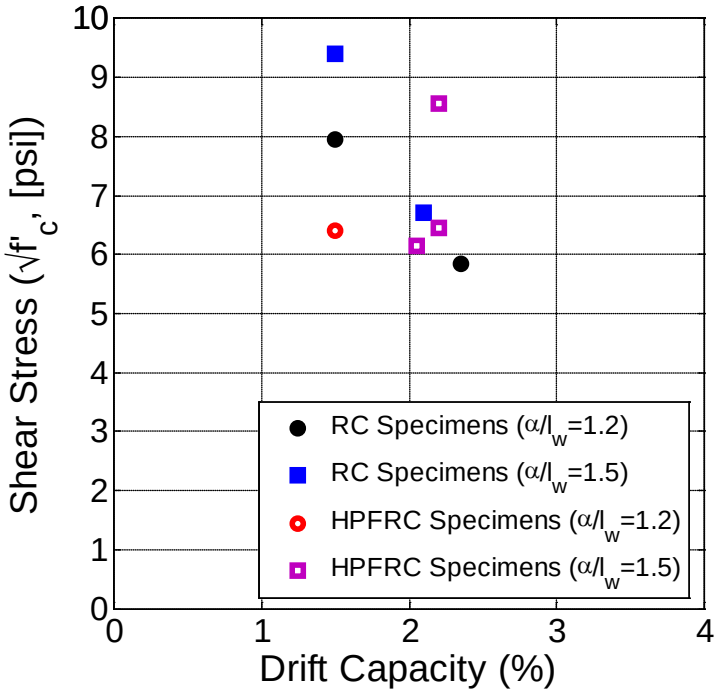

Fig. 5-26 Peak Shear Stress versus Drift Capacity for Test Specimens in this Study

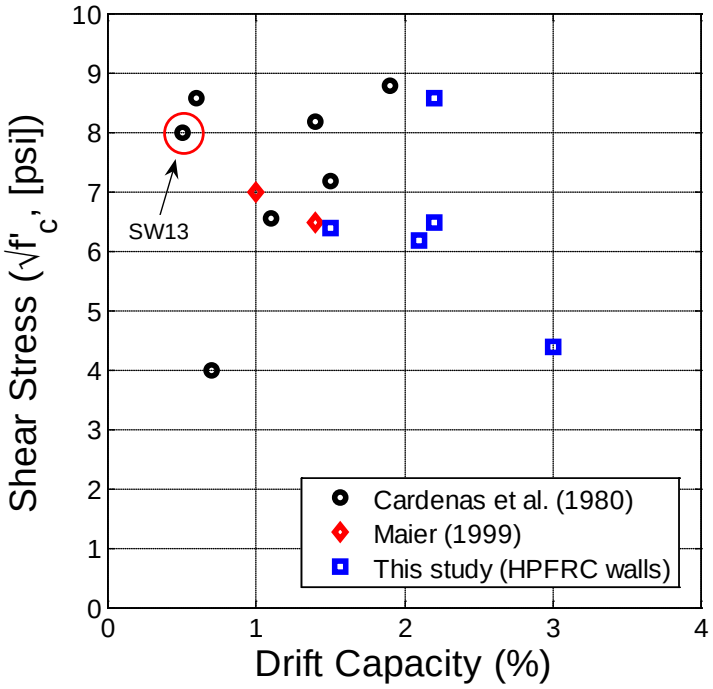

Note: Specimen SW13 (Cardenas et al., 1980) and all HPFRC walls in this study were tested under reversed cyclic loading. All other specimens were tested under monotonic loading.

Fig. 5-27 Comparison of Peak Shear Stress versus Drift Capacity for Walls with No or Little Confinement Reinforcement in the Boundary Regions

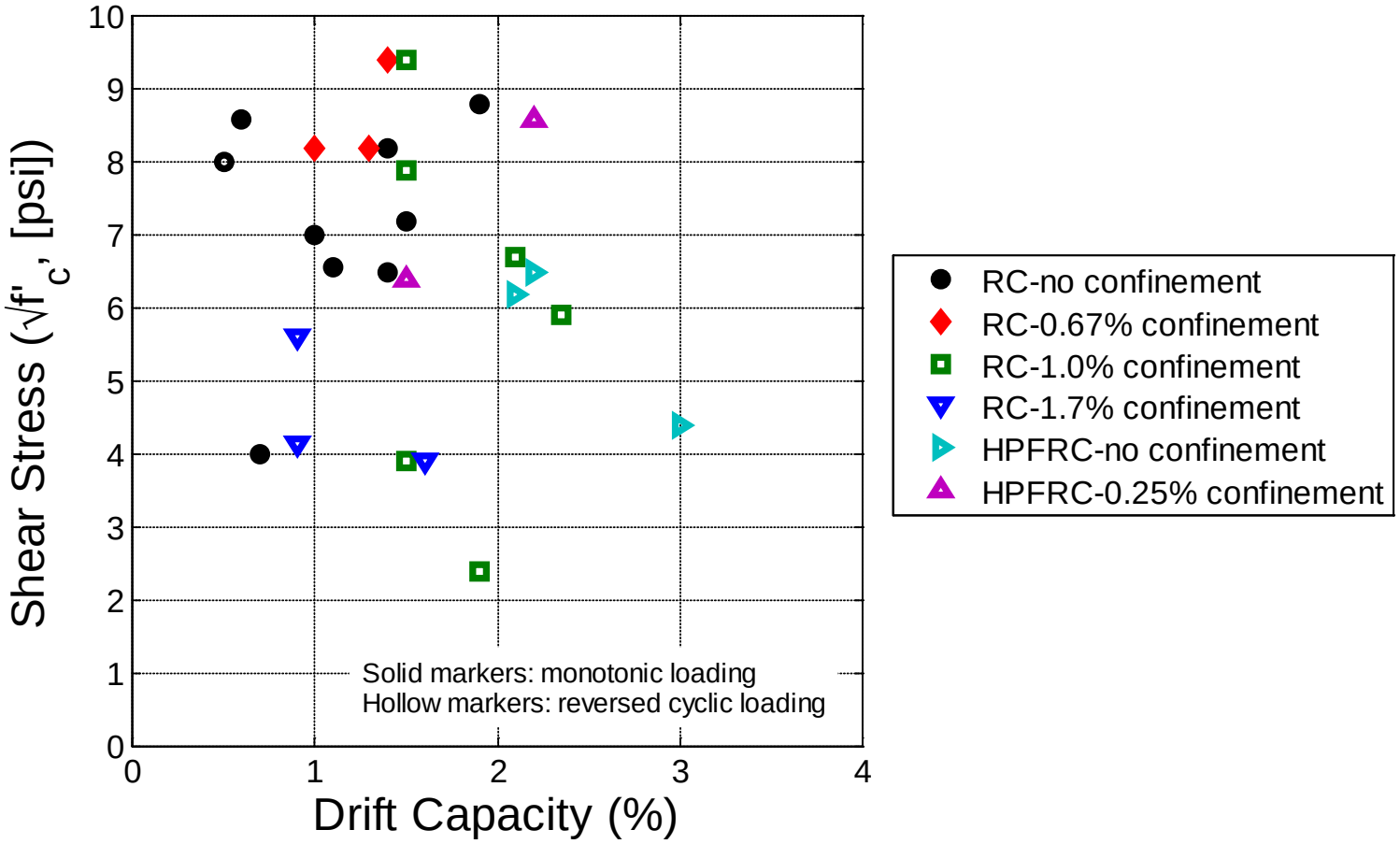

Fig. 5-28 Peak Shear Stress versus Drift Capacity versus for Wall Specimens with Various Confinement Reinforcing Ratios

Appendix A: Strain Gauges Location

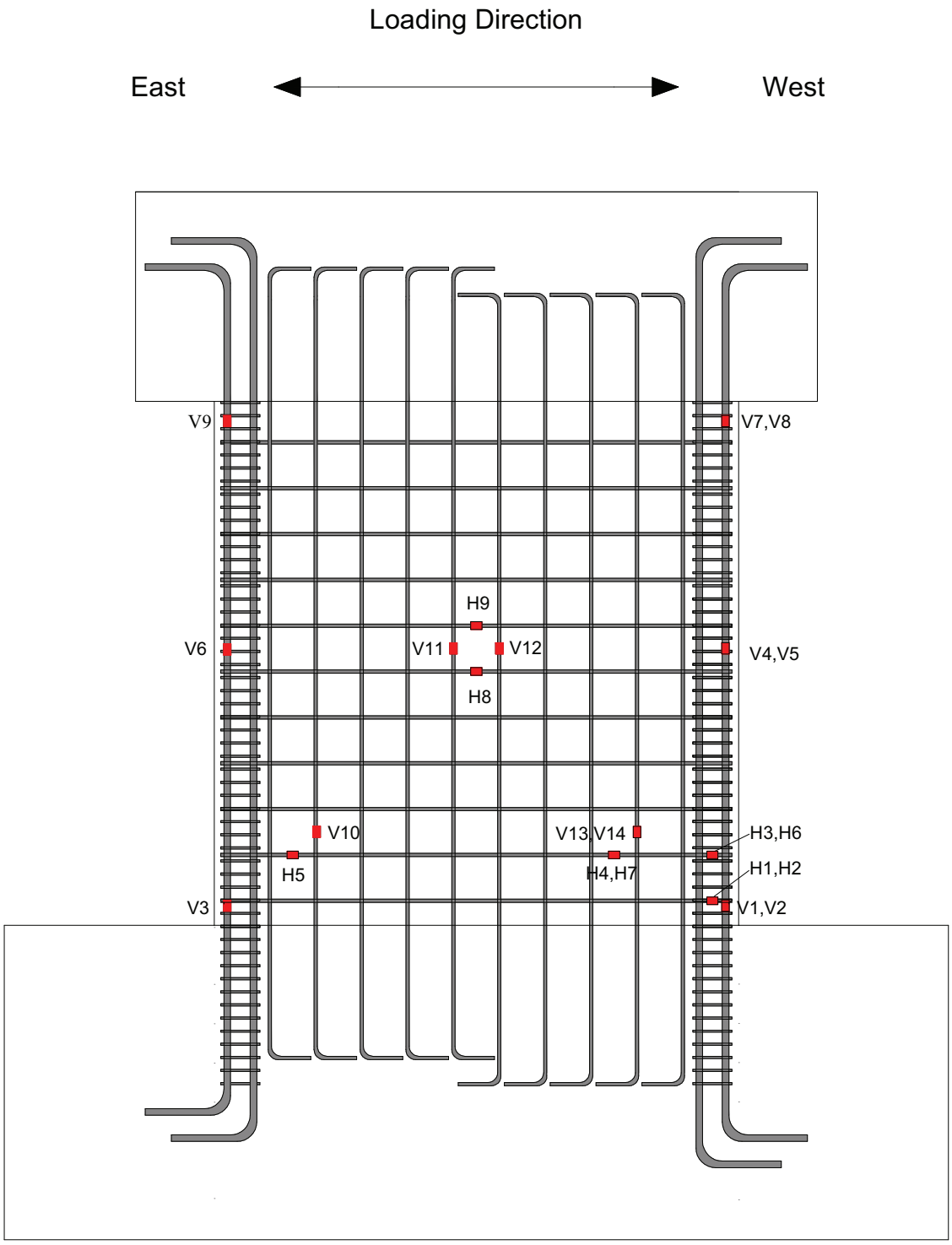

Fig. A-1 Strain Gauges Locations for Specimen S1

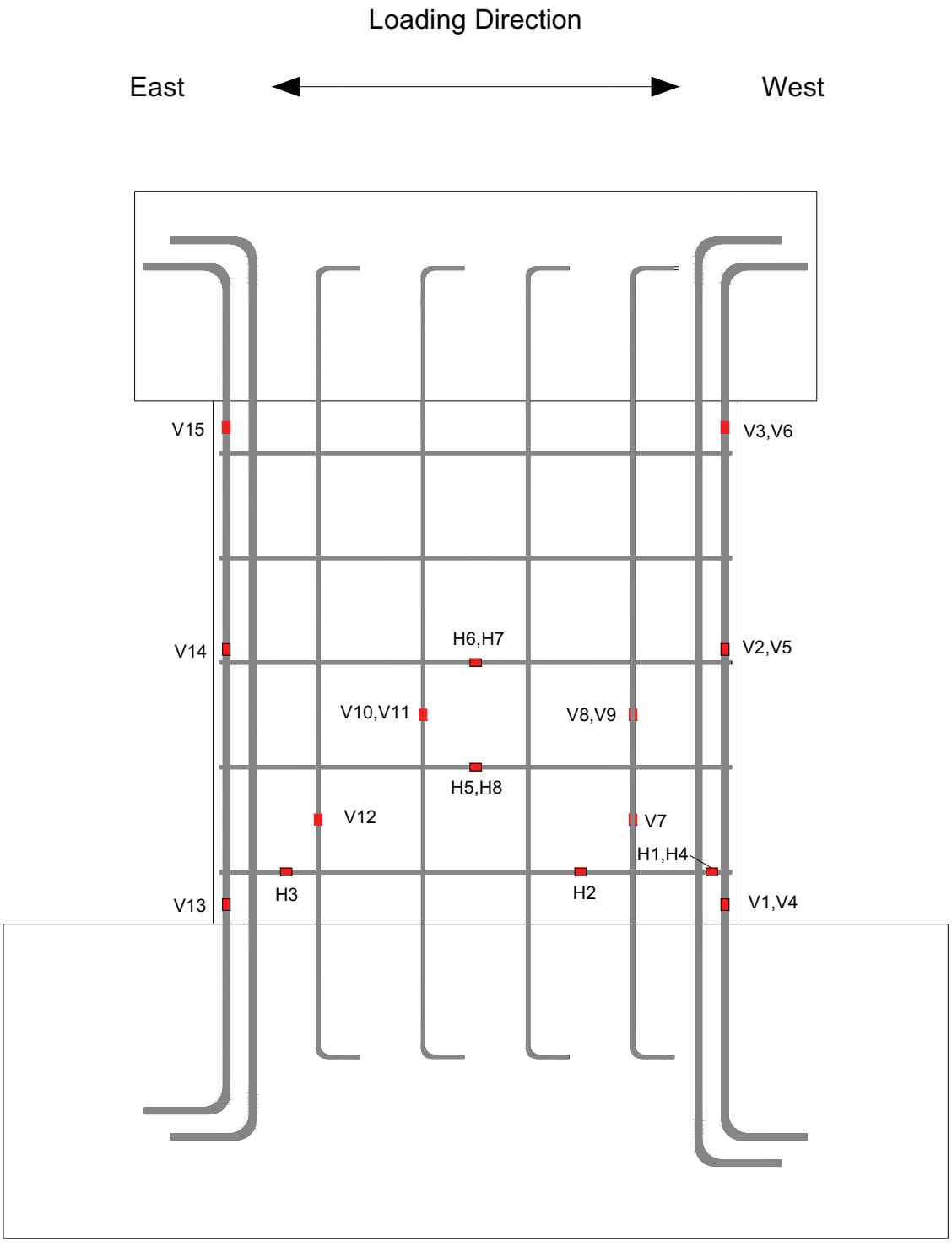

Fig. A-2 Strain Gauges Locations for Specimen S2

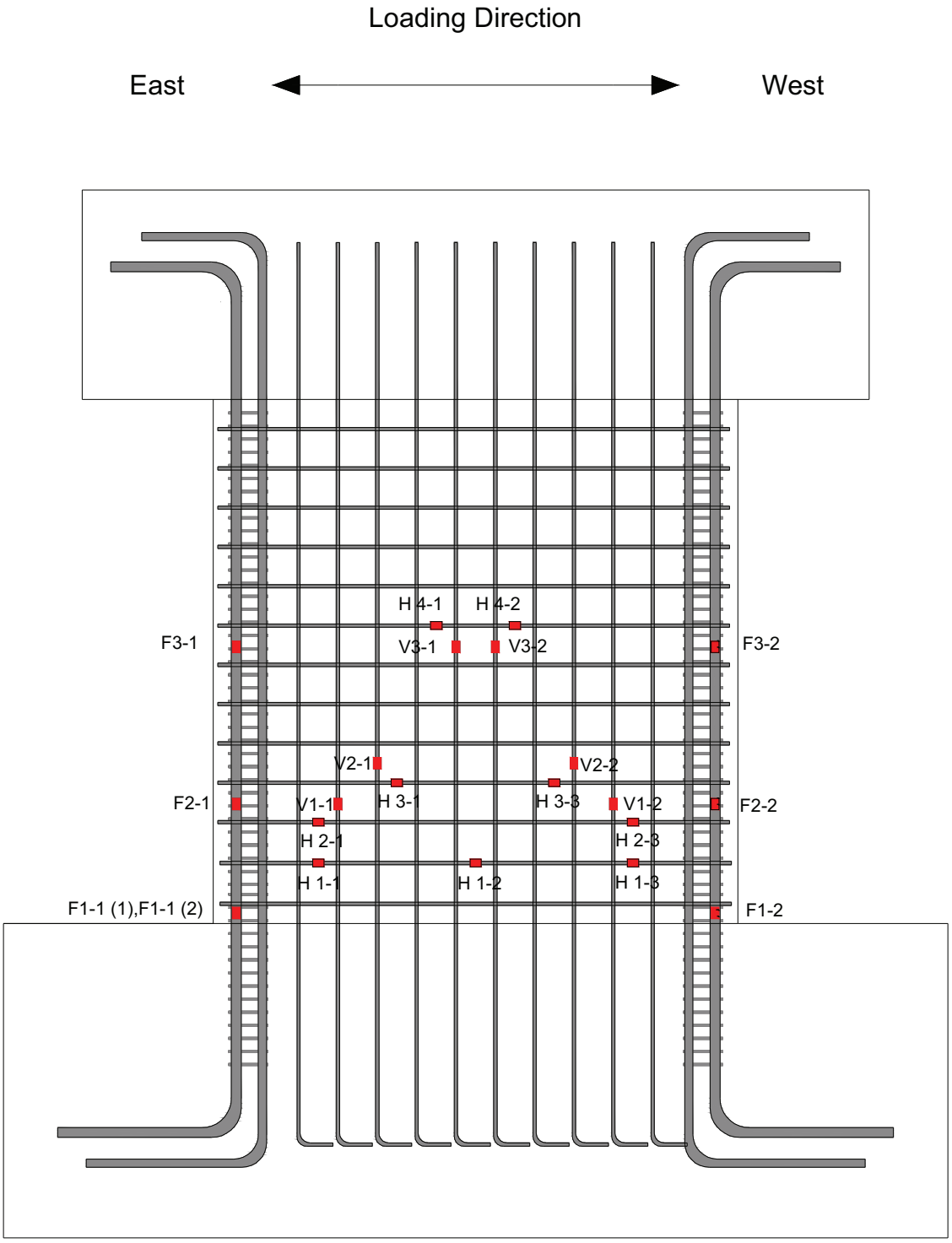

Fig. A-3 Strain Gauges Locations for Specimen S4

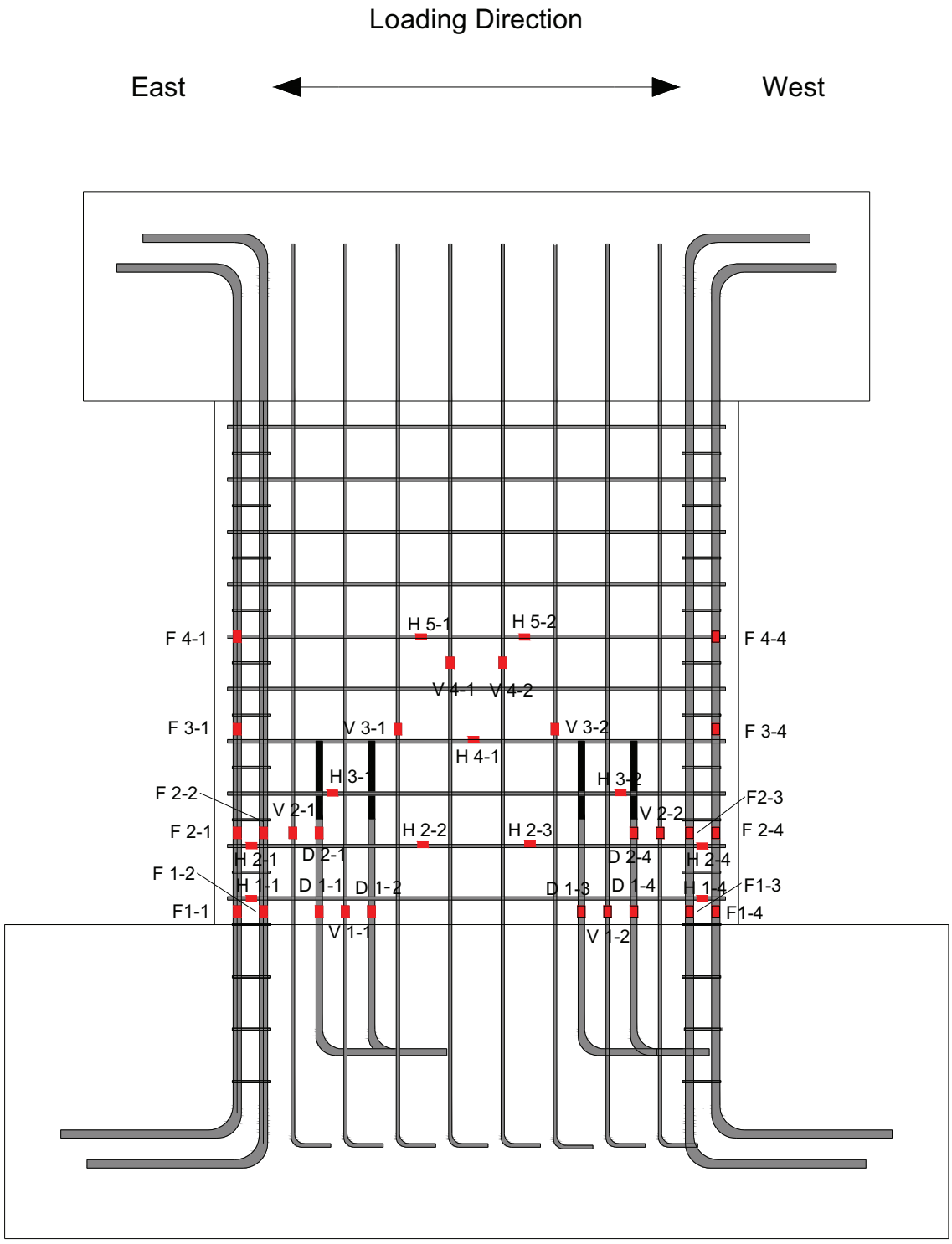

Fig. A-4 Strain Gauges Locations for Specimen S5

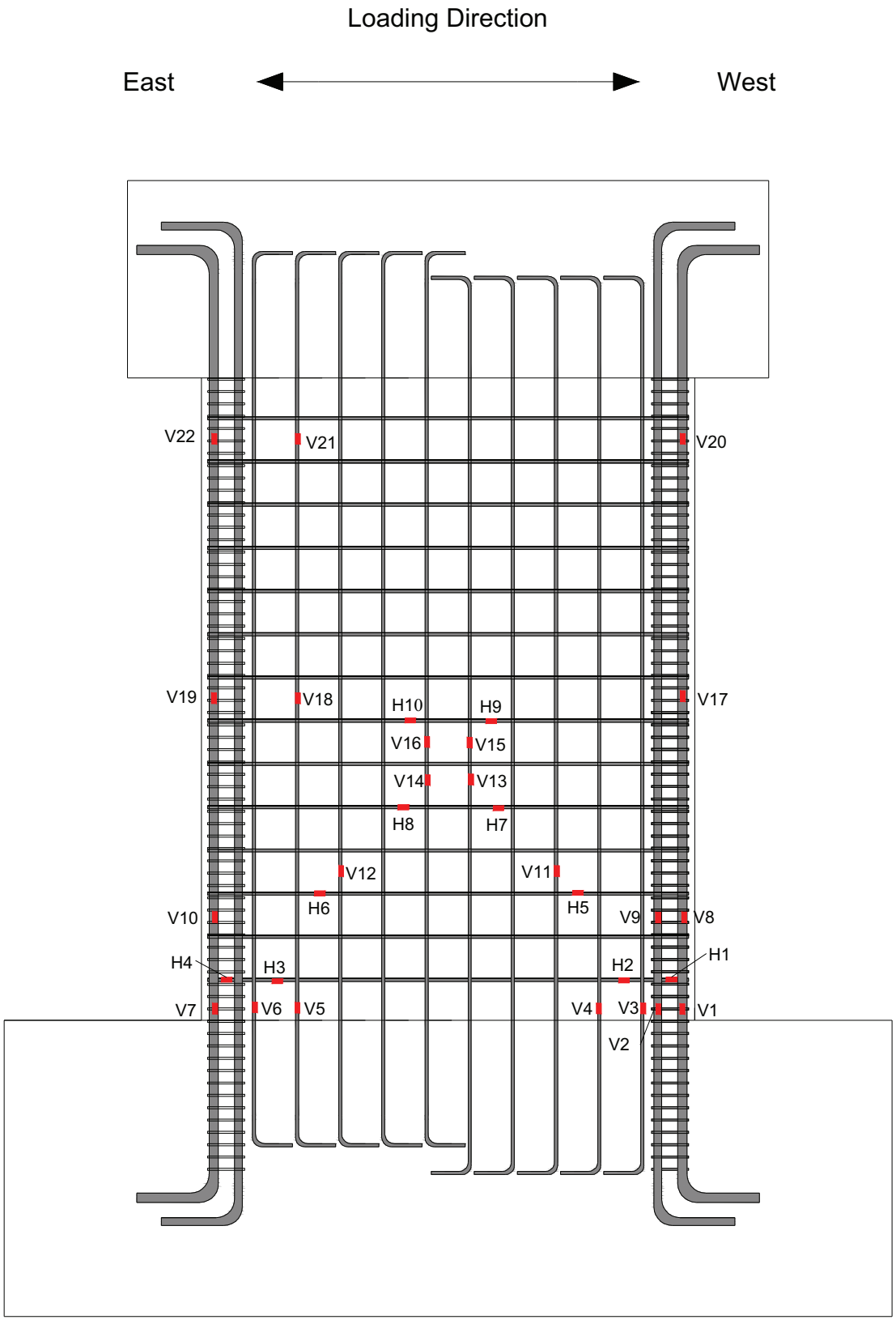

Fig. A-5 Strain Gauges Locations for Specimen S6

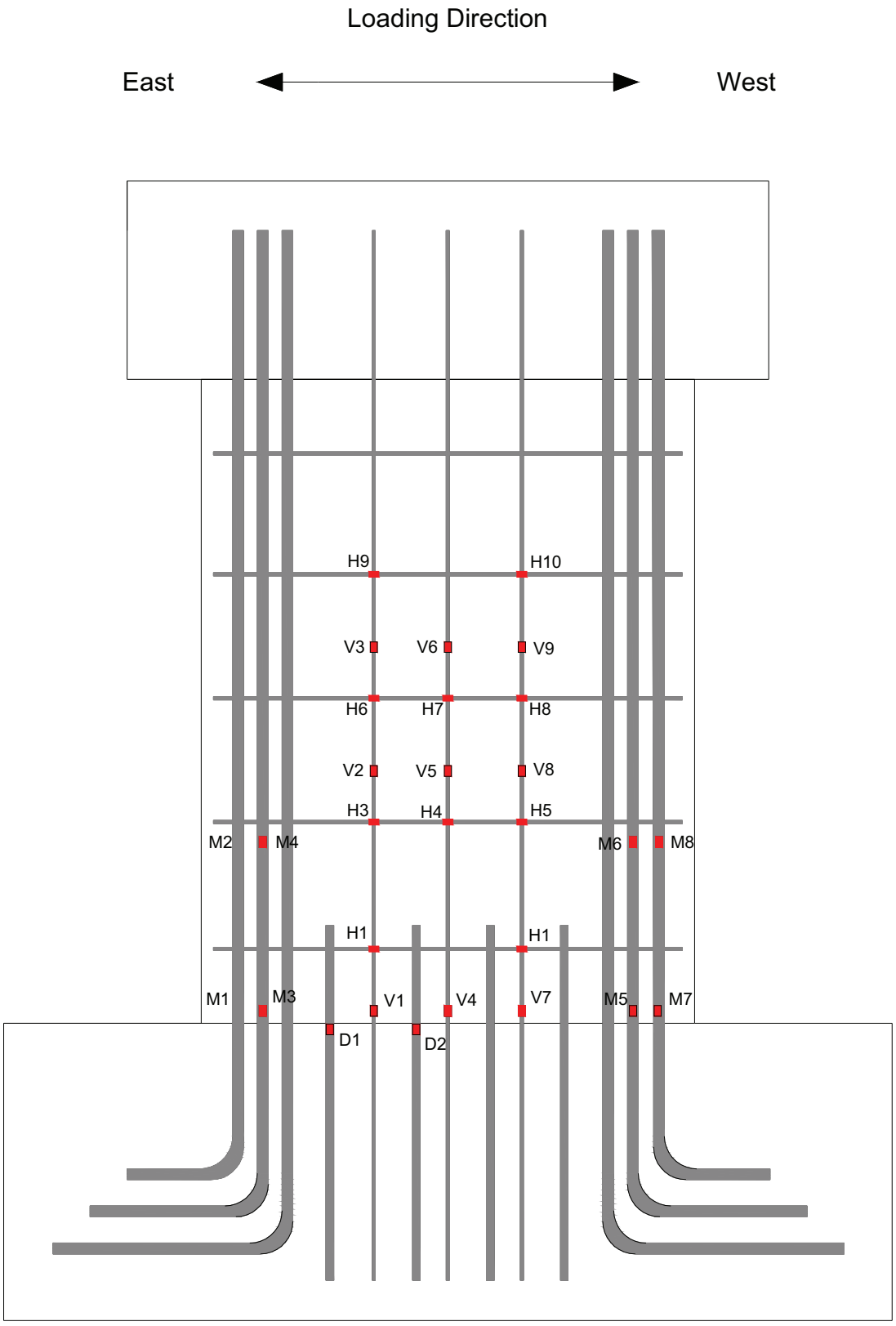

Fig. A-6 Strain Gauges Locations for Specimens S7 and S8

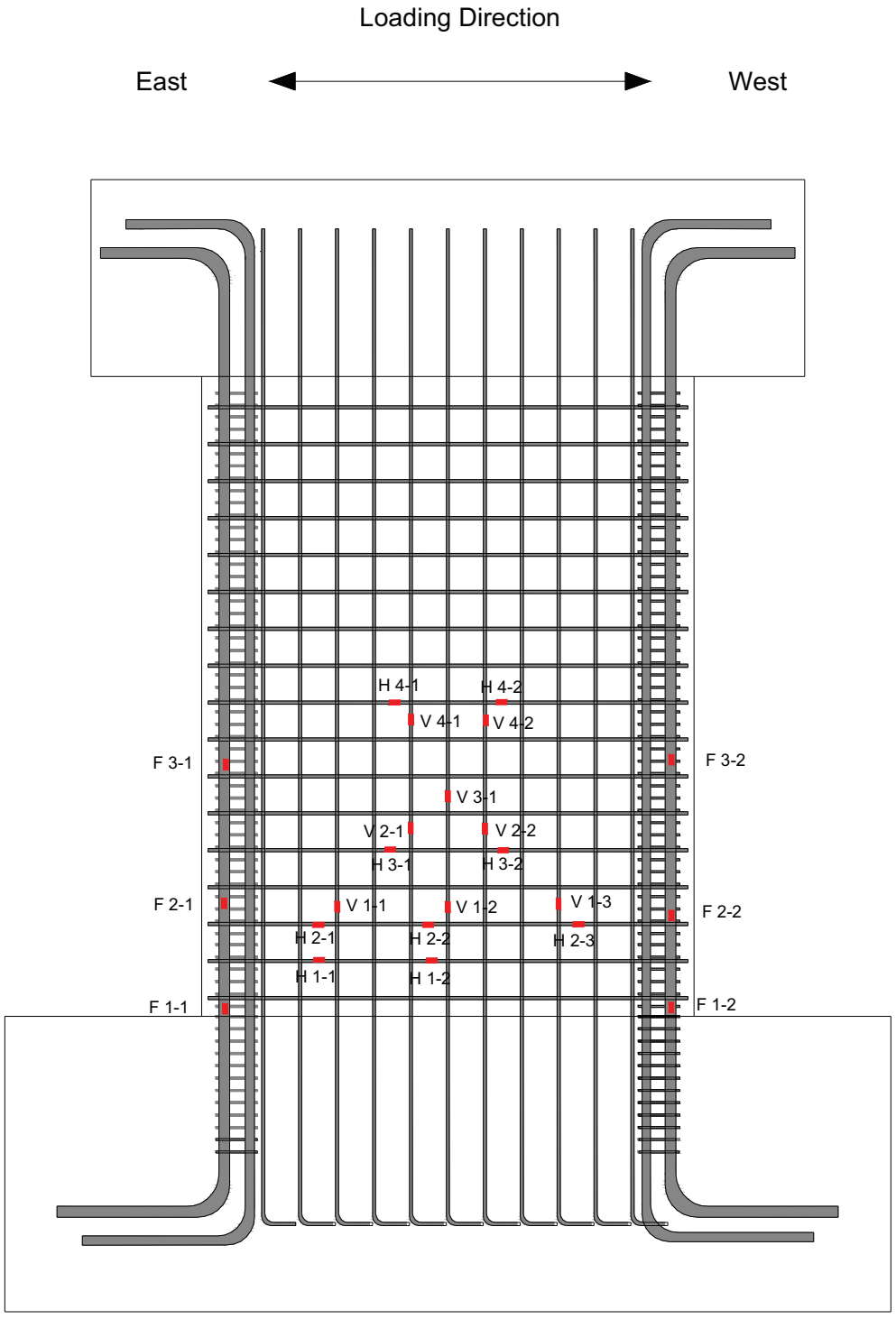

Fig. A-7 Strain Gauges Locations for Specimen S9

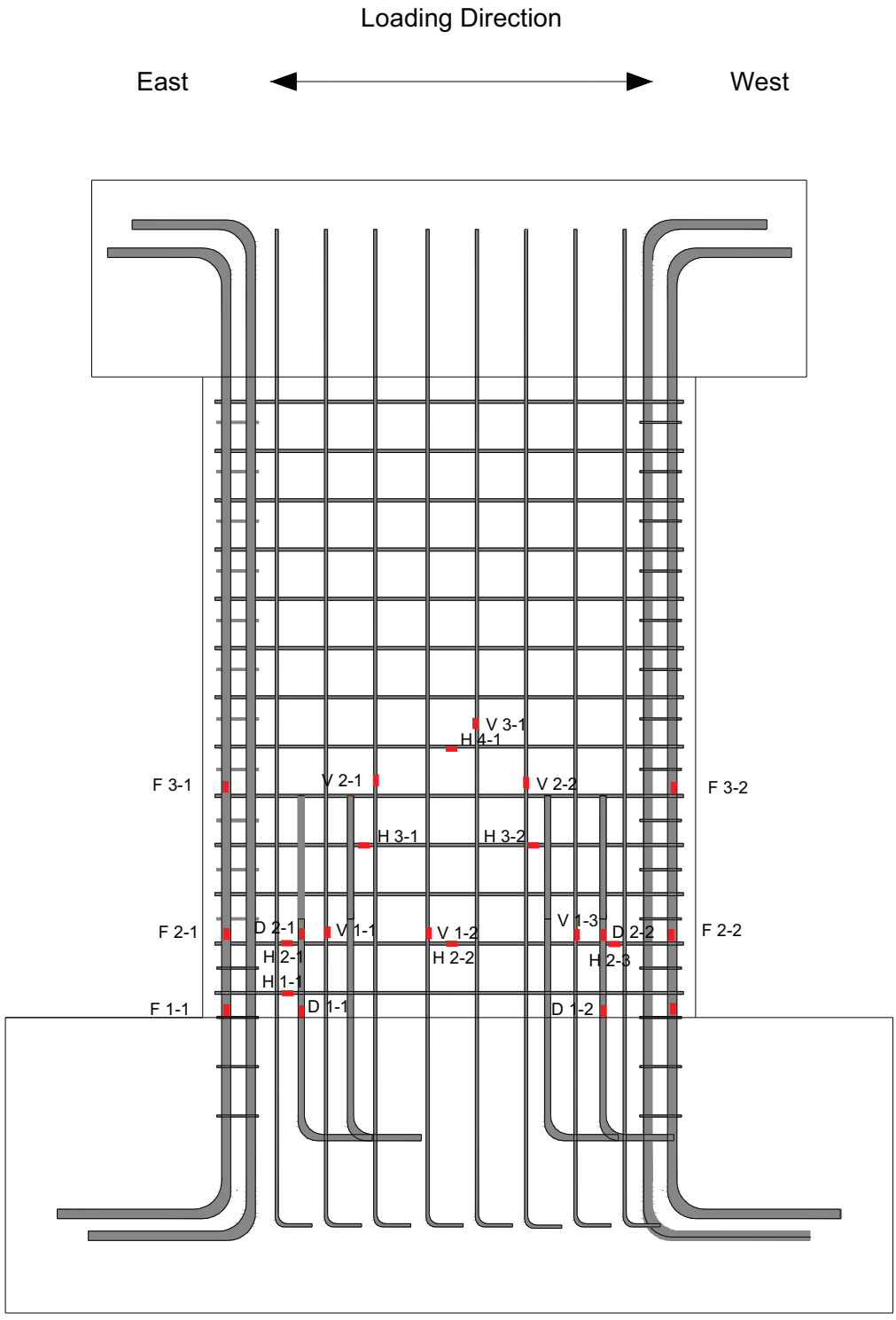

Fig. A-8 Strain Gauges Locations for Specimen S10

REFERENCES

ACI Committee 318, “Building Code Requirements for Reinforced Concrete (ACI 318-71)”, American Concrete Institute, Detroit, Michigan, 1971.

ACI Committee 318, “Building Code Requirements for Reinforced Concrete (ACI 318-83)”, American Concrete Institute, Detroit, Michigan, 1983.

ACI Committee 318, “Building Code Requirements for Reinforced Concrete (ACI 318-89)”, American Concrete Institute, Detroit, Michigan, 1989.

ACI Committee 318, “Building Code Requirements for Reinforced Concrete (ACI 318-99)”, American Concrete Institute, Farmington Hill, Michigan, 1999.

ACI Committee 318, “Building Code Requirements for Reinforced Concrete (ACI 318-2002)”, American Concrete Institute, Farmington Hill, Michigan, 2002.

ACI Committee 318, “Building Code Requirements for Reinforced Concrete (ACI 318-2005)”, American Concrete Institute, Farmington Hill, Michigan, 2005.

ACI Committee 318, “Building Code Requirements for Reinforced Concrete (ACI 318-2008)”, American Concrete Institute, Farmington Hill, Michigan, 2008.

Aktan A. E., and Bertero V. V., “RC Structural Walls: Seismic Design for Shear.”, Journal of Structural Engineering, Vol. 111, No. 8, August 1985, pp. 1775-1791.

Aoyama, H., “Design Philosophy for Shear in Earthquake Resistance in Japan.”, International Workshop on Concrete in Earthquake, University of Houston, Houston, Texas, 1991.

Ashour, A.A., Ghazi, S.H., and Wafa, F.F., “Shear Behavior of High-Strength Fiber Reinforced Concrete Beams.”, ACI Structural Journal, Vol. 89, No. 2, March-April 1992, pp. 176-184.

ASTM, “Standard Specification for Steel Wire, Deformed, for Concrete Reinforcement. (A492-02)”, ASTM International, West Conshohocken, PA, 2002.

ASTM, “Standard Specification for Steel Wire, Carbon, for General Use (A853-04).”, ASTM International, West Conshohocken, PA, 2004.

ASTM, “Standard Test Method for Flexural Performance of Fiber-Reinforced Concrete. (Using Beam with Third-Point Loading) (C1609/C1609M-05).”, ASTM International, West Conshohocken, PA, 2005.

Barda F., Hanson J. M., and Corley W. G., “Shear Strength of Low-Rise Walls with Boundary Elements.”, ACI Special Publications, Reinforced Concrete in Seismic Zones, SP-53-8, 1977, pp.149-202. (Also, Research and Development Bulletin, No. RD043.01D, Portland Cement Association.)

Benjamin, J.R. and Williams H.A., “The Behavior of One-Story Reinforced Concrete Shear Walls.”, Proceeding of the American Society of Civil Engineers, Journal of the Structural Division, Vol. 83, No. ST.3, May 1957, pp. 1254-1 to 1254-49. (Also, Transactions, ASCE, Vol. 124, 1959, pp.669-708.)

Benjamin, J.R. and Williams H.A., ”Behavior of One-Story Reinforced Concrete Shear Walls Containing Openings.”, ACI Journal Proceedings, Vol. 55, November 1958, pp. 605-618.

Benjamin J.R., and Williams H.A., ” Reinforced Concrete Shear Walls Assemblies.”, Journal of Structural Division, ASCE, Vol. 86, No. 8, 1960, pp.1–32.

Buzzini, D., Dazio, A., and Trub, M., “Quasi-Static Cyclic Tests of Three Hybrid Fibre Concrete Structural Walls.”, Report No. 297, Institute of Structural Engineering, Swiss Federal Institute of Technology, April 2006.

Canbolat B. A., Parra-Montesinos G. J. , Wight J. K., “Experimental Study on Seismic Behavior of High-Performance Fiber Reinforced Cement Composite Coupling Beams.”, ACI Structural Journal, Vol. 102, No. 1, January-February, 2005, pp. 159-166.

Cardenas A. E., Hanson J. M., Corley W. G., and Hognestad E., “Design Provisions for Shear Walls.”, ACI Journal, Vol. 70, No. 23, Code Background Paper, Background Material used in preparing ACI 318-71, March, 1973, pp. 221-230.

Cardenas, A.E., Russell, H.G., and Corley, W.G., “Strength of Low-Rise Structural Walls.”, ACI Special Publications, SP-63-10, 1980, pp. 221-241.

CEN Technical Committee 250/SC8, ”Eurocode 8: Earthquake Resistance Design of Structures – Part 1: General Rules,” (ENV 1998 1-1, 1-2, 1-3), CEN, Brussels, 1995.

Chao, S.-H., Naaman, A.E., and Parra-Montesinos, G.J. “Bond Behavior of Seven-Wire Strands Embedded in Fiber Reinforced Cementitious Composites.”, PCI Journal, Vol. 51, No. 6, 2007, pp. 56-71.

Chao, S.-H., Naaman, A. E., and Parra-Montesinos, G. J. "Bond Behavior of Reinforcing Bars in Tensile Strain-Hardening Fiber Reinforced Cement Composites.", ACI Structural Journal, V. 106, No. 6, November-December, 2009, pp. 897-906.

Choi, C.A., “Improvement of Earthquake-Resistant Performance of Squat Shear Walls under Reversed Cyclic Loads.”, Key Engineering Materials, Vol. 324-325, 2006, pp. 535-538.

Chompreda, P. and Parra-Montesinos, G. J. “Deformation Capacity and Shear Strength of Fiber Reinforced Cement Composite Flexural Members Subjected to Displacement Reversals.”, Research Report No. UMCEE 05-03, Department of Civil and Environmental Engineering, University of Michigan, 2005.

Collins M., and Mitchell D., “A rational approach to shear design: The 1984 Canadian Code Provisions.” ACI Journal, Vol. 83, 1986.

Corley, W.G., Fiorato, A.E., and Oesterle R.G., “Structural Walls.”, ACI Special Publication, SP-72-04, December, 1981.

Craig, R., Mahadev, S., Patel, C., Viteri, M. and Kertesz, C., “Behavior of Joints Using Reinforced Fibrous Concrete.”, ACI Special Publication SP-81, 1984, pp.125-167.

Filiatrault, A., Ladicani, K., and Massicotte, B., “Seismic Performance of Code Designed Fibre Reinforced Concrete Joints.”, ACI Structural Journal, Vol. 91, No. 5, September-October 1994, pp. 564-571.

Filiatrault, A., Sylvain, P., and Houde, J., “Seismic Performance of Steel-Fiber Reinforced Concrete Interior Beam-Column Joints.”, ACI Structural Journal, Vol. 92, No. 5, September-October 1995, pp. 534-552.

Fintel M., “Shearwalls - An Answer for Seismic Resistance?”, Concrete International, Vol. 13, No. 7, July 1991, pp. 48-53.

Greifenhagen, C. and Lestuzzi, P., “Static Cyclic Tests on Lightly Reinforced Concrete Shear Walls.”, Engineering Structures, Vol. 27, 2005, pp. 1705-1721.

Gulec, C.K., Whittaker, A.S., and Stojadinovic, B., “Shear Strength of Squat Rectangular Reinforced Concrete Walls.”, ACI Structural Journal, Vol. 105, No. 4, July-August 2008, pp. 488-497.

Gulec, C.K., Whittaker, A.S., and Stojadinovic, B.,”Peak Shear Strength of Squat Reinforced Concrete Walls with Boundary Barbells or Flanges.”, ACI Structural Journals, Vol. 106, No. 3, May-June 2009, pp. 368-377.

Gupta, A. and Rangan, B.V., “High-Strength Concrete (HSC) Structural Walls.”, ACI Structural Journals, Vol. 95, No. 2, March-April 1998, pp. 194-205.

Henager, C.H., “Steel Fibrous, Ductile Concrete Joint for Seismic-Resistant Structures.”, ACI Special Publication SP-53, 1977, pp. 371-379.

Hidalgo P. A., Ledezma C. A., and Jordan R. M., “Seismic Behavior of Squat Reinforced Concrete Shear Walls.” Earthquake Spectra, Vol. 18, No. 2, May 2002, pp. 287-308.

Khuntia, M., Stojadinovic, B., and Goel, S. C., "Shear Strength of Normal and High-Strength Fiber Reinforced Concrete Beams without Stirrups.", ACI Structural Journal, Vol. 96, No. 2, March-April 1999, pp. 282-289.

Kim K., Parra-Montesinos G., “Behavior of HPFRCC Low-Rise Walls Subjected to Displacement Reversals.” High Performance Fiber Reinforced Cement Composites (HPFRCC) Workshop, Ann Arbor, USA, 2003.

Kwak, Y.K., Eberhard, M.O., Kim, W., and Kim, J., “Shear Strength of Steel Fiber-Reinforced Concrete Beams Without Stirrups”, ACI Structural Journal, Vol. 99, No. 4, July-August 2002, pp. 530-538.

Lefas, I.D., Kotsovos, M.D. and Ambraseys, N.N., “Behavior of Reinforced Concrete Structural Walls: Strength, Deformation Characteristics and Failure Mechanism.”, ACI Structural Journal, Vol. 87, No. 1, January-February 1990, pp. 23-31.

Lehmans, D., Moehle, J.P., and Mahin, S., “Experimental Evaluation of the Seismic Performance of Reinforced Concrete Bridge Columns.”, Journal of the Structural Engineering, Vol. 130, No. 6, 2004, pp. 869-879.

Lestuzzi, P. and Bachmann, H., “Displacement Ductility and Energy Assessment from Shaking Table Tests on RC Structural Walls.”, Engineering Structures, Vol. 29, 2007, pp.1708-1721.

Li, V.C., Ward, R., and Hamza, A.M., “Steel and Synthetic Fibers as Shear Reinforcement.”, ACI Materials Journal, Vol. 85, No. 5, 1992, pp.499-5-8.

Li, V.C., “From Micromechanics to Structural Engineering – The Design of Cementitious Composites for Civil Engineering Applications.”, JSCE Journal of Structural Mechanics and Earthquake Engineering , Vol. 10, No. 2, 1993, pp.37-48.

Liao, W.-C.; Chao, S.-H.; Park, S.-Y. and Naaman, A. E., "Self-Consolidating High Performance Fiber Reinforced Concrete: SCHPFRC." High Performance Fiber Reinforced Cement Composites: HPFRCC-5,Mainz, Germany, July 2007.

Lopes, M.S. [(a)], “Experimental Shear-Dominated Response of RC Walls. Part I: Objectives, Methodology and Results.”, Engineering Structures, Vol. 23, 2001, pp.229-239.

Lopes, M.S. [(b)], “Experimental Shear-Dominated Response of RC Walls. Part II: Discussion of Results and Design Implications.”, Engineering Structures, Vol. 23, 2001, pp. 564-574.

Maier, J., “Shear Wall Tests.”, Concrete Shear in Earthquake, University of Houston, Texas, 1992, pp.85-94.

Mansur, M.A., Ong, K.C.G., and Paramsivam, P., “Shear Strength of Fibrous Concrete Beams without Stirrups.”, Journal of Structural Engineering, Vol. 112, No. 9, September 1986, pp.2066-2079.

Markovic, I, Walraven, J.C., and van Mier, J.G.M., “Development of High-Performance Hybrid Fiber Concrete.”, 4th International Workshop on HPFRCC, June 2003.

Markovic, I, Walraven, J.C., and van Mier, J.G.M., “Tensile Reponse of Hybtid-Fiber Concrete.”, 6th RILEM Symposium on FRC – BEFIB 2004, September, 2004.

Massone, L. M., and Wallace, J. W., “Load-Deformation Responses of Slender Reinforced Concrete Walls.”, ACI Structural Journal, Vol. 101, No. 1, January-February, 2004, pp. 103-113.

Matamoros, A.B., and Sozen, M.A., “Drift Limits of High-Strength Concrete Columns Subjected to Load Reversals.”, Journal of Structural Engineering, Vol. 129, No. 3, 2003, pp. 297-313.

Mindess, S., Young, J.F., and Darwin, D., “Concrete”, Prentice Hall, 2003, 2nd edition, 644 pp.

Mo, Y.L. and Kuo, J.Y., “Experimental Studies on Low-Rise Structural Walls.”, Materials and Structures, Vol. 31, August-September 1998, pp. 465-472.

Moehle, J.P., and Wallace, J.W., “Ductility and Detailing Requirements of Shear Wall Buildings.”, Proceedings of the Fifth Chilean Conference of Seismology and Earthquake Engineering, Santiago, Chile, 1989, pp.131-150.

Naaman, A. E., "Fiber Reinforcement for Concrete.", Concrete International, Vol. 7, No. 3, March 1985, pp. 21-25.

Naaman, A. E., "New Fiber Technology (Cement, Ceramic, and Polymeric Composites).", Concrete International, Vol. 20, No. 7, July 1998, pp. 57-62.

Narayanan R., and Darwish I. Y. S., “Use of Steel Fibers as Shear Reinforcement.”, ACI Structural Journal, Vol. 84, No. 3, May-June 1987, pp. 216-227.

Narayanan, R., and Darwish, I.Y.S., “Fiber Concrete Deep Beam in Shear.”, ACI Structural Journal, Vol. 85, No. 2, March-April 1988, pp. 141-149.

Naaman, A.E., and Reinhardt, H.W., “Characterization of High-Performance Fiber Reinforced Cement Composites-HPFRCC.”, High Performance Fiber Reinforced Cement Composites 2 (HPFRCC 2), Proceedings of the Second International RILEM Workshop, Ann Arbor, USA, Edited by Naaman A.E. and Reinhardt H.W., RILEM Publications S.A.R.L., Cachan Cedex, France, June 1996, pp.1-24.

Oesterle, R.G., Fiorato, A.E., Johal, L.S., Carptenter, J.E., Russell, H.G., and Corley, W.G., “Earthquake-Resistant Structural Walls-Test of Isolated Walls.”, PCA Construction Technology Laboratories/National Science Foundation, Washington, D.C., November 1976, 315 pp. (available as PB 27-14670 from National Technical Information Service).

Oesterle, R.G., Aristizabal-Ocha, J.D., Fiorato, A.E., Russell, H.G., and Corley, W.G., "Earthquake-Resistant Structural Walls, Phase II.", PCA Construction Technology Laboratories/National Science Foundation, Washington, D.C., October 1979, 327 pp. (available as PB 80-132481 from National Technical Information Center)

Oestterle, R. G., Aristizabal-Ochoa, J. D., Shiu, K. N., and Corley, W. G., "Web Crushing of Reinforced Concrete Structural Walls.", ACI Journal, Vol. 81, No. 22, May-June, 1984, pp. 231-241.

Palermo, D. and Vecchio, F.J., "Behavior of Three-Dimensional Reinforced Concrete Shear Walls.", ACI Structural Journal, Vol 99, No. 1, January-February, 2002, pp. 81-89.

Parra-Montesinos, G.J., and Wight, J.K., "Seismic Response of Exterior R/C Column-to-Steel Beam Connections.", Journal of Structural Engineering, Vol. 126, No. 10, October 2000, pp. 1113-1121.

Parra-Montesinos G., "HPFRCC in Earthquake-Resistant Structures: Current Knowledge and Future Trends." High Performance Fiber Reinforced Cement Composites (HPFRCC) Workshop, Ann Arbor, USA, 2003.

Parra-Montesinos G., "High-Performance Fiber-Reinforced Cement Composites: An Alternative for Seismic Design of Structures." ACI Structural Journal, Vol. 102, No. 5, September-October 2005, pp. 668-675.

Parra-Montesinos, G.J., Peterfreund, S.W., and Chao, S.-H., "Highly Damage Tolerant Beam-Column Joints Trough the Use of High-Performance Fiber Reinforced Cement Composites.", ACI Structural Journal, Vol. 102, No. 3, May-June, 2005, pp.487-495.

Parra-Montesinos G., Canbolat, B.A., and Jeyeraman, G.R., "Relaxation of Confinement Reinforcement in Structural Walls Through the Use of Fiber Reinforced Cement Composites.", Eighth National Conference on Earthquake Engineering, April 2006, San Francisco, California.

Parra-Montesinos G., and Chompreda, P., "Deformation Capacity and Shear Strength of Fiber-Reinforced Cement Composite Flexural Members Subjected to Displacement Reversals.", Journal of Structural Engineering, Vol. 133, No. 3, March 2007, pp. 421-431.

Pauley T. M. [(a)], “The Design of Ductile Reinforced Concrete Structural Walls for Earthquake Resistance.”, Earthquake Spectra, Vol. 2, No. 4, 1986, pp.783-823.

Pauley T., Priestley M. J. N., Synge A. J., “Ductility in Earthquake Resisting Squat Shearwalls.” ACI Journal, Vol. 79, No. 26, January-August 1982, pp. 257-269.

Salonikios, N. T., Kappos, J. A., Tegos, A. I., Penelis, G. G., “Cyclic Load Behavior of Low-Slenderness Reinforced Concrete Walls: Design Basis and Test Results.”, ACI Structural Journal, Vol. 96, No. 4, July-August 1999, pp. 649-660.

Salonikios, N. T., Kappos, J. A., Tegos, A. I., Penelis, G. G., “Cyclic Load Behavior of Low-Slenderness Reinforced Concrete Walls: Failure Modes, Strength and Deformation Analysis, and Design Implications.”, ACI Structural Journal, Vol. 97, No. 1, January-February 2000, pp. 132-142.

Salonikios, T. N., “Analytical Prediction of the Inelastic Response of RC Walls with Low Aspect Ratio.”, Journal of Structural Engineering, Vol. 133, No. 6, June 2007, pp. 844-854.

Shah, S.P., and Naaman, A.E., “Mechanical Properties of Glass and Steel Fiber Reinforced Mortar.”, ACI Journal, Vol. 23, No. 1, January 1976, pp. 50-53.

Shah, S.P., and Rangan, B.V., “Fiber Reinforced Concrete Properties.”,(1971), ACI Journal, Vol. 68, No. 2, February 1971, pp. 126-135.

Shah, S.P., Stroven, P., Dalhuisen, D., and Van Stekelenburg, P., “Complete Stress-Strain Curves for Steel Fibre Reinforced Concrete in Uniaxial Tension and Compression.”, Testing and Test Methods of Fibre Cement Composites, RILEM Symposium 1978, Construction Press, Lancaster, 1978, pp. 399-408.

Sharma, A.K., “Shear Strength of Steel Fiber Reinforced Concrete Beams.”, ACI Journal, Vol. 83, No. 4, July-August 1986, pp. 624-628.

Sittipunt, C., and Wood, S. L., "Influence of Web Reinforcement on the Cyclic Response of Structural Walls.", ACI Structural Journal, Vol. 92, No. 6, November-December 1995, pp.1-12.

Sittipunt, C., Wood, S. L., Lukkunaprasit, P., and Pattararattanakul, P., "Cyclic Behavior of Reinforced Concrete Structural Walls with Diagonal Web Reinforcement." ACI Structural Journal, Vol. 98, No. 4, July-August 2001, pp. 554-562.

Synge, A.J., "Ductility of Squat Shear Walls.", Research Report 80-8, Department of Civil Engineering, University of Canterbury, Christchurch, New Zealand, February, 1980.

Thomsen, J.H., and Wallace, J.W., "Displacement-Based Design of Reinforced Concrete Structural Walls: Experimental Studies of Walls with Rectangular and T-Shaped Cross Sections.", Report No. CU/CEE-95/06, Department of Civil and Environmental Engineering, Clarkson University, Potsdam, N.Y., 1995.

Thomsen, J.H. and Wallace, J.W., "Displacement-Based Design of Slender Reinforced Concrete Structural Walls-Experimental Verification.", Journal of Structural Engineering, Vol. 130, No. 4, April 2004, pp. 618-630.

Uniform Building Code, "International Conference of Building Officials", Whittier, California, 1967.

Uniform Building Code, "International Conference of Building Officials", Whittier, California, 1970.

Uniform Building Code, "International Conference of Building Officials", Whittier, California, 1991.

Uniform Building Code, "International Conference of Building Officials", Whittier, California, 1994.

Uniform Building Code, "International Conference of Building Officials", Whittier, California, 1997

Vecchio, F. J., and Collins, M. D., "The Modified Compression-Field Theory for Reinforced Concrete Elements Subjected to Shear.", ACI Journal, Vol. 83, No. 2, March-April 1986, pp. 219-231.

Wallace J. W., "New Methodology for Seismic Design of RC Shear Walls." Journal of Structural Engineering, Vol. 120, No.3, March 1994, pp. 101-130.

Wallace J. W. [(a)], "Seismic Design of RC Structural Walls. Part I: New Code Format." Journal of Structural Engineering, Vol. 121, No. 1, January 1995, pp.75-87.

Wallace J. W. [(b)], "Seismic Design of RC Structural Walls. Part II: Applications." Journal of Structural Engineering, Vol. 121, No. 1, January 1995, pp. 88-101.

Wallace, J.W., and Moehle, J.P., "The 3 March 1985 Chile Earthquake: Structural Requirements for Bearing Walls Buidlings.:, EERC Report No. UCB/EERC-89-5, Earthquake Engineering Research Center, University of California at Berkeley, Berkeley, California, 1989.

Wallace, J. W., and Moehle, J. P, "Ductility and Detailing Requirements of Bearing Wall Buildings.", Journal of Structural Engineering, Vol. 118, No. 6, June 1992, pp.1625-1644.

Wallace, J.W. and Orakcal, K., "ACI 318-99 Provisions for Seismic Design of Structural Walls.", ACI Structural Journal, Vol. 99, No. 4, July-August 2002, pp. 499-508.

Wight, R.G., and Erki, M.A., "Steel Fiber Reinforced Concrete for Shear-Wall Coupling Beams.", Proceedings of the Second University-Industry Workshop on Fiber Reinforced Concrete and Other Advanced Materials, Toronto, 1995, pp. 363-377.

Wiradinata, S. and Saactioglu, M., "Tests of Squat Shear Walls under Lateral Load Reversals.", Proceedings of the Third U.S. National Conference on Earthquake Engineering, Vol. 2, August 1986, Charleston, South Carolina, pp. 1395-1406.

Wood, S. L., "Minimum Tensile Reinforcement Requirements in Walls.", ACI Structural Journal, Vol. 86, No. 5, September-October 1989, pp. 582-591.

Wood S. L., "Shear Strength of Low-Rise Reinforced Concrete Walls." ACI Structural Journal, Vol. 87, No. 1, January-February 1990, pp. 99-107.

Wood S. L., "Performance of Reinforced Concrete Buildings during the 1985 Chile Earthquake: Implications for the Design of Structural Walls.", Earthquake Spectra, Vol. 7, No. 4, 1991, pp. 607-638.